UNIVERSITY OF SOUTHAMPTON
Faculty of Engineering and the Environment
Institute of Sound and Vibration Research

Force Response of Locust Skeletal Muscle

by

Emma Wilson

Thesis for the degree of Doctor of Philosophy

December 2010

UNIVERSITY OF SOUTHAMPTON

ABSTRACT

FACULTY OF ENGINEERING AND THE ENVIRONMENT
INSTITUTE OF SOUND AND VIBRATION RESEARCH

Doctor of Philosophy

FORCE RESPONSE OF LOCUST SKELETAL MUSCLE

by Emma Wilson

The force response of the locust hind leg extensor muscle to input excitation pulses is modelled. Despite the processes behind muscle contraction being well established, no broadly valid method of modelling skeletal muscle exists. Studies that compare the merits of existing models are extremely scarce and researchers make various assumptions in order to simplify the complex, nonlinear behaviour of the muscle. Locusts provide an opportunity to develop a muscle model in a simpler system, that will still show similar properties to that of mammalian muscles. In developing a model previous work is considered, and complexity is introduced in the experimental conditions in stages. This meant a model could be built up in parts. This approach reduces the need for questionably valid assumptions.

The main focus of this work is modelling activated isometric muscle. Experimental data was collected by stimulating the extensor muscle and measuring the force generated at the tibia. In the first instance the response to individual stimulus pulses is modelled. This is extended to develop a predictive model capable of estimating the isometric force response to general pulse train inputs. In developing the model, data was fit to existing models, and from this an improved isometric model developed. The effect of changing the isometric muscle length is considered. Commonly changing the muscle length is assumed to just scale the force response. This assumption is poor. The dynamics of the force response were found to be modified by the change in muscle length, and the isometric model adapted to include this dependency.

Results related to the non-isometric behaviour are also presented. Passive muscle is usually just modelled over the lengthening period, however, the whole stretch-shorten cycle is considered here. A model, adapted from the standard linear model, is developed to describe the passive force response.

Contents

List of Figures

List of Tables

Declaration of Authorship

I, Emma Wilson, declare that this thesis titled, 'Force Response of Locust Skeletal Muscle' and the work presented in it are my own. I confirm that:

- This work was done wholly or mainly while in candidature for a research degree at this University.
- Where any part of this thesis has previously been submitted for a degree or any other qualification at this University or any other institution, this has been clearly stated.
- Where I have consulted the published work of others, this is always clearly attributed.
- Where I have quoted from the work of others, the source is always given. With the exception of such quotations, this thesis is entirely my own work.
- I have acknowledged all main sources of help.
- Where the thesis is based on work done by myself jointly with others, I have made clear exactly what was done by others and what I have contributed myself.
- Parts of this work have been published as

1. E. Wilson, E. Rustighi, B.R. Mace, P.L. Newland. A model of force generation by locust skeletal muscle in response to individual stimuli. In:*Proceedings of the ASME 2009 IDETC/CIE*, San Diego, USA. ASME
2. E. Wilson, E. Rustighi, P.L. Newland, B.R. Mace. A predictive model of the isometric force response of the locust extensor muscle. In:*Proceedings of the 32nd Annual International Conference of the IEEE Engineering in Medicine and Biology Society*, 2010.
3. E. Wilson, E. Rustighi, B.R. Mace, P.L. Newland. Isometric Force generated by locust skeletal muscle: responses to single stimuli. *Biological Cybernetics*, 102(6):503-511, 2010.
4. E. Wilson, E. Rustighi, B.R. Mace, P.L. Newland. Modelling the isometric force response to multiple pulse stimuli in locust skeletal muscle. *Biological Cybernetics*. 104(1-2):121-136, 2011.

Acknowledgements

I would like to acknowledge and thank my supervisors, Dr. Emiliano Rustighi, Professor Brian Mace and Professor Philip Newland, both for their initial ideas on the project and for their continued support. Their academic guidance, understanding and encouragement were valuable, both throughout the project, and during the writing of the thesis. My thanks also go to Dr. David Simpson and Professor Stephen Elliott for their useful suggestions at each review meeting.

Grateful thanks are also due to Dave Edwards and the ISVR technicians for both technical support and in making components for the experimental rigs, to Oliver Dewhirst for use of his acquisition unit and to those responsible for maintaining the locust colony at Southampton University.

Finally, I would like to thank Stuart Bennett for proof reading of the thesis and all of those who supported me in any respect during the completion of the project.

Abbreviations

AIC	**A**kaike's **I**nformation **C**riterion
BIC	**B**ayesian **I**nformation **C**riterion
CE	**C**ontractile **E**lement
CFT	**C**onstant **F**requency **T**rain
ETi	**E**xtensor **Ti**bia
FES	**F**unctional **E**lectrical **S**timulation
FETi	**F**ast **E**xtensor **Ti**bia
FT	**F**emoro-Tibial
FTI	**F**orce **T**ime **I**ntegral
HRT	**H**alf **R**elaxation **T**ime
IPF	**I**nter **P**ulse **F**requency
IPI	**I**nter **P**ulse **I**nterval
IRC	**I**sometric **R**ecruitment **C**urve
LDS	**L**inear **D**ynamic **S**ystem
LMN	**L**ocal **M**odel **N**etwork
LN	**L**inear **N**onlinear
LNL	**L**inear **N**onlinear **L**inear
LRT	**L**ate **R**elaxation **T**ime
NCFT	**N**on **C**onstant **F**requency **T**rain
ODE	**O**rdinary **D**ifferential **E**quation
PE	**P**arallel elastic **E**lement
PF	**P**eak **F**orce
RFI	**R**elative **F**usion **I**ndex
SE	**S**eries elastic **E**lement
SETi	**S**low **E**xtensor **Ti**bia
SLM	**S**tandard **L**inear **M**odel
SNL	**S**tatic **N**on-**l**inearity
SR	**S**arcoplasmic **R**eticulum
TPT	**T**ime to **P**eak **T**ension

Symbols

Muscle Specific

$F_m(t)$	Muscle force	N
$F(t)$	Normalised muscle force	
$\hat{F}_m(t)$	Estimated muscle force	N
$\hat{F}(t)$	Estimated normalised muscle force	
F_o	Maximum isometric force	N
F_V	Force-velocity relation	N
$\tilde{F}_V$	Normalised force-velocity relation	
F_L	Force-length relation	N
$\tilde{F}_L$	Normalised force-length relation	
F_{CE}	Force developed by the contractile element	N
F_{PE}	Force developed by the passive element	N
l_m	Muscle length	mm
l_o	Muscle rest length	mm
l_f	Muscle fibre length	mm
l_{of}	Muscle fibre rest length	mm
$\tilde{l}_m$	Normalised muscle length, $\tilde{l}_m = l_m/l_o$	
l_{min}, l_{max}	Upper and lower bonds for the admissible range of muscle lengths	mm
x_{ms}	Distance muscle shorterned from rest, positive for contracting muscle	mm
v_{ms}	Muscle shortening velocity, positive for contracting muscle, $v_{ms} = \dot{x}_{ms}$	mms^{-1}
x_m	Muscle displacement from rest, positive for lengthening muscle	mm
v_m	Muscle velocity, positive velocity for lengthening muscle, $v_m = \dot{x}_m$	mm s^{-1}
a_m	Muscle acceleration, positive acceleration for lengthening muscle, $a_m = \ddot{x}_m$	mm s^{-2}

v_o	Maximal shortening velocity	mms^{-1}
$\tilde{v}_m$	Normalised muscle velocity, $\tilde{v}_m = v_m/v_o$	
$u(t)$	Neural stimulus	
$a(t)$	Activation	
$\beta(t)$	T-tubuli depolarisation in cascade model	
$\gamma(t)$	Free calcium concentration in cascade model	
$C_N(t)$	Calcium concentration in muscle filaments in LNL models	
$\mu(t)$	Fitness variable to account for fatigue	
Locust Specific		
ΔL	Relative length change of extensor	mm
λ	Femoral-tibial angle	
λ_r	Relative femoral-tibial angle	
θ_b, θ_c	Internal joint angles	
Aquisition Settings, Inputs and Outputs		
n	Number of input pulses	
d	duration of input pulses	
$V_{\max}$	amplitude of input pulses	V
V_{in}	voltage used to stimulate muscle	V
V_{bridge}	bridge voltage setting in wheatstone bridge circuit of transducer amplifier	V
V_{S}	voltage used to drive shaker	V
V_{LC}	voltage output from load-cell	V
V_x	low-pass filtered voltage output from laser	V
F_{tib}	force measured at the tibia	N
Model Parameters Used in Simulations		
τ_1, τ_2, τ_c, τ_R,	Model time constants	s
θ_3, θ_2, θ_1, θ_0	Constants, model parameters	s^3, s^2, s, -
A, b_o, a	Constants, model parameters	s^{-1}
b_1, B, k, m	Constants, model parameters	
$\theta^{(n)}$	Estimated parameters when fitting to the n^{th} pulse of a CFT	
d_m,..,d_o	Model coeffcients	
$a_{(n-1)}$,.., a_o	Model coeffcients	
k_{l1}, k_{l2}, k_{l3}	Linear spring coefficients	Nmm^{-1}
k_{n1},k_{n2},k_{n3}	Nonlinear spring coefficients	Nmm^{-3}
c_d, c_e	Linear damping coefficients	Nsmm^{-1}
c_{d1}	Nonlinear damping coefficient	Nsmm^{-2}
c_{d2}, c_{e2}	Noninear damping coefficients	Nsmm^{-3}

Chapter 1

Introduction

Muscles and tendons are the interface between the nervous system and skeletal dynamics [1]. The neural and muscular systems are dynamically coupled. Both systems play a role in movement and force generation [2] and are both utilised to control locomotion. This is demonstrated by Fig. 1.1 which gives a representation of the neuromuscular control during locomotion. Neural activity causes muscles to contract, thus muscles can be thought of as the actuators that do the work in moving the skeleton [3]. It is essential in the analysis of the neuro-muscular-skeletal control system to have an understanding of these actuators and mathematical descriptions of their dynamics [4].

By studying muscular function in a system where the neural components are well understood and simple, a greater insight into the neuromuscular system can be gained [5]. This thesis is concerned with the behaviour of invertebrate muscle, namely the extensor muscle of the locust metathoracic (hind) leg. Many studies on muscular function focus on vertebrate muscle. The functional processes that occur during contraction are similar in invertebrate muscle [6, 7], with calcium being the key regulatory factor of contraction. The muscles of invertebrates differ from those of vertebrates due to details of innervation. Invertebrate muscle is innervated by only a small number of neurons. These neurons are often identifiable, hence the neural events leading to contraction are tractable and relatively easily produced in experiment. The neural components controlling the locust hind leg extensor muscle are well known [8–13] and simple. This, combined with the muscles relatively large size, makes it ideal to study.

1.1 Motivation

Muscle models can provide an important step in enhancing our understanding of the neuromuscular system. It could be argued that the best description of a system is the system itself [16].

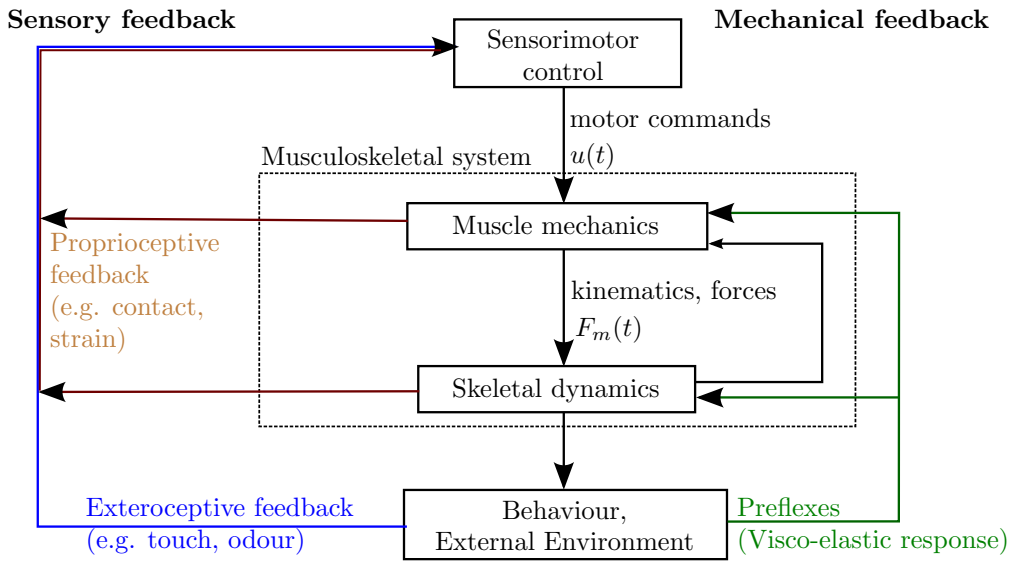

FIGURE 1.1: Neuromuscular control during locomotion. The central nervous system generates motor commands that activate the musculoskeletal system. The musculoskeletal system acts on the external environment, causing movement. Both neural and mechanical feedback play roles in controlling locomotion. Muscle mechanics play a central role in determining the movement. Figure adapted from [14, 15].

However, it is hard to extract information from the actual system, especially given that the muscle is history dependent and fatigues after repeated stimulation [17, 18]. A mathematical model highlights the important functions of the muscle system and can provide a predictive insight into its behaviour. The model should provide a simplified representation of the system's behaviour which is easier to interpret. A model with predictive capabilities is able to provide insight into how the muscle will respond to a given input.

Skeletal body dynamics are induced by muscular contraction. Being able to predict the response of a muscle to a given input enables one to infer the resultant body dynamics. Figure 1.1 shows how the musculoskeletal system is coupled into locomotion. Musculoskeletal modelling has uses in controlling movement, such as in functional electrical stimulation (FES) as well as helping to build devices that restore function after injury [19]. The characterisation of the functional role of the muscle is also useful in the development of robotic devices that are driven by virtual muscles [15].

An improved model of the locust skeletal muscle will inform on the general behaviour of invertebrate and mammalian muscle with the eventual aim of improving models of human muscles, embracing prosthetic construction and muscle therapy. An accurate muscle model can help to drive FES protocols by enabling the prediction of the force response to a range of inputs, removing the need to record the actual muscle response to such a large range of inputs. This helps to minimise fatigue, reduce the number of necessary tests, and can speed up the process

of identifying the optimal stimulation routine [20]. Furthermore, the relatively simple neural components of the locust hind leg extensor muscle mean that coupling a muscle model into the neural system (as in Fig. 1.1) is a realistic goal. In characterising the neuromuscular control system that is utilised during a simple task such as a kick or walking more insight would be gained on neuromuscular control. This could provide a better control strategy for the development of robotic devices such as hexapod robots.

In vertebrates a wide range of models have been used to describe muscle responses. Despite the processes behind muscle contraction being well established no broadly valid method of modelling skeletal muscle exists. Two main factors are thought to be responsible for this. Firstly, researchers tend to deal solely with their own model: studies that compare the merits of different types of model are extremely scarce. Secondly, the muscle is a highly complex non-linear system; this leads to researchers making various assumptions in order to simplify the behaviour. As a result, models of the muscle range from black-box models, that are derived solely from input-output characteristics, to models based on the detailed properties of tissue that take the system's physiology into account [21]. Due to the lack of comparative studies it is difficult to establish which model to use and to know if a simpler model would be as good at describing the behaviour. By building up a model through introducing complexity in the experimental conditions in stages, fewer assumptions are necessary. For example, the contractile and activation components of the muscle are often assumed to be uncoupled. By comparing how the isometric force response changes dependent on the length this assumption can be investigated. Also, in developing a model, previous research is considered and existing models are fitted to data. In doing this, existing models can be assessed in terms of both the goodness of fit and in relation to parameter definitions.

1.2 Comparisons Between Invertebrate and Vertebrate Muscle

The muscles of invertebrates differ from those of vertebrates due to details of the innervation. Vertebrate muscle is supplied by a large number of nerve fibres, and the number of motor units which are in a state of active contraction are varied in order to control the tension developed [11]. This method of contraction uses a large number of muscle fibres and correspondingly large numbers of nerve fibres to innervate them. In contrast, invertebrate muscle is innervated by only a small number of motor axons [22]. In invertebrate muscle each nerve fibre exerts a particular physiological effect [11] with the effects being common to every muscle fibre.

Despite differences in the innervation between vertebrate and invertebrate muscle the contractile components are similar. The molecular basis of force generation, thin filament structure

and the fact that Ca^{2+} is the key regulatory factor in contraction are common features to both vertebrate and invertebrate muscle [6].

The locust extensor tibia (ETi) muscle is an invertebrate muscle and so each neuron stimulates a different physiological effect. It is innervated by only two excitatory neurons. In studying muscular function in an invertebrate, as opposed to a vertebrate, the effect of each input to each neuron can be separated. This makes the response more tractable and also allows for consistency in stimulation. The locust ETi in particular is an ideal muscle to study due to the fact that the neural components are well described in the literature [8–13]. Furthermore, it has a relatively large size for an invertebrate muscle, making the practicalities of measuring the force response easier.

Locusts provide an opportunity to develop a muscle model in a simpler system, that will still show similar properties to that of mammalian muscle. The problem is further simplified by studying a simply innervated muscle, thus further reducing the number of assumptions that need to be made regarding the system behaviour.

1.3 Physiological Basis of Muscle Contraction

In developing a model it is important to understand the physical processes that underlie contraction. The structure of skeletal muscle and processes behind its contraction are summarised in this section.

1.3.1 Muscle Structure

The function of a tissue is reflected in its structure [4]. The function of skeletal muscle is to generate force, or produce movement. The structure of skeletal muscle is an essential element to understanding how the muscle produces force. The muscles of invertebrates and vertebrates share fundamental similarities [6].

Figure 1.2 shows the components of which skeletal muscle is comprised and the functional arrangement of these. Skeletal muscle is made up of bundles of fibres, each fibre being a multi-nucleated cell. These fibres are arranged in bundles (known as fasciculi). Within the muscle, each of these bundles is lined with connective tissue. Each fibre is made up of myofibrils, with these in turn being comprised of arrays of myofilaments [23]. Two primary types of protein are contained within the myofilaments, actin and myosin. The myofilaments are divided into serial repeating regions termed sarcomeres. The sarcomeres are the smallest functional unit of the muscle.

A specialised plasma membrane, the sarcolemma, surrounds each muscle fibre. Electrical impulses conducted by the sarcolemma travel along transverse-tubules (T-Tubules). These are narrow tubes which invaginate the Sarcolemma. The electrical impulses, or action potentials, are the trigger for muscle contraction. The Sarcoplasmic Reticulum (SR) surrounds the sarcomeres; this is an internal membrane system. The primary function of the SR is to store calcium ions; these are released when the muscle is activated. The membrane of the SR has pumps for the active transport of calcium ions back into it.

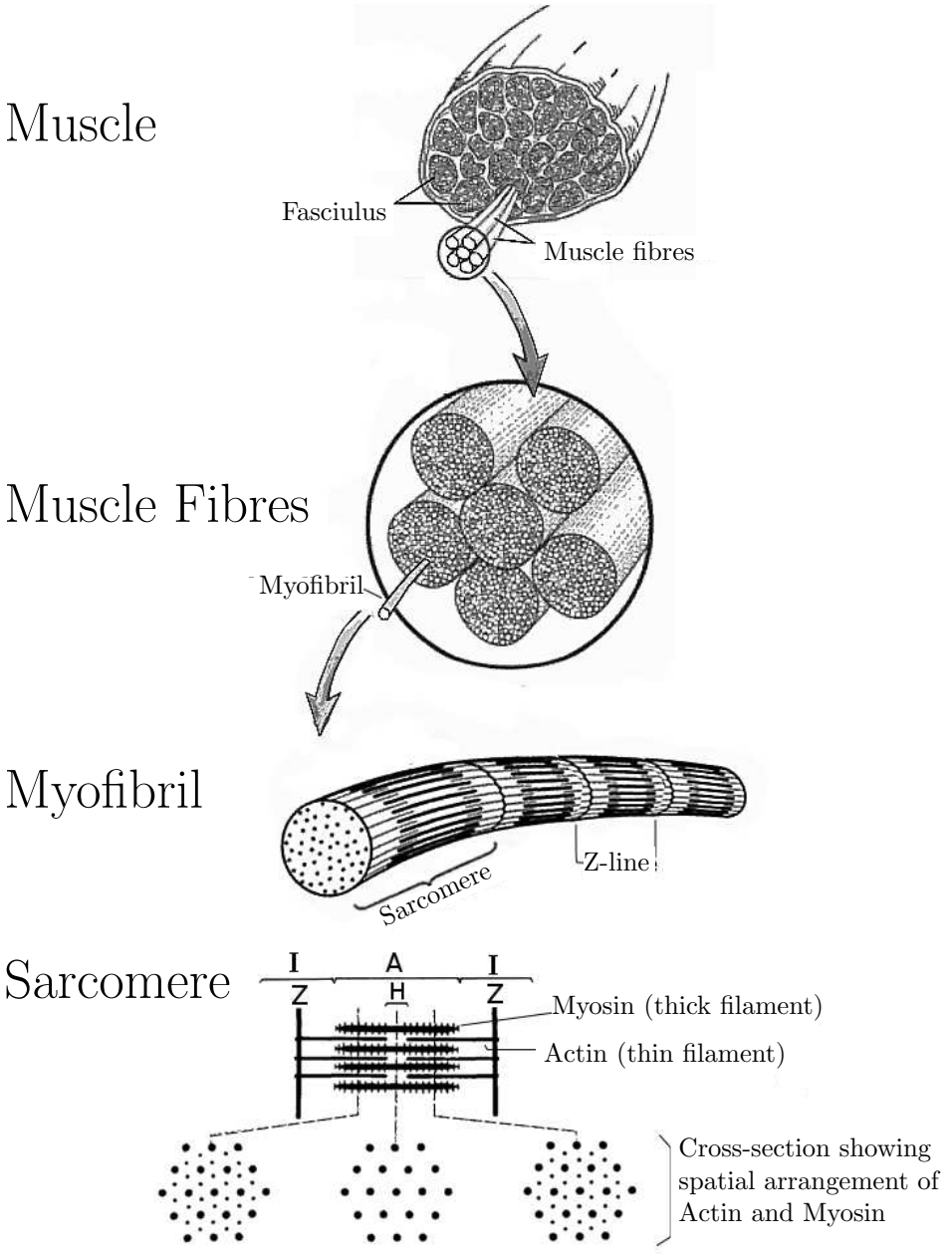

FIGURE 1.2: Structure of skeletal muscle, adapted from [24]. Each major component of the muscle structure is shown.

1.3.2 Activation-Contraction Dynamics

Although some ambiguity remains in the finer details, the processes behind muscle contraction are well established [4]. The calcium ion, Ca^{2+}, is known to be a regulator in many biological processes. All nucleated animal cells have the calcium messenger system as one of their fundamental control schemes [25]. Calcium is also fundamental to muscle contraction, being the key regulatory factor of muscle contraction at the molecular level in all types of muscle [26].

In the absence of stimulation, calcium ions are accumulated in the SR by an ATP (adenosine triphosphate) driven protein pump, which pumps calcium ions out from the sarcoplasm [4]. In the absence of Ca^{2+} in the sarcoplasm, tropomyosin blocks access to the myosin binding site of actin. In rest conditions there is a large calcium ion concentration gradient between the inside and outside of the SR, but the permeability of the membrane is low. Neural stimulation causes a depolarising signal to propagate, spreading along the T-tubules. The change in membrane potential is effective in causing the muscle to contract [27]. This signal is transmitted to the SR and temporarily increases the permeability of the membrane, causing calcium ions to be released into the sarcoplasm. The released ions bind to tropomyosin, resulting in the myosin having access to binding sites on actin. Myosin hydrolyses ATP and undergoes a conformational change into a high-energy state. The head group of myosin binds to actin forming a cross-bridge between the thick and thin filaments. The energy stored by myosin is released, and ADP and inorganic phosphate dissociate from myosin. The resulting relaxation of the myosin molecule entails rotation of the globular head, which induces longitudinal **sliding of the filaments** [27]. This process happens continuously, hundreds of times each second as long as the calcium is attached to tropomyosin. This causes the length of each sarcomere to decrease and the muscle to contract via a paddling type action. Relaxation occurs when the muscle is no longer stimulated, and the calcium is pumped back into the SR [28].

The function of cross-bridges as tension generators, and the sliding filament mechanism of muscle contraction is virtually universally accepted [29]. The sliding filament mechanism is based on the findings of Huxley *et al* [30, 31]. It states that length changes occur due to a relative sliding motion between the thick and thin filaments, with the length of each filament remaining substantially unaltered. The sliding filament mechanism is supported by the fact that the lengths of the muscle A-bands do not alter when the muscle is stretched or shortened, and by the fact that electron microscopy shows each myofibril to be made up of two sets of filaments [30, 31].

1.4 Approach

The behaviour of the locust hind leg extensor muscle is investigated in this thesis. The aim is to develop a simple mathematical model capable of describing the force response of the muscle to pulse train inputs for a range of initial conditions. A mathematical model consists of a set of assembled equations that describe a physical system or process [32]. The muscle is a biological physical system. Bernotas *et al* [33] recognised that all physical systems are non-linear with infinite dimensions. Hence, in characterising the muscle by using a mathematical model with fixed dimensions, it is inevitable that the system will be simplified. In simplifying a system the resultant model needs to retain a valid description of the behaviour, yet be of reduced dimension [32]. Modelling should provide a simplified representation of the system and should promote understanding of the system's behaviour. There are advantages to using as simple a model as possible to describe a system, with model characteristics responsible for observed effects being more evident in simpler models [34]. Hence, in this study no prior assumptions are made to define the model complexity. In developing a model we also consider the ability of existing models to describe the force response of the muscle, and compare the performance of a range of models.

The main focus of this work is modelling activated, isometric muscle. In the isometric case the muscle is held at constant length. In modelling activated, isometric muscle the model inputs are the neural stimulus and the muscle length, with the output being the developed force. By fully characterising the isometric behaviour a strong foundation is built. This is used to investigate how controlled departures from isometric conditions affect the developed force.

The muscle is a complex non-linear system. To limit the number of simplifying assumptions needed to model the force response the conditions during experiments were constrained; by using increasingly fewer constraints on the experimental conditions a model of the muscle behaviour can be built up. First the isometric (muscle held at constant length) force response to a single input pulse is considered, this case provides an important building block for further development of a model. Next the isometric force responses to constant frequency pulse trains, then to random pulse train inputs, are measured. From this a general isometric model is developed. The muscle length is then changed; during stimulation the muscle is held isometrically at a range of differant lengths, thus enabling the effect of changing the muscle length on the isometric force to be established. Finally the effect on the force in changing both the muscle length and velocity is considered.

1.5 Contributions

By studying the response of the locust extensor muscle to a range of different conditions more insight into the system is gained. This thesis provides more data and information on the specific locust extensor muscle-joint system, as well as contributing to the more general field of muscle modelling. Movement, and the corresponding neuromuscular control system is still not fully understood [14]. Locust specific contributions can be used to try to understand muscular function, movement and locomotion in a simple invertebrate. General modelling results have potential applications to other species as well as the locust in particular. The contributions of this thesis are outlined below,

Muscle Measurement

1. There have been relatively few studies on invertebrate muscle and modelling its response. Experimental data and its analysis provide more information on the behaviour of invertebrate muscle, namely the locust extensor muscle.

2. Related to the extensor muscle of the locust hind leg, a method of calculating the joint dimensions of the hind leg femoral-tibial joint without dissecting the joint has been developed.

3. A new experimental method to measure the relationship between muscle force and muscle velocity has been used.

Muscle Modelling

1. Systematic testing of the best model order to describe the isometric force response to a single input pulse has shown it to be well described using a linear second order model. This model provides a building block for further investigation of the system.

2. For the isometric response, the case where input pulses are closely spaced so that responses sum is investigated. Assuming the system is quasi-linear and investigating how the parameters of a linear model of each individual pulse change depending on the input conditions provides with more insight into the behaviour of the muscle.

3. Investigation and comparison of existing muscle models has led to the development of a new model capable of predicting the isometric force response to pulse train inputs. This new model eliminates some of the problems such as parameter redundancy that were found in existing models.

4. The assumption made in existing models that the activation and contraction dynamics are not coupled and can be modelled as two distinct systems in series is tested. There is found to be coupling between the two systems.

5. A dynamic model to describe the passive force-velocity-displacement characteristics of the extensor muscle has been developed.

1.6 Outline

The remainder of this thesis is organised as follows

Chapter 2 reviews the literature, and evaluates existing methods used to model the force response of muscle. **Chapter 3** provides an outline of the experimental methods used to measure the force response of the locust hind leg extensor muscle under a range of different conditions. **Chapter 4** looks at how the isometric response of the muscle to each individual input can best be modelled. An analysis of how parameters and model orders change with input conditions is provided. **Chapter 5** uses a range of models to describe the isometric force response. An optimum model is developed and presented. **Chapter 6** examines the effect of changing the muscle length on the isometric behaviour, while **Chapter 7** examines the effect on the force of changing the muscle velocity and length. **Chapter 8** concludes the thesis: contributions made and avenues for future investigation are given.

Chapter 2

Models Describing the Response of Skeletal Muscle

2.1 Introduction

In modelling a muscle as a dynamic system one attempts to describe a set of processes that convert an input, which is often some neural stimulus, into an output, which is often muscle force. The processes through which a motor neuron spike is commonly modelled to be transformed into a force by the musculo-tendon complex are summarised in Fig. 2.1. The assumption that the transformation of a neural input $u(t)$ into a muscle force $F_m(t)$ can be modelled in two stages is shown in Fig. 2.1A. Figures 2.1A and B sumarise the processes thought to occur in each of these stages. In the first stage the neural input is converted into an activation. In the second stage the muscle activation acts through the muscle-tendon complex to develop a force, which is exerted on the environment. This chapter summarises and evaluates the state of the art of models developed to describe the force response of skeletal muscle.

Virtually all existing models assume that the activation and contraction dynamics are uncoupled, as in Fig. 2.1A, leading to models of the activation and contraction dynamics being developed in separate stages. Muscle activation is used to represent an intermediate state in muscle contraction and is similar to Hill's concept of active state [36, 37]. The assumption has physical justification since the activation represents some internal muscle tissue state that is thought to be associated with the Ca^{2+} triggering of the contractile process [1]. Ebashi and Endo [26] defined the activation as representing the relative amount of calcium bound to tropopnin; this is a common conceptual assumption [28, 35, 38–41]. The activation is a concept of modelling and itself is immeasurable [38]. It is a relative quantity, with the activation $a(t) = 1$ when the muscle has been maximally excited. Activation is the output of the

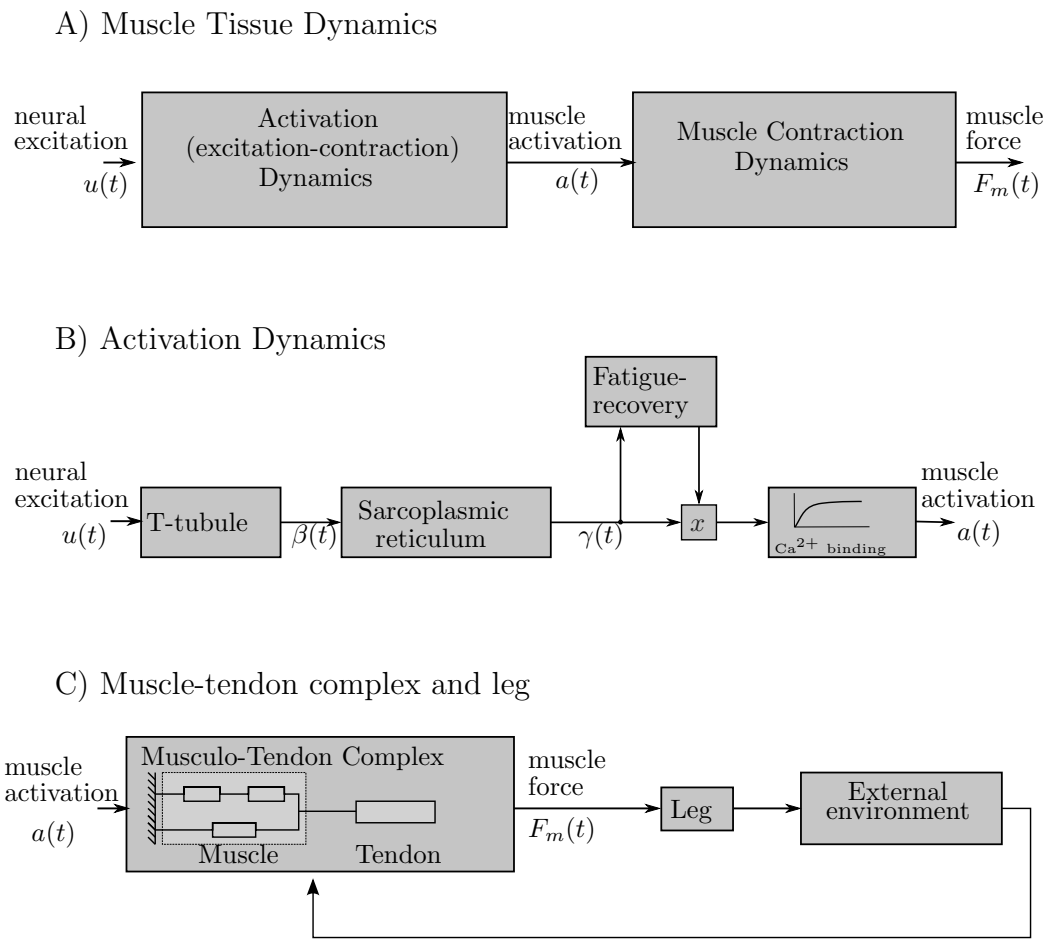

FIGURE 2.1: A system model showing the modelled stages that occur during the neuromuscular transform: A) a neural input, $u(t)$ is transformed into a muscle force, $F_m(t)$ in two stages, with activation and contraction dynamics assumed uncoupled (adapted from Zajac [1]). B) Muscle activation model (adapted from Riener and Quintern [35]) summarising the processes occurring when a neural input, $u(t)$ is transformed into an activation, $a(t)$; C) musculo-tendon complex and leg: the muscle is activated through the musculo-tendon complex and leg; this causes a force to be exerted on the environment. A feedback loop represents the fact that the reaction force influences the response of the muscle (adapted from Ghigliazza and Holmes [28]).

excitation-contraction dynamics, and input to the contractual mechanism. The processes that occur during activation are shown in Fig. 2.1B.

Muscle contraction dynamics model how the muscle activation is transformed into a muscle force. The developed force is commonly assumed to depend upon the level of muscle activation, muscle velocity and muscle length. Traditionally in modelling the muscle contractile dynamics the relative muscle activation is held constant at maximum (a(t)=1) and a model of the dynamics is then developed for constant activation.

By modelling the activation and contraction dynamics as two distinct systems, as is common practice, one assumes that the activation and contraction dynamics are uni-directional and

independent of each other. This assumption is used as it simplifies the system [1, 42], however there is data to suggest that there is coupling between the two systems [18, 43–47]. Huijing [47] concludes that the muscle activation and length-force characteristics are not independent, with history of activation, and shortening and lengthening of the muscle affecting the force-length relationship of muscle. By assuming uni-directional independent activation and contraction dynamics, these history dependent effects cannot be modelled.

2.2 Activation Dynamics

2.2.1 Isometric Equivalence

During an isometric contraction the muscle is activated but held at constant length. An example of such a contraction is pushing against a solid wall where the muscle is activated but there is no resultant movement. Due to the fact that it simplifies the problem, modelling the isometric force is a useful building block in developing an overall model [48].

Commonly, as in Fig. 2.1A the activation and contraction dynamics are assumed to be uncoupled. If the effects of any elasticity are also assumed small then the force generated in an isometric contraction is dependent only on the muscle activation. Due to the proportionality that is commonly assumed to exist between the isometric force and muscle activation, this section discusses both isometric force models and pure activation models.

Hill, [37] used the term 'active state' to define the force that the muscle exerts when its contractile component is held at a constant length. In an isometric contraction these conditions are met if the compliance of the muscle fibres is assumed small. Making these assumptions, and combining a model of the isometric force response (which in effect gives the muscle activation) with contraction dynamics, means a model that is valid for static and dynamic contractions can be developed [35, 48, 49].

Modelling the isometric force is a popular choice in developing a muscle model. This is due to the reduced system complexity in holding the muscle length constant and the use of the isometric force as a building block. There are a range of methods to model the isometric force response. These include linear approximations [41, 50–55] , models that take the steps that occur during muscle activation (Fig. 2.1B) into account [20, 28, 39, 40, 56–61], and using local model networks [62–65]. The most prevalent ways of modelling isometric muscle are discused in more detail below.

2.2.2 Linear Models

Linear models are attractive due to their simplicity and ease of analysis. Linearisation of an inherently non-linear system, however, will always lead to a loss of information [66].

Mannard and Stein [51] investigate the frequency response of isometric contractions of the cat soleus muscle. They find that for isolated input pulses, or low stimulation rates, the muscle behaves as a critically damped second order system. For different values of mean stimulation rate, muscle length or active units the nerve-muscle system could be described by a family of second order systems, the parameters of each system being dependent upon input conditions. If the system were truly linear the frequency response to any input would be equivalent to the Fourier transform of the impulse response; the impulse response of the muscle system being approximately equivalent to the response to a single pulse [67]. The fact that the parameters of the linear model depend upon input conditions suggests that the system is modelled as quasi-linear. It can be linearised about a given input, but the linear model changes due to the relatively long time constants associated with the non-linearities. As the stimulation rate increases errors in fits increase, and a linear frequency response becomes a less good model. This is probably due to increasing non linear summation of the responses to individual stimuli [51].

Baratta and Solomon [54] also find the frequency response of muscle to be well described by a linear second order system. Their model consists of a linear second order model with double real poles and a pure time delay. They find different muscles have different pole values. Likewise, Bobet *et al* [50] describe isometric muscle using a linear-second-order system, this being a critically damped low-pass system. Like Mannard and Stein [51], they find that to provide a good fit to data, parameters of the model need to be allowed to vary. In their model estimated coefficients were held constant across each interpulse interval (IPI) but allowed to vary between input pulses. In effect they model the muscle as a linear, time-varying system. Zhou *et al* [68] confirm a model of the medial gastrocnemius muscle of the cat to be second order. They found that if the effect of the joint is included an extra pole and zero improved the model.

It is suggested by Mannard and Stein [51] that the fact that a second order model provides a good fit may indicate that, despite many rate constants being involved in activation-contraction coupling and the sliding filament model ([27, 29, 69, 70]), only two constants are rate limiting. Further research by Bawa *et al* [52, 53] suggests that one rate constant is associated with viscoelastic properties and the other with the reuptake of calcium into the SR.

In support of using a second-order model Bobet *et al* [48] find that the critically damped second order model provides close to the best possible fit when using a linear model. However, they

also found that no linear model provides a good fit to to the data. This indicates that for most conditions a linear model is not capable of providing a good description of muscle force. This is also indicated through the fact that parameters in the linear models of Mannard and Stein [51] and Bobet *et al* [50] need to change dependent on input conditions for acceptable fits to be obtained.

2.2.2.1 Non-Linear Effects

The isometric muscle force response is inherently non-linear and while under certain conditions a linear assumption may be valid, one cannot model the general behaviour well using just a linear time invariant model [39].

The response to a single stimulus is known as a twitch response [23]. If the muscle is re-stimulated whilst there is still some contractile activity from a previous pulse then responses will sum. If the muscle is stimulated such that it does not relax between inputs, then a smooth sustained contraction, termed tetanus, occurs [23]. Figure 2.2 represents wave summation and tetanus.

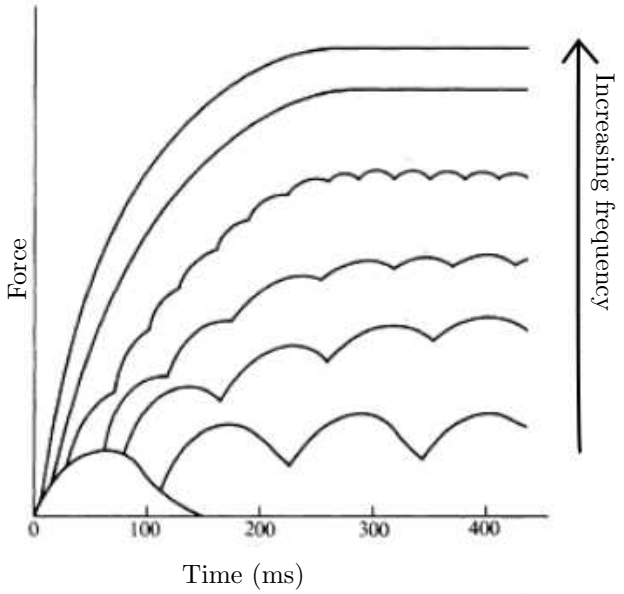

FIGURE 2.2: Representation of the non-linear summation of responses that occurs when the inputs are closely spaced. Adapted from [23]

Repetitive stimulation of muscles produce tensions that sum non-linearly [50, 71–75]. Stein and Parmiggiani [71] report a less-than-linear summation (depression) during the rising phase of a twitch and a more-than-linear summation (facilitation) during the falling stage. They attribute this depression to a first order saturable reaction and facilitation to increasing stiffness of the muscle facilitating force transmission, and to Ca^{2+} release mechanisms [52, 53].

This non-linear summation is investigated by Stein *et al* [71, 72]. The experimentally determined force response to $n-1$ pulses was subtracted from that to n pulses, leaving the contribution of the n^{th} pulse. This is demonstrated in Fig. 2.3A with the resultant contributions given in Fig. 2.3B. This approach is also used by Raikova *et al* [74, 75] and Celichowski *et al.* [76]. They model the summation of twitches for various types of motor units by describing the response to constant frequency trains (CFTs) in terms of the response to each individual stimulus. In their work an analytical function is used which describes the twitch shape using six parameters [76]. Given that other studies found the response to each pulse to be well described by a second order system, a model with fewer parameters may provide equally good fits to the measured response.

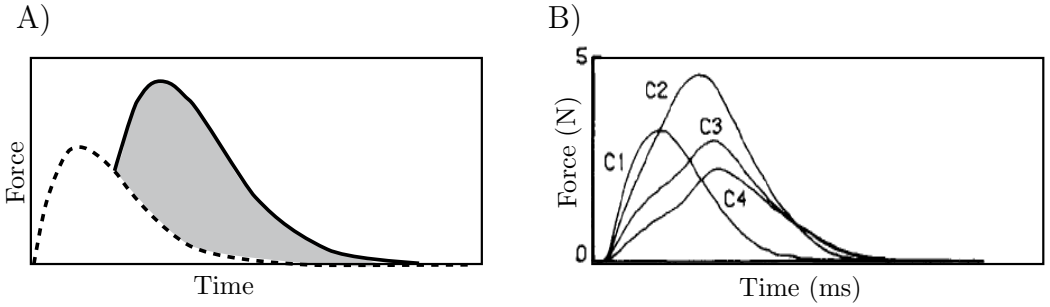

FIGURE 2.3: Contribution to overall force response by each individual pulse response A) Illustrates how the response to a second pulse (shaded) can be extracted from the response to two pulses, B) Contributions of the first 4 pulses of a CFT, from [72]. C1 - C4 give the contributions due to the 1^{st}-4^{th} pulse.

Although the contributions of individual pulses have been extracted by assuming a quasi-linear system, much of this work has focused on the qualitative behaviour. There has been little attempt to quantify the changes in pulse shapes and use this to model entire contractions. In this thesis the contribution from individual stimuli in CFTs is investigated in Chapter 4.

2.2.3 Hammerstein Models

A Hammerstein structure (static non-linearity[1] (SNL) followed by linear dynamics (LDS)) is a common choice for modelling electrically stimulated muscle [33, 42, 48, 64, 77, 78]. Often all the dynamics of the muscle system are contained in the LDS and the SNL is assumed to be a function of the electrode/nerve coupling characteristics [77]. Figure 2.4 gives a Hammerstein model structure, this is a NL (nonlinear - linear) system. The linear dynamic system (muscle dynamics) is commonly represented as a second order system [33, 42, 77, 78]. The SNL is assumed to represent the recruitment, this is often represented by a isometric recruitment curve (IRC) which has the form given in Figure 2.5. The stimulus activation level can be varied by changing the stimulation frequency, pulse width or pulse amplitude.

[1] A static non-linearity is described by a non-linear function which does not vary with time

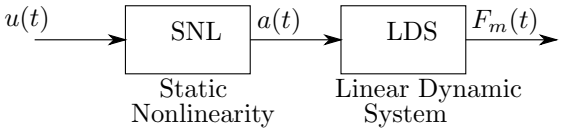

FIGURE 2.4: Hammerstein Model Structure. The system is comprised of a static nonlinearity (N) followed by a linear dynamic system (L), it is a NL system.

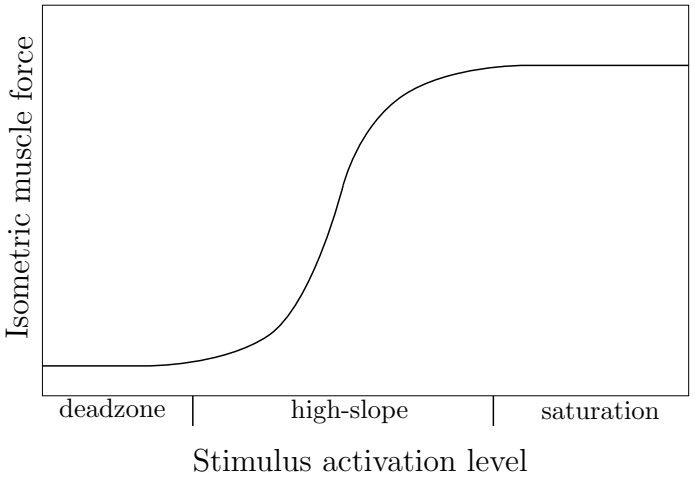

FIGURE 2.5: Isometric recruitment curve (IRC), the effect of input on muscle force is shown.

Although a Hammerstein model is a common choice for modelling electrically stimulated muscle it is argued that it is not a very accurate method. The poles of the muscle system change with the level of activation [64]. Each muscle twitch has a different shape dependent upon the level of activation [77] (see Sec. 2.2.2.1). These changes in the dynamic properties of the muscle cannot be accounted for using a Hammerstein structure as it is assumed that the muscle dynamics are linear. The activation and contraction blocks are uncoupled and unidirectional, so the activation cannot influence the dynamics.

2.2.4 Cascade Model

Another popular choice for modelling the activation dynamics is a system made up of two coupled second order ODEs (effectively one fourth order ODE) followed by a non-linearity [28, 35, 39, 41, 49, 79, 80]. This is a specific case of a Wiener system. The Wiener structure is similar to the Hammerstein structure, but the non-linearity is placed after the linearity. The model is of LN (linear - nonlinear) structure. This model is based on the cascade of processes that occur during activation, as summarised in Fig. 2.1B. A feedback loop is shown in Fig. 2.1 this is used to account for muscle fatigue. In a cascade model the fatigue loop is often ignored. The first of the differential equations is assumed to convert the neural input, $u(t)$,

into a T-tubuli depolarisation $\beta(t)$, and the second to convert this depolarisation into a free calcium concentration $\gamma(t)$, as

$$\ddot{\beta}(t) + \phi_1\dot{\beta}(t) + \phi_2\beta(t) = \phi_3 u(t) \tag{2.1}$$

$$\ddot{\gamma}(t) + \phi_4\dot{\gamma}(t) + \phi_5\gamma(t) = \phi_6\beta(t) \tag{2.2}$$

ϕ_1 - ϕ_6 are muscle specific constants. The muscle activation $a(t)$ is then estimated from the free calcium concentration $\gamma(t)$. Commonly a non-linear sigmoid shaped function (with similar shape to that used in the Hammerstein structure) is used to estimate the muscle activation from the free calcium concentration. This transform is modelled by Riener and Quintern [35] and Ghigliazza and Holmes [28] as

$$a(t) = \frac{a_0 + (\rho\gamma(t)\mu(t))^2}{1 + (\rho\gamma(t)\mu(t))^2} \tag{2.3}$$

where ρ and a_0 are muscle specific constants with $a_o \approx 0$, and $\mu(t)$ is a fitness variable used to account for fatigue. This method of modelling the isometric force is thought to capture the essential dynamics of the system. This form of model, originally used by Hatze [39] has also been adopted by Riener and Quintern [35], Ghigliazza and Holmes [28], Holmes *et al* [79], Van Zandwijk [41] and Zakotnik *et al* [49, 80]. The model structure, as related to a Wiener model is given in Fig. 2.6.

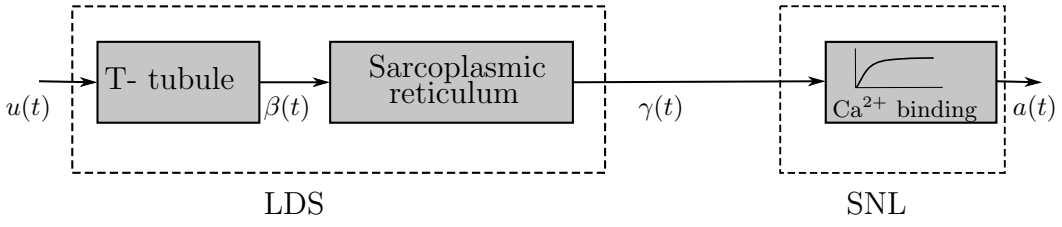

FIGURE 2.6: Block diagram of the LN cascade model structure; this structure is a special case of a Wiener model with a LDS proceeding a SNL.

This method uses a much higher model order than others to describe the system dynamics, with a fourth order ODE used, as opposed to second order. It may be that a fourth order model is required to capture the necessary dynamics, or it could overfit the data. There have been no comparative studies that include the cascade model; where used it is just stated, and hence from the literature it is unclear whether the model overfits, or fourth order dynamics are necessary. This, given the popularity of the model, is strange. The lack of comparison between existing models is unfortunately a prevalent theme in muscle modelling [48].

2.2.5 Local Models

Non-linear models of the muscle response which are based upon local model networks (LMN) have also been developed [62–65, 81]. In using LMNs the nonlinear modelling task is divided into smaller subtasks, each sub-task is then handled locally by a simpler model [81]. A scheduler is used to decide, based on the current operating conditions, how relevant each model is. The models are weighted according to relevance and the overall model given as the sum of the weighted models.

In a sense the LMN approach is a more formalised way of extending the finding [50, 64, 71, 72, 74, 75] that the shape of each response to an individual input pulse (and similarly the system dynamics), differ dependent upon input conditions. LMNs are able to capture the changing dynamics of the muscle system. Hunt *et al* [64] find the dynamic performance of combined local models to be significantly better than the performance of a model with Hammerstein structure. The downsides to using a LMN approach are that it can involve the identification of a large number of parameters [81], and in the model complexity the physical relevance of the model may be lost [34].

2.2.6 Contemporary Nonlinear models

To the author's knowledge only two previous studies compare the performance of existing isometric models [48, 82]. Furthermore, of these only Bobet *et al* [48] compare different models by fitting to measured data. Bobet *et al* [48] find the models of Ding *et al* [20] and Bobet and Stein [73] to give the best fits to data. Using terminology from Frey Law and Shields [82] we refer to these models as contemporary nonlinear models. These models are of LNL (linear - nonlinear - linear) structure. The two models have similar structures, each consisting of low pass-filters in series with a static non-linearity. The time constant of one of the filters becomes large at high levels of activation.

By standardising the governing equations for these two models and writing each in the same format, as a series of coupled first order differential equations and non-linear equations, the relationship between the models is more clear.

2.2.6.1 Bobet and Stein Model

Bobet and Stein's [73] model takes a pulse train as input and gives the isometric force as the output. A block diagram of the muscle model is given in Fig. 2.7. The model is an extension to using a second order linear model. The model consists of two first order differential equations

which act as low pass filters, separated by a static non-linearity which saturates force. The second of the differential equations has a variable rate constant that varies with the force.

$$\dot{q}(t) + aq(t) = \sum_{i}^{n} \delta(t - t_i) \tag{2.4}$$

$$x(t) = \frac{q(t)^m}{q(t)^m + k^m} \tag{2.5}$$

$$\dot{F}(t) + bF(t) = Bbx(t) \tag{2.6}$$

$$b = b_o \left(1 - \frac{b_1 F(t)}{B}\right)^2 \tag{2.7}$$

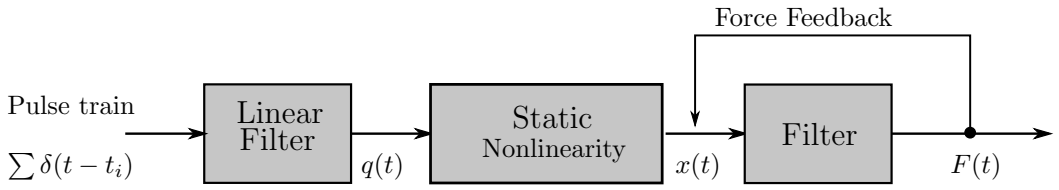

FIGURE 2.7: Block diagram showing the stages through which a pulse train input is transformed into a force in Bobet and Stein's [73] model.

The model has 6 parameters, a, b_o, b_1, B, k, m. It is speculated that the first filter (Eq.(2.4)) represents calcium release and re-uptake. The static non-linearity may represent calcium binding to troponin (Eq. (2.5)). The final filter could account for (Eq. (2.6)) the cross-bridge dynamics, with the non-linearity in rate constant (Eq. (2.7)) accounted for by cross-bridge detachment.

2.2.6.2 Ding et al Model

The model developed by Ding *et al* [20, 60, 61] is of higher order than that of Bobet and Stein [73], but uses the same number of parameters. The structure of the model is given in Fig. 2.8. It consists of three first-order low pass filters in series, with a static non-linearity which occurs before the final filter.

$$\dot{q}(t) + \frac{q(t)}{\tau_c} = \sum_i^n R_i \delta(t - t_i) \tag{2.8}$$

$$\dot{C}_N(t) + \frac{C_N(t)}{\tau_c} = \frac{q(t)}{\tau_c} \tag{2.9}$$

$$x(t) = \frac{C_N(t)}{k + C_N(t)} \tag{2.10}$$

$$\dot{F}(t) + \frac{F(t)}{\tau_1 + \tau_2 x(t)} = Ax(t) \tag{2.11}$$

$$R_i = 1 + (R_o - 1) \exp\left(\frac{-(t - t_i)}{\tau_c}\right) \tag{2.12}$$

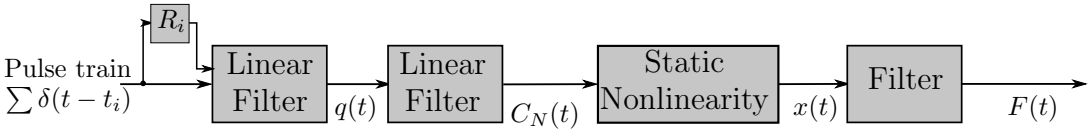

FIGURE 2.8: Block diagram showing the stages through which a pulse train input is transformed into a force in Ding *et als* [20] model.

The model has six parameters, $\tau_c, R_o, A, k, \tau_1, \tau_2$. The term R_i (Eq. (2.12)) is used to account for the non-linear summation when fibres are stimulated by two closely spaced pulses. Equations (2.8) and (2.9) represent the muscle activation and are said to do this by modelling the dynamics of the rate limiting step that leads to formation of the Ca^{2+}-troponin complex. The variable C_N is said to represent the normalised amount of the Ca^{2+} complex. The development of mechanical force from activation is represented by Eq. (2.10) and (2.11).

2.3 Contraction Dynamics

The muscle contraction dynamics describe how a muscle activation is converted into a muscle force [1]. Since the activation and contraction dynamics are almost always assumed uncoupled, as in Fig. 2.1C, to describe the contraction dynamics it is common that the muscle is maximally activated, so that $a(t) = 1$. For cases where the activation is submaximal the contractile model developed under maximal activation is scaled by the activation.

Muscles are made up of series of fibres. The arrangement of these fibres depends on the muscular function [23, 83–85]. Common functional arrangements of muscle fibres are given in Fig. 2.9.

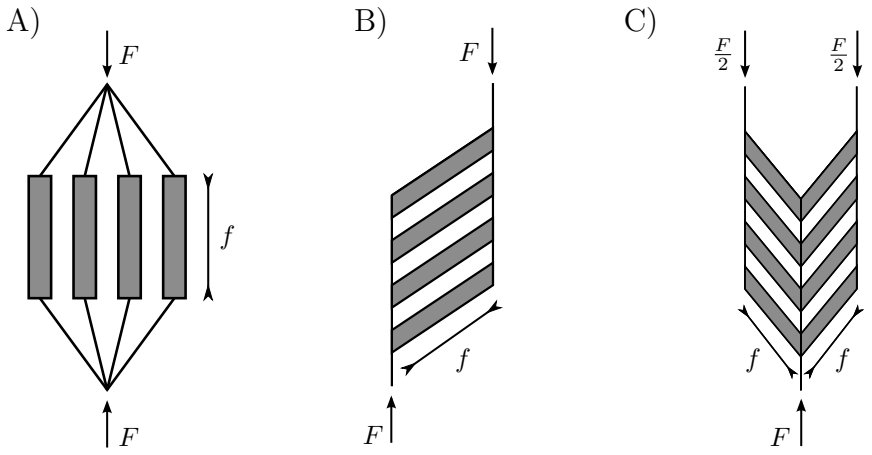

FIGURE 2.9: Different arrangements of muscle fibres within a muscle. The boxes represent the muscle fibres and the lines radiating from these the tendons. Double headed arrows (f) indicate the direction of force exerted by individual fibres and single headed arrows (F) the direction of force exerted by the whole muscle. A) Parallel muscle B) Pennate muscle C) Bi-pennate muscle. Adapted from [86]

During muscular contraction, it is the sliding filaments in the individual sarcomeres that shorten the muscle. Thus, the fibres shorten in a direction parallel with their line of action. The shortening of the global muscle occurs as a result of the shortening of each individual fibre. To describe contraction of the whole muscle it is commonly assumed that the properties of fibres are just scaled up from sarcomeres, and muscle properties scaled up from fibres. A factor is used to account for the pennation angle [1, 39]. This approach ignores the individual differences in force, displacement, velocity and timing of each sarcomere [47].

2.3.1 Hill-Model

A.V. Hill [36] was an early pioneer in muscle research, finding that during shortening as well as doing mechanical work a muscle produces extra heat. The extra heat is proportional to the distance shortened [36]. Thus, the total energy produced in excess of an isometric contraction is given as $(F_m + a_h)x_{ms}$, where F_m is the force of the muscle, x_{ms} the distance shortened and a_h a constant of proportionality which relates the heat of shortening to distance shortened [36, 38, 87]. By definition, the rate of extra energy liberation during an isometric contraction is zero, therefore,

$$(F_m + a_h)v_{ms} = (F_o + a_h)b_h \tag{2.13}$$

where $v_{ms} = (dx_{ms}/dt)$, the muscle shortening velocity, F_o is the maximal isometric force and b_h is a constant which defines the absolute rate of energy liberation. This relation can be re-written to give Hill's characteristic equation, often referred to as the Hill equation,

$$(F_m + a_h)(v_{ms} + b_h) = (F_o + a_h)b_h = \text{constant} \tag{2.14}$$

or equivalently

$$F_m = \frac{F_o b_h - a_h v_{ms}}{b_h + v_{ms}} \tag{2.15}$$

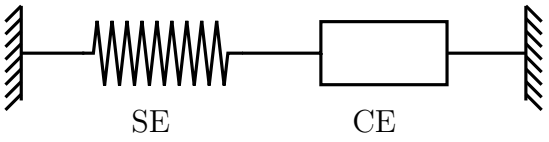

FIGURE 2.10: Hill's model of skeletal muscle. The model comprises a contractile element (CE) which is characterised by Eq. (2.14) in series with an elastic element (SE). Adapted from [87]

Based on experimental observations Hill went on to conclude that active skeletal muscle is a two-component system consisting of an undamped purely elastic element in series with a contractile element, as shown in Fig. 2.10. The properties of this contractile element are governed by Eq. (2.14). Hill states that there are probably also viscoelastic and viscous elements as well.

2.3.2 Hill-Type Lumped Component Models

A Hill-type lumped-component model is frequently used in bio-mechanical models of the musculo-skeletal system [1, 15, 28, 39, 40, 42, 57, 59–61, 79, 85, 88–92]. It is a popular choice due to its mathematical simplicity. In the lumped component model, the Hill model (Fig. 2.10) is commonly supplemented with an extra parallel elastic component (PE) in parallel with the contractile element. Popular functional arrangements of the elements are given in Fig. 2.11.

Commonly, as in Fig. 2.11, muscle is viewed as consisting of three basic structural elements: the contractile element (CE) which is active and controllable, the passive and negligibly damped series elastic element (SE) and the parallel elastic element (PE) which is both passive and negligibly damped. Variations to the general model given in Fig. 2.11 exist [93].

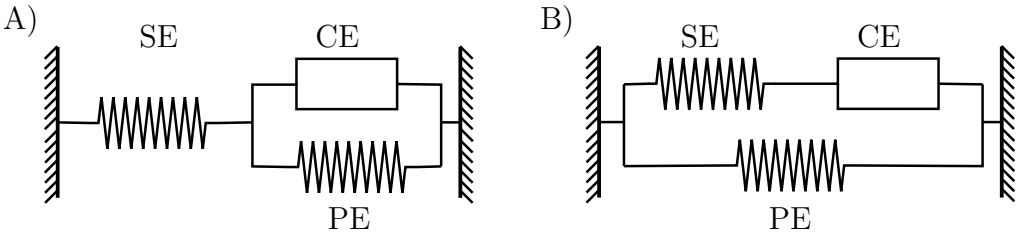

FIGURE 2.11: Popular functional arrangements of Hill-type lumped component models. A) Hill model with PE component in parallel with the CE. B) Hill model with PE component in parallel with both the SE and CE. Adapted from [87]

The model assumes that all the fibres are excited at exactly the same time, and the properties are scaled up from that of a sarcomere. Under these assumptions the lumped component models provide an equivalent representation of the actual distributed system [1, 39]. The lumped component model is a conceptual model so does not apply to actual components.

2.3.2.1 Contractile Element

The behaviour of the CE is key to the active muscle response. The CE is active and controllable. Hill used his equation to describe the response of the contractile element (Eq. (2.14)). However, Hill's equation applies only to limited contractile conditions [4, 36, 87] : maximal activation, shortening contractions, from optimal muscle length, l_o. Optimal muscle length is defined as the length at which the muscle develops the greatest active tension [94]. In a relaxed state the length of the muscle is usually at optimal length [95]. Constraining conditions for which the model is valid limits its physiological applications [34]. Therefore, as an extension to Hill's equation and to include the full range of muscle lengths the contractile force is commonly assumed [1, 28, 42, 57, 79, 96] to be given by

$$F_{CE} = a(t) \cdot F_L(l_m) \cdot F_V(v_m) \tag{2.16}$$

where $a(t)$ is the activation, $F_V(v_m)$ is a force-velocity relation which is assumed to be a function of the muscle velocity only, and $F_L(l_m)$ is a force-length relation, assumed to be a function of the muscle length only. In expressing the contractile force as a function of force-length, force-velocity and activation properties as in Eq. (2.16) one assumes mutual independence of these properties [97]. The activation, $a(t)$ is obtained from isometric experiments (see Sec. 2.2). The F_V and F_L relations are essentially established by fitting to experimental data [38, 98–100].

The F_L relation gives the relation between isometric length and muscle force. Typically, to estimate the force length relation the muscle is held at a range of different lengths and at each

length the isometric force in response to maximal activation recorded. The resultant force-length relation of the contractile element has the form given in Fig. 2.12A. In Fig. 2.12A, l_o refers to the muscle rest length, at which the maximum isometric force F_o is produced. Figure 2.12B gives the force velocity relation, in which the shortening velocity is defined as negative, and where v_o defines the maximal shortening velocity. The F_L component of the contractile force is generally assumed to vanish outside the range $l_{\min} < l_m < l_{\max}$. The lengths $l_{\min}$ and $l_{\max}$ are the lower and upper bound for the admissible range of muscle lengths, outside of which damage may occur [28].

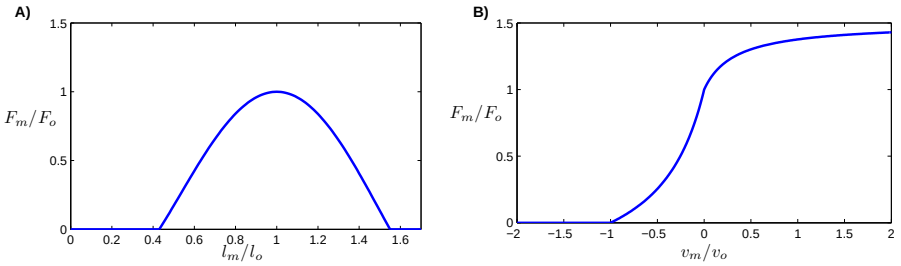

FIGURE 2.12: Normalised force response under maximum activation A) Relation between isometric force and muscle length, B) Relation between muscle force and velocity

The sliding filament mechanism of muscular contraction [27, 101] provides an explanation for the shape of the force-length curve of the CE shown in Fig. 2.12A. Contraction occurs due to a relative sliding motion between thick and thin filaments, with the length of each filament remaining substantially unaltered [27]. The degree of overlap of these filaments affects the developed tension. This is demonstrated in Fig. 2.13. Various equations have been used to fit to force-length data, however equations that describe the F_L relation in Hill-type models are not based on the physical processes as given in Fig. 2.13; they just provide a fit to the measured behaviour.

To estimate the F_V relation, again the muscle is maximally excited. It is initially held at a given length (often optimal length) by a force, F_1, which is then suddenly reduced to F_2 which enables the muscle to shorten. The force F_1 is then plotted against the shortening velocity. The muscle is released against a range of different forces, giving a force-velocity profile.

The Hill-hyperbola of Eq. (2.14) describes the response of the contractile element to shortening at optimal length. To describe the total force-velocity relation two equations are commonly used, one to describe shortening ($v_m \leq 0$) and the other lengthening ($v_m > 0$). The form of the F_V relation of the CE is shown in Fig. 2.12B. The F_V relation has been estimated by many groups [28, 39, 102]. The vast majority find data comparable to the Hill-hyperbola over the shortening range. Although Hill's relation relates the force-velocity to muscle energetics the F_V relation is essentially, like the F_L relation, just a fit to experimental data [38]. One proposed F_V relation given in terms of the normalised muscle velocity $\tilde{v}_m = \dot{l}_m/v_o$ is [28],

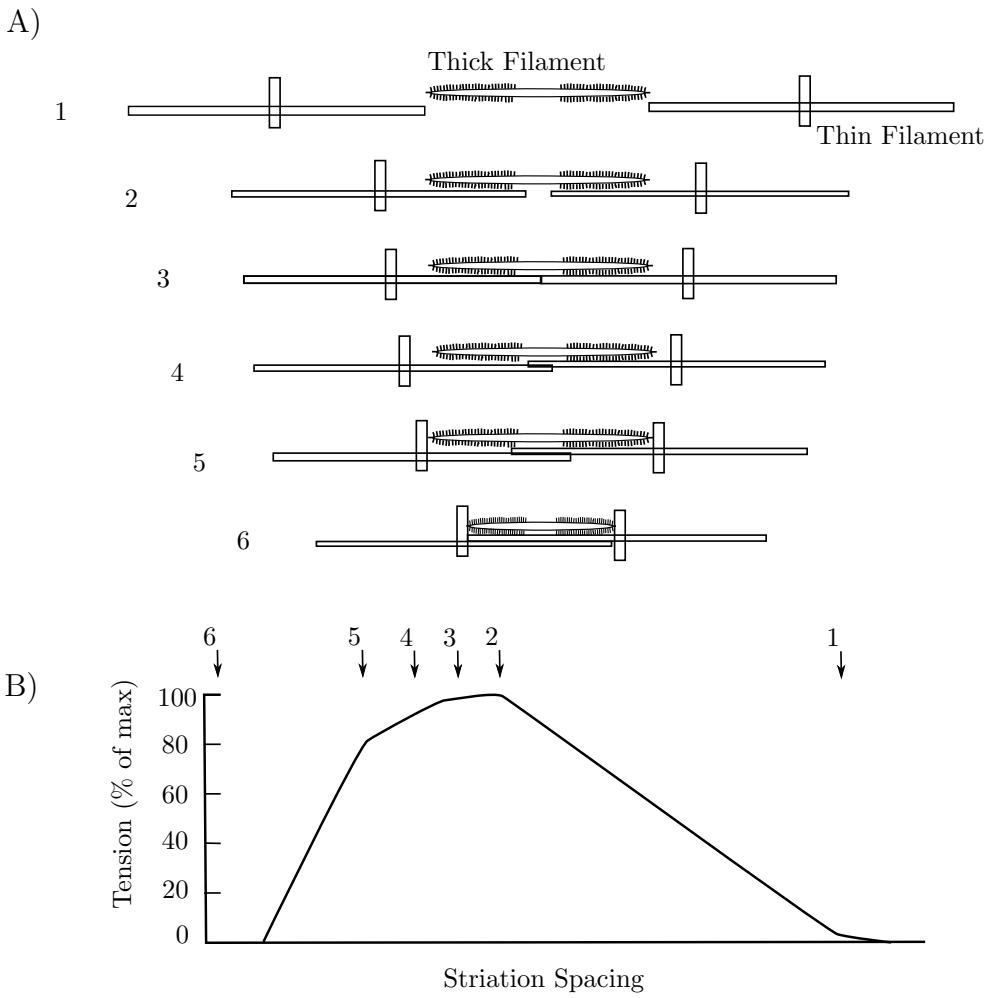

FIGURE 2.13: Features of the force-length curve explained using sliding filament theory. From stages 1-2 the proportion of bridges of the thick filament which are overlapped by the corresponding thin filament increases constantly (assuming uniformly distributed cross-bridges where present). Thus the number of cross-bridges that can be formed increases and so the tension increases. There is a plateau in force from stages 2-3 as there is no further increase in the number of cross-bridges that can be formed. As the thin filaments start to overlap (3-4) the force starts to decrease. From stages 4-6 the ends of the thick filament collide with the z-lines. This reduces the number of crossbridges capable of generating tension and there is a corresponding decrease in tension. Figure adapted from [101].

$$\tilde{F}_V = \begin{cases} \dfrac{1 - \tilde{f}\dfrac{1+\tilde{b}}{\tilde{f}-1}\tilde{v}_m}{1 - \dfrac{1+\tilde{b}}{\tilde{f}-1}\tilde{v}_m} & , \tilde{v}_m > 0 \text{ (Lengthening)}, \\ \dfrac{1-\tilde{v}_m}{1+\dfrac{\tilde{v}_m}{\tilde{b}}} & , \tilde{v}_m \leq 0 \text{ (Shortening)} \end{cases} \tag{2.17}$$

where the parameters $\tilde{b}$ and $\tilde{f}$ are constants for each muscle. Since $\tilde{b}$ and $\tilde{f}$ are constants, the

shortening region of Eq. (2.17) is mathematically equivalent to the classic Hill equation of Eq. (2.14).

This form of equation (2.17) is commonly used to model the F_V relation, although particular equations describing the lengthening and shortening portions differ. Alternatively, Giat *et al* [96] present the force-velocity relationship using one equation which describes force as a function of shortening or lengthening velocities as,

$$F_V = 1 + \arctan(c_{g1}\tilde{v}_m^3 + c_{g2}\tilde{v}_m^2 + c_{g3}\tilde{v}_m) \tag{2.18}$$

where c_{g1}, c_{g2} and c_{g3} are muscle specific parameters.

This method of describing the CE assumes that the F_V component is unaffected and uncoupled from the muscle length. This is an important and arguable assumption. Brown *et al* [57, 102] observe that active shortening and active lengthening regions of the force velocity curve cannot be scaled congruently for all lengths; to account for this a length dependency is included in the F_V relation,

$$\tilde{F}_V = \begin{cases} \dfrac{v_o - v_m}{v_o + (c_{vo} + c_{v1}l_m)v_m} & , v_m \leq 0 \text{ (Shortening)}, \\ \dfrac{b_v - (a_{vo} + a_{v1}l_m + a_{v2}l_m^2)v_m}{b_v + v_m} & , v_m > 0 \text{ (Lengthening)}. \end{cases} \tag{2.19}$$

where a_{vo}, a_{v1}, a_{v2}, b_v, c_{vo} and c_{v1} are introduced as constants. Brown *et al*'s [57] equation for the shortening section of the F_V relation is similar to that of Hills, but also includes some dependency upon current length. If this length dependency is removed then the relation becomes mathematically equivalent to Hills relation.

2.3.2.2 Series Elastic Element

The SE element is a non-contractile component of the muscle that lies in series with the contractile element. The SE components store energy when stretched and contribute to the elasticity of muscle. Some chose to neglect the SE [1, 28, 42, 57, 79, 91]. Zajac [1] argues that including a SE means that the fibre lengths and velocities will not be proportional to sarcomere lengths and velocities and that in many muscles tendon compliance dominates, so any series elasticity within muscle fibres should be ignored. Others equivalently assume that the SE has infinite stiffness and can hence be ignored.

2.3.2.3 Parallel Element

The PE is generally assumed to generate force only where the muscle is stretched beyond the optimal muscle length. If the SE is assumed infinitely stiff then the PE describes the passive tension developed when the CE is inactivated (more details on passive tension are given in Sec. 2.4). The response of the PE is commonly assumed to be negligibly damped [28] and the force it develops assumed only to be a function of length. In some cases some viscous damping is included [79]. The response of the PE modifies the force length curve of the muscle and the total force-length curve is described by the sum of the response of the contractile and parallel element, as shown in Fig. 2.14.

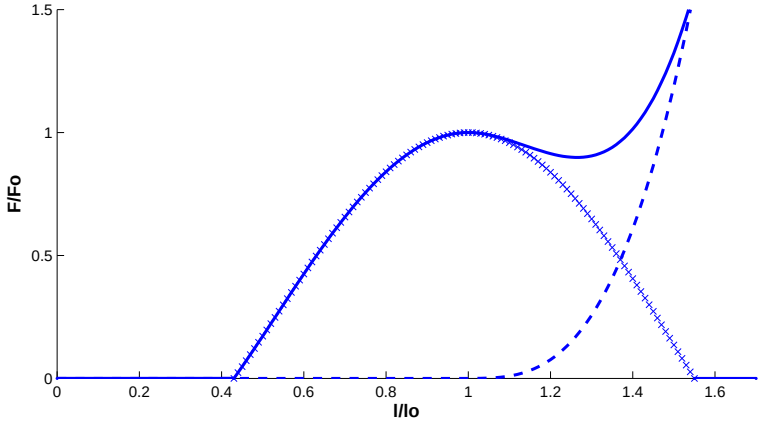

FIGURE 2.14: Relation between muscle length and force. The total force length relation (——) is given as the sum of the active (×××) and passive (– – –) contributions.

2.3.3 Issues with Hill-Type Models

Lumped component, Hill-type models (introduced in Sec. 2.3.2) are widely used [1, 15, 28, 39, 40, 42, 57, 59–61, 79, 88, 90, 91]. Their popularity stems from their mathematical simplicity and the ease with which model parameters can be estimated [38, 87]. They have been shown to capture a variety of experimental findings [88] and utilised effectively for the study of higher excursion tasks [38, 103]. However, they are not widely used to study movements that involve lower speeds and submaximal activation [88]. Such conditions are relevant to naturally occurring, normal, everyday movements [88, 97, 104]. Perreault *et al* [97] and Barratta *et al* [104] conclude that Hill-type models have the largest error when applied to naturally occurring movements, suggesting that the model has limited functional relevance.

A primary source of error in Hill-type models is that the force response of the contractile element is assumed to be instantaneous and single valued. However, length, velocity and activation are not independent determinants of muscle function [4, 5, 47]. The muscle is well

known to exhibit history dependent behaviour [18, 43], which includes force enhancement and force depression, fatigue and sag [105]. The steady-state isometric force following stretching of a muscle is greater than the force for a purely isometric contraction [57, 105–113]. This is known as force enhancement. Similarly the maximum force following shortening is depressed [108, 113, 114]; this is termed force depression. This behaviour cannot be predicted using Hill models as the equations implicitly assume a unique relation between force, velocity and length.

Hill-type models are considered to be phenomenological. Regardless of anatomical locations or levels of muscular organisation within a muscle all elastic properties are pooled into either the SE or PE element. All contractile properties that do not involve elasticity are concentrated in the CE [47]. Another issue with Hill-type models is that the division of forces between the CE and PE and separations of elongation between the SE and CE is somewhat arbitrary [87]. Although the model is phenomenological this arbitrary division makes it hard to associate the theoretical elements of the model with any biological structure [87]. Furthermore, rather than the force-velocity and force-length properties of the CE being obtained as a resultant behaviour of a combination of simpler elements, the CE introduces the F_V and F_L relations.

2.3.3.1 Modifications to Hill-Type models

Adapted Hill-models have been utilised to account for the errors associated with assuming an invariant force-velocity and force-length relation [56–59, 97, 102, 115–117]. Brown *et al* [56–59, 102, 115] build a 'next generation' model to account for these effects. In their model the force-velocity relation is a function of length as well as velocity (see Eq. 2.19). They include coupling between the activation and a delayed representation of muscle length; sag and fatigue are also accounted for in the activation model. Similarly Shue *et al* [116, 117] incorporate length dependent coupling between activation and velocity in a model with Hill-type structure. These models are able to replicate some of the known interactions between muscle velocity, length and activation as well as some history dependency. However, the overall models are relatively complicated, with many parameters and governing equations compared to Hill-type models.

2.3.3.2 Alternative to Hill-type Models

In addition to the issues discussed in the previous sections, Hill-type models do not tend to describe the chemo-mechanical energy conversion process (energetics) that occur during the transformation from a neural action potential to force [118]. Commonly the Electromyography (EMG) is recorded, and the EMG signal (lightly filtered and rectified) is used as the input to the muscle model [38]. The EMG measures the electrical activity of the muscle, and EMG driven models rely on measured muscle activity to estimate muscle force. Alternatively, activation

can be considered as almost instantaneous, with deactivation a slower process, and modelled as a first order relation [38]. There being no correlate between the activation model used in some Hill-type models to the processes that occur during contraction may contribute to the inability of these models to perform well at sub-maximal levels of activation.

In this work an alternative approach is used to model the isometric force. The model is based on the muscle energetics, and is of similar form to the models of Bobet and Stein [73] and Ding *et al* [20] described in section 2.2.6. Instead of using the EMG signal as a model input, the stimulus pulse is used directly. The processes that are modelled during the transformation from input to muscle force can be linked to the physiological processes that occur during muscle contraction described in section 1.3. This approach provides more insight into the physiological phenomenon, and muscle energetics during contraction. Hill-models perform worst at low levels of activation, this may be due to the fact they are unrelated to the events that occur during the electro-chemical transform.

One of the main attractions of Hill-type models is their mathematical simplicity. In this thesis a simple alternative is presented. The model of isometric force at a fixed length contains six parameters, and is made up of two coupled first order differential equations. This model is able to predict the isometric force response to a wide range of inputs, including physiological relevant inputs. The model is extended to an isometric model that can describe the force response at any isometric length. This introduces an extra five parameters to the model, and includes coupling between the activation and contraction dynamics. This number of additional parameters is equivalent in some cases to the number of parameters introduced by the FL relation in Hill-models (i.e. in the model of Ghigliazza and Holmes the FL relation is described by 5 parameters). The developed model has the distinct advantage that coupling between the activation and contraction dynamics is included. The model is more physiologically relevant than a Hill-type model, and provides an alternative that is able to model the force at a wide range of levels of activation. Furthermore, modelling the force response to a voltage input, as opposed to the electrical activity of the muscle (EMG input) has more direct relevance in aiding with FES stimulation protocols.

2.3.4 Huxley-Type Models

There also exist biophysical models describing muscle behaviour [4]. These models are based on the sliding filament theory of contraction. They describe the muscle behaviour based on the current state and attachment and detachment rates of crossbridges. The original and simplest model of this form is presented by Huxley [119]. These models form a conceptual foundation for contraction. They are, however, rarely used with biomechanical application, such as to model global muscle forces or motions [87]. This is attributed to the fact that these models

are mathematically complex and represent sarcomere as opposed to fibre behaviour [4]. These models do not address the interaction between electrical stimulation and calcium activation, dependence of activation upon length or sarcomere inhomogeneity [87].

2.4 Passive Muscle Properties

2.4.1 Mechanism for Passive Force Development

The force developed in an inactivated muscle is termed the passive force. The passive muscle force develops due to the presence of the giant protein titin [120–123]. Within the sarcomere, titin connects the M-line (centre of sarcomere) to the Z-line (end of sarcomere) as shown in Fig. 2.15. The section between the Z-line and the thick filament (i.e. edge of the A-band) is extensible and acts as an elastic molecular spring [122]. It is this section that gives the muscle its passive tension, as well as centring the thick filaments.

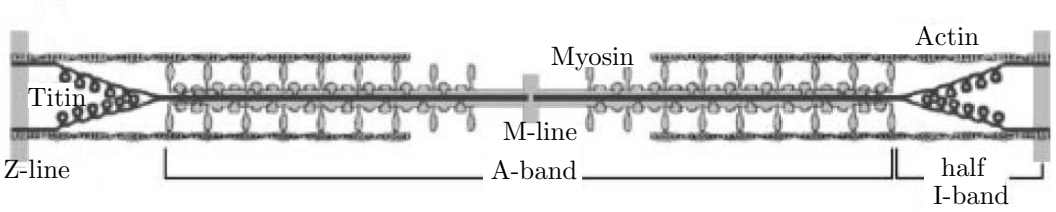

FIGURE 2.15: A schematic diagram of titin, myosin (thick filament) and actin detailing the location of titin within the sarcomere. Taken from [124]

When stimulated, muscles contract and activated muscles can only exert a pulling force. Therefore, muscles often work in agonist-antagonist pairs [28]. These pairs consist of an extensor muscle (agonist) which increases the joint angle when activated, and a flexor (antagonist) which acts in the opposite sense. Figure 2.16 gives a representation of an agonist-antagonist pair. When one muscle of the pair is activated it contracts while the other undergoes passive lengthening. If the activation of the muscle is then stopped, passive shortening can occur in one of the pair and lengthening in the other back to the joint rest position.

2.4.2 Modelling Passive Force Development

Little attempt has been made to characterise the contractile response of passive muscle. However, passive contraction, as well as passive lengthening can occur in muscles that act as agonist-antagonist pairs. Models describing the response of passive muscle commonly only describe the force response of the muscle as it undergoes lengthening from rest conditions. In these models the passive force is commonly assumed to be negligibly damped and described

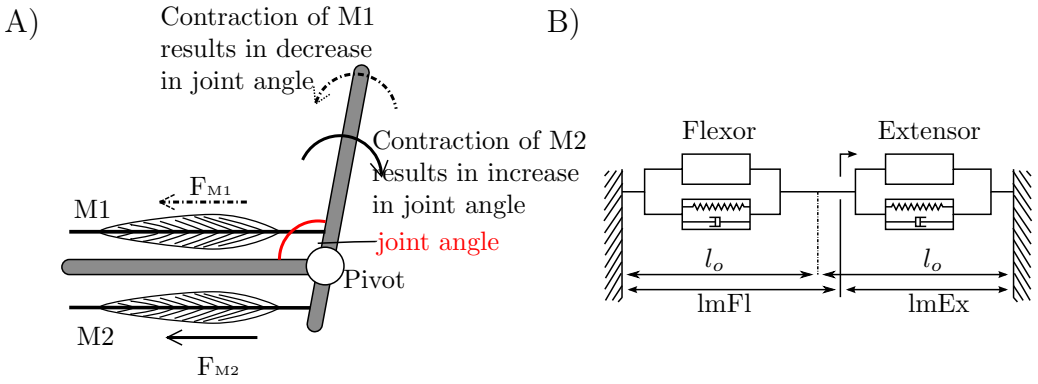

FIGURE 2.16: Agonist-antagonist pair. A) Shows how the two muscles work together to enable the joint to move in both directions. B) Gives a phenomenological Hill-type representation of a agonist-antagonist pair, adapted from Ghigliazza and Holmes [28].

by a non-linear spring. The force is assumed to be zero for cases where the muscle length is shorter than the optimal length. For lengthening from the optimal length the non-linear spring is often described algebraically as either a power law or exponential. Both forms of equations produce relations similar to that given in Fig. 2.14.

Biological materials are known to display both viscous and elastic behaviour [23]. Passive muscle has also been measured to behave viscoelastically [125–128]. If the muscle is considered as a viscoelastic material the shape of the passive curve will be influenced by the initial muscle length, stretch history and rate of change of length as well as the current length [129]. Thus, if a passive model is based only on the lengthening response of the muscle from optimal length, it cannot describe this viscoelastic behaviour. There has been little attempt to characterise the viscoelastic behaviour of passive skeletal muscle [130]. However, there has been some attempt to model the viscoelastic behaviour of smooth muscle[2] and other biological materials [23, 126, 131]. Tian *et al*, [131] model the passive mechanical properties of a leech body wall using a combination of series and parallel non-linear springs and dampers. Similarly, the passive response of larangal soft tissue and rabbit detrustor smooth muscle have been modeled using Kelvin/Voigt type viscoelastic models [132–134].

2.5 Invertebrate Specific Models

There have been a number of studies that measure the force response of invertebrate muscle [5, 9, 49, 135–141], however, there have been few attempts to develop a model describing the response.

[2]Smooth muscle is one of three types of muscle found in the body of mammals, the others being skeletal and cardiac muscle. Smooth muscle is found in the walls of internal organs and blood vessels (excluding the heart). The muscle has the form of thin layers of sheet so does not appear striated. It contracts without conscious control

Full and Ahn [142] use a Hill-type model with the form given in Fig. 2.11B in developing a model of the hind leg of the death head cockroach. Similarly, a Hill-type model is used by Zakotnik *et al* [49, 80] to model the response of the extensor muscle to SETi stimulation. Zakotnik *et al* [49, 80] use standard F_V and F_L relations and do not measure these properties directly. Their activation model is extended from the cascade model described in Sec. 2.2.4 and is given by

$$\frac{\delta^2\beta}{\delta t^2} + \phi_1\frac{\delta\beta}{\delta t} + \phi_2\beta = u(t) \tag{2.20}$$

$$\frac{\delta^2\gamma}{\delta t^2} + \phi_3\frac{\delta\gamma}{\delta t} + c(f)\phi_4\gamma = \beta(t) \tag{2.21}$$

$$c(t) = \frac{t^2}{K_1 + t^2} - \frac{t^2}{K_2 + t^2} + 1\ ; t \equiv 1/f \tag{2.22}$$

where $u(t)$ gives the input action potential and $\gamma(t)$ the active state of the muscle. The model has 6 parameters, ϕ_1, ϕ_2, ϕ_3, ϕ_4, K_1 and K_2.

Cofer *et al* [143] also use a Hill-type model to model the locust hind leg flexor and extensor muscle in a neuromechanical simulation of a locust jump. The model converts a change in muscle membrane voltage to tension using a sigmoid shaped curve (similar approach to using a Hammerstein model with IRC curve, see Sec. 2.2.3). The tension value is then scaled based on the muscle length, using a F_L curve. The scaled tension is then applied to the muscle by a force generator to produce a contraction. A Hill-type model is again used to describe the behaviour of cockroach muscle by Ghigliazza and Holmes [28, 79]. Parameters of their model are found by fitting to data from a cockroach.

Each of these studies embodies the muscle model into an overall system. The muscle models are just used as actuators to describe the overall response. For example Cofer *et al* [143] study locust jumping and are more concerned with the details of other mechanical components in the system, Full and Ahn [142] use their model in describing wedging behaviour, Zakotnik *et al* [49, 80] to characterise locust scratching and Ghigliazza *et al* [28, 79] as a component in describing locomotion.

2.6 Conclusions

A wide range of methods have been used to model the response of skeletal muscle. There exists very little literature describing comparisons between existing models. Even in cases where the modelling method is similar, e.g. Hill-type, there is still little crossover between the models of

different researchers. The individual components of the models (e.g. F_V relation) are described using different sets of equations by different research groups.

Muscle is a complex system, therefore simplifying assumptions are used to model it. These assumptions limit the range of applicability of the model, but help to reduce the complexity of the system. There is a trade-off between having a simple tractable model and a precise complex model. Studying invertebrate muscle simplifies the neural part of the neuro-muscular system. Despite this there have been few attempts to describe the force response of invertebrate muscle.

Chapter 3

Materials and Methods

3.1 Introduction

Force measurements were made under two different conditions: isometric and non-isometric. This required two distinct experimental set ups. This chapter summarises the experimental set ups and acquisition methods used in obtaining data. The chapter starts by describing the length and mass measurements recorded in each locust. Next, an introduction to the anatomy and neurology, relevant to the hind leg extensor muscle, of the locust (*Schistocerca gregaria*, Forskål) is provided. Details of the femoral-tibial (FT) joint are then described. During isometric experiments force was measured external to the muscle, at the tibia. The method of estimating the muscle force from the tibial force, which involves estimating joint dimensions in each locust, is then provided. Next the set up, stimulation protocol and acquisition methods used to measure the isometric force response are described. Finally the set ups, inputs and acquisition methods used to measure the force response under non-isometric conditions are provided.

3.2 Locusts

Adult locusts (*Schistocerca gregaria*, Forskål) of both sexes, taken from a colony at the University of Southampton, were used for experiments. The sex, length, mass, femur length, tibial length and femur width of each locust were recorded. Leg measurements refer to the left (looking from ventral side, with head at top) hind leg. To measure the lengths, specific reference points on the locusts were used for consistency between measurements in different animals. The reference points used to measure the lengths are defined in Fig. 3.1. Callipers with accuracy of ±0.01mm were used to measure lengths. The locust mass was recorded by

placing it on a balance with measurement accuracy of ±0.005g. Table 3.1 summarises the mean measurements in 25 adult locusts, taken from the colony.

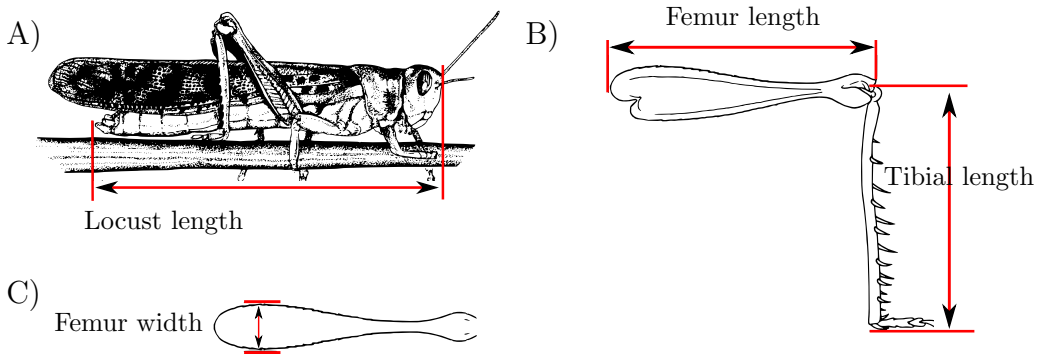

FIGURE 3.1: Definitions of length measurements in each locust. In each locust measurements were taken between the same visually identifiable reference points.

TABLE 3.1: Sample mean measurements with confidence interval at the 95% confidence level, (25 locusts)

Measurement	Sample mean, $\bar{x}$	Conf interval of mean
Locust length (mm)	44.6	$43.4 \leq \mu \leq 45.9$
Femur length (mm)	20.1	$19.4 \leq \mu \leq 20.5$
Tibial length (mm)	19.3	$18.8 \leq \mu \leq 19.9$
Femur width (mm)	3.96	$3.83 \leq \mu \leq 4.10$
Locust mass (g)	1.47	$1.34 \leq \mu \leq 1.61$

3.3 The Locust Hind Leg Anatomy

The hind legs of locusts are specialised for powerful kicking and jumping movements. As a result, the hind leg is significantly larger than than the front and mid legs. The hind leg joints are: thoraco-coxal, coxal-troxhanteral, trochantero-femur, femoro-tibial, tibio-tarsal and tarso-ungual [8]. The components of the hind leg and these joints are depicted in Fig. 3.2A. The muscle of interest in this thesis is the extensor tibia (ETi). This muscle contracts to extend the tibia about the femoro-tibial (FT) joint. Figure 3.2B shows the FT joint more clearly with the muscles that move the tibia, tarsus and unguis given. The much enlarged size of the extensor muscle, relative to the flexor is evident in Fig. 3.2B.

3.3.1 Structure of the Extensor Muscle

The hind leg extensor muscle is a bi-pennate muscle. Muscle fibres attach between the extensor apodeme and the femur cuticle. The fibres vary in length, due to the shape of the femur and the fact that the attachment angles of fibres to the apodeme vary. A plan diagram of the left

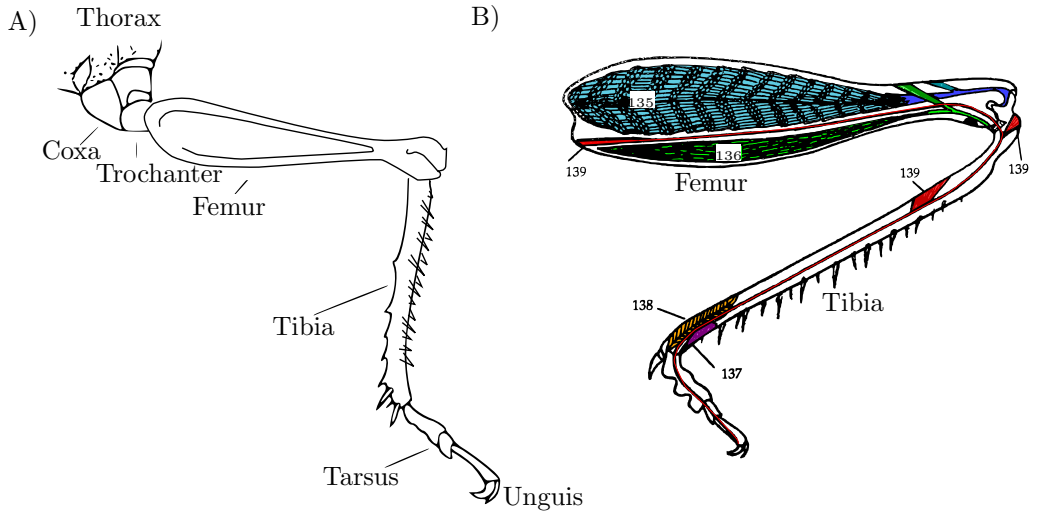

FIGURE 3.2: A) Components of the locust hind leg. B) Locust hind leg, from [8]. The muscles are numbered according to convention: 135 extensor tibia, 136 flexor tibia, 137 levator tarsi, 138 depressor tarsi, 139 retractor unguis.

ETi, viewed from the ventral surface, is given in Fig. 3.3. This provides a representation of the structure of the ETi.

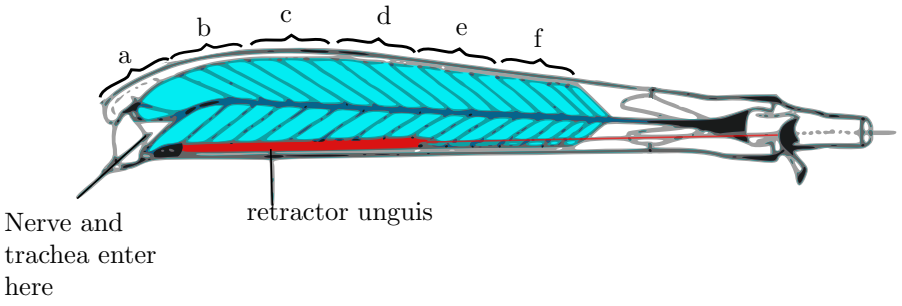

FIGURE 3.3: Plan view of the left ETi viewed from the ventral surface. taken from [9]. Marked regions a-f contain different fibre structures and innervations. The retractor unguis muscle is also shown, this muscle controls movement of the unguis.

Experiments were performed in which the entire extensor muscle was exposed. This was done by removing the ventral section of the femur, flexor muscle and air-sacs. During dissection the exposed section was bathed in locust saline. Toludine blue was used to highlight features of the muscle, enabling individual fibres and corresponding pennation angles to be seen. Images of the exposed extensor were taken down the microscope (Wild, Germany) for a range of FT angles. For the required magnification it was not possible to fit the whole muscle into a single picture. Therefore, sections of the muscle were photographed, then combined using reference

points. An image of the extensor muscle, obtained using the described method, is given in Fig. 3.4. The variation of fibre length and pennation angle along the muscle is clear.

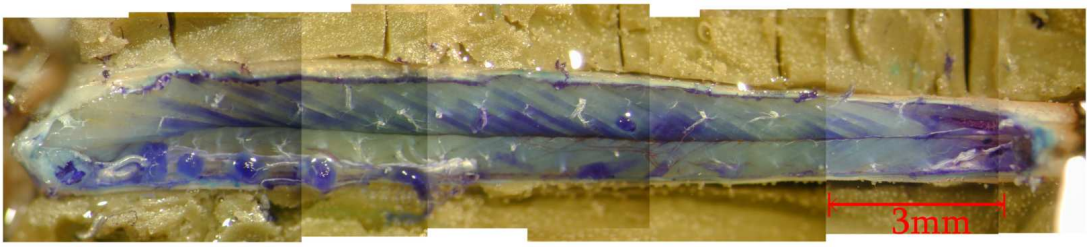

FIGURE 3.4: Photograph of the exposed extensor muscle, taken at an FT angle of 90°.

3.3.2 Innervation of the Extensor Muscle

The physiology and control of the ETi muscle of the locust hind leg has been throughly studied [8–10, 12, 13]. The ETi is innervated by only four neurons [9], each of which has been uniquely identified. These neurons consist of a fast (FETi) and slow (SETi) excitatory motor neuron, a common inhibitor (CI) and a dorsal unpaired motor neuron (DUMETi). During fast movements, such as jumping or kicking, both FETi and SETi are active. For slow movements, such as walking, only SETi is active. The axon supply to the ETi from the point of entry to the end of the femur is given by Hoyle [9]. The extensor muscle innervation is common to multiple units; muscle units are not supplied with independent nerve branches. Different regions of the extensor muscle play different functional roles [9]. This thesis is concerned with the force response to FETi stimulation. The mechanical response to FETi dominates the overall response of ETi [9]. FETi stimulation is relatively easily produced during experiment and the stimulation routine used in experiments is described in Sec. 3.5.1.

3.3.3 The Femoral-Tibial Joint

The FT joint is a hinge joint so movement of the tibia is in-plane. The joint is controlled by the flexor tibia and extensor tibia muscles that work as an agonist-antagonist pair. Contraction of the extensor muscle extends the tibia, whereas contraction of the flexor causes tibial movement in the opposite direction. The range of movement of the FT joint is from approximately 10°, where the flexor and tibia lie almost parallel, to 160° when the tibia is fully extended [144].

The FT joint is specialised for jumping and kicking. Jumping and kicking are high-speed, high-power movements. Muscle cannot produce high-power, high-speed movements as there is a trade off between velocity and force. Such behaviour is captured by Hill's equation (Eq. (2.14)). The FT joint has a section of sclerotised cuticle, known as the semilunar process. Prior to a jump the tibiae are held flexed for 300-600ms [145], during this time the flexor and

extensor muscles co-contract isometrically. This co-contraction distorts the semilunar process. The semilunar process stores approximately half of the energy which is released during a jump or kick [145]. This enables the resultant high-power, high-velocity jumping or kicking movement to occur. A diagram showing the anatomy of the femoro-tibial joint and the semilunar process is given in Fig. 3.5.

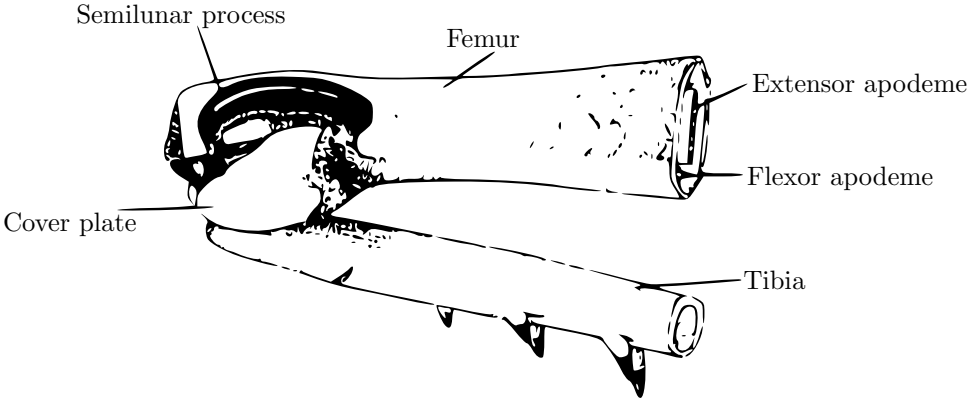

FIGURE 3.5: Anatomy of FT joint, showing the semilunar process.

The mass of the extensor is approximately 5 times that of the flexor [8]. The extensor muscle can exert a stronger force than the flexor. During co-contraction the relatively weak flexor muscle must pull with the same force as the strong extensor. The joint is specialised so co-contraction can occur. When the tibia is fully flexed (i.e. FT angle=10°) the extensor tendon is working at a significant mechanical disadvantage. The hind leg contains a lump (Heilter's lump) and the flexor tendon rides on top of this lump. The lump changes the angle with which the flexor tendon pulls on the tibia which gives the flexor mechanical advantage meaning that co-contraction of a relatively weak flexor and strong extensor muscle can occur.

3.4 Joint Transform

3.4.1 Calculating Muscle Force from Tibial Force

In the isometric experiment forces were measured external to the muscle, at the tibia (Sec. 3.5.1). The internal muscle force needs to be found from the known external force [146]. To calculate muscle force from the tibial force, knowledge of the FT joint is required.

The structure of the FT joint was assumed to match Heitler's description [147]. This assumes that the joint is a hinge joint and that, due to the relative distal origin of the extensor muscle,

the extensor apodeme remains parallel to the femur. The assumed structure is given in Fig. 3.6 with **ABCD** assumed to be rigid and free to pivot about **B**.

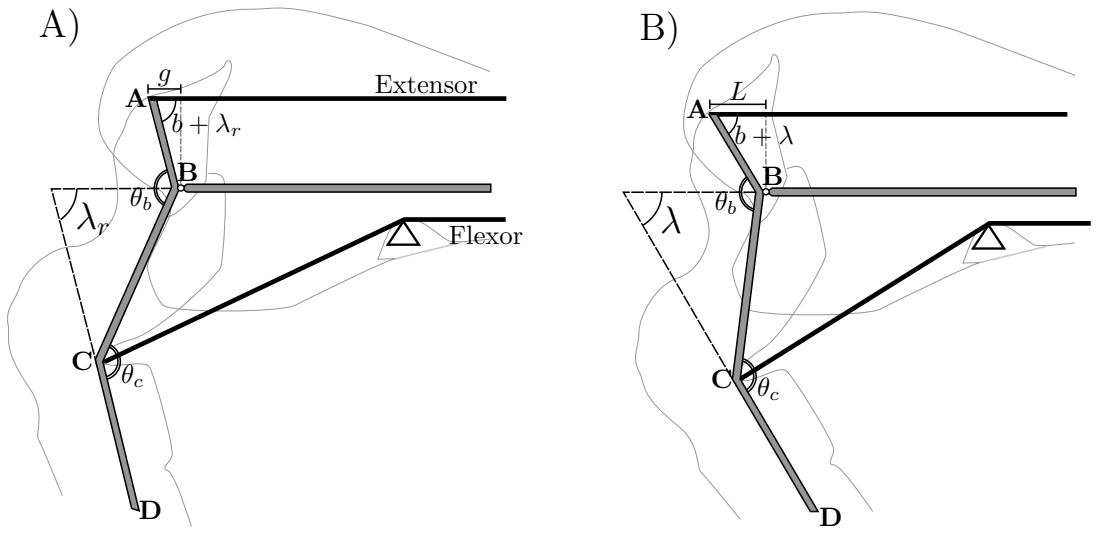

FIGURE 3.6: Assumed structure of the FT joint, adapted from [147]. A) The extensor muscle is at resting length, B) the extensor muscle is at a general length.

An expression for the relative length change of the extensor, $(L - g)$ in Fig. 3.6, is obtained from the joint geometry as

$$\Delta L = a\cos(b + \lambda) - c \tag{3.1}$$

with

$$a = \overline{\mathbf{AB}}, \quad b = \theta_b - \theta_c, \qquad c = \overline{\mathbf{AB}}\cos(\theta_b - \theta_c + \lambda_r)$$

Here λ is the FT angle and λ_r the angle at which the lengths are measured relative to, the dimension $\overline{\mathbf{AB}}$ and angles θ_b and θ_c are defined in Fig. 3.6. The lengths were measured relative to the muscle resting length ($\lambda_r = 80°$), hence the relative length change ΔL gives the change from muscle resting length.

After isometric experiments, the extensor muscle was exposed for length measurements by cutting a window in the distal part of the femur close to the FT joint. The overlying flexor and air-sacs were dissected out. The FT angle was varied from 20° to 140° . Figure 3.7 gives an example of the change in length ΔL against FT angle λ in one locust. By curve fitting, using a least-squares estimate, to a plot of ΔL against λ using Eq. (3.1) estimates could be obtained for the length $\overline{\mathbf{AB}}$ and angle $\theta_b - \theta_c$ for each locust. Figure 3.7 gives an example of the fit.

In order to convert the measured tibial force into a muscle force, equilibrium of moments can be taken about the joint pivot point. In isometric experiments there was no joint rotation,

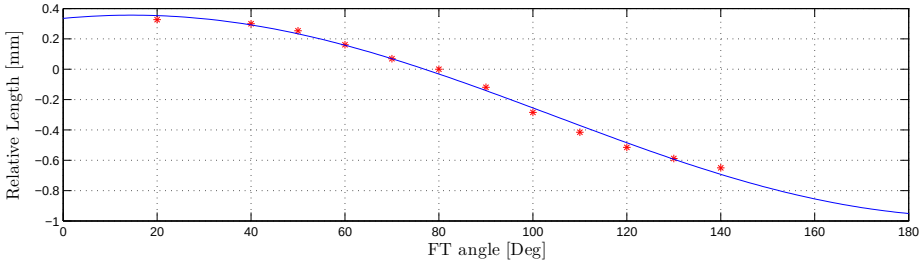

FIGURE 3.7: Example of data (*) and fit (—) for relative muscle length at different FT angles for one locust.

TABLE 3.2: Mean estimates for $\overline{\mathbf{AB}}$ and $\theta_b - \theta_c$ with confidence intervals at the 90% confidence level (25 locusts)

Measurement	Sample mean, $\bar{x}$	Conf interval of mean
Length of $\overline{\mathbf{AB}}$ (mm)	0.46	$0.42 \leq \mu \leq 0.49$
Angle $\theta_b - \theta_c$ (rad)	0.15	$0.06 \leq \mu \leq 0.23$

therefore the moment due to the tibial force can be equated to the moment due to the muscle force. To do this, as well as knowing $\overline{\mathbf{AB}}$, $\theta_b - \theta_c$ and λ, the location of the pivot point and the perpendicular distance from the line of action of the tibial force to the pivot, are also required. The pivot point **B** was found by tracking a point on the tibia as the femur was rotated (this was done prior to the dissection to find $\overline{\mathbf{AB}}$ and $\theta_b - \theta_c$). A circle could be fitted between points (justifying the hinge joint assumption), with the centre of rotation found at the centre of the circle. Figure 3.8 provides an example of the tracked points, fitted circle and the corresponding pivot point. The point of measurement on the tibia was marked and recorded for each locust. Hence, once the pivot point was located, the moment due to the tibial force could be found straightforwardly. This moment was equated to the moment due to the muscle force, which could be calculated for each locust using the relevant values of $\overline{\mathbf{AB}}$ and $\theta_b - \theta_c$ for each locust. Re-arrangement gave the corresponding muscle force at a given FT angle from the measured tibial force.

3.4.2 Joint Estimates

Table 3.2 provides a summary of estimates for $\overline{\mathbf{AB}}$ and $\theta_b - \theta_c$ using the method described above. The obtained lengths for $\overline{\mathbf{AB}}$ and $\theta_b - \theta_c$ can be compared to Heitler's [147] who measured $\overline{\mathbf{AB}}$=0.76mm and $\theta_b - \theta_c = 0.018$ radians in one locust with tibial length of 21mm. These measurements are of comparable order of magnitude and the variability could be accounted for by variation between locust colonies. Heitler's measurements were obtained from scale drawings and photographs of the dissected joint. The method described above leaves the joint intact. The distal end of the femur is encased in a hard cuticle, the semi-lunar process. Dissecting this away to expose the joint is difficult and causes some loss of structural integrity of the joint.

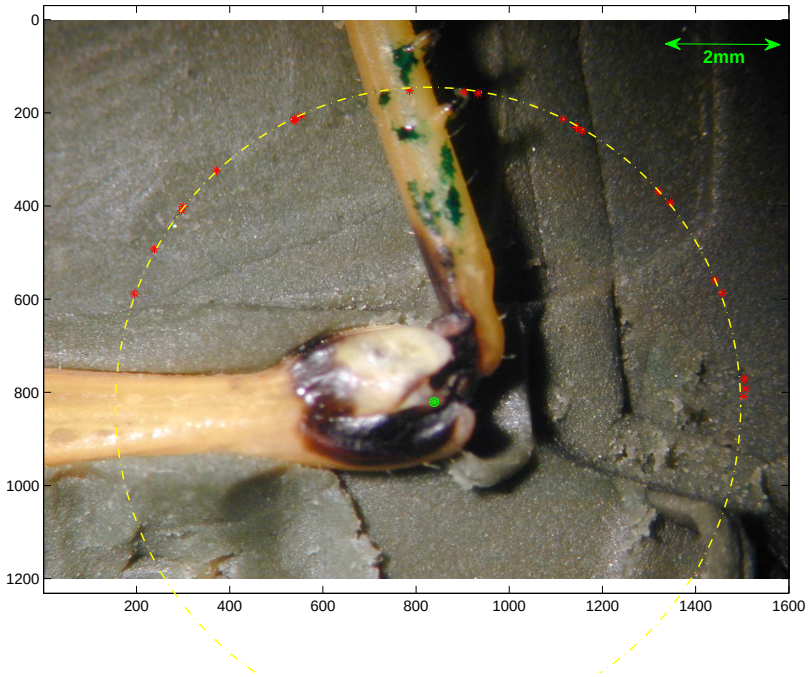

FIGURE 3.8: Example of tracking a point on tibia to find the centre of rotation. A circle (- . -) was fitted to the tracked points (x) on the tibia as the joint was rotated to give the pivot point (⊗).

After estimation of joint dimensions using the method described a few joints were dissected open and dimensions measured. Estimated angles and lengths were found to be similar between the two methods, although exact measurements from dissection were difficult due to the difficulties in determining exact insertion points. Estimates using the method described, where the joint dimensions were estimated from tracking changes in muscle length, are shown superimposed on a dissected joint in Fig. 3.9 for a range of FT angles. The method of determining joint dimensions without joint dissection and direct measurement is thought to provide reasonably accurate estimates of the joint dimensions, the merits in this method lying in the fact that no joint dissection is necessary. The inaccuracies of this method arise from tracking the mark imprecisely and difficulties in exactly determining the FT angle. FT angle measurements are accurate to about $\pm$ 0.035rad.

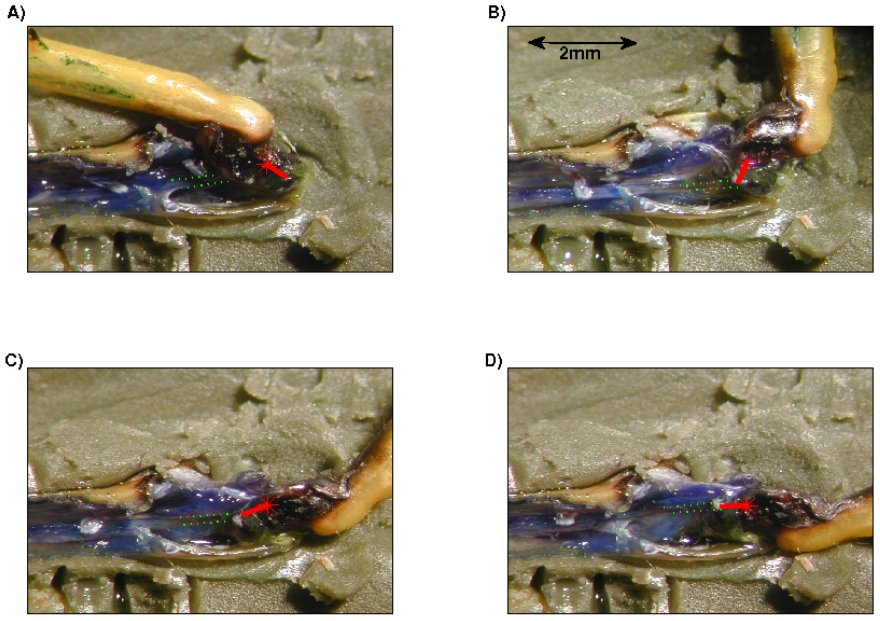

FIGURE 3.9: Photographs of dissected joint at a range of FT angles showing estimate for $\overline{\mathbf{AB}}$ (—) and the pivot point (*), where visible the edges of the extensor apodeme (- - -) are marked. A) FT angle = 15°, B) FT angle = 85°, C) FT angle = 130°, D)FT angle = 155°.

3.5 Force Measurements

3.5.1 Isometric Measurements

Locusts were securely fixed ventral side up using modelling clay. The left (looking from ventral side, with head at top) hind leg was clamped ventral side up so that the femur was fixed but the tibia and tarsi of the leg were free to move with their full range [144]. The FT angle was set to 80° using a protractor, with a pin used to hold the tibia at 80°. A schematic of the set up is given in Fig. 3.10. A photograph of the set-up is shown in Fig. 3.11.

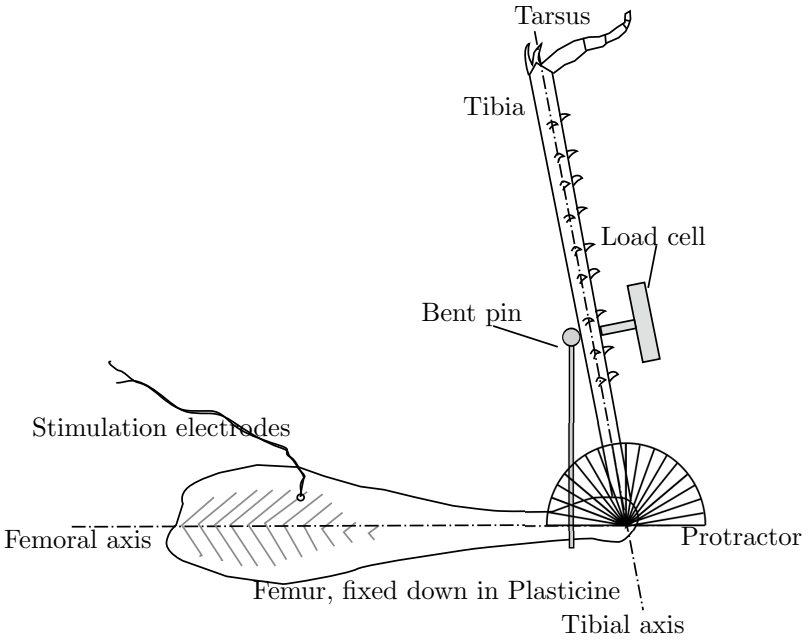

FIGURE 3.10: Schematic of force experiments. Stimulation electrodes were used to activate the extensor muscle and cause the tibia to exert a pushing force on the load cell.

FIGURE 3.11: Photograph of isometric force experiments. The locust was mounted under a microscope.

During experiments the muscle was held isometrically by constraining the FT angle at 80°. Figure 3.12 depicts the maximum tetanic force, measured at a fixed point along the tibia, for 5 locusts at a range of FT angles. The force measured at the tibia is maximum when the FT angle is set to 80°. The signal to noise ratio is improved by using the angle at which the maximum force was recorded, therefore an angle of 80° was used throughout experiments.

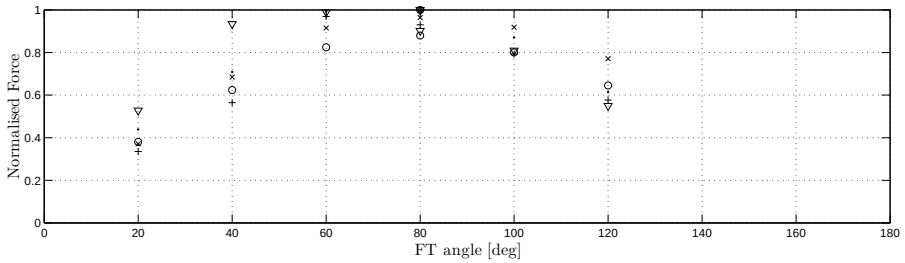

FIGURE 3.12: Maximum force measured at the tibia during tetanic stimulation for a range of FT angles. Results from 5 locusts shown, a different symbol is plotted for each locust. The force was normalised in each locust by dividing by the maximum tetanic force recorded in each locust.

During a jump the ETi produces a maximum isometric force of approximately 15N [12], this provides an upper-bound on the ETi force. However, in response to a single input pulse the maximum force developed by the ETi can be much lower, of the order of 1N. It is important that the maximum force is within the range of measurement, but that it is also possible to resolve small force changes. In experiments forces are measured at the tibia. The expected maximum force, measured at mid-point along the tibia, is 0.5N. As well as using equipment suitably matched to measure the expected force, conditions must be isometric. Therefore, any defections must be very small, such that an isometric approximation is acceptable. An S100 SMD (Strain Measurement Devices, USA) thin film load cell, with range up to 1N was used to measure the force at the tibia. Under a force of 0.5N the tip deflection of the load cell was measured to be less than 0.4mm. During the full range of motion the movement of the mid-point of the tibia is of the order of 25mm, therefore departures from isometric conditions due to load cell deflection were assumed to be negligible.

The output of the load cell was fed into a Fylde FE-369-TA (UK) transducer amplifier to amplify and filter the signal prior to acquisition. The filter cut-off frequency was set to 1kHz (-3dB). Both the input to the muscle, and the load cell output, were recorded with a sampling frequency of 2.2kHz using a Cambridge Electronic Design 1401 A/D interface using Spike2 software.

Measuring the force at the tibia, as opposed to cutting the apodeme and attaching a force transducer directly to the apodeme has the advantage that the muscle remains *in vivo*. Conditions during testing will be physiologically relevant as it will not be possible to shorten or

stretch the muscle beyond what the structure of the FT joint permits. During the force measurement stage no dissection is necessary, meaning the response should be more relevant to conditions in which 'normal movement' occurs. The muscle was assumed to be held isometrically during force measurements. This was done by constraining the tibial position using a load cell and pin. Due to mechanical compliance of the femoral tibial joint system, although tibial movement is constrained to be negligible, there may be some departure from isometric conditions. The assumption that the muscle is held isometrically was tested by estimating the maximum expected movement of components of the femoral tibial joint system.

The apodeme can be considered to be a stiff link [12] but other components of the joint that may provide some serial elasticity are the semi-lunar process and the tibia. During the experiment the tibia is stressed in the same direction as in a jump. Heitler [145] measures approximately 2° of tibial bending in response to a force of 0.02N when the tibia is treated like a cantilever of length 14.5mm. This corresponds to a stiffness of approximately 80Nmm^{-1}. Considering that the peak forces measured at the tibia, during preliminary experiments, are of the order of 0.8N, there is likely to be less than 0.01mm deflection of the tibia when stressed during experiments.

The other element that may contribute towards a departure from equilibrium is the semi-lunar process. By using the relation of Gabriel [148], which relates the deformation of the semi lunar process to the applied load, an expected maximum deformation could be calculated. The maximum tetanic force of 10N, recorded during preliminary experiments, provides an upper bound for the applied load. According to Gabriel's relation 10N of force would result in up to 0.19mm of joint deformation. This value is a very conservative upper-bound and in practice the deformation of the semi-lunar process is likely to be significantly less. This deformation assumes co-contraction of the flexor and extensor with a small FT angle so that the flexor has significant mechanical advantage over the extensor [8, 144]. Neither of these conditions were met during experiment. Considering that during the whole range of motion of the FT joint the total displacement of the apodeme from rest is approximately ±0.5mm, it is possible that the motion is not small enough to ignore. However, in practice this motion is expected to be significantly less. Furthermore, around an FT angle of 80° preliminary experiments indicated that the force-length relation tends towards a plateau. Hence, although movements in the apodeme may not be small enough to ignore, it is thought that the resultant changes in the force profile are negligible and so assuming the measured force to be equivalent to the isometric force response is acceptable.

In measuring the force at the tibia the flexor muscle could also contribute to the overall measured force. Steps were taken to ensure that the measured force due to the flexor muscle was negligible. The stimulation electrodes were inserted directly into the extensor muscle and so should not cause activation of the flexor muscle. To remove the passive contribution due to the flexor (also removes passive contribution due to the extensor) once the leg was in position,

as in Fig. 3.10, the force was zeroed prior to stimulation. In doing this it is assumed that neither muscle is activated when the force is zeroed so just the passive component of force is removed. This approach assumes that the passive resistance is constant for a given muscle length; passive muscle displays some visco-elastic behaviour. However, for zero velocity conditions as in the isometric case this assumption is reasonable. Since the locust is alive during experiments, co-contraction may occur, also since the load cell constrains the leg movement the locust may, instinctively, push back against it. The output signal from the load cell was continually monitored throughout the experiments. Any activity could be seen clearly on the force trace and the force was zeroed only when no activity was evident on the force trace. The force returned to zero after each contraction. Therefore it is thought acceptable that zeroing removes only the passive components of the force.

It is also assumed that the measured output (contractile force) is entirely due to the given input. Since the locust is alive during experiments it is possible that voluntary or reflexive activity may contribute to the measured force, these contributions would not be as a direct result of the input and so are undesirable. Voluntary movements are clearly shown on the force trace and any force traces that include extra voluntary movements were discarded. Sensory feedback comes from the femoral chordotonal organ, hair sensilla which monitor joint angle and campaniform sensilla which monitor cuticle strains [149, 150]. During this set up conditions were isometric, so the joint angle is unchanged during each experiment, furthermore, the contact area on the tibia is only very small. Under these conditions the sensory feedback is minimal and so not considered further for isometric conditions. In later experiments, where conditions departed from isometric, the nerve N5 supplying the muscle was cut in the thorax to avoid neural feedback loops.

3.5.1.1 Stimulation Protocol

The extensor muscle was stimulated by implanted electrodes. Points of attachment of the extensor muscle are visible as dark patches on the femur cuticle [9]. The sixth attachment point from the proximal end of the femur was used as a marker to place the electrodes on the anterior side (this corresponds to the outside region c in [9], defined in Fig. 3.3).

Pulses of 3ms duration and 5V amplitude were used to activate the muscle. Pulses of 3ms duration were used as they give a consistent response. In preliminary tests the stimulus pulse amplitude was increased until a single, unitary amplitude response was elicited, as to rule out the potential confounding factors caused by inhibitory motor neuron activation. Similar amplitude levels were then used in experiments (5V). In using the lowest possible stimulation level it is assumed that only the FETi is excited. The number of input pulses (n) and interpulse interval (IPI) were varied during experiment. The pulse duration (d) and amplitude ($V_{\max}$)

were kept constant. The recorded force was normalised by dividing by the maximum tetanic force (recorded during a 40 pulse, 67Hz train of input pulses) for each locust.

Different patterns of stimulation were considered; constant frequency pulse trains (CFTs) and non-constant frequency pulse trains (NCFTs). In measuring the response to a CFT a Master-8 pulse stimulator (A.M.P.I., Israel) was used to generate the pulse train neural stimulus to the muscle. This hardware enabled constant frequency pulse trains of given pulse number, pulse duration, interpulse frequency (IPF) and amplitude to be input to the muscle. The pulse output was triggered by inputing a voltage pulse greater than 1V to Master-8. A different approach was used to measure the response to a NCFT. This was due to the fact that the programable output of Master-8 does not lend itself to generating NCFTs. To generate a NCFT the times of the individual pulses in the NCFT were defined by generating a MATLAB vector of zeros everywhere, except one at the start time for each input pulse. This was output by a measurement computing USB 2527 data acquisition board. This output was amplified so that the maximum of the signal was greater than 1V and input to the Master-8. A stimulus pulse was thus generated by the Master-8 each time the programmed Matlab signal was non-zero.

3.5.1.2 Data Acquisition

Figure 3.13 shows a block diagram summarising the stages involved in acquisition, the inputs and recorded outputs. During isometric experiments the voltage input to the stimulation electrodes and the voltage out from the transducer amplifier are measured (Fig. 3.13). The experimental data is used to develop a muscle model, capable of describing the muscle force in terms of the input. Therefore, the voltage output needs converting into a muscle force. Calibration experiments were used to find the tibial force from the output voltage (V_{out}). Figures 3.14A and B summarise the calibration set up. An example of calibration results are given as Fig. 3.14C, where a straight line was fitted to data to obtain a calibration factor. The method used to convert the tibial force into a muscle force is given in Sec. 3.4.

Time delays between the input stimulus and measured force response, caused by both the hardware and neural transmission within the locust, were removed. The response was assumed to be instantaneous. As a result of this assumption this work does not consider time delays in the muscle model caused by neural transmission.

3.5.1.3 Isometric Experiments at Different Lengths

In addition to isometric experiments where the FT angle was held at 80°, isometric experiments were also performed at a range of FT angles. This enabled the effect of muscle length on the

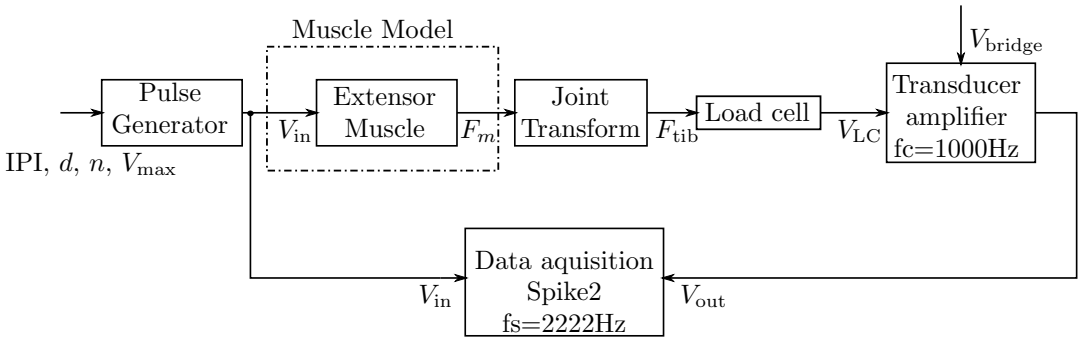

FIGURE 3.13: Block diagram to show stages involved in the acquisition of signals during experiment.

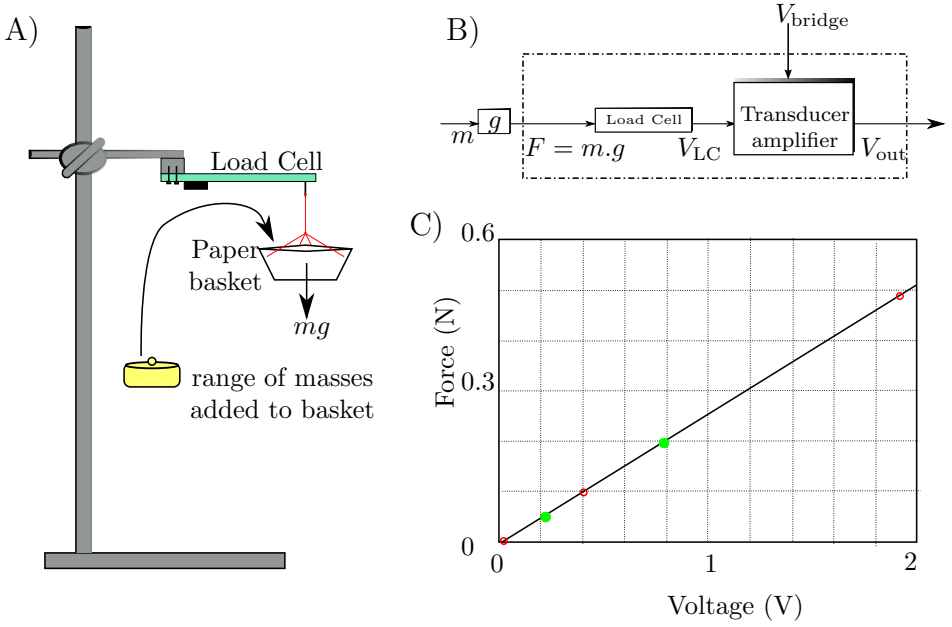

FIGURE 3.14: Calibrating to find force from voltage. A) Diagram of the experimental set up ; B) block diagram of calibration; C) example of calibration result during loading (○) and unloading (●).

isometric force to be assessed, thus testing the assumption that the activation and contraction dynamics are uncoupled. The experimental set up was as described in Sec. 3.5.1, but the FT angle varied from 80°.

There are limitations as to how much data can be collected from each locust before factors such as fatigue[1], or muscle damage due to the inserted wires start to affect results. Changing the angle imposes further limits on the amount of repeatable data that can be collected from each locust. The resultant change in muscle length as a result of changing the FT angle whilst the stimulation wire is still inserted causes some muscle damage. The alternative is to remove and replace the wires each time but, again, this causes some muscle damage. Therefore, only

[1]Muscle fatigue is characterised by the failure of a muscle to maintain the required or expected force output.

a limited set of data is recorded at each FT angle. Further details on the repeatability and specific data recorded at each FT angle are provided in Chapter 6.

3.5.2 Non-Isometric Experiments

In previous experiments the extensor muscle was held isometric, therefore the muscle velocity was zero. Experiments were also performed in which the effect on the force of changing the muscle velocity, as well as the length, were measured.

3.5.2.1 Experimental Set-Up

As with the isometric experiments, locusts were securely fixed in modelling clay with the left hind leg clamped ventral side up. A window in the ventral surface, extending to above the FT joint, was made in the femur cuticle to expose the flexor apodeme. The flexor apodeme and any air sacs were then dissected out, exposing the extensor apodeme.

A diagram of the experimental set up is provided in Fig. 3.15 and a photograph in Fig. 3.16. During these experiments forces were measured directly at the apodeme; as opposed to at the tibia as was the protocol in the isometric experiments. In these experiments, unlike in the isometric case, the load cell must measure a pulling as well as pushing force at the tibia. To measure the pulling force, the load cell needed to be attached to the tibia. Unfortunately, preliminary experiments were unable to find a way of attaching the load cell to the tibia and produce accurate, repeatable results when the position of the tibia was changed. The solution to this issue was to grasp the apodeme directly with forceps. This method has the disadvantage that the joint is no longer left intact. The advantage of this approach is that factors such as joint friction and the passive flexor force will not be recorded. Furthermore, the displacement range of the shaker is within the range of muscle length changes during normal movements.

Custom modified forceps were used to grab the extensor apodeme. The forceps modifications were: the length was significantly shortened, the tips were filed down to firmly grip the apodeme, and a small bolt was drilled through which enabled the forceps to clamp firmly shut. These forceps were allowed to clamp shut around the extensor apodeme. The end of the apodeme on the distal side of the forceps from the ETi muscle was cut away and the tibia removed. The forceps were attached to a S100 SMD (Strain Measurement Devices, USA) thin film load cell with range up to 20N. A load cell with increased range to that used in isometric experiments was used to allow for the fact that forces at the apodeme are much higher than at the tibia. This load cell was mounted on a shaker (LDS, type 101). A stand was built; this was used to hold the head unit of a Keyence LK-G32 CCD laser displacement sensor and

measure the displacement of the load cell. The shaker-load cell-laser system was mounted on a manipulator, allowing the clamped position to be altered.

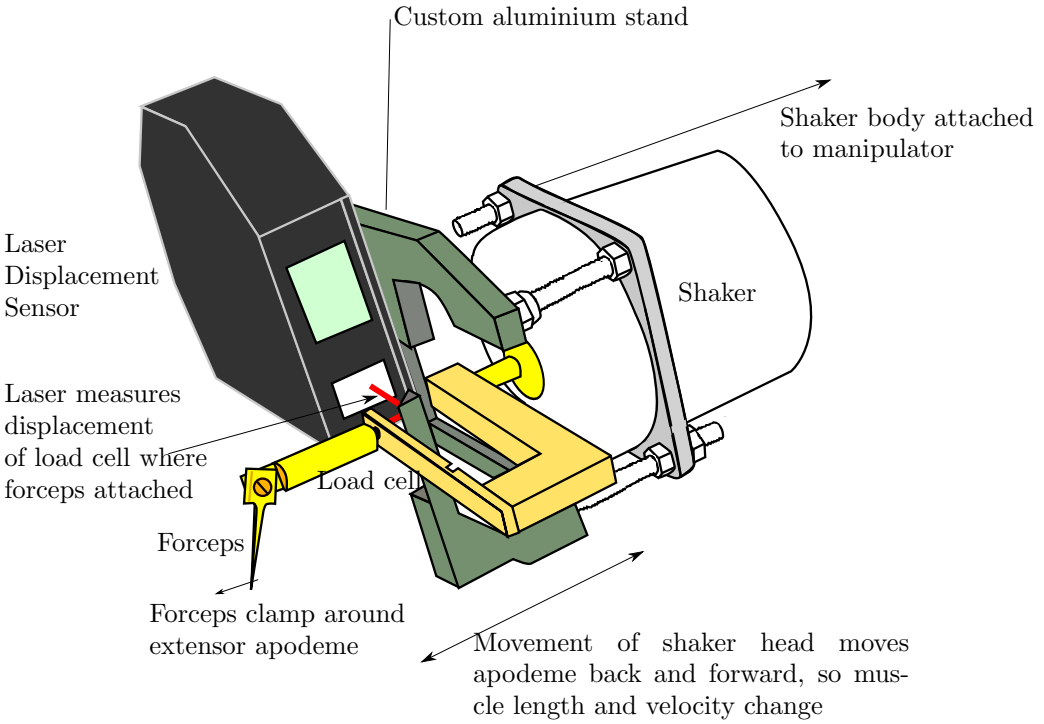

FIGURE 3.15: Diagram showing set up for non-isometric experiments. The laser system was attached to the shaker body (green section) and used to measured displacement. The forceps and load cell system (yellow section) were attached to the shaker head, and used to shake the apodeme and measure the force.

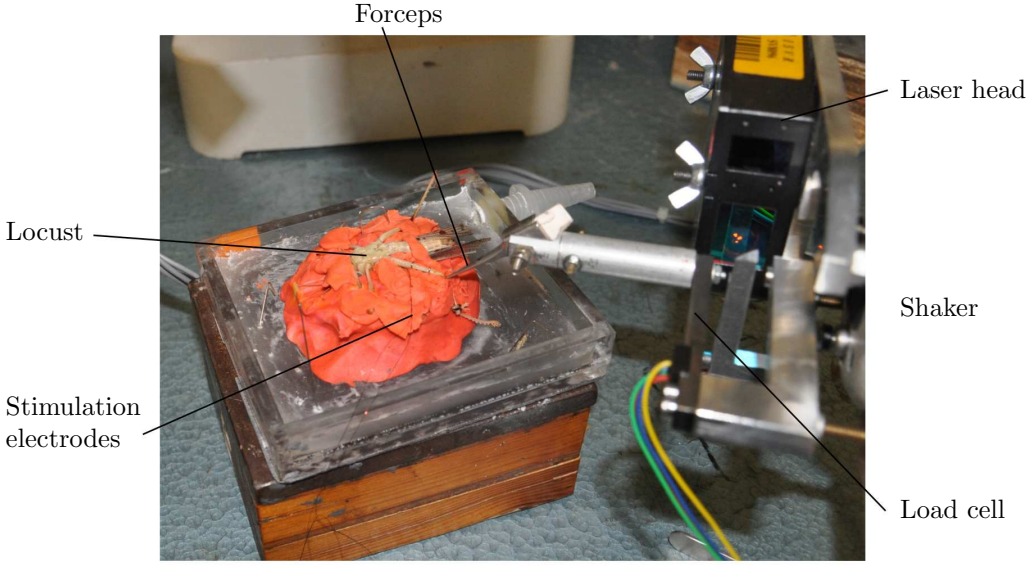

FIGURE 3.16: Photograph of the non-isometric experiments.

During experiments it is the displacement of the end of the load cell that is measured. Due to space constraints, this was done using a 45° mirror to reflect the laser beam. The muscle

displacement is determined by the displacement at the tip of the forceps. The forceps system is rigidly linked to the end of the load cell so this should be equivalent to the measured displacement. However, the angle of the mirror system was slightly off 45°, resulting in measured displacements being scaled by a factor from the tip displacement. Calibration experiments were used to determine the scale factor to convert the measured displacement into a tip displacement. These were carried out by using a second laser head to measure the displacement of the tip of the forceps, whilst simultaneously measuring the displacement using the laser-mirror system. Calibration experiments were also performed, so as to convert the transducer amplifiers voltage output (V_{out}) into the corresponding force at the tip of the forceps.

3.5.2.2 Data Acquisition

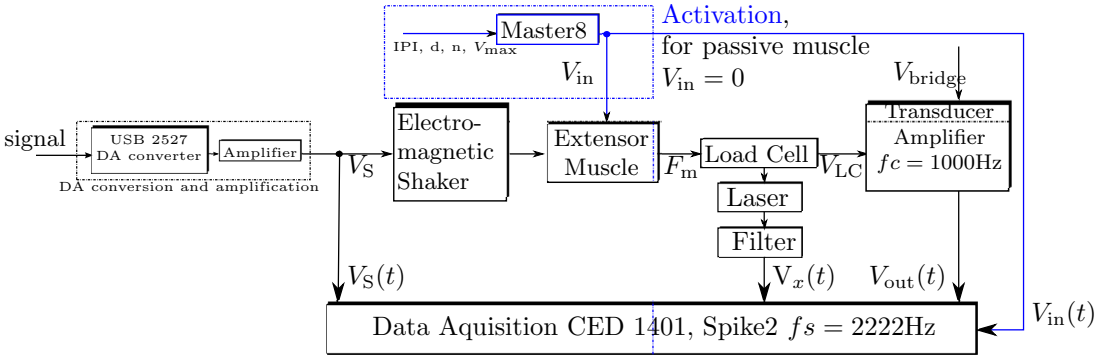

FIGURE 3.17: Block diagram of non-isometric experiment.

The shaker was driven using the analogue output of a USB 2527 Measurement Computing data acquisition system. The voltage driving the shaker was recorded using Spike2 software, with a sampling frequency of 2222Hz. The output of the load cell was fed into a Flyde FE-369-TA transducer amplifier, to filter and amplify the signal prior to acquisition. The filter cut-off frequency was set to 1KHz (-3dB). The output of the laser displacement sensor was low-pass filtered with a cut-off frequency of 1KHz. Both the laser and load cell outputs were also recorded using Spike2 software, with a sampling frequency of 2222Hz. Figure 3.17 provides a block diagram of the experimental set up.

3.5.2.3 Input to Shaker

The expected displacement range (from rest) of the muscle under normal physiologically relevant conditions was found by considering the results of preliminary experiments that measured the relative length change at different FT angles (see Sec. 3.4.1). The displacement range was estimated to be of the order of ±0.5mm. During normal walking the FT angle changes by 90° in around 0.1s [151], which results in an average muscle velocity of 5mms^{-1}. Instantaneous

velocities may be higher and are assumed to be of the order of $\pm 10 \text{mms}^{-1}$. During experiments the shaker was driven to produce apodeme movements relevant to this range (± 0.5mm, $\pm 10 \text{mms}^{-1}$).

The shaker input is also limited by the system's frequency response. The magnitude response of the shaker-load-cell-forceps system is given in Fig. 3.18. Results are shown for the displacement measured using the mirror system and the displacement measured at the forceps tip. There exists a scale factor between the two measurements in the range up to 30Hz. There is a system anti-resonance around 40Hz. Shaker inputs were frequency limited to be below 30Hz to avoid the anti-resonance and operate in the range where there is a frequency independent relation between the measured displacement and tip displacement.

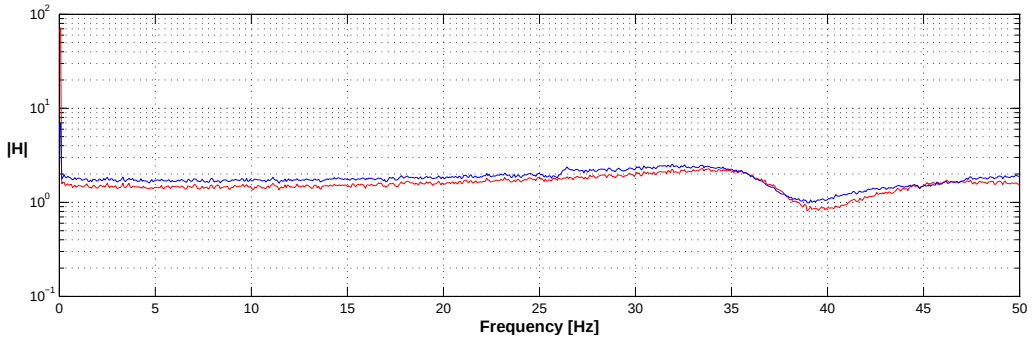

FIGURE 3.18: Displacement magnitude response of shaker-load-cell-forceps system. The displacement is measured both at the forceps tip (—) and at the end of load cell using a mirror (—).

The described set up was used to obtain both the passive and active responses under non-isometric conditions. To measure the passive response the muscle was not stimulated. The extensor apodeme was grabbed as described above. The real-time force output from the load-cell was displayed on a monitor. The manipulator on which the shaker, load-cell, and forceps system was mounted was then used to move the end of the forceps backwards and forwards in line with the muscle apodeme. To find the muscle rest length, the muscle was shortened so that the response displayed upon the monitor was just zero. The rest length was used as the start point for experiments.

To obtain the active response the resting length was again used as a start point for experiments. To avoid possible neural feedback loops due to the muscle movement a small window was made in the thorax to expose the nerve N5 supplying the muscle, which was then cut. During experiment the open thorax was continuously bathed in locust saline. Stimulation was elicited using the same protocol as the isometric experiments, described in Sec. 3.5.1. During experiments, both the stimulus input to the muscle and the voltage driving the shaker could be varied. The stimulus input, shaker input and output voltages from the laser and transducer amplifier were all recorded during experiment.

3.5.2.4 Response With Nothing Attached

During experiments where the muscle length is changed a component of the measured force is the force required to accelerate the mass of the load-cell-forceps system. This force was measured by shaking the system without attaching the forceps to anything. The resultant response to three input types is shown in Fig. 3.19. During these experiments the displacement was measured. This displacement signal was used to calculate the acceleration of the system. The force required to accelerate the mass of the load-cell-forceps system should be equivalent to the mass of these components multiplied by the acceleration. The mass of the components was measured to be 0.015kg. The resultant estimated force is also given in Fig. 3.19. It is clear that the load-cell-forceps system can be modelled as an accelerating mass. The force response is well described as the mass of the system times the acceleration. In experimental results the force contribution due to accelerating the mass is removed by subtracting 0.015× acceleration. This means that the force developed by the extensor muscle is isolated.

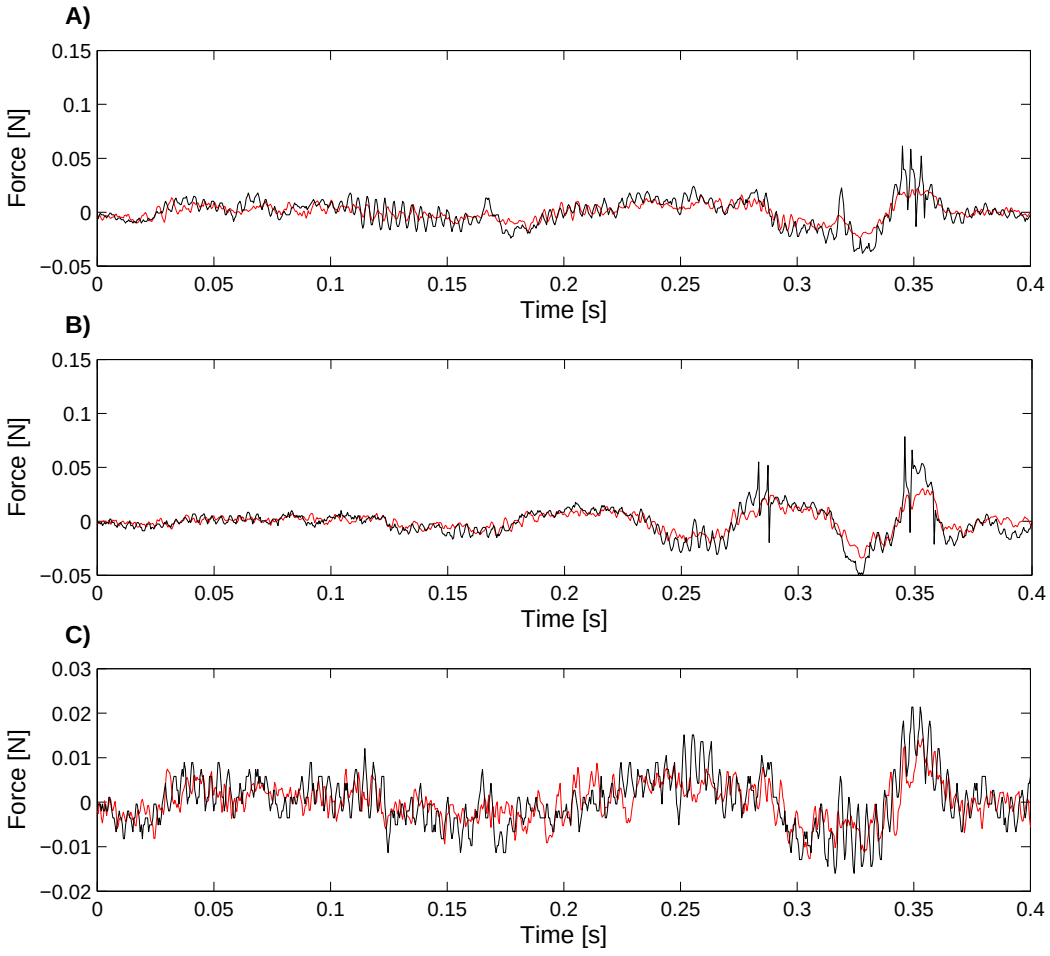

FIGURE 3.19: Estimated (—) and measured (—) force due to accelerating the mass of the load cell-forceps system.

3.6 Conclusions

The main experimental protocols were summarised in this chapter. Experimental details, relevant to specific results, are included with the results in subsequent chapters for clarity. All experiments for this thesis were performed by the author.

Two distinct experimental set ups were used to measure the muscle force under isometric and non-isometric conditions. This was necessary due to the extra complexity of the non-isometric experiments. In each locust there are practical constraints on the amount of data that can be obtained before factors such as fatigue start to affect results. This was a consideration when deciding on the best stimulation routines. Due to practical limitations, separate sets of locusts were used for isometric and non-isometric experiments. Locusts in the colony are quantitatively different, due to their differing anatomy and morphology. However, the general qualitative behaviour of all locusts is similar. In each set of experiments at least five different locusts were tested so as to investigate the statistical variations of the general behaviour.

Chapter 4

Isometric Force Response to Single and Multiple Pulses: Analysing the Contribution of Individual Pulses

4.1 Introduction

The isometric force contribution due to individual stimulus pulses is analysed in this chapter. Having a clear understanding of how the muscle behaves in response to a single input pulse is important for further investigation of the muscle under more physically relevant conditions. This further investigation is given in Chapters 5-7. In Chapter 5 the isometric response to pulse train inputs is considered. Chapter 6 uses the findings of Chapters 4 and 5 as building blocks to look at how the isometric force response is affected by changes in the muscle length. This is further developed in Chapter 7, where the muscle velocity is not constrained to be zero, and the force response under non-isometric conditions is analysed.

In this chapter, first a model that describes the twitch response of the locust extensor muscle is developed from experimental data. The isometric twitch response provides an important building block to a more general model. In developing a model it was assumed that the response to a single isolated stimulus was linear. The twitch response can be well approximated as linear because many of the non-linear effects that occur when pulses sum [50, 71–75] do not occur. There are merits in using as simple a model as possible to describe a system since model characteristics, essential to observed effects, are often more evident in simpler models [34]. The

behaviour of a single twitch is simple enough to allow models of a range of orders to be fitted to data. Hence, no assumptions or prior models are used to define the model order in this study. Models of various orders are fitted to data. Doing this enables the best model order to describe the twitch response to be found and removes any assumptions regarding the model order. This approach differs to that used in the development of other mathematical muscle models. Often studies deal with the authors' own models and few studies comparing models of different orders exist.

Next, the study of the twitch response is extended by considering the response to trains of pulses. By decomposing the response to constant frequency trains (CFTs) of varying frequencies and number of pulses into the response to each individual pulse, the behaviour of a muscle to a wide range of inputs can be investigated. The ability to describe the response to each pulse using linear models of various orders is investigated. Model parameters are allowed to vary from one pulse response to the next. Examining how these vary with the pulse train history gives insight into how the response of the muscle to each pulse changes with pulse number or frequency. In effect this assumes that the response is quasi-linear, i.e. the response to a pulse is linear, but the model parameters change slowly with time: the time constants associated with nonlinear effects (summation, depression, etc) are much larger than the time constants associated with the response to an individual pulse.

4.2 Methods

The physical set up is described in Chapter 3. Here, the specific stimulation protocol and method of extracting the response to each pulse are described in more detail.

4.2.1 Stimulation Protocol

To determine the twitch response the extensor muscles of seven locusts were excited by both five and ten pulse trains, with interpulse intervals (IPIs) of 10s and 1s respectively. In these pulse trains the response to one stimulus pulse had decayed to zero before the arrival of the subsequent stimulus input. Hence, the force response to isolated pulses was found by averaging the response to each of the 15 stimulus pulses. Two pulse trains, with IPIs ranging from 0.1s to 0.015s were also used to excite the extensor muscles of these seven locusts.

The extensor muscles of a further 14 locusts were stimulated using n pulse CFTs, where $n = 1, 2, ..., 20$. This was done for an interpulse frequency (IPF) of 12.5Hz and another of 40Hz. Stimulus trains of 1 to 20 pulses were delivered to the muscle at both IPFs. The results were used to calculate the response to the n^{th} pulse. The higher frequency CFT (40Hz)

corresponds to the frequency at which muscle tetanus first occurred. Instantaneous frequencies can naturally be much higher that tetanus frequencies, often reaching 100Hz during a kick [152].

4.2.2 Extracting Individual Pulses

Where input pulses are not well separated isolated twitches are not generated and summation of responses occurs. If the response were linear the response to two pulses would be equivalent to the response to two individual pulses added together. It it well known that the muscle does not behave linearly [39]. In estimating the response contributed by each pulse it was assumed that the response was quasi-linear, with the time constants of the non-linearities being long in comparison to the responses of individual pulses [50, 71]. The response to two pulses was assumed to be equivalent to the response of two individual pulses, with the specific form of each individual pulse dependent upon the input history, and not equivalent as in the linear case. To estimate the force contributed by each individual pulse the response to $n-1$ pulses was subtracted from the response to n pulses (Fig. 4.1). This method has inaccuracies that were mainly due to the response not being exactly repeatable (as demonstrated in Fig. 4.1). Furthermore, fatigue and recovery inevitably affect the muscle response and hence errors accumulate when subtracting the response to $n-1$ pulses from that to n pulses. During some experiments the locust moved and any data that included clear movement artefacts are not included in the analysis.

In Fig. 4.1 there is a clear change in magnitude between the response of the first pulse in a two pulse train and the response to a single pulse. The response to a two pulse train with IPI=100ms is shown for an additional three locusts in Fig. 4.2, with the twitch response superimposed. The behaviour given in Fig. 4.2 is representative of the behaviour across all locusts, this shows that in each case the magnitude of the single pulse is either very similar, or more than that of the first pulse in a two pulse train. Since the locust cannot know that a second pulse is coming this discrepancy is likely to be due to the input history and the fact that the single pulses were input to the muscle prior to the two pulse trains.

4.3 Model Estimation Algorithms

Three different methods were used to estimate the best model and parameters for the twitch response. These were: fitting in the frequency domain, fitting in the time domain using an ODE solver, and fitting in the time domain using an ARX model. The estimation algorithms used are described in more detail below.

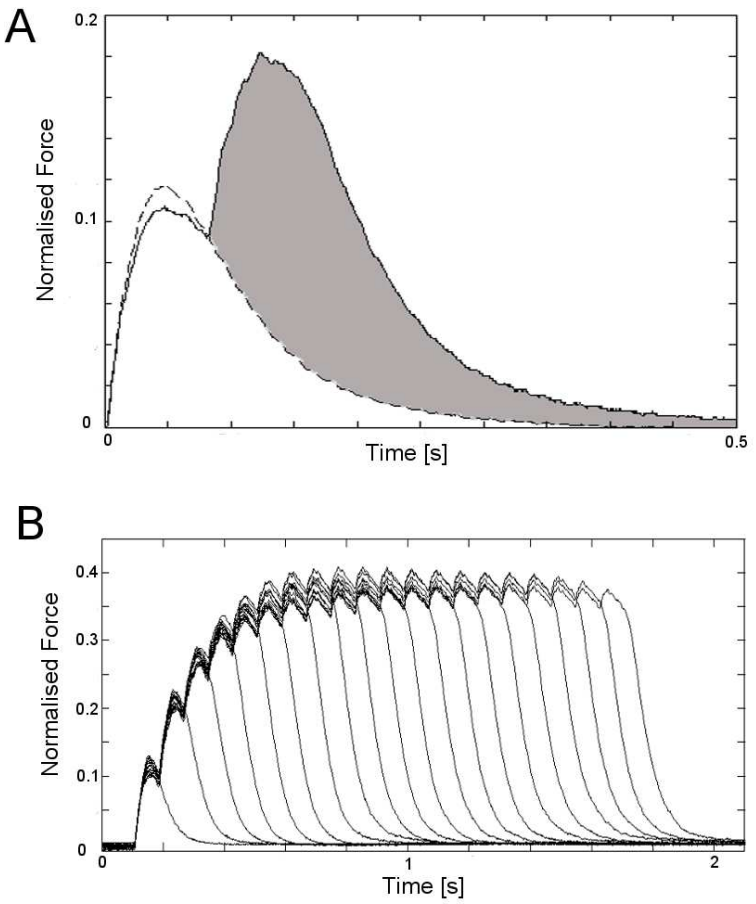

FIGURE 4.1: Examples showing how pulses are extracted. A) Example showing how the response to a second pulse is extracted. The response to a single input (- - -) is subtracted from the response to two stimuli (—), IPI=0.08s. The resultant response to a second pulse in shown as the shaded area. B) Example data showing the force response to an n pulse CFT (IPF=12.5Hz), where n = 1...20. The contribution from the n^{th} pulse is found by subtracting the response to $n-1$ pulses from the response to n pulses.

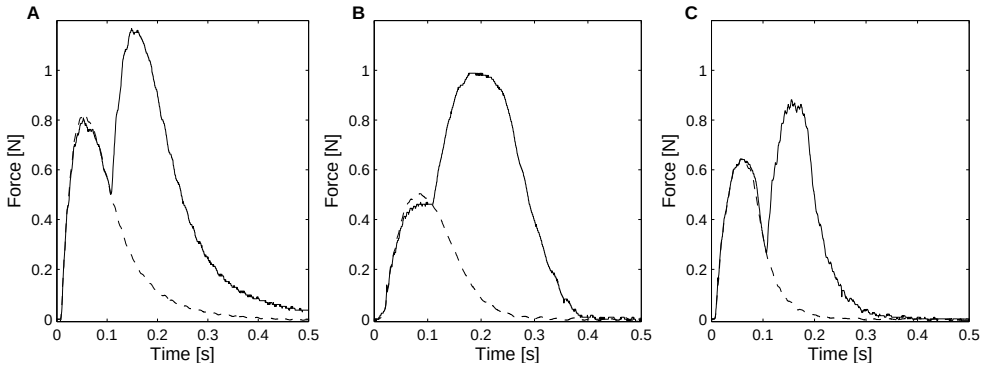

FIGURE 4.2: A-C) Response of three different locusts to a single pulse (– – –) and a two pulse train with IPI=100ms (——).

4.3.1 Frequency Domain Identification

Fitting was performed in the frequency domain. The time series data was Fourier transformed to give the data in the frequency domain. It was assumed that the twitch response is the response to an impulse. A model of the form

$$G(s) = \frac{d_m s^m + d_{m-1} s^{m-1} + ... + d_o}{s^n + a_{n-1} s^{n-1} .... + a_o} = \frac{N(s)}{D(s)} \tag{4.1}$$

was fitted to data, where m is the number of zeros in the transfer function and n the number of poles. These numbers were varied during estimation to find the model order that gave the best fit. Increasing the number of zeros did not improve the fit to data, hence the model given in Eq. (4.2) was simplified to

$$G(s) = \frac{d_o}{s^n + a_{n-1} s^{n-1} .... + a_o} = \frac{N(s)}{D(s)} \tag{4.2}$$

To estimate the coefficients d_o, $a_{n-1}...a_o$ a least squares approach was adopted, by minimising

$$J = \sum_{k=1}^{r} w(\omega_k) \left| G(j\omega_k) D(j\omega_k) - N(j\omega_k) \right|^2 \tag{4.3}$$

where $G(j\omega_k)$ is the transfer function of the original data (found from the Fourier transform of the impulse response data), $N(j\omega_k)$ and $D(j\omega_k)$ are the numerator and denominator of the transfer function being estimated, r is the length of the data, w a weighting function, and ω_k gives the frequencies at which the cost function is evaluated. The coefficients, d_o, $a_{n-1}...a_o$ are given by [153]

$$x = (A^T A)^{-1} A^T b \tag{4.4}$$

where

$$x = \begin{bmatrix} a_{n-1} & \dots & a_1 & a_o & d_o \end{bmatrix}^T$$

$$A = \begin{bmatrix} G(j\omega_1)(j\omega_1)^{n-1} & \dots & G(j\omega_1)(j\omega_1) & G(j\omega_1) & -1 \\ G(j\omega_2)(j\omega_2)^{n-1} & \dots & G(j\omega_2)(j\omega_2) & G(j\omega_2) & -1 \\ \vdots & \vdots & \vdots & \vdots & \vdots \\ G(j\omega_r)(j\omega_r)^{n-1} & \dots & G(j\omega_r)(j\omega_r) & G(j\omega_r) & -1 \\ \end{bmatrix}$$

$$b = \begin{bmatrix} -G(j\omega_1)(j\omega_1)^n & -G(j\omega_2)(j\omega_2)^n & \dots & -G(j\omega_r)(j\omega_r)^n \end{bmatrix}^T$$

The response was weighted by frequency so that emphasis could be given to the frequency range of interest. Most of the power in the force response signal was contained to frequencies below 80Hz, hence these frequencies were given a weighting of one. The weighting factor was rolled off above 80Hz to zero at 200Hz. Frequencies above 200Hz were discarded to avid fitting to noise in the signal. An initial estimate for the coefficients was made from Eq. (4.4). More accurate estimates were then found by applying the Gauss-Newton algorithm to the minimisation problem,

$$\min \sum_{k=1}^{r} w(\omega_k) \left| G(j\omega_k) - \frac{N(j\omega_k)}{D(j\omega_k)} \right|^2 \tag{4.5}$$

The estimation was implemented in MATLAB using the function `invfreqs`.

4.3.2 Identification in the Time Domain: Differential Equation Approach

The relationship between input and output was assumed to be described by the nth order ODE,

$$\frac{d^n F_m(t)}{dt^n} + a_{n-1}\frac{d^{n-1} F_m(t)}{dt^{n-1}} + ... + a_o F_m(t) = d_o u(t) \tag{4.6}$$

where $F_m(t)$ represents the output force and $u(t)$ the input. The input, $u(t)$ was found by normalising the measured input, $V_{\text{in}}(t)$, so that the area under the pulse was equal to one and defining $t = 0$ as the time at which the twitch is generated. An initial estimate was made for the parameters a_o-a_{n-1}, d_o and a solution for the ODE found using a fourth order Runge-Kutta method. Iteration using a Gauss-Newton algorithm was used to solve the non-linear least squares problem of finding the coefficients a_o-a_{n-1}, d_o. The function minimised was,

$$\min \sum_{k=1}^{r} (F_m(t) - \hat{F}_m(t))^2 \tag{4.7}$$

where $F_m(t)$ is the measured force and $\hat{F}_m(t)$ the estimated force

4.3.3 Identification in the Time Domain: Filter Approach

The response was modelled using a AutoRegressive model with eXogeneous input (ARX model). This is a discrete time model, as opposed to the continuous time model of section 4.3.2. The form of an ARX model in the general case (not specifically applied to the twitch model) is

$$P(q)y(t) = R(q)z(t) + e(t) \tag{4.8}$$

$$P(q) = 1 + p_1 q^{-1} + ... + p_n q^{-n} \tag{4.9}$$

$$R(q) = r_1 q^{-1} + ... + r_m q^{-m} \tag{4.10}$$

where $e(t)$ is input/output measurement noise, $z(t)$ is the input sequence and $y(t)$ the output. q^{-1} denotes the backward shift operator $q^{-1}y(t) = y(t-1)$. In estimating an ARX model it was assumed that the error could be neglected. The ARX prediction model for the estimated output, $\hat{y}$ can then be written as

$$\hat{y}(t|\theta) = R(q)z(t) + (1 - P(q))z(t) \tag{4.11}$$

where the model parameters are written as $\theta = [-p_1, ..., -p_n, r_1, ..., r_m]^T$. This can be written as a linear regression problem

$$\hat{y}(t|\theta) = x^T(t)\theta \tag{4.12}$$

where $x(t) = [y(t-1), ..., y(t-n), z(t-1), ..., z(t-m)]^T$.

To apply an ARX modelling approach to the twitch model, the relationship between input and output was again assumed to be described by the n^{th} order ODE given in Eq. (4.6). Using a third order model as an example the estimation algorithm using an ARX modelling approach is detailed in the following steps.

The differential equation,

$$\frac{d^3F_m(t)}{dt^3} + a_2\frac{d^2F_m(t)}{dt^2} + a_1\frac{dF_m(t)}{dt} + a_o = d_o u(t) \tag{4.13}$$

is first discretised, where F_m gives the output and u the input. Using an Euler approximation,

$$\frac{dF_m}{dt} \approx \frac{F_m(n+1) - F_m(n)}{T} \tag{4.14}$$

$$\frac{d^2F_m}{dt^2} \approx \frac{F_m(n+2) - 2F_m(n+1) + F_m(n)}{T^2} \tag{4.15}$$

$$\frac{d^3F_m}{dt^3} \approx \frac{F_m(n+3) - 3F_m(n+2) + 3F_m(n+1) - F_m(n)}{T^3} \tag{4.16}$$

These expressions were substituted into (4.13), with $n = n - 3$, to give

$$\begin{aligned} &\frac{F_m(n) - 3F_m(n-1) + 3F_m(n-2) - F_m(n-3)}{T^3} + \\ &a_2\left(\frac{F_m(n-1) - 2F_m(n-2) + F_m(n-3)}{T^2}\right) + \\ a_1&\left(\frac{F_m(n-2) - F_m(n-3)}{T}\right) + a_0F_m(n-3) = d_0u(n-3) \end{aligned} \tag{4.17}$$

Simplifying Eq. (4.17) and equating coefficients gives

$$F_m(n) = -c_1F_m(n-1) - c_2F_m(n-2) - c_3F_m(n-3) + c_4u(n-3) \tag{4.18}$$

where

$$c_1 = -3 + a_2T \tag{4.19}$$

$$c_2 = 3 - 2a_2T + a_1T^2 \tag{4.20}$$

$$c_3 = -1 + a_2T - a_1T^2 + a_0T^3 \tag{4.21}$$

$$c_4 = d_0T^3 \tag{4.22}$$

The difference equation (4.18) can be put into matrix form as

$$Y = SP \tag{4.23}$$

where

$$Y = F_m(n) \tag{4.24}$$

$$S = [-F_m(n-1) - F_m(n-2) - F_m(n-3)u(n-3)] \tag{4.25}$$

$$P = \begin{bmatrix} c_1 \\ c_2 \\ c_3 \\ c_4 \end{bmatrix} \tag{4.26}$$

The pseudo Matrix inverse was used to give the coefficients in P

$$P = (S^T S)^{-1} S^T Y \tag{4.27}$$

Equations (4.19)-(4.22) can then be used to estimate the 'continuous' coefficients $a_2 - a_0$, d_0.

In using this method the input signal needs to be persistently excitatioral [153]. A persistently excitatioral signal generates an input-output data set that is rich enough for the estimates to converge to their true values [154]. The response to a single pulse is well approximated as an impulse response, however an impulse input is too transient to be a good input for the ARX model estimation. Therefore, the response was assumed to be equivalent to an impulse response and integrated to give the step response. The step response was used as the output and a step as input to the ARX model. The advantage of this approach is that the step input provides continuous excitation as the signal is not zero at any time after the start time.

4.3.4 General Form of Model

It was found that increasing the number of zeros in the estimated model when using the frequency domain estimation did not improve the fit. Therefore, estimated transfer functions were assumed to be of the form

$$TF_d = \frac{\theta_0^{(n)}}{\theta_d^{(n)} s^d + \theta_{d-1}^{(n)} s^{d-1} + ... + 1} \tag{4.28}$$

where d is equivalent to the model order and $\theta_j^{(n)}$; $j = 0, ..., d$ are the estimated model parameters found by fitting to the n^{th} pulse in a CFT.

The resultant error between the measured data x and estimated response x_e is defined as

$$E = \frac{\sum_i (x_i - x_{e,i})^2}{\sum_i (x_i)^2} \times 100\% \tag{4.29}$$

with the sums being taken over all measured data points, i. The specific definition of the error to be minimised affects the final estimate of the model parameters, in terms of bias and/ or random error. In this case the error is defined as the normalised sum of the square differences between estimated and actual data. The fact that differences are squared (as opposed to for example taking the mean absolute error) means that small differences will be reduced, but large differences greatly amplified. This error measure will therefore favour estimated models with a lot of small discrepancies between the measured data and the estimate, as opposed to a model with a few large differences. The choice to normalise by the sum of the measured data may further affect estimates, and such limitations in the optimization should be kept in mind during the analysis of models.

4.4 Force Response to Isolated Pulses

The average twitch force, as was measured in seven different locusts, is shown in Fig. 4.3. Both the actual muscle force and the normalised force, obtained by dividing by the maximum tetanic force (recorded during a 40 pulse 67Hz input train) for each locust, are shown. Qualitatively the behaviour of each locust is similar: the rise time is fast in comparison to the decay time and the system is heavily damped. However, the specific shape of each pulse varies, due at least in part to variability in the locusts' morphology. An example of the response to the 15 individual pulses, used to obtain the average twitch response of one locust is shown in Fig. 4.4. This shows that within each locust the variability is small.

Each twitch response can be characterised by specific measurements. To characterise each response we used the following measurements (as defined by Frey Law and Shields [82]); peak force (PF), defined as the maximum recorded force; force-time integral (FTI), defined as the area under the force trace; half relaxation time (HRT) defined as the time for the force to decay from 90% to 50% of the peak force; late relaxation time (LRT), defined as the time for the force to decay from 40% to 10% of the peak force; and the time to peak tension (TPT) defined as the time required to reach 90% of the peak force from time zero. Figure 4.5 defines each measurement in relation to the measured twitch response.

The chosen model order (the number of poles and zeros) inevitably affects the fit to the measured data. As the model order is increased the errors in fit will decrease, as with more parameters the better the fit of the model to data [155]. However, although increasing the model complexity improves the accuracy of the fit in terms of minimising the error, if the

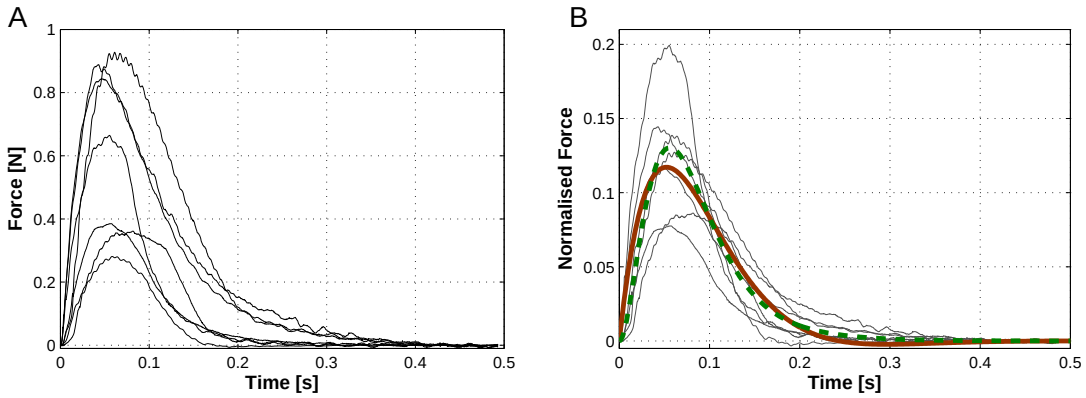

FIGURE 4.3: Average twitch response as measured in 7 different locusts, A) gives the actual muscle force, B) the normalised muscle force. The individual locust data is measured (—) and means estimated using a frequency domain fit to two pole (- - -) and three pole (—) models.

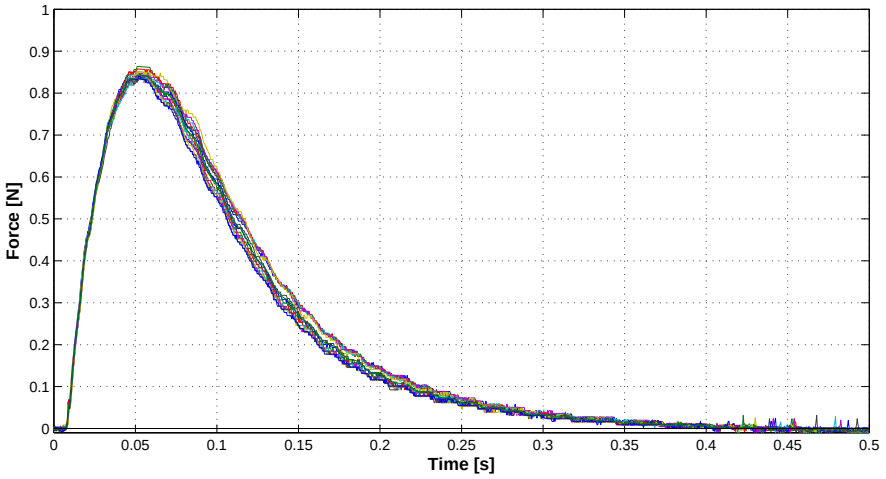

FIGURE 4.4: Example of 15 repeated twitches in one locust.

model order is too high the accuracy of the estimated parameters decreases [153]. Problems such as overfitting occur, e.g. fitting to the noise in the data.

A plot of the error between measured data and the estimated response (calculated using Eq. (4.29)) for models with one zero and different numbers of poles is shown in Fig. 4.6. These errors were calculated from fitting in the time domain, using a least squares approach. The corresponding frequency domain errors are not shown as for high model orders (above 3rd order) the inverse of a singular matrix was required and so no estimates could be made for higher order models. Figure 4.6 shows the effect of increasing the number of poles on the error; increasing the number of zeros in the estimation gave no improvement in fit. It was found that a transfer function with three poles and no zeros provided the best fit (in terms of minimising error, without overfitting) between estimated and actual data; acceptable fits were

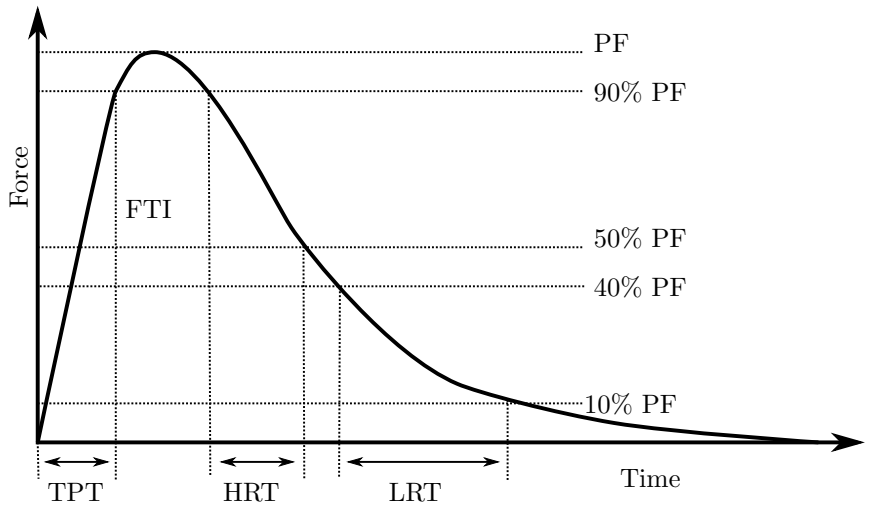

FIGURE 4.5: Definition of twitch characteristics: peak force (PF), force time integral (FTI), half relaxation time (HRT), late relaxation time (LRT) and time to peak tension (TPT)

also obtained when a transfer function with two poles and no zeros was used. When the model order was above three there was negligible improvement in the fit and the inverse of a singular matrix was sometimes involved in the estimation in the frequency domain. This suggests that a fourth order model is too high a model order.

There is no benefit to a model which when compared to data has errors that are less than the repetition error in the experiment. This indicates that the model overfits the data. The standard deviation provides an indication of the spread of experimental results. Table 4.1 gives the mean twitch parameters for a second and third order estimated model (using frequency domain fit), as well as parameters relevant to the mean experimental response and normalised standard deviation (n.s.d). The results given in Table 4.1 are summarised in Fig. 4.7. Error bars are plotted in Fig. 4.7, these give the upper and lower 95% confidence limits for the estimate of the mean of experimental data. For each model (second and third order) the errors predicted in the force characteristics are greater than the repetition errors in the experiments. For the twitch response, only second and third order models are considered further.

An estimate of the average modelled response using both a two and three pole model is also given in Fig. 4.3B. This was obtained by reconstructing the response using the average parameters, $\bar{\theta}$. The second and third order models have similar shapes but there are some discrepancies; the second order model predicts a lower maximum force, shows more undershoot at the end of the pulse, and rises faster from time $t = 0$. In Fig. 4.3B, the 'mean' is the response of an abstract locust whose parameters, θ are the means of those estimated. This measure of the average response differs from that obtained by averaging the time series data, both methods have the potential to generate average behaviour that does not represent the behaviour of any locust. Averaging across the time series data would smear the response, for example the total

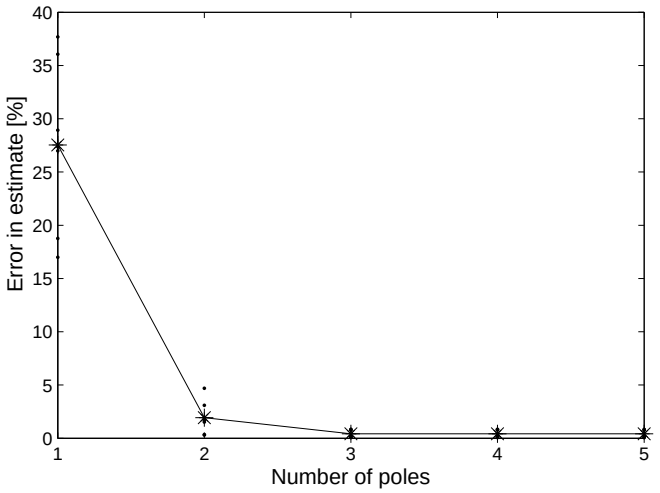

FIGURE 4.6: Errors in fit to twitch response when using models with one zero and increasing numbers of poles, both data from individual locusts (·) and means (*) are plotted. The reduction in error when using models with more than three poles is negligible.

TABLE 4.1: Model parameters and errors for twitch response. For each locust the specific twitch characteristics are extracted from the mean twitch response. The characteristics of the 2nd and 3rd order model fits, from fitting in the frequency domain, are also extracted. The normalised standard deviation (n.s.d.), defined as $\sigma/\mu \times 100\%$, is given for experimental twitch responses

		Average Mean (μ)				
		PF	FTI	HRT	LRT	TPT
L1	Mean	0.84 (nsd 0.69%)	99.4 (nsd 5.3%)	45.5 (nsd 4.9%)	95.2 (nsd 6.7%)	31.3 (nsd 4.4%)
	2 poles	0.81	99.0	51.1	81.0	28.1
	3 poles	0.85	99.0	49.2	88.3	29.4
L2	Mean	0.39 (nsd 2.0%)	38.8 (nsd 5.0%)	30.4 (nsd 9.2%)	62.6 (nsd 13%)	35.0(nsd 3.6%)
	2 poles	0.36	38.0	44.2	52.9	30.4
	3 poles	0.40	38.3	36.8	60.7	36.8
L3	Mean	0.66(nsd 4.5%)	56.9(nsd 7.0%)	20.2(nsd 19%)	52.0(nsd 9.7%)	35.0(nsd 2.0%)
	2 poles	0.63	55.5	37.3	41.4	27.1
	3 poles	0.69	55.8	30.4	44.2	33.6
L4	Mean	0.89(nsd 1.9%)	108.4(nsd 2.9%)	52.4(nsd 5.0%)	114.1(nsd 7.2%)	31.7(nsd 2.9%)
	2 poles	0.83	108.7	55.2	97.1	27.6
	3 poles	0.87	108.7	53.8	105.8	28.5
L5	Mean	0.93(nsd 2.2%)	114.7(nsd 5.9%)	51.5(nsd 3.8%)	62.6(nsd 11%)	46.0(nsd 1.3%)
	2 poles	0.85	112.9	55.7	63.5	40.0
	3 poles	0.94	114.2	47.4	72.2	46.9
L6	Mean	0.36(nsd 2.1%)	40.7(nsd 7.0%)	32.7(nsd 14%)	30.8(nsd 19 %)	50.6(nsd 6.3%)
	2 poles	0.34	39.2	49.7	46.9	42.3
	3 poles	0.38	40.8	37.3	39.1	56.6
L7	Mean	0.30(nsd 9.4%)	24.3(nsd 10%)	33.1(nsd 11%)	27.1(nsd 100 %)	58.9(nsd 8.7%)
	2 poles	0.26	23.8	39.1	35.9	33.6
	3 poles	0.29	24.2	31.3	32.7	43.2

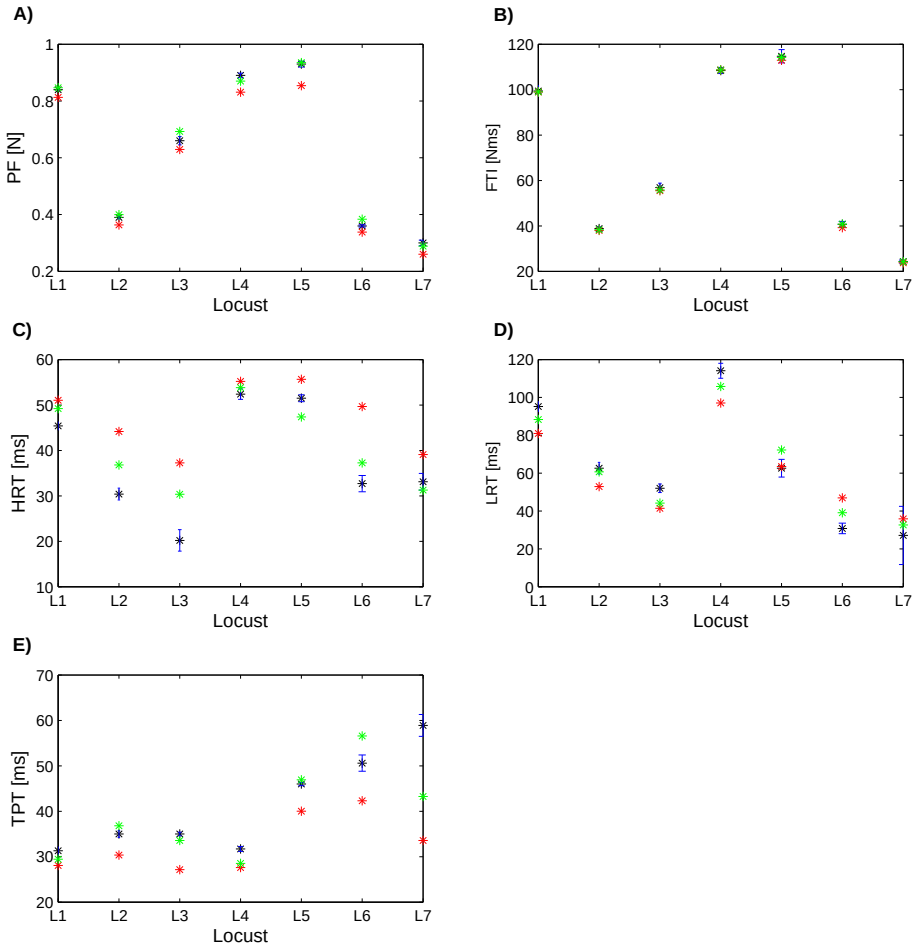

FIGURE 4.7: A-E) Specific force characteristics of measured and modelled twitch response in 7 locusts. The mean characteristics of the measured data (*) are plotted with error bars that indicate the upper and lower 95% confidence limits. The modelled characteristics when using a 2nd order (*) and 3rd order model (*) are also plotted.

contraction time of the average locust would be equivalent to the maximum total contraction time measured across the locusts. In the presented model the estimated parameters are directly related to the gain and poles of the system. The poles of a system define the rate of decay, and oscillatory behaviour of the response. Averaging across parameters effectively averages the time decay and oscillatory behaviour of each pole, and so averaging the parameters produces a representation of the average behaviour in terms of the total magnitude, rise, and decay times which are the salient features of interest. The use of average parameters to provide an idea of the average locust behaviour does have potential dangers, as does any averaging method, of misrepresenting the behaviour. However, a comparison between the model using average parameters and mean measurements of specific twitch characteristics given in Tab. 4.1 shows that estimates are similar, with differences likely due to the choice of model, this shows that

in this case averaging the parameters is reasonable.

An example of the estimated response in the time domain for one locust, obtained using each fitting method for both a two and three pole model, is shown in Fig. 4.8. The associated estimated parameters are given in Table 4.2. This shows that the coefficients estimated using the different methods are, as expected, similar. The parameters relevant to the second and third order fits are similar, with the extra contribution due to $\theta_3^{(1)}$ in the third order model small. In the ARX model $\theta_3^{(1)}$ is very small and the resultant improvement in fitting error between the second and third order models is, therefore, small.

TABLE 4.2: Example of parameters estimated for one locust (**L2**) when fitting to twitch response, using a second and third order model for different fitting methods.

	Second Order Model				Third Order Model				
Fit	$\theta_2^{(1)}$	$\theta_1^{(1)}$	$\theta_0^{(1)}$	Err %	$\theta_3^{(1)}$	$\theta_2^{(1)}$	$\theta_1^{(1)}$	$\theta_0^{(1)}$	Err %
Freq.	0.0020	0.071	0.0077	1.53	1.77×10^{-5}	0.0020	0.080	0.0077	0.24
ODE	0.0019	0.070	0.088	1.08	1.07×10^{-5}	0.0019	0.075	0.0088	0.35
ARX	0.0025	0.070	0.0076	2.52	1.12×10^{-6}	0.0024	0.070	0.0076	2.2

The fit to one locust using each method is given as an example (Fig. 4.8); fits to other locusts have similar characteristics. Both two and three pole models give good fits to the data with errors of 1.53 and 0.24% respectively for the second and third order models when using the frequency domain estimation. The frequency domain and ODE methods give the best fits to data in terms of minimising error. The fit using an ARX model is not as good. The ARX method has limitations; the input-output error was neglected and the input signal assumed to be exactly known. Furthermore, the input signal needs to be sufficient to excite all relevant modes in the model for identification. Using the ODE method is more computationally expensive and produces similar results to the computationally efficient frequency domain method. Therefore, further fits to single input pulses will be presented for just the frequency domain method.

Due to the small errors in the estimates it is thought that the assumptions of a linear model with the twitch response being equivalent to an impulse response are acceptable for isolated pulses. The second order model predicts a force that rises too quickly from $t = 0$ and has too much overshoot towards the end of the response in comparison to the modelled data. A better fit is obtained using a third order model. This is also confirmed by comparing the specific force characteristics given in Table 4.1.

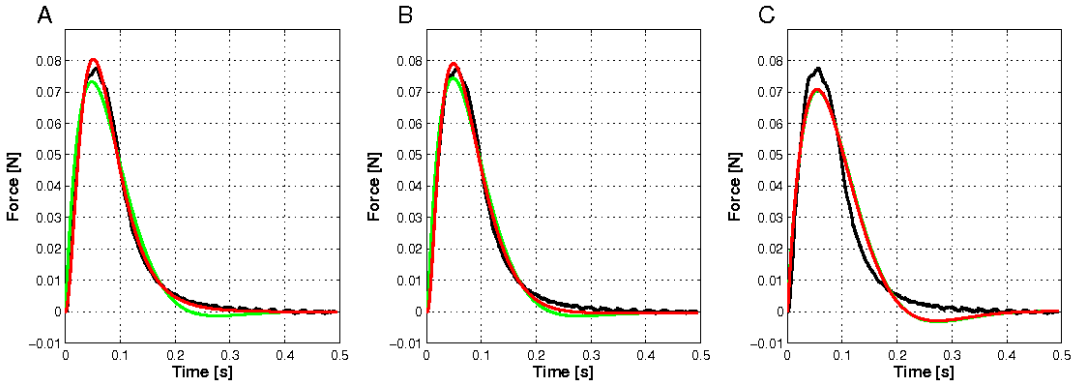

FIGURE 4.8: Example of force response to input pulse (—) and fits using second (—) and third order (—) models for one locust. A) fits using frequency domain method, B) fits using ODE method, C) fits using ARX method.

4.5 Force Response to Second Pulse

The extensor muscle response to a train of two pulses is next considered. These trains do not generate isolated twitches, so summation of muscle responses occurred. The force contributed by the second stimulus was calculated by subtracting the recorded response to a single stimulus from the total recorded response to two stimuli and time shifting the response by the IPI [71]. An example of this is given in Fig. 4.1A, the shaded area giving the response to the second pulse. There is a slight discrepancy in the peaks of the first pulses, most likely caused by the fact that muscle is a physiological, time varying entity that may respond differently given slight environmental fluctuations. Since the response to the second pulse was time shifted by the IPI so that it starts at time zero, data before the start of the second pulse was effectively neglected in the analysis of the response to the second pulse.

The responses of the extensor muscle of seven locusts to two stimulus pulses for IPFs of 12.5Hz and 40Hz are shown in Fig. 4.9. Some measurement noise is visible in the recordings. As with the twitch response, the responses of each locust are similar but specifics differ between locusts, due in part to their variable morphology. The twitch contraction time (time to reach peak force in response to a single input) was approximately 0.05s. This corresponds to an IPF of 20Hz. In Fig. 4.9B the IPF was greater than the twitch contraction frequency and the pulses can be seen to fuse into one pulse. When the IPF was lower two distinct peaks were evident, as in Fig. 4.9A.

Results when both two and three pole models were fitted to second pulse data are presented. Model orders greater than three, as with the isolated pulses, were found to overfit the data: inverses of nearly singular matrices were involved in the frequency domain estimation. An example of the data from one locust and the fit to both models is shown in Fig. 4.10. The response of this extensor muscle was in general representative of the response of each locust. From the experimental data (Fig. 4.10A) it is clear that forces do not sum linearly. As the IPF increases the maximum force and time to reach peak force increase. Facilitation (more-than-linear summation) is evident during the falling stage of the second pulse and some depression (less-than-linear summation) during the rising stage. As the IPF increases the depression and facilitation increase. The simulated pulses obtained from the two pole fit show too much undershoot towards the end of the response and underpredict the maximum force (Fig. 4.10B): these issues increase with increasing IPF. The third order model reproduces the general shape well; the estimated magnitude of the peak force and contraction time compare well with experimental data. However, the last part of the pulse is somewhat oscillatory. The oscillations arise as the poles are found using a least squares fit and happen to be complex (although highly damped). If poles were constrained to be real then the oscillations do not occur but errors in the least squares fit increase.

The error when using a two pole model increases significantly with IPF: the mean error was approximately 2% for isolated pulses (IPF=0). This increased to 7% when the IPF was increased to 67Hz (Fig. 4.11). The errors in fit of the three pole model were of the order of 1%, and the error increased by less than 1% across the range of IPF values. Thus, while a second order model fits the response to an isolated twitch reasonably well, the response to the second pulse requires at least a third order model.

Fig. 4.12 shows the estimated second pulse parameters as a function of IPF for the third order model. Each parameter increases with IPF until saturating above an IPF of approximately 40Hz. There are variations in parameter values between locusts, but the general shape of how the parameters change is similar for all locusts.

The response of the 'average locust' to two pulses when a three pole model is used to describe the second pulse was calculated (Fig. 4.9). This was found by first reconstructing the twitch response using the average of parameters[1] $\bar{\theta}^{(1)}$, as estimated from fitting to a single pulse response, then reconstructing the second pulse contribution using a new set of average parameters, $\bar{\theta}^{(2)}$, found when fitting to a second pulse for a given IPF. The total average response to two pulses was then found by time shifting the estimate for the response to the second pulse by the IPI, and adding this to the estimate of the twitch response. The third order model provides a good description of the average behaviour. The poles of the response to a second pulse reconstructed using the average parameters were calculated. The third order model poles are a complex conjugate pair with one real pole. As the IPF increases these poles became more oscillatory and the magnitude of their real part decreases.

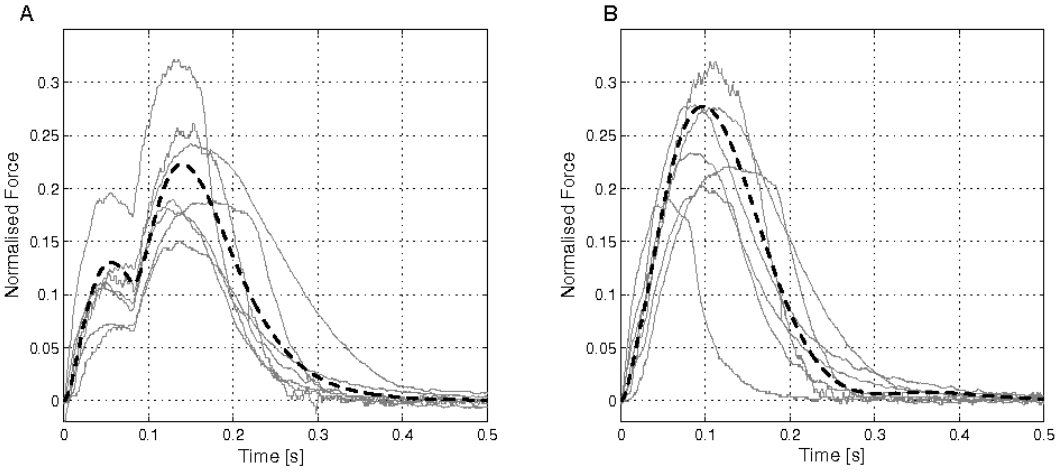

FIGURE 4.9: Force response to two input pulses: individual locust data (light continuous) and response of the three (heavy dashed) pole model estimated using parameter means; (A) IPF=12.5Hz, (B) IPF=40Hz. The mean third order average model response gives a representation of the behaviour of the average locust.

[1] Averaging parameters gives a different result to averaging across time series data. This is discussed further in terms of a single twitch in the preceding section.

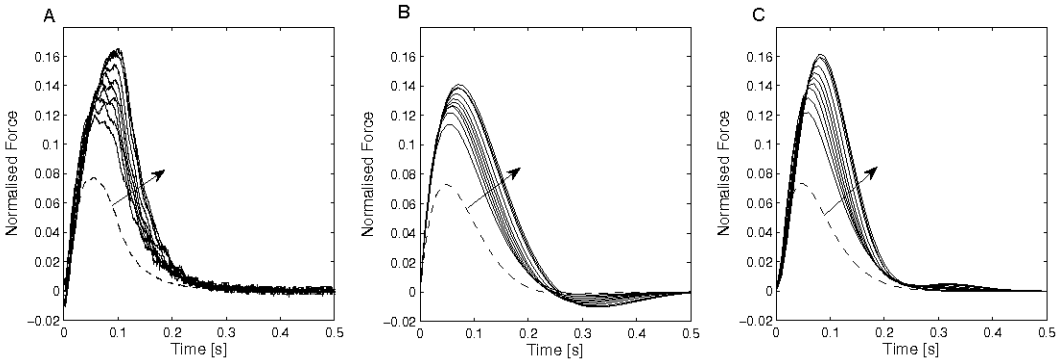

FIGURE 4.10: Comparison between isolated twitch (- - -) and force contributed by a second stimulus for various IPFs. Arrows show change as IPF is increased, (A) Experimental data (B) Fits using 2nd order model, (C) Fits using 3rd order model. The second order model underestimates the peak response and predicts too much undershoot towards the end of the pulse compared to the measured data, with the third order model providing a better description of the behaviour.

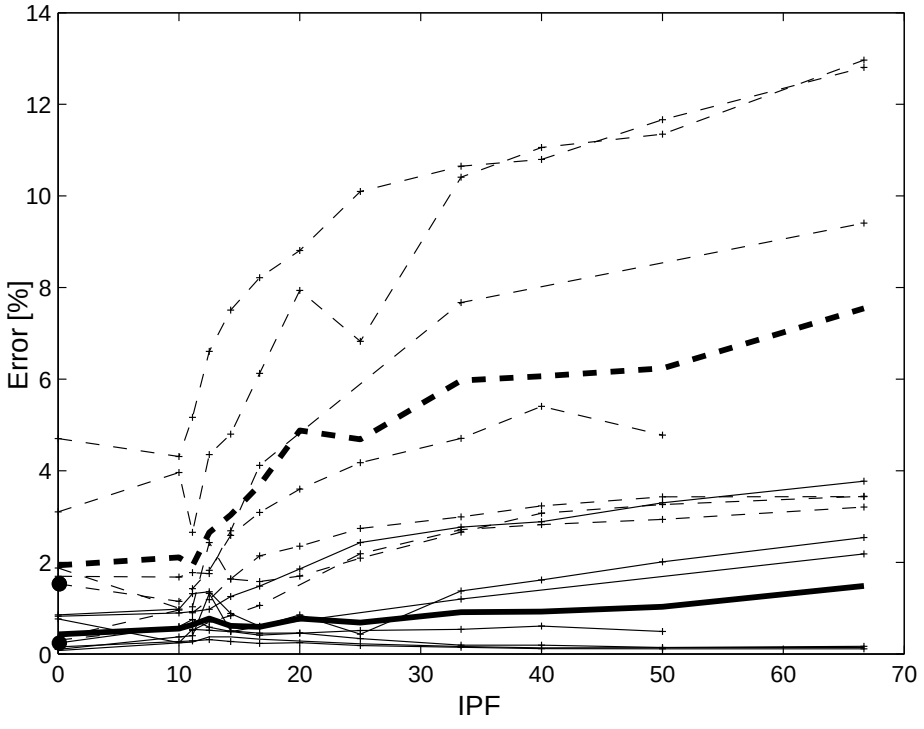

FIGURE 4.11: Errors in fit to the 2nd pulse for second-order model (- - -) and third order-model (—), with average errors given in bold. The mark (·) indicates the lines which refer to the individual locust used as an example and plotted in Fig. 4.10. Errors increase significantly with IPF for the second order model, while the goodness of fit of the third order model is less dependent on IPF.

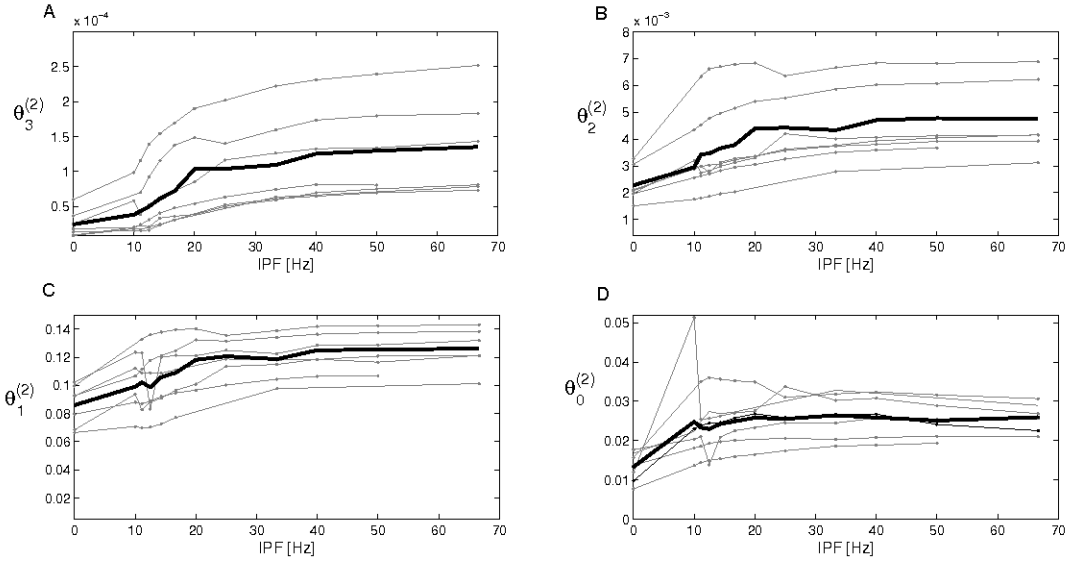

FIGURE 4.12: Change in parameters θ_i with IPF for the second pulse, estimated for each locust using a 3rd order model (A,B,C,D), with means given in bold. Parameters increase with IPF before saturating above an IPF of approximately 40Hz.

4.6 Force Response to nth Pulse

The extensor muscle response to longer CFTs was also analysed. The pulses were not well separated, so that summation of the muscle responses occurred. To estimate the forces generated by each pulse the response to $(n-1)$ pulses was subtracted from the response to n pulses. This was done for $n = 1...20$ (where $n = 1$ is equivalent to an isolated pulse). One CFT with an IPF higher (IPF=40Hz) than the twitch contraction frequency and one with a lower IPF (IPF=12.5Hz) were used.

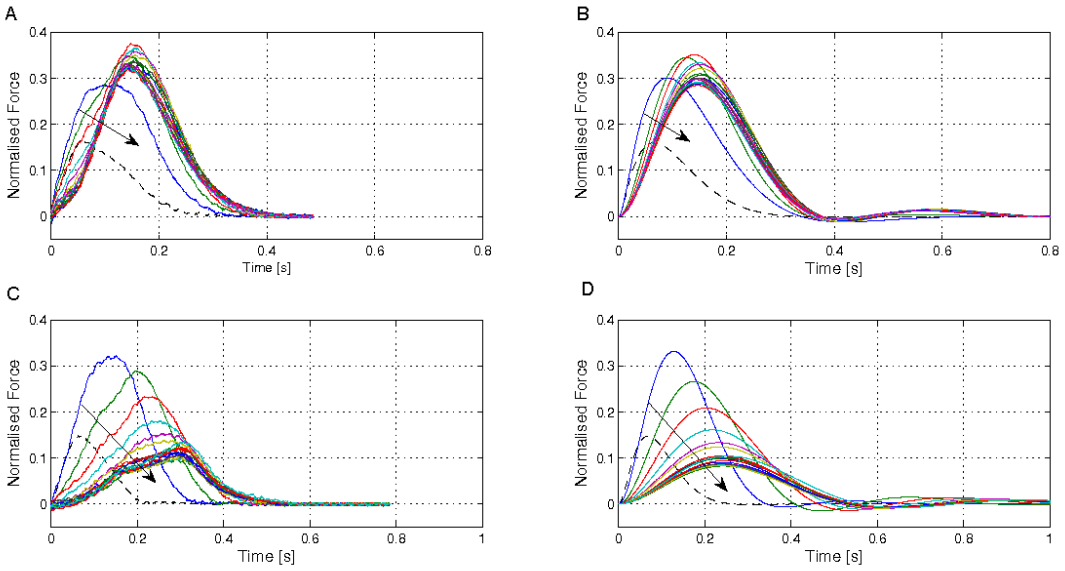

FIGURE 4.13: Force contributed by the nth stimulus in a CFT: $n = 1$ shown by a dashed line and arrows show change as n increases from 2, (A) Experimental data, IPF=12.5Hz, (B) Fit to IPF=12.5Hz data using 3rd order model, (C) Experimental data, IPF=40Hz, (D) Fit to IPF=40Hz data using 3rd order model.

Figure 4.13 shows example data from one locust, showing the force contribution of the n^{th} pulse in a pulse train when the IPF=12.5Hz and 40Hz. It is clear that the forces do not sum linearly. When the IPF=12.5Hz the magnitude and contraction time of the pulses increase over the first three pulses, with each pulse showing increased facilitation and depression. After the first three pulses the pulse shape remains approximately constant, with only slight fluctuations in amplitude. Comparing this to the case when the IPF=40Hz shows that the pulse shape depends on the IPF. When the IPF=40Hz there is an initial increase in the maximum force and contraction time from the first pulse to the second pulse. Subsequent pulses show more early depression, the magnitude decreases from the magnitude of the second pulse, and the contraction time increases. After approximately 8 pulses the pulse shape again saturates and becomes approximately constant. The magnitudes of these pulses, when n is high, are less

than those of the isolated twitches ($n = 1$), with the contraction time being much larger and the decay time smaller.

The estimated errors when fitting to the n^{th} pulse are shown in Fig. 4.14. For an IPF of 12.5Hz the three pole model provides a good fit to the data. Estimated errors are small for all pulses, with the average error being less than 1% for the whole range of pulse numbers. When the IPF was increased to 40Hz the fit was not as good (Fig. 4.13), the time at which the maximum force occurred was not modelled accurately. Estimated errors when the IPF=40Hz increase with pulse number from 0.5% for the first pulse up to almost 4% for the 20th pulse. For both IPFs the end of the modelled response is oscillatory. Fitting to data using fourth order and higher order models gives slight reductions in errors as would be expected. For some locusts, however, this reduction in error was negligible and using frequency domain methods to estimate models resulted in the inversion of nearly singular matrices. This suggests that in some cases a fourth order model overfits the data. In cases where a fourth, or higher order, model improved the fit the modelled peak force when the IPF=40Hz still occurred too early and, although slightly reduced, oscillations in the tail of the response were still evident. In general, as the IPF or n increases the errors increase. Considering also that the fitted responses wrongly predicted the time at which the peak force occurs and that the fits became oscillatory, even when higher model orders are used, suggests that the assumptions of a linear response may not hold well for such cases.

The estimated parameters for each locust obtained using a third order model are shown in Fig. 4.15 with the mean parameter values in bold. It is clear that there is wide variation between individual locusts in the estimated parameters. However, the general trends and qualitative relation between pulse number and parameters are similar. With the exception of θ_0 for IPF=40Hz, as the pulse number increases the parameter values increase and eventually saturate. Parameter values are higher when the IPF=40Hz. This supports the observations from Fig. 4.12 that as the IPF or n increase the parameters increase and eventually saturate. The parameter θ_0 when IPF=40Hz was an exception to this trend, increasing for small n then decreasing. This effect is due to the fact that the peak pulse amplitudes when IPF=40Hz decrease when n is greater than 2. The fact that tetanus was reached at around 40Hz may account for the decrease, the individual pulse amplitude decreasing resulting in the overall force not increasing above a certain value.

Figures 4.16 and 4.17 show the responses of 12 locusts to a 20 pulse train when the IPF=12.5Hz and 40Hz respectively. Again the responses for each locust are qualitatively similar, however, the magnitude and decay time vary significantly between locusts. Responses were reconstructed from models using the average parameter values estimated for each individual pulse, i.e. at each time a pulse was input, the average model parameters $\bar{\theta}$ are used to describe the response to the next pulse (Figs. 4.16, 4.17). Using mean parameters gives a representation of the response

of the 'average locust'. The model of the average locust provides a good representation of the behaviour over most of the response, except at the end where the modelled response is too oscillatory. The response to each individual pulse in a 20 pulse CFT is given also in Figs. 4.16 and 4.17, both the actual data from one locust and the modelled response being presented. The results again show that the modelled response is oscillatory at the end of the pulse. It is also clear that a steady state pulse shape is reached when the IPF=12.5Hz. When the IPF=40Hz (Fig. 4.17B) for higher n the shapes of successive pulse responses are similar. The increase and the subsequent decrease in the pulse magnitude when IPF=40Hz is very clear. Comparing the modelled response and the response for one locust also shows that as the IPF and/or n increase the modelled pulse shape shows increasing deviation from the actual pulse shape.

By calculating the poles of the model it was found that the average model poles show the same characteristics as those seen for individual locusts. In general, the magnitude of the real part of the poles tends to decrease with pulse number before reaching an approximately constant value. The real parts of the poles are smaller when the IPF=40Hz compared to when the IPF=12.5Hz, supporting the observation that as the IPF or n increase the response to each input deviates more from the response of the isolated pulse. For the first pulse one of the poles has a large magnitude so decays quickly, contributing little to the overall response, hence explaining why for a single pulse a second order fit is acceptable.

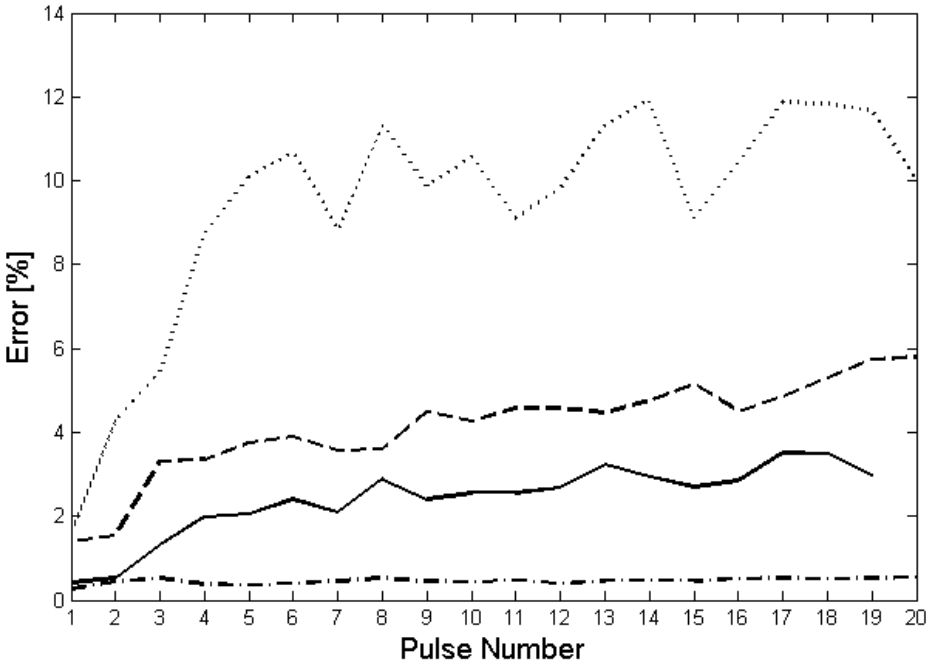

FIGURE 4.14: Median errors when fitting to the nth pulse in a CFT, The fit using a 2 pole model for IPF=12.5Hz (- - -) and IPF=40Hz (. . .) and the fit using a 3 pole model for IPF=12.5Hz (- . -) and IPF=40Hz (—) are given.

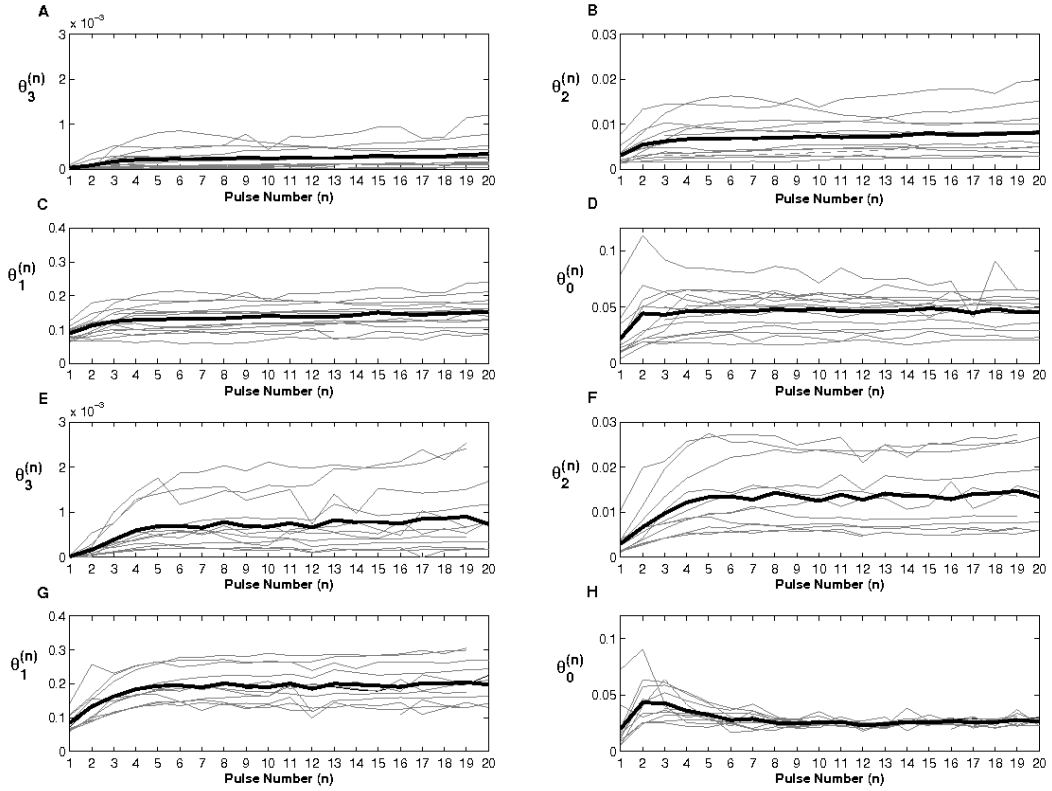

FIGURE 4.15: Change in parameter values with pulse number, n in a CFT, A,B,C,D show parameter changes in a CFT of IPF=12.5Hz and E,F,G,H in a CFT of IPF=40Hz. Parameters were estimated for each locust using a 3rd order model, with means (bold). In general, except for the estimate of θ_0 when using a third order model (H), parameter values increase before saturating at pulse numbers greater than approximately six.

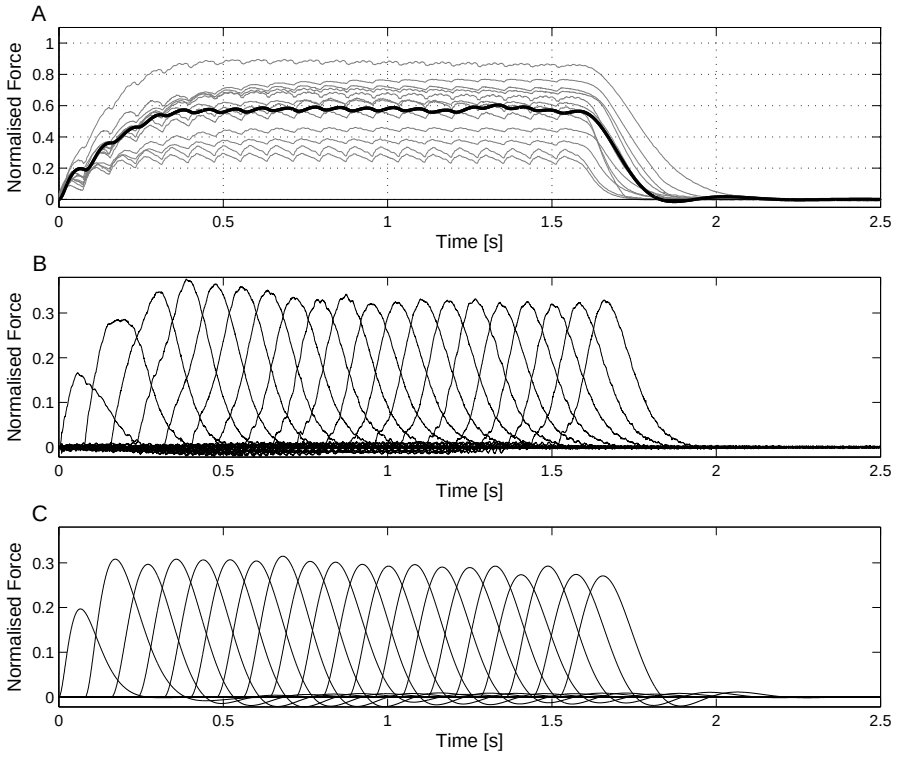

FIGURE 4.16: Force response to a 20 pulse CFT (IPF=12.5Hz). (A) The individual locust data is measured and mean (bold) estimated from average model parameters. (B) Experimentally decomposed responses from one locust. (C) Estimated response for each pulse. The main discrepancies in fit are that the end of the modelled pulse is slightly oscillatory.

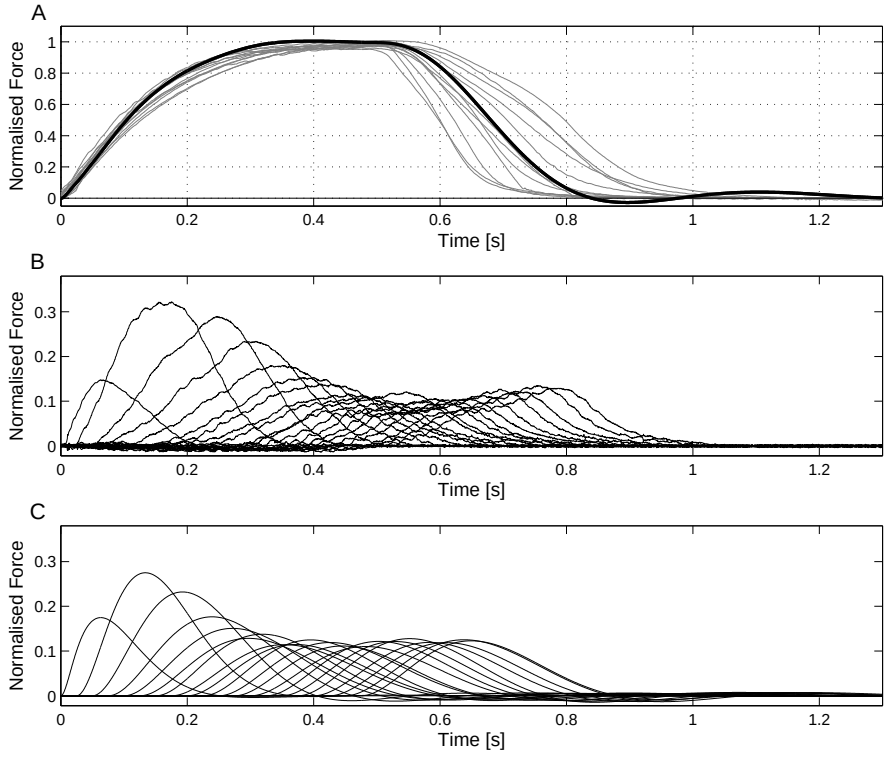

FIGURE 4.17: Force response to a 20 pulse CFT (IPF=40Hz) for twelve locusts. (A) The individual locust data (faint lines) is measured and 'average locust' (bold) estimated from average model parameters. (B) Experimentally decomposed responses from one locust. (C) Estimated response for each pulse. The main discrepancies in fit are that the location of the peak force occurs too soon in modelled data and that the end of the modelled response is oscillatory.

4.7 Discussion

4.7.1 Estimated Models

In modelling each contraction in CFTs using a linear model with a simple form, changes in both the form of the model and model parameters are easily tracked. This is in contrast to the few previous studies that have been done on decomposing muscle force into contributions from individual stimuli [50, 74–76]. In these, where models were developed, a general model was fitted to each contraction, with no attempt made to minimise model order or investigate how the model may change over the course of the CFT. More focus was given to the properties of each force trace (e.g. twitch contraction time) as opposed to the estimated model parameters.

The locust extensor muscle shows similar nonlinear summation to mammalian muscle with facilitation and depression occurring in pulses that are not well separated [71, 72]. This similarity is expected. Ebashi [7] recognised that calcium was the key regulatory factor of muscle contraction at the molecular level in all kinds of muscle. Facilitation and depression are thought to be caused, at least in part, by mechanisms involving calcium [71, 72]. The facilitation is thought to be caused by an improved transmission of force and prolonged release of Ca^{2+} [72] and the depression by a first order saturable reaction, such as Ca^{2+} binding to troponin [71]. There have been relatively few studies into insect muscle [80]. Demonstrating that facilitation and depression occur in the locust extensor muscle reinforces the hypothesis that calcium is key to muscular contraction and that mechanisms involving calcium are responsible for some of the non-linear behaviour.

The summation of successive pulses in a CFT was nonlinear in the sense that the responses to subsequent stimuli differ. However, in most cases the responses to individual pulses in a CFT could be modelled as quasi-linear, with the time constants of nonlinear effects being large compared to the pulse response. This shows that the processes responsible for nonlinear effects are slow compared to the processes involved in each individual contraction. Trends were seen in parameters estimated for successive pulses in the CFT. In general the value of the parameters describing each subsequent pulse increase before saturating and reaching a constant value. The fact that the parameter values saturate suggests that the processes behind the nonlinear behaviour are saturable. This ties in with the non-linearities being caused by the processes suggested by [72] and [71] (improved force transmission, prolonged release of Ca^{2+}, first order saturable reaction such as Ca^{2+} binding to troponin).

Both well-separated pulses and low IPF two-pulse trains can be modelled adequately using a second order, linear model; use of a third order model improves the fit. Modelling the response as a second order system is supported by research by [50–53] and [156]. As the IPF increases for the two pulse train, the errors using a two pole model increase and a three pole model

becomes necessary to model the response. The fact that an extra parameter is needed suggests an extra process in the contraction becomes important as the IPF increases. This is confirmed by the fact that the magnitude of the real parts of all the poles (including the extra pole) decreased as the IPF increased. This indicates an increase in the associated time constants.

Muscular contraction is well described by Huxley's sliding filament theory [27]. Mannard and Stein [51] suggest that despite many rate constants being involved in activation, as described by Huxley's theory, only two are rate-limiting. However, as pulses sum and the IPF increases the present study finds an extra process becomes important. [52, 53] suggest that of the two observed rate-limiting steps one is involved with visco-elastic properties and the other with the reuptake of Ca^{2+} into the sarcoplasmic reticulum. Possible processes responsible for the extra parameter found here are the limited number of available binding sites, or the increase in Ca^{2+} concentration that occurs as pulses sum.

A third order model is not a common choice for modelling isometric muscle. However, Zhou *et al* [68] find that although the muscle alone is best described by a second order model with double poles and a time delay, when the joint is included in measurements the model is modified by the introduction of an extra pole and zero. In the experiments described here the effect of the joint is also included in measurements. More commonly the response of isometric muscle is described by two coupled, linear, second order ordinary differential equations (effectively one fourth order ODE) followed by a non-linear term. In some locusts, however, a fourth order model was found to overfit the data. In other locusts, using a fourth or higher order model slightly reduced errors in the fit, yet the location of peak force was still wrongly predicted and the end of the response still modelled as too oscillatory.

When the IPF is high and the number of pulses in the train increases, the errors in using a third order linear model increase. The main discrepancies in the fit were not reduced substantially by using a linear model of higher order. The large errors when long, high frequency pulse trains were used suggest that the assumption that the response to each pulse is linear may not hold. The main discrepancies between measured and estimated data were in the location of the peak force and across the decaying part of the response, which was modelled as being too oscillatory.

4.7.2 Linear Approximation

In estimating a model of the twitch it was assumed that the response was linear. The muscle is known to exhibit non-linear properties [1, 39, 50, 71–73, 88]. In the case of a single twitch, however, it was found that the nonlinearities are weak and a linear model provides a good fit to data. Here, a linear model is taken to mean that the relation between input and output can be described using a linear equation, where a linear equation is an algebraic relation in which each term is a constant or the product of a single variable and a constant. The justification for

using a linear model to describe the twitch response can be found by considering the processes that occur during muscle contraction.

It is thought that saturable reactions involved in the activation process do not affect the twitch response, as the input is very low, hence the muscle operates in a linear region well before the occurrence of saturation. The binding of calcium ions to troponin is a saturable reaction that occurs during muscle activation; saturation occurs due to the limited number of available binding sites. For the case of a single twitch however, the input is low, resulting in few binding sites being occupied during contraction [24]. Moreover, since the input pulses are well separated the muscle relaxes between stimulations, freeing binding sites as calcium is pumped back into the SR and returning the muscle to its original state. The response to a single input pulse should also not be modified by the increasing stiffness of the muscle because the muscle is in a relaxed state when the next stimulus pulse occurs since the pulses are well separated.

Muscle fatigue can be characterised by the muscles failure to maintain the force output [17]. Fatigue often occurs during repeated activation of the muscle and is increased by increasing the stimulation frequency or intensity [20]. Single stimulus pulse inputs should not cause muscle fatigue as the stimulus is of very low intensity and frequency. The relative importance of muscle properties are task specific [88], hence muscle fatigue is not relevant to the single twitch response. Thus it is thought that a linear model fits well to the response to an isolated pulse since many of the effects that introduce non-linearities are unlikely to occur in the response to a single pulse. This is not the case for pulses that are not well separated such that summation occurs.

4.8 Conclusions

The dynamics of the responses of individual pulses vary depending on the input conditions. This is attributed to the non-linear behaviour of the muscle. For most cases this behaviour could be approximated as quasi-linear. When the IPF was low and the number of pulses in the train small, a second order model provided a reasonable fit to each pulse and a third order model a better fit. The fit using a second order model deteriorates with increasing IPF. For moderate IPF and longer CFTs the second order model breaks down and a third order model is necessary to model each pulse. When the input comprised long CFTs of high IPF the assumption that the response was linear could not be confirmed. No linear model of any order provided a good fit to individual pulse data.

In this chapter the behaviour and dynamics of individual pulses that make up summed isometric contractions were considered. This provides more insight into the behaviour of the muscle and the non-linear summation of the response to individual pulses under isometric conditions,

providing a solid background for the studies in subsequent chapters. In the next chapter the response to pulse train inputs is considered.

Chapter 5

Isometric Force Response to Pulse Trains: A Predictive Model of the Isometric Force Response

5.1 Introduction

In the preceding chapter, the response to each pulse in a CFT was considered. Fitting a model to each pulse in a CFT provides insight into the behaviour of the muscle during a sustained contraction. It does not, however, provide a model of the force response that has predictive capability. In each instance force was fitted to measured data, as opposed to being modelled. A predictive model is developed in this chapter.

In this chapter, predictive isometric models that exist in the literature are considered. A new model, adapted from an existing model is also presented. The ability of the existing isometric models to predict the isometric force response to pulse train inputs is assessed alongside the new Adapted model. The modelling capabilities of the models are compared by considering goodness of fits in the least squares sense and using Akaike's and Bayesian information criteria (AIC, BIC). The ability of each model to describe the underlying behaviour, i.e. the response of each individual pulse in a contraction, is also investigated. The new Adapted model was found to provide the best description of the isometric force response. This model was further investigated with regard to parameter sensitivity and the behaviour of the model as related to physiological processes.

5.2 Methods

The ability of a range of models to capture the isometric force response to a pulse train input of the form

$$u(t) = \sum_{i=1}^{n} \delta(t - t_i) \tag{5.1}$$

is assessed in this chapter. Input pulses (3ms in duration and of 5V amplitude) are assumed to be equivalent to impulses. The preceding chapter showed that the assumption of the response to each individual pulse being equivalent to the impulse response was reasonable. The physical set up is described in Chapter 3, however the specifics of the stimulation protocol are discussed below.

5.2.1 Fitting Algorithm

In the preceding chapter, fits to individual pulse data were found using a black-box model. In this chapter, the model structures are pre-determined (these are defined in the subsequent section). Model structures are based on those used in the literature and use prior knowledge. Parameters of such models are determined by fits to measured data. Assuming a prior model structure, then estimating corresponding parameters is a form of grey-box modelling. Grey-box models are based on both experimental data and physical insight into the system. The advantage of this approach is that some *a priori* knowledge about the system can be introduced.

Parameters were estimated by finding the values that gave the smallest squared differences between the model and measured force data, when using training data. This was done using the MATLAB function `lsqnonlin` and a fixed step ODE solver. An initial estimate for parameters was made, then parameter values iterated using a trust-region-reflective algorithm to find the parameters which provided the best fit to data [157]. The parameter optimisation routine was re-run using a range of initial parameter estimates to avoid estimating local minima.

The data was split into training and test data sets. The model parameters were estimated using the training data, and minimising the least squares error between the training data and the estimated response. The model and these estimated parameters were then applied to test data. The fit to the test data was used to evaluate the model. This method ensures that the trained model parameters do not overfit the model. Using a separate training data set to estimate model parameters reduces overfitting, which as noted previously occurs when the model fits to noise as opposed to the underlying relation [158].

5.2.2 Stimulation Routine

In experiments the amount of data that can be collected is limited as muscle fatigue increases with input. Fatigue is characterised by the failure of the muscle to maintain the expected force output and is seen in results as a reduction in the maximum force over time in response to a repeated input. The inclusion of a suitable recovery period counteracts the effects of fatigue, however there is a trade off as this increases the time that the stimulating electrodes are inserted into the muscle, and so the chances of the muscle becoming damaged. As well as this physical constraint, care was take to ensure that both training and test data contained a rich range of frequencies to stimulate a range of muscle behaviour.

By stimulating the model with more physiologically relevant inputs, developed models can be tested over a relevant range of behaviour. During experiments the ETi muscle is stimulated directly, leading to contraction of the entire muscle due to activation of the terminals of the FETi motor neuron. FETi activity is associated with fast movements such as those that occur during jumping, kicking or hopping [8, 10, 144, 152, 159]. Examples of the FETi spike signal recorded during a kick were taken from the literature. These signals were simplified, as shown in Fig. 5.1, by replacing each maximum with a single input pulse (of 3ms duration and 5V amplitude). Five physiological inputs were found using this method with FETi data taken from Fig. 2A in [152], Figs. 4A and 8A in [159] and Fig. 5 from [144]. Five simplified kick signals were obtained and they are shown in Fig. 5.2. Table 5.1 summarises the properties of these kick signals. These kick signals were used as inputs to provide physiologically relevant test data.

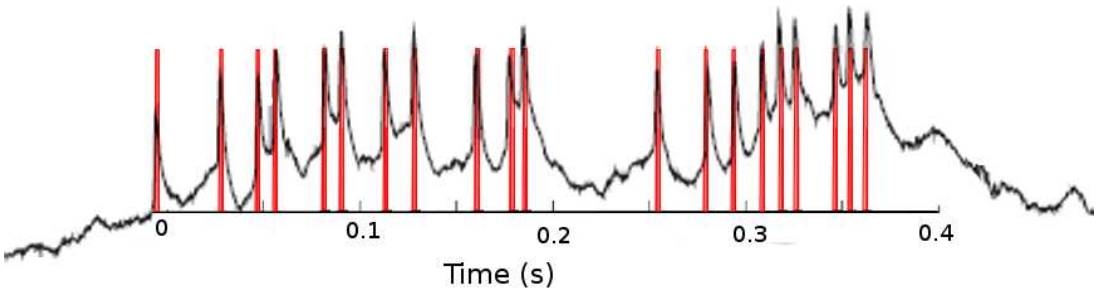

FIGURE 5.1: Method of obtaining simplified kick input. Each spike in the FETi recording (—) is approximated as a pulse of 3ms duration and 5V magnitude (—).

In addition to physiological inputs, some general pulse inputs were also used to stimulate the muscle. The highest instantaneous frequency in the FETi activity recorded during a kick is of the order of 100Hz. Signals with instantaneous frequencies up to 100Hz were therefore used to stimulate the muscle. If the muscle is stimulated repeatedly with inputs that result in high

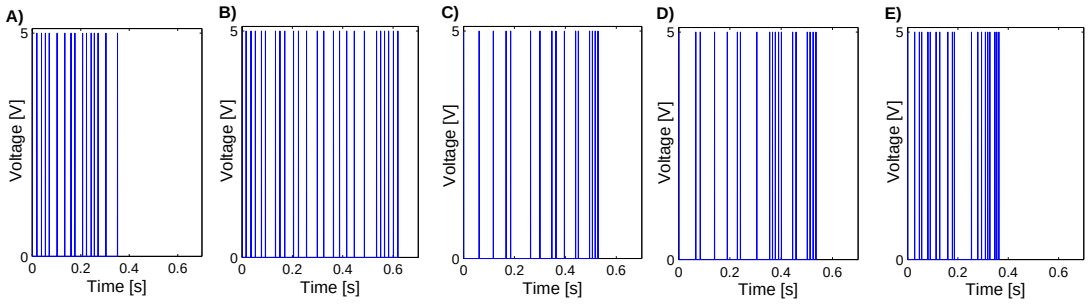

FIGURE 5.2: Simplified kick inputs used to stimulate muscle. A) Kick signal 1, obtained from Fig. 2A in [152], B) Kick signal 2, obtained from Fig. 4A in [159], C) Kick signal 3, obtained from Fig. 8A in [159], D) Kick signal 4, obtained from Fig. 8A in [159], E) Kick signal 5, obtained from Fig. 5 in [144].

	Duration of activity (ms)	Number of spikes	Lowest instantaneous frequency (Hz)	Highest instantaneous frequency (Hz)
Kick1	336	16	20	78
Kick2	688	25	20	63
Kick3	567	17	5	90
Kick4	544	19	15	90
Kick5	381	20	15	108
Mean	503	19	15	86

TABLE 5.1: Summary of the properties of the FETi signals recorded during a kick.

force outputs, the muscle fatigues [96]. This results in the decay of maximum force over time. To minimise the effects of fatigue, high-frequency pulse trains were separated by 5 individual pulses with IPI of 5s. As well as minimising fatigue, the inclusion of these separated pulses enables any decay in force levels, due to fatigue, to be monitored. Schematic representations of the input types used to stimulate the muscle are given in Fig. 5.3. The specific stimulation protocol is summarised in Fig. 5.4, with an example of the input and force output in the time domain given in Fig. 5.5.

To evaluate model performance, parameters were estimated using a training data set, and the performance evaluated using a different test data set. The set of training data was chosen by training the model with different combinations of the different data sets shown in Fig. 5.4. The physiological data was not used in training as this provides good test data to assess the ability of the model to predict the response to a physiologically relevant input. Combinations of all other data sets were used. The final set of training data was chosen as it provided small errors when fitting to test data, including physiologically relevant data, whilst keeping the cost of input data low. Training data consisted of five isolated pulses, a 40 pulse CFT with IPI=15ms, a pulse train of 29 pulses which increased then decreased in frequency (back to initial value) with a maximum frequency of 100Hz and minimum of 10Hz, and a 60 pulse train which decreased then increased in frequency (back to start value) with a minimum frequency

of 1Hz and maximum of 50Hz. The training data sets are shown in Fig. 5.5 by the highlighted sections. Test data consisted of both general pulse trains and physiological kick type data.

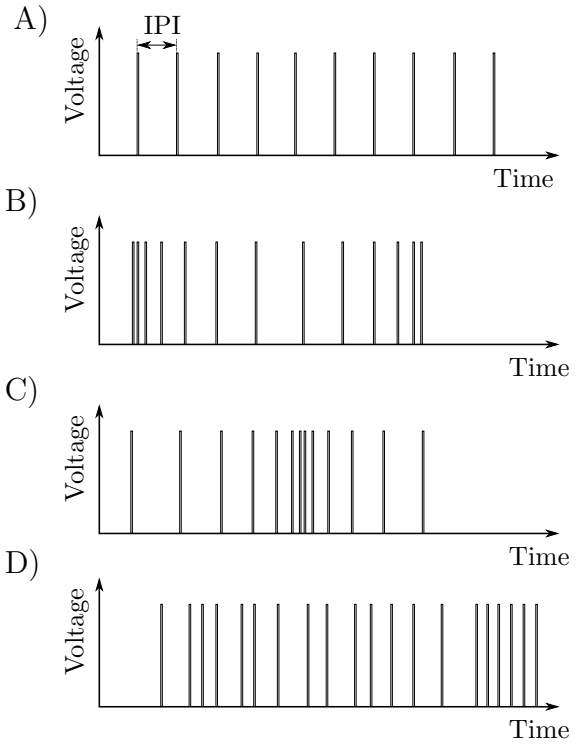

FIGURE 5.3: Schematic representation of different input types. A) CFT, B) NCFT of decreasing-increasing frequency, C) NCFT of increasing-decreasing frequency, D) NCFT Physiological type input.

5.3 Candidate models

A range of different models were used to describe the isometric force response. These models were selected due to their popularity, and the fact they all take a pulse train $u(t)$ as an input and produce isometric force $F_m(t)$ as an output. The force $F_m(t)$ was normalised with respect to the maximum tetanic force in each locust and models fitted to normalised data. In this chapter all experiments were performed at an FT angle of 80°. This means that for each locust one factor is used to convert all tibial force recordings into a muscle force. In normalising the data this factor is changed, but no information is lost. The modelled normalised force can be converted into an actual force. The following models from the literature were used to describe the isometric force response.

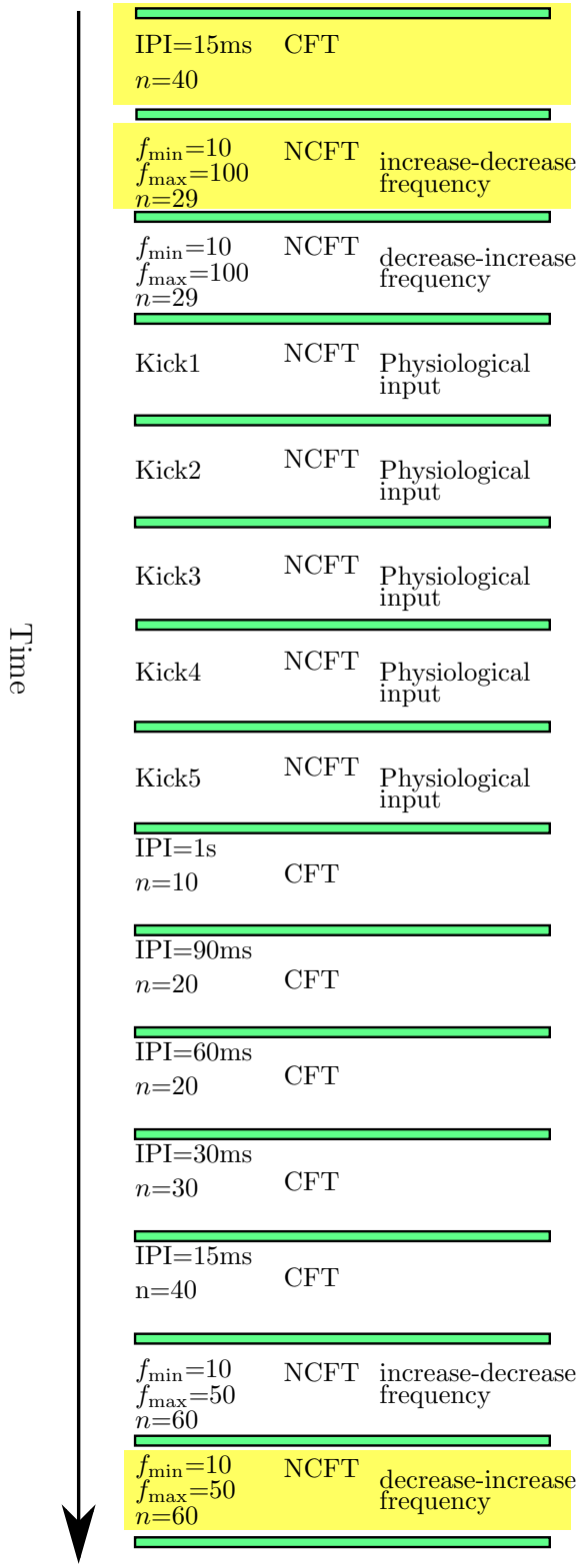

FIGURE 5.4: Routine used to stimulate ETi muscle. Each pulse train is separated by a 5 pulse CFT with IPI=5s; this input is represented by the rectangular green blocks. The highlighted sections indicate the training data set. In the increasing-decreasing and decreasing-increasing NCFTs $f_{\min}$ defines the minimum instantaneous frequency and $f_{\max}$ the maximum.

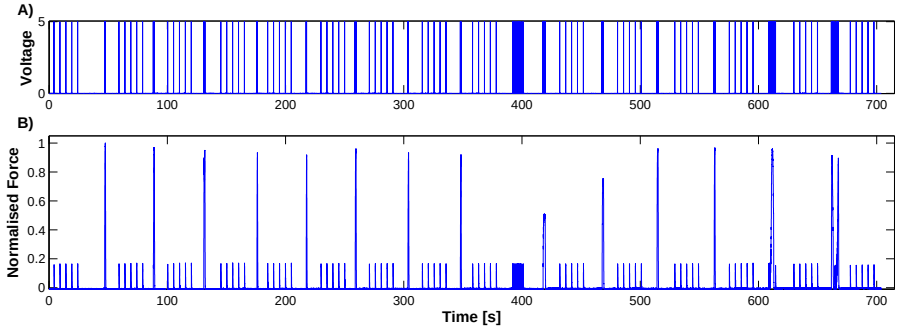

FIGURE 5.5: Example of A) input, B) output data used to fit to and assess models

5.3.1 Linear Model

In the analysis of individual pulses (Ch. 4) it was found that a third order model was of optimal order for fitting over a range of pulse frequencies, therefore a linear model of third order is used, i.e.

$$\theta_3 \dddot{F}(t) + \theta_2 \ddot{F}(t) + \theta_1 \dot{F}(t) + F(t) = \theta_0 u(t) \tag{5.2}$$

This model has 4 parameters θ_3, θ_2, θ_1, θ_0 with units of s^3, s^2, s, and dimensionless respectively, for the case where the force is normalised.

5.3.2 Wiener Model

For a pulse train input of the form given in Eq. (5.1), the Hammerstein model reduces to a linear model and so is not considered, instead the related Wiener model is considered. A second-order linear differential equation is used to describe the linear dynamics. A second-order model was chosen as this is a popular choice for the linear section of a Hammerstein model. Furthermore, a second order model provided an acceptable linear fit to the twitch response (Ch. 4). The static nonlinearity was assumed to have a similar form to that of existing models [28, 35],

$$\theta_2 \ddot{q}(t) + \theta_1 \dot{q}(t) + q(t) = \theta_0 u(t) \tag{5.3}$$

$$F(t) = \frac{q(t)^m}{q(t)^m + k^m} \tag{5.4}$$

This model has 5 parameters θ_2, θ_1, θ_0, m, and k with units of s^2, s, dimensionless, dimensionless, and dimensionless respectively, for the case where the force is normalised. A dummy variable $q(t)$ is used to couple the nonlinear to the linear model.

5.3.3 Cascade Model

The cascade model is a special case of a Wiener model. Unlike the Wiener model described above the linear dynamics are assumed to be of fourth-order. This model is a popular choice in the literature [28]. It is given by,

$$\theta_4 \dddot{q}(t) + \theta_3 \ddot{q}(t) + \theta_2 \ddot{q}(t) + \theta_1 \dot{q}(t) + q(t) = \theta_0 u(t) \tag{5.5}$$

$$F(t) = \frac{q(t)^m}{q(t)^m + k^m} \tag{5.6}$$

This model has 7 parameters, θ_4, θ_3, θ_2, θ_1, θ_0, m, and k with units of s^4, s^3, s^2, s, dimensionless, dimensionless, and dimensionless respectively, for the case where the force is normalised. The variable $q(t)$ is a dummy variable, used to couple the nonlinear and linear equations. It is commonly assumed to represent the calcium release from the SR [28]. It is often the case that the linear dynamics (Eq. 5.5) are written as two coupled second order ODEs, with the T-tubuli depolarisation response given as an intermediate step to finding the calcium release [28].

5.3.4 Ding et al Model

Ding *et al* [20] find their model gives good fits to data. It is given by

$$\dot{q}(t) + \frac{q(t)}{\tau_c} = u(t) \tag{5.7}$$

$$\dot{C}_N(t) + \frac{C_N(t)}{\tau_c} = \frac{q(t)}{\tau_c} \sum_i^n R_i \tag{5.8}$$

$$x(t) = \frac{C_N(t)}{k + C_N(t)} \tag{5.9}$$

$$\dot{F}(t) + \frac{F(t)}{\tau_1 + \tau_2 x(t)} = A x(t) \tag{5.10}$$

$$R_i = 1 + (R_o - 1) \exp\left(\frac{-(t_i - t_{i-1})}{\tau_c}\right) \tag{5.11}$$

This model has 6 parameters, τ_c, τ_1, τ_2, A, R_o, and k with units of s, s, s, s^{-1}, dimensionless, and dimensionless respectively, for the case where the force is normalised. The variables R_i, $C_N(t)$, $q(t)$ and $x(t)$ are intermediate stages in the model. The variable $q(t)$ is used as an

intermediate in calculating $C_N(t)$, which is said to represent the normalised amount of the Ca^{2+} complex. The variable $x(t)$ describes the non-linear saturation, and R_i (dimensionless) is used to account for nonlinear summation when the muscle is stimulated by two closely spaced pulses, where t_i defines the time of the i^{th} stimulation.

5.3.5 Bobet and Stein Model

Bobet and Stein [73] present a model that they find to provide good fits to the force produced by cat muscle. The model is

$$\dot{q}(t) + aq(t) = u(t) \tag{5.12}$$

$$x(t) = \frac{q(t)^m}{q(t)^m + k^m} \tag{5.13}$$

$$\dot{F}(t) + bF(t) = Bbx(t) \tag{5.14}$$

$$b = b_o \left(1 - \frac{b_1 F(t)}{B}\right)^2 \tag{5.15}$$

This model has 6 parameters, a, m, k, b_o, b_1, and B with units of s^{-1}, dimensionless, dimensionless, s^{-1}, dimensionless, and dimensionless respectively, for the case where the force is normalised. The parameter a is thought to represent the decay of free calcium concentration, m and k define a nonlinearity that might represent the binding of calcium ions to troponin, and B is a scale factor. The nonlinearity in Eq. 5.14 is thought to represent the decay of force under different conditions.

5.4 Development of Adapted Model

The model of Ding *et al* [20] (described by Eqs. (5.7) - (5.11)) provides reasonable fits to data, however, the physiological meaning of the model and parameters is hard to interpret. A sensitivity analysis by Frey Law and Shields [82] that looks at trying to better understand the relationship between model parameters and muscle contractile properties finds the parameter definitions of Ding *et al* to only be partially supported. Furthermore, no physical reason was given, or could be found, as to why the time constants in Eqs. (5.7) and (5.8) should be the same. Therefore, a model variation in which the time constant in Eq. (5.7) was allowed to differ from that in Eq. (5.8) was investigated, giving the model the following form:

$$\dot{q}(t) + \frac{q(t)}{\tau_R} = u(t) \tag{5.16}$$

$$\dot{C}_N(t) + \frac{C_N(t)}{\tau_c} = \frac{q(t)}{\tau_c} \sum_i^n R_i \tag{5.17}$$

$$x(t) = \frac{C_N(t)}{k + C_N(t)} \tag{5.18}$$

$$\dot{F}(t) + \frac{F(t)}{\tau_1 + \tau_2 x(t)} = Ax(t) \tag{5.19}$$

$$R_i = 1 + (R_o - 1) \exp\left(\frac{-(t_i - t_{i-1})}{\tau_c}\right) \tag{5.20}$$

This introduces an extra parameter, τ_R. It was found that the resultant fit was insensitive to the value of the parameter τ_R, and good fits could be obtained for a range of values of τ_R. The original model was thus simplified and adapted in an attempt to reduce parameter redundancy and make the essential characteristics of the model clearer. The form of the simplified model is given as

$$\dot{C}_N(t) + \frac{C_N(t)}{\tau_c} = u(t) \tag{5.21}$$

$$x(t) = \frac{C_N(t)^m}{C_N(t)^m + k^m} \tag{5.22}$$

$$\dot{F}(t) + \frac{F(t)}{\tau_1 + \tau_2 x(t)} = Ax(t) \tag{5.23}$$

This model has 6 parameters, τ_c, τ_1, τ_2, m, k, and A. For the case where $F(t)$ is normalised the time constants τ_1, τ_2 and τ_c have units of seconds, A units of s^{-1}, and all other parameters are dimensionless. This model is termed the 'Adapted model'.

In the Adapted model, the order of the model is reduced, and the parameter τ_R neglected, hence, the state variable $q(t)$ is not required. The relation between input and output is second rather than third order. The variable R_i, which was said to account for the non-linear summation in response to two closely spaced pulses, has been removed. This was done as R_i is a function of discrete as opposed to continuous time, so it is hard to physically interpret its influence on a continuous time system and model. Instead, an extra parameter, m, was included to allow the specific form of the non-linearity to change. Figure 5.6 shows how the saturation curve changes with the value of m.

The developed model needs to be capable of capturing the nonlinear behaviour and the changing shape of individual pulses found in Chapter 4 (see Figs. 4.10, 4.16, 4.17). To better understand the behaviour of the model described in Eqs. (5.21)-(5.23) and establish if it is capable of

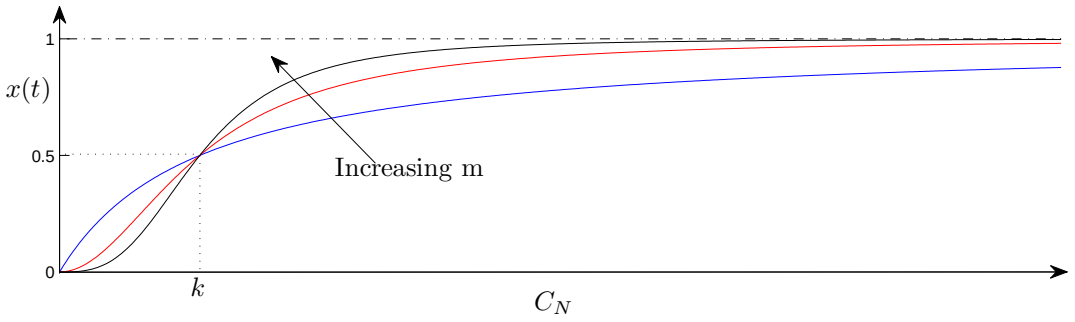

FIGURE 5.6: The change in saturation nonlinearity given in Eq. (5.22) with m.

capturing this behaviour, the total force response and corresponding contribution by each individual pulse was computed when using the model. This was done for both a high and low frequency CFT. The ability of the model to replicate the behaviour of Figs. 4.16 and 4.17 was assessed. In each simulation parameters were fixed with $\tau_c = 0.1$, $\tau_1 = 0.1$, $\tau_2 = 0.1$, $k = 1$, $A = 5$, $m = 2$. Figure 5.7 gives the results of this simulation. From this it is clear that the model is able to capture the fundamentals of the underlying behaviour and is a reasonable candidate model. Therefore the Adapted model described by Eqs. (5.21)-(5.23) is also used as a candidate model.

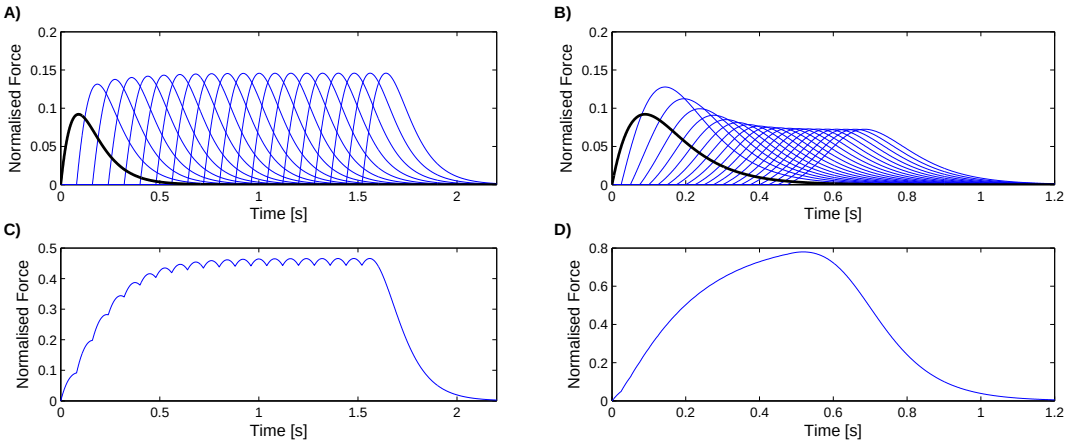

FIGURE 5.7: Simulated force response when using the model given in Eqs (5.21)-(5.23). A) Contribution of individual pulses to total force response for low frequency CFT (12.5Hz), B) contribution of individual pulses to total force response for high frequency CFT (40Hz), C) total force response for low frequency CFT (12.5Hz), D) total force response for high frequency CFT (40Hz). Corresponding experimental data is given in Figs. 4.16 and 4.17.

5.4.1 Behaviour of the Model Under Different Assumptions

It has been shown that the Adapted model is capable of capturing the nonlinear behaviour and changing shape of the individual pulse responses. To establish if a further simplified form of

the Adapted model is also capable of modelling this behaviour, the response of the model to given parameters under different assumptions was investigated. In each simulation parameters were again fixed so $\tau_c = 0.1$, $\tau_1 = 0.1$, $\tau_2 = 0.1$, $k = 1$, $A = 5$, $m = 2$.

5.4.1.1 Assumption 1

Small C_N was assumed. This linearises the problem and the model equations become

$$\dot{C}_N(t) + \frac{C_N(t)}{\tau_c} = u(t) \tag{5.24}$$

$$\dot{F}(t) + \frac{F(t)}{\tau_1} = AC_N(t) \tag{5.25}$$

The resultant force responses are given in Fig. 5.8. It is clear that by linearising the model one cannot replicate the changing pulse shapes seen in experimental data.

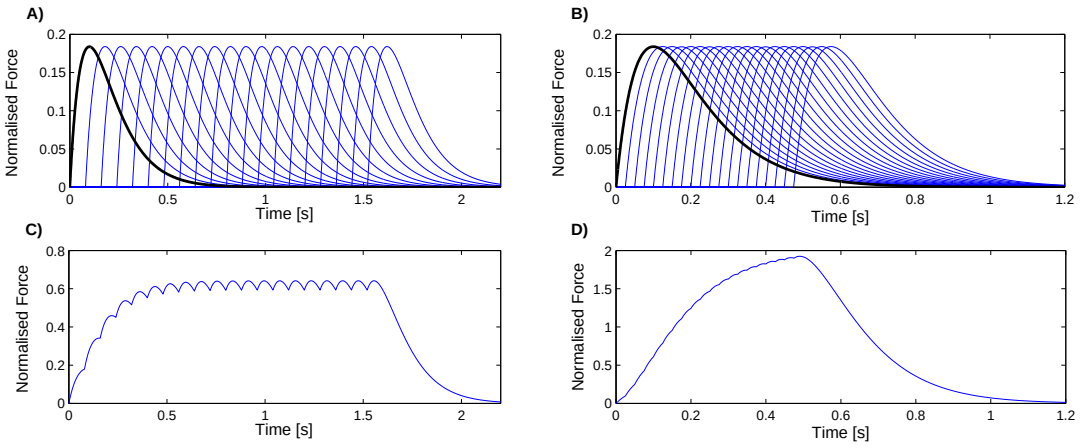

FIGURE 5.8: Simulated force response when using the Adapted model with Assumption 1. A) Contribution of individual pulses to total force response for low frequency CFT (12.5Hz), B) contribution of individual pulses to total force response for high frequency CFT (40Hz), C) total force response for low frequency CFT (12.5Hz), D) total force response for high frequency CFT (40Hz).

5.4.1.2 Assumption 2

It is assumed that $\tau_2 = 0$, giving the following model:

$$\dot{C}_N(t) + \frac{C_N(t)}{\tau_c} = u(t) \tag{5.26}$$

$$x(t) = \frac{C_N(t)^m}{C_N(t)^m + k^m} \tag{5.27}$$

$$\dot{F}(t) + \frac{F(t)}{\tau_1} = Ax(t) \tag{5.28}$$

This model has 5 parameters, τ_c, τ_1, m, k, and A. The corresponding force behaviour is given in Fig. 5.9. The model is able to replicate the changing pulse shape. The change in pulse shape is dependent upon the frequency, this is also the case in the experimental data. The model with $\tau_2 = 0$ is capable of describing the fundamentals of the underlying behaviour. The Adapted model with $\tau_2 = 0$ is therefore used as a candidate model. This model is termed the 'Simplified Adapted model'.

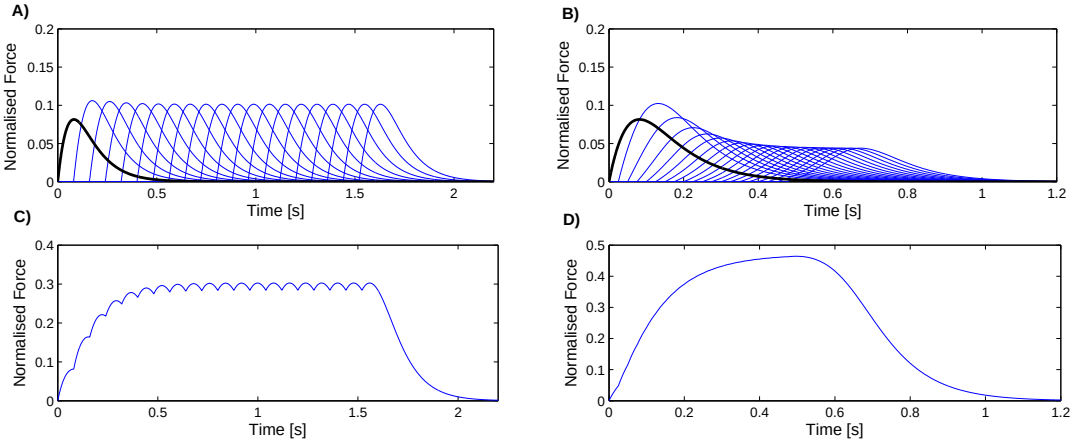

FIGURE 5.9: Simulated force response when using the Adapted model with Assumption 2. A) Contribution of individual pulses to total force response for low frequency CFT (12.5Hz), B) contribution of individual pulses to total force response for high frequency CFT (40Hz), C) total force response for low frequency CFT (12.5Hz), D) total force response for high frequency CFT (40Hz).

Assumption 3

It is assumed that that the nonlinearity appears only as a multiplying factor to the time constant τ_2 and so the modelled force is,

$$\dot{C}_N(t) + \frac{C_N(t)}{\tau_c} = u(t) \tag{5.29}$$

$$x(t) = \frac{C_N(t)^m}{C_N(t)^m + k^m} \tag{5.30}$$

$$\dot{F}(t) + \frac{F(t)}{\tau_1 + \tau_2 x(t)} = AC_N(t) \tag{5.31}$$

Figure 5.10 depicts the simulated force behaviour under this assumption. In each case the pulse magnitude increases, the removal of the extra non-linear term means that the force saturation is not modelled and the simulated force keeps increasing with increasing input. In real data there is a limit to the maximum force (tetanus). This is not replicated, hence this simplification of the model is poor and so not considered further.

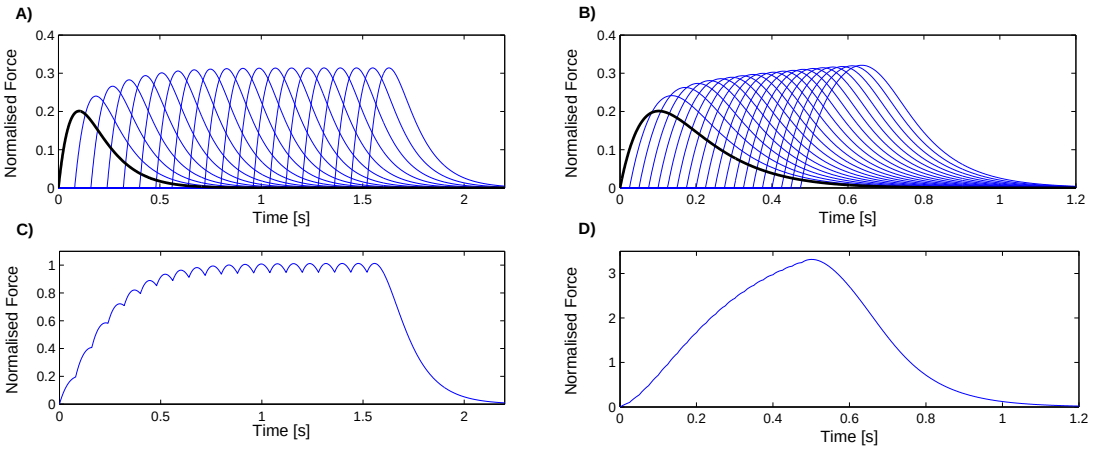

FIGURE 5.10: Simulated force response when using the Adapted model with Assumption 3. A) Contribution of individual pulses to total force response for low frequency CFT (12.5Hz), B) contribution of individual pulses to total force response for high frequency CFT (40Hz), C) total force response for low frequency CFT (12.5Hz), D) total force response for high frequency CFT (40Hz).

5.5 Performance of Models

The performance of each model (Linear, Wiener, Cascade, Ding, Bobet and Stein, Adapted, Simplified Adapted) was assessed by looking at goodness of fits, AIC and BIC, parameter sensitivity and the capability of the model to replicate the underlying behaviour of individual pulses.

5.5.1 Goodness of Fits

For each model, parameters were estimated in five different locusts; Tables 5.2 to 5.8 give estimated parameters and errors for each model. The errors in estimation using each model are summarised in Table 5.9. Presented errors refer to the least squares fit between model and data. Errors in the fit to training data (E_{train}), the fit test data which consists of general pulse trains (E_{test1}[1]), and the fit to test data from kick type inputs (E_{kick}[2]), are given. An example of the fit to training data for one locust (termed locust LE) using each model is given in Fig 5.11, the fit to pulse train test data in Fig. 5.12, and kick test data in Fig 5.13. This locust is representative of, and produced qualitatively similar results to the set of locusts.

TABLE 5.2: Estimated parameters and least square errors between measured and modelled data when using a **Linear model**. Errors are given as percentages for the fit to training data (E_{train}), the fit to general pulse data (E_{test1}) and the fit to kick type inputs (E_{kick}).

Locust	θ_3 (s^3)	θ_2 (s^2)	θ_1 (s)	θ_0	E_{train}	E_{test1}	E_{kick}
LA	8.0×10^{-6}	3.3×10^{-3}	0.28	0.025	11	14	10
LB	4.2×10^{-6}	5.4×10^{-3}	0.23	0.022	10	14	7.8
LC	4.1×10^{-5}	3.6×10^{-3}	0.26	0.023	13	16	10
LD	2.8×10^{-5}	4.0×10^{-3}	0.26	0.024	13	15	9.1
LE	2.5×10^{-5}	3.6×10^{-3}	0.26	0.024	12	15	10
Mean	2.1×10^{-5}	4.0×10^{-3}	0.26	0.023	12	15	9.4

TABLE 5.3: Estimated parameters and least square errors between measured and modelled data when using a **Wiener model**. Errors are given as percentages for the fit to training data (E_{train}), the fit to general pulse data (E_{test1}) and the fit to kick type inputs (E_{kick}).

Locust	θ_2 (s^2)	θ_1 (s)	θ_0	m	k	E_{train}	E_{test1}	E_{kick}
LA	1.0×10^{-3}	0.011	0.20	1.6	0.013	2.7	2.9	1.8
LB	5.9×10^{-6}	0.011	0.19	1.6	8.8×10^{-5}	3.7	4.1	2.7
LC	1.6×10^{-6}	0.010	0.17	1.6	2.0×10^{-5}	2.9	2.7	1.6
LD	9.4×10^{-7}	0.012	0.17	1.6	1.1×10^{-5}	2.9	2.3	1.5
LE	1.9×10^{-1}	0.011	0.17	1.6	2.3	2.5	2.5	1.2
Mean	3.8×10^{-2}	0.011	0.18	1.6	0.46	2.9	2.9	1.8

TABLE 5.4: Estimated parameters and least square errors between measured and modelled data when using a **Cascade model**. Errors are given as percentages for the fit to training data (E_{train}), the fit to general pulse data (E_{test1}) and the fit to kick type inputs (E_{kick}).

	θ_4 (s^4)	θ_3 (s^3)	θ_2 (s^2)	θ_1 (s)	θ_0 -	m -	k -	E_{train}	E_{test1}	E_{kick}
LA	2.2×10^{-6}	1.1×10^{-4}	0.018	0.20	0.0030	1.6	0.035	3.0	2.6	3.0
LB	3.8×10^{-6}	2.0×10^{-4}	0.018	0.20	0.0014	1.6	0.020	4.5	4.0	4.5
LC	3.0×10^{-6}	2.0×10^{-4}	0.018	0.20	0.0073	1.6	0.093	4.1	3.5	4.3
LD	2.6×10^{-6}	2.0×10^{-4}	0.018	0.20	0.0044	1.6	0.052	3.8	2.8	2.4
LE	2.1×10^{-6}	2.0×10^{-4}	0.018	0.20	0.0093	1.6	0.12	3.2	3.2	2.7
Mean	2.7×10^{-6}	2.0×10^{-4}	0.018	0.20	0.0051	1.6	0.060	3.7	3.2	3.4

The linear model provides the poorest fit to data. The model is unable to describe the range of behaviour and both under- and over-predicts the isometric force. This inability to describe the

[1] Test1 data includes all test data except the physiological kick data
[2] Kick data includes just the physiological kick data

TABLE 5.5: Estimated parameters and least square errors between measured and modelled data when using **Ding model**. Errors are given as percentages for the fit to training data (E_{train}), the fit to general pulse data (E_{test1}) and the fit to kick type inputs (E_{kick}).

Locust	τ_c (s)	τ_1 (s)	τ_2 (s)	A (s^{-1})	R_o	k	E_{train}	E_{test1}	E_{kick}
LA	0.019	0.14	0.16	5.3	0.73	0.19	1.7	1.6	3.0
LB	0.022	0.079	0.24	5.3	0.92	0.25	1.3	1.7	3.1
LC	0.027	0.087	0.17	5.6	1.3	0.28	2.1	1.5	2.6
LD	0.036	0.093	0.18	5.3	1.2	0.23	1.5	1.0	3.0
LE	0.023	0.11	0.18	5.3	1.1	0.24	1.7	1.5	3.3
Mean	0.023	0.10	0.19	5.4	1.0	0.24	1.7	1.5	3.0

TABLE 5.6: Estimated parameters and least square errors between measured and modelled data when using **Bobet and Stein's model**. Errors are given as percentages for the fit to training data (E_{train}), the fit to general pulse data (E_{test1}) and the fit to kick type inputs (E_{kick}).

Locust	a (s^{-1})	m	b_o (s^{-1})	b_1	B	k	E_{train}	E_{test1}	E_{kick}
LA	15	2.5	8.4	0.27	1.0	0.72	1.3	0.83	0.80
LB	16	2.7	8.7	0.13	0.97	0.77	1.5	1.6	0.98
LC	15	2.4	9.5	0.19	0.96	0.71	1.8	1.1	0.83
LD	16	2.4	7.9	0.09	0.99	0.63	1.6	0.86	0.81
LE	14	2.4	8.7	0.15	0.97	0.75	1.4	0.94	0.74
Mean	15	2.5	8.6	0.17	0.99	0.72	1.5	1.1	0.83

TABLE 5.7: Estimated parameters and least square errors between measured and modelled data when using the **Adapted model**. Errors are given as percentages for the fit to training data (E_{train}), the fit to general pulse data (E_{test1}) and the fit to kick type inputs (E_{kick}).

Locust	τ_c (s)	τ_1 (s)	τ_2 (s)	k	A (s^{-1})	m	E_{train}	E_{test1}	E_{kick}
LA	0.076	0.12	0.06	0.70	6.2	2.1	1.3	0.62	0.57
LB	0.059	0.066	0.15	0.52	5.3	1.7	0.94	1.1	1.0
LC	0.074	0.072	0.09	0.56	6.2	1.8	1.6	0.85	0.69
LD	0.064	0.079	0.12	0.44	5.5	1.6	1.3	0.60	1.1
LE	0.077	0.080	0.09	0.60	6.1	1.9	1.2	0.79	0.71
Mean	0.070	0.083	0.10	0.57	5.8	1.8	1.3	0.80	0.82

TABLE 5.8: Estimated parameters and least square errors between measured and modelled data when using the **Simplified Adapted model**. Errors are given as percentages for the fit to training data (E_{train}), the fit to general pulse data (E_{test1}) and the fit to kick type inputs (E_{kick}).

Locust	τ_c (s)	τ_1 (s)	k	A (s^{-1})	m	E_{train}	E_{test1}	E_{kick}
LA	0.076	0.14	0.80	7.1	2.4	1.4	0.71	0.73
LB	0.065	0.13	0.78	7.5	2.7	1.5	1.6	0.98
LC	0.073	0.12	0.73	7.7	2.5	1.8	1.0	0.83
LD	0.066	0.14	0.64	7.2	2.4	1.6	0.85	0.81
LE	0.077	0.13	0.77	7.5	2.5	1.4	0.91	0.73
Mean	0.071	0.13	0.75	7.4	2.5	1.5	1.0	0.81

TABLE 5.9: Summary of average errors estimated using each model. Errors are given as percentages for the fit to training data (E_{train}), the fit to general pulse data (E_{test1}) and the fit to kick type inputs (E_{kick}).

Model type	E_{train}	E_{test1}	E_{kick}
Linear	12	15	9.4
Wiener	2.9	2.9	1.8
Cascade	3.7	3.2	3.4
Ding *et al*	1.7	1.5	3.0
Bobet and Stein	1.5	1.1	0.83
Adapted	1.3	0.80	0.82
Simplified Adapted	1.5	1.0	0.81

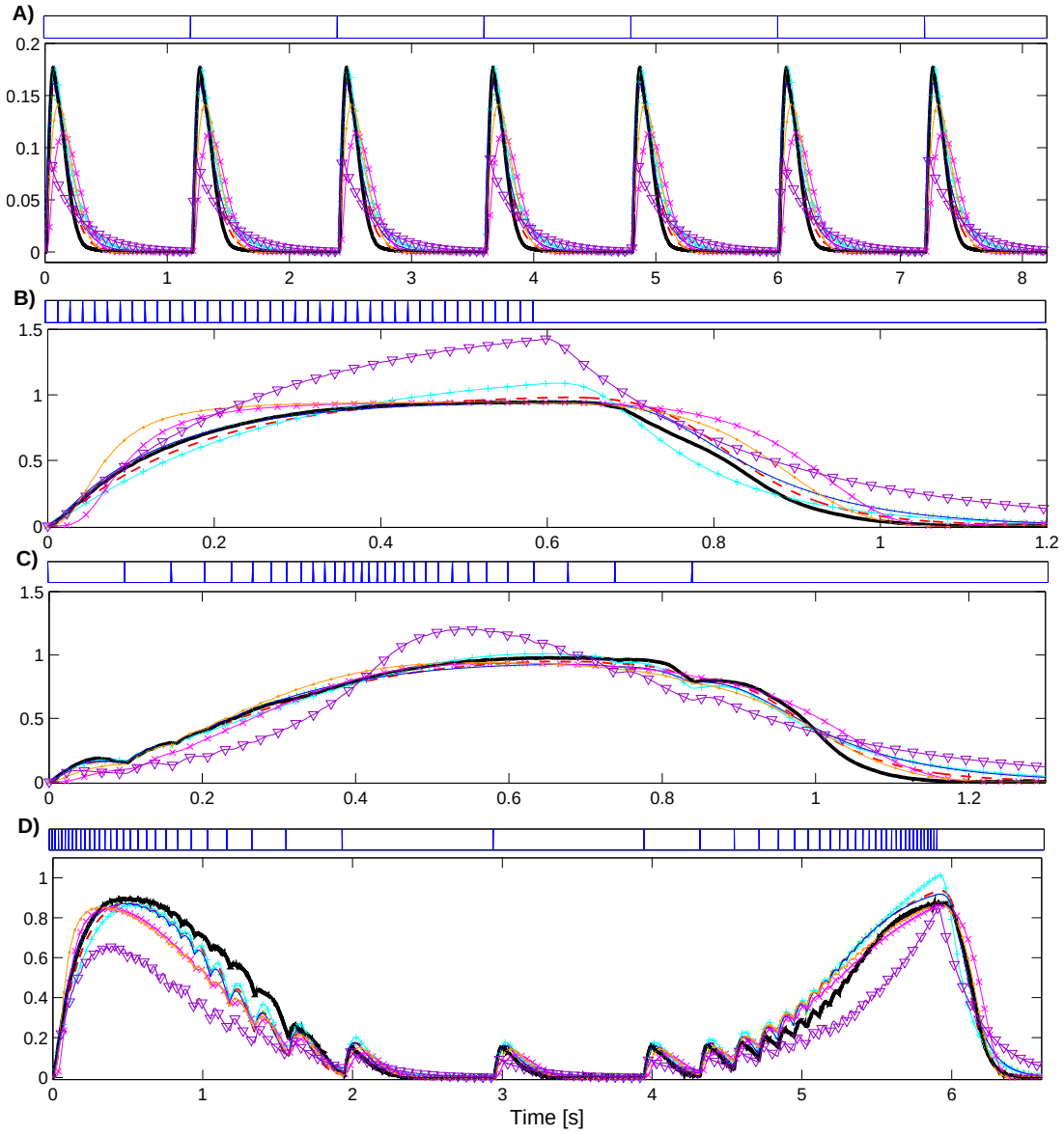

FIGURE 5.11: A-D) Fitting each model to each set of training data (bold) to estimate parameters. The input pulse train used to generate each force response is shown above each graph of force response. Fitted models are: Linear (-▽-), Wiener (_._._), Cascade (-×-), Ding *et al* (-+-), Bobet and Stein (—), Adapted (- - -), Adapted simple (...).

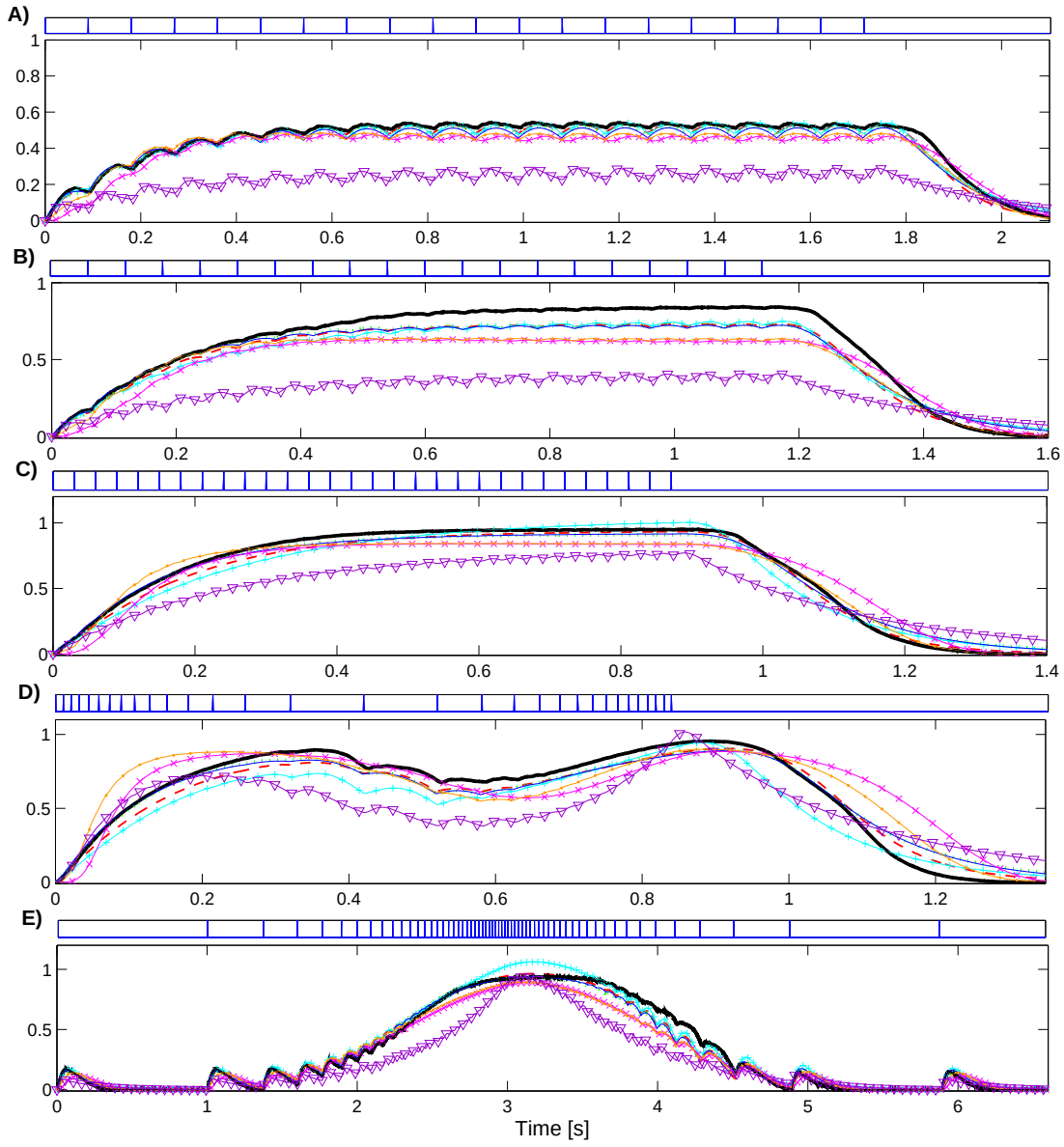

FIGURE 5.12: A-E) Comparison between measured (bold) and modelled force data for pulse train inputs. The input pulse train used to generate each force response is shown above each graph of force response. Fitted models are: Linear (-▽-), Wiener (.-.-.), Cascade (-×-), Ding *et al* (-+-), Bobet and Stein (—), Adapted (- - -), Adapted simple (...).

behaviour is expected from the analysis in the preceding chapter. A linear model was found to produce a good fit to the twitch response. When summation occurs non-linear effects become important, and a linear model cannot describe the behaviour unless coefficients describing each individual pulse response are allowed to change (even in this case, high frequency, high pulse number trains cannot be modelled well).

The inclusion of a static nonlinearity, as in the Wiener and Cascade Models, provides an improvement on the linear fit. The static non-linearity allows some of the nonlinear behaviour to be described. The Cascade model is of higher order, yet gives larger errors than the Wiener

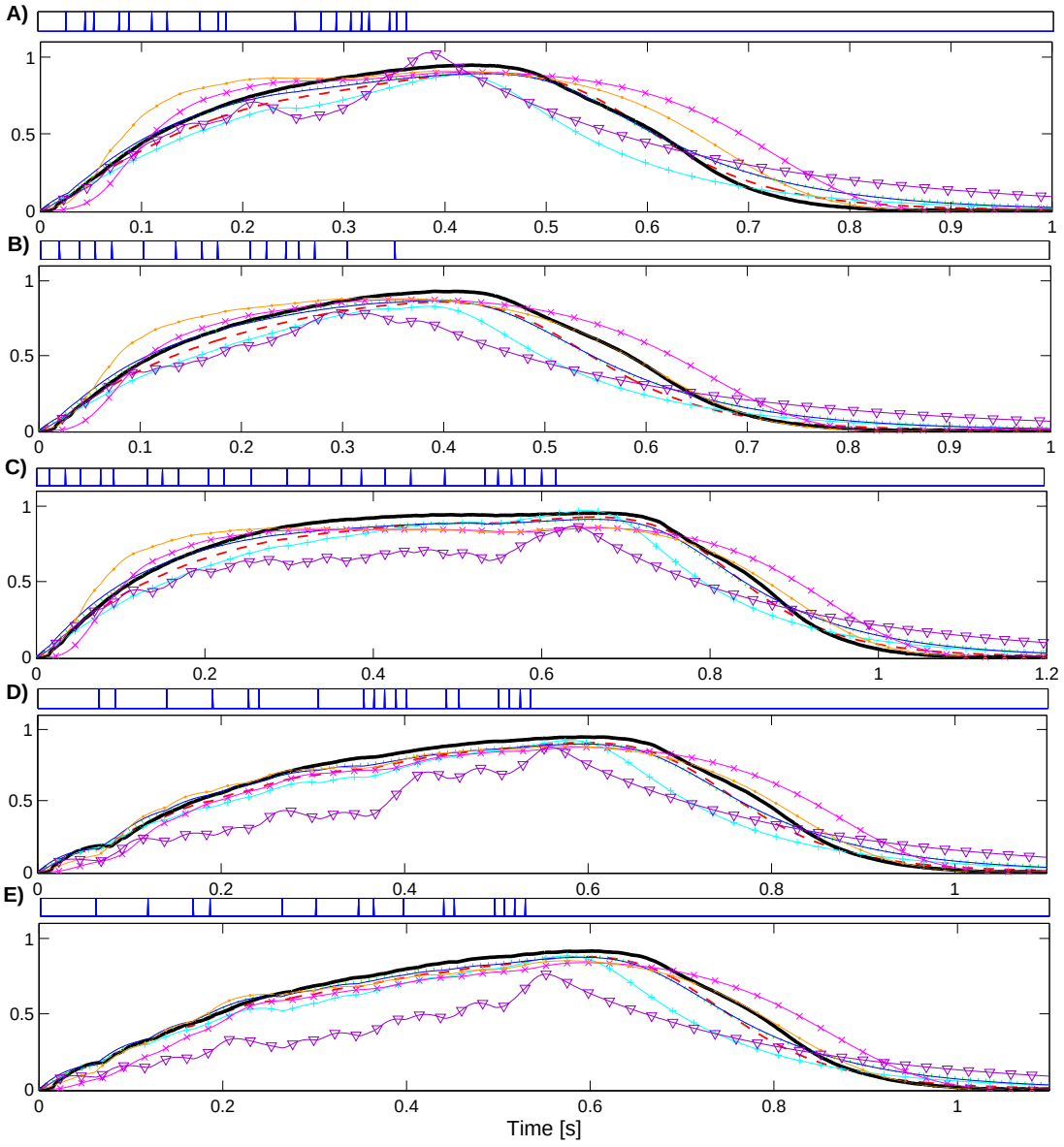

FIGURE 5.13: A-E) Comparison between measured (bold) and modelled force data for kick type inputs. The input pulse train used to generate each force response is shown above each graph of force response. Fitted models are: Linear (-▽-), Wiener (.-.-.), Cascade (-×-), Ding *et al* (-+-), Bobet and Stein (—), Adapted (- - -), Adapted simple (...).

model. This suggests that in the Cascade model a local minimum may be estimated. The fact that in the Cascade model for most locusts some of the parameters (θ_1, θ_2, m) do not change from their initial estimates suggests that the model has redundant parameters. In the Wiener model there is a lot of variability in some of the parameters (θ_2, k) between locusts. The Wiener, Cascade and Linear models give lower errors when fitting to the kick data compared to the training data. They are better at replicating the response to short high-frequency pulse trains (kick type inputs), than the force response to lower frequency pulse trains.

Models of linear-nonlinear-linear (LNL) structure (Ding, Bobet and Stein, Adapted and Simplified Adapted models), with the exception of the model of Ding *et al*, outperform models with the simpler linear-nonlinear (LN) structure (Wiener and Cascade). The fit to kick data is worse in the model of Ding *et al* when compared with the Wiener model. In the model of Ding *et al* the fit to kick data is much worse than the fit to general test data. This suggests that this model is less good at predicting physiologically relevant behaviour and better suited to lower frequency pulse train inputs.

The improved fit obtained with LNL models, with the exception to that of Ding *et al*, is attributed to the increased structural complexity of the LNL models, however a good fit does not prove that a model is correct, but suggests that it is a better option than a model that fits the data poorly. The LN structure assumes linear dynamics; there is no nonlinear element that changes the system's time constants. The LNL models all provide similar fits to training data. In each LNL model any differences in estimated parameters between locusts are small and likely to be as a result of the fact that the measured force responses of each locust are quantitatively different.

The performances of Bobet and Stein's model, the Adapted model and the Adapted Simplified model are similar in terms of kick errors. The Adapted model provides a better fit to general pulse train data. The estimated force traces for just these three models are shown in Figs. 5.14 to 5.16 for a clearer view of the model dynamics. The three models are of similar form and the modelled force-time traces are similar. The Adapted Simplified model and the model of Bobet and Stein predict very similar force trajectories. Marginally better fits to data are given by the Adapted Simplified model when compared to Bobet and Stein's model. The form of the Adapted Simplified model is similar to that of Bobet and Stein, yet the model has one less parameter as the variation in time constant with force level is not included (the parameter b_1 is effectively zero). This suggests that the force feedback included in Bobet and Stein's model is not necessary when describing the isometric force response of the locust extensor muscle. It should also be noted that the errors presented in Table 5.6 when fitting using Bobet and Stein's model are much lower, especially at low levels of contraction than those quoted by Bobet and Stein [73]. This could be attributed to the training data used by Bobet and Stein not being 'rich' enough.

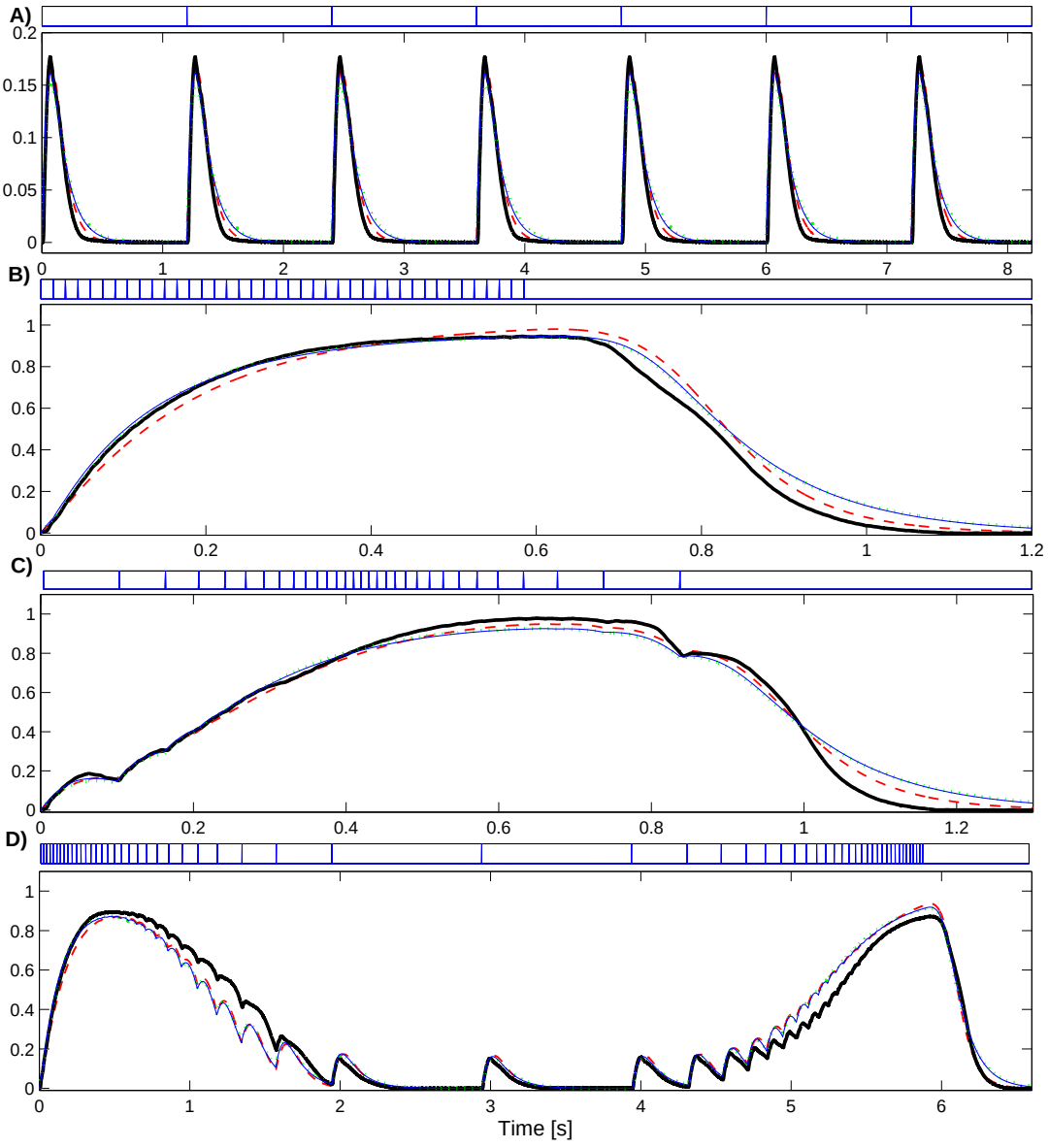

FIGURE 5.14: A-D) Fitting each model to training data (bold) to estimate parameters. The input pulse train used to generate each force response is shown above each graph of force response. Fitted models are: Bobet and Stein (—), Adapted (- - -), Adapted simple (...).

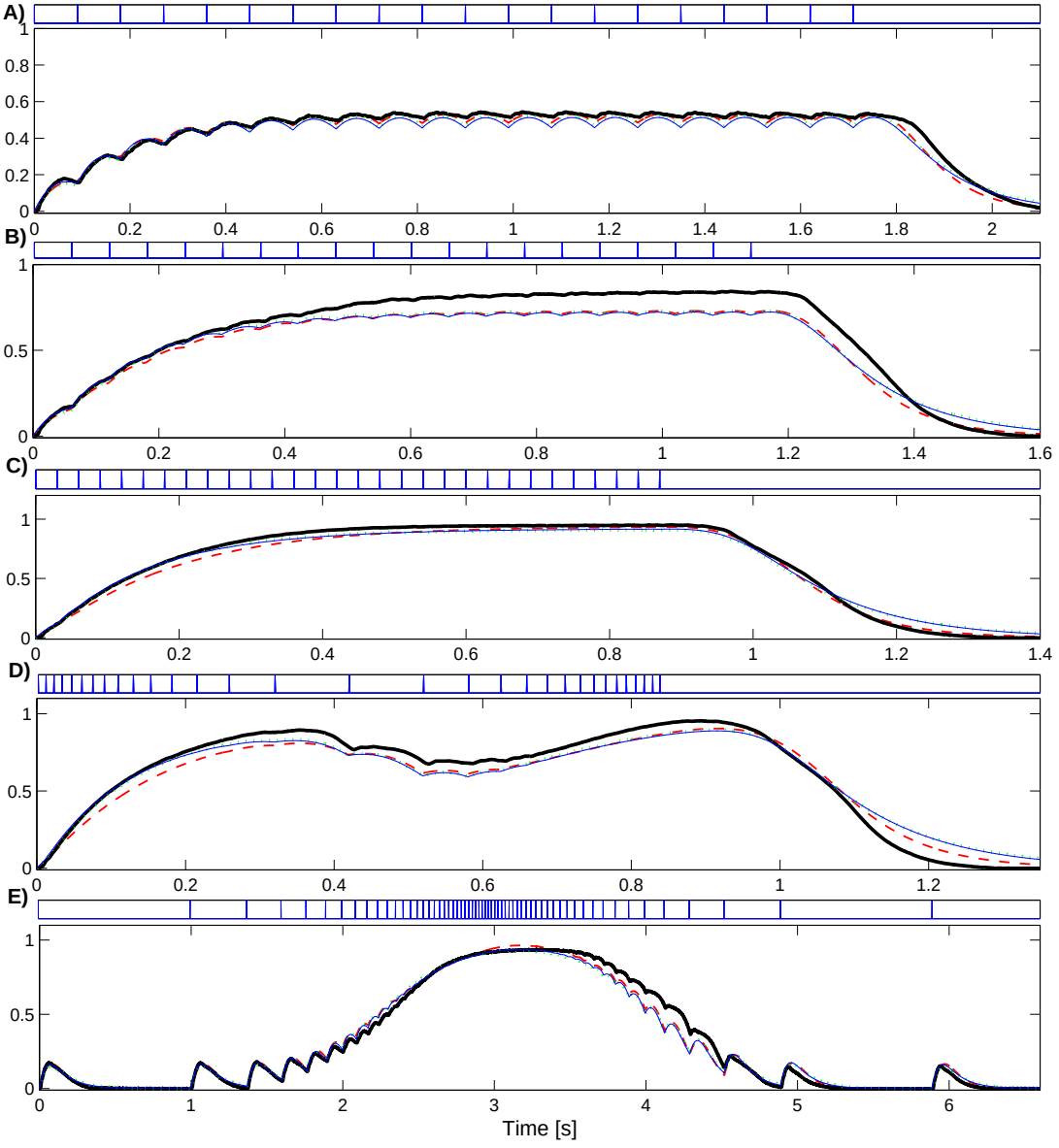

FIGURE 5.15: A-E) Comparison between measured (bold) and modelled force data for pulse train inputs. The input pulse train used to generate each force response is shown above each graph of force response. Fitted models are: Bobet and Stein (—), Adapted (- - -), Adapted simple (...).

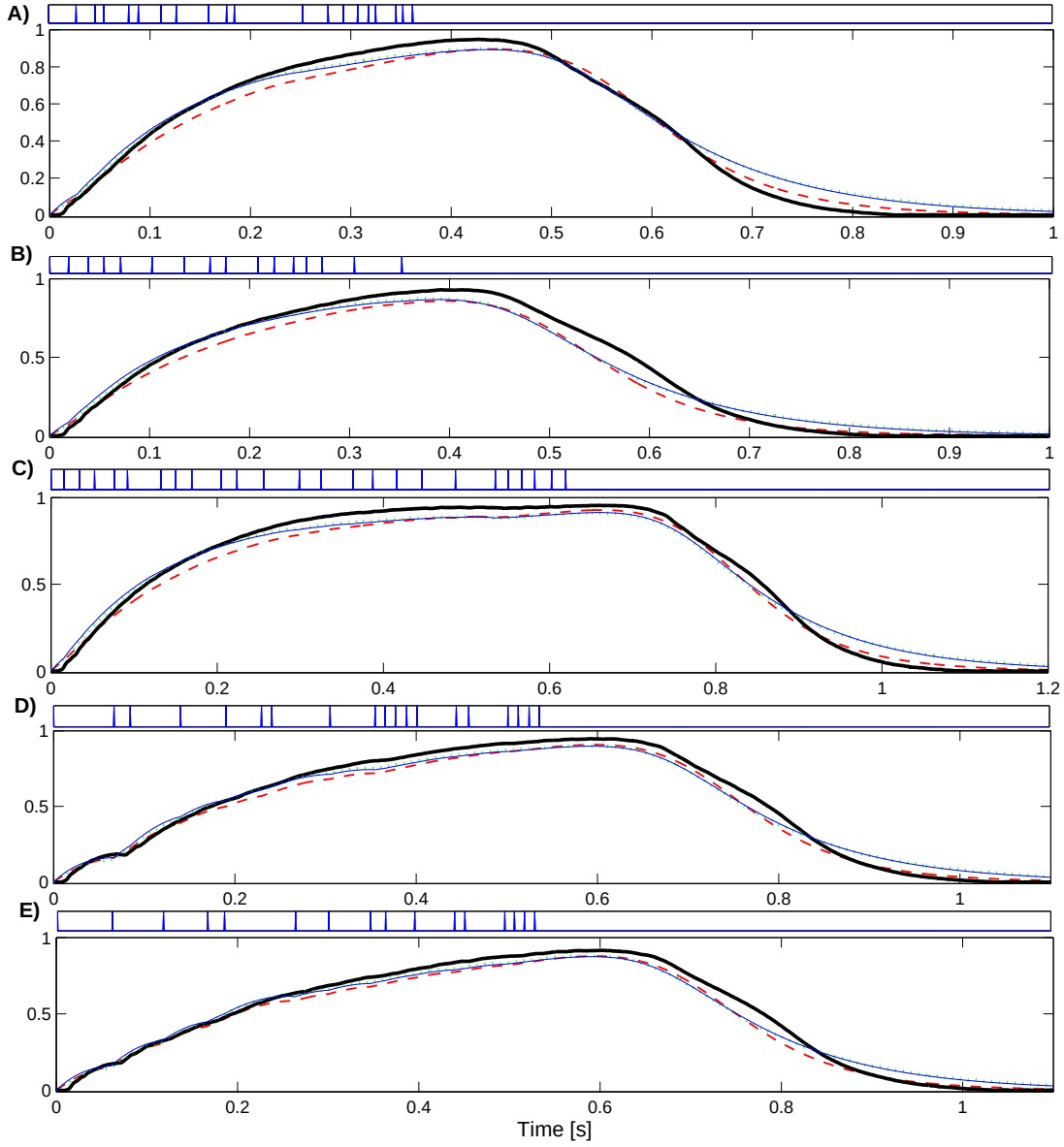

FIGURE 5.16: A-E) Comparison between measured (bold) and modelled force data for kick type inputs. The input pulse train used to generate each force response is shown above each graph of force response. Fitted models are: Bobet and Stein (—), Adapted (- - -), Adapted simple (...).

5.5.2 Model Selection Using AIC and BIC

Comparing least square errors between measured and modelled data indicates the goodness of fit of each model. However, the least squares statistic does not take into account the trade-off between model complexity and estimation errors. Models of increased complexity can better adapt to fit to data. However, additional parameters may fit to measurement noise and not describe any important processes. This can make the underlying governing behaviour harder to interpret. Using solely the model that gives the lowest mean square error will often just lead to the largest model being selected as best. The 'best' model should balance simplicity and goodness of fit; model characteristics essential to observed effects are often more evident in simpler models [34].

Akaike's information criterion (AIC) [155] is used as a tool for model selection. This method takes account of the trade off between model complexity (measured as the number of model parameters) and accuracy. AIC attempts to find the model that provides the best description of the data whilst keeping the number of free parameters to a minimum. The AIC in the general case is defined by

$$\mathrm{AIC} = 2k - 2\,\ln(\ell(\hat{\theta}|x)) \tag{5.32}$$

where k is the number of parameters, and $\ell(\hat{\theta}|x)$ the likelihood function of the model parameters θ, given the data x. The second term tends to decrease as more parameters are added to the approximate model, while the first gets larger [155]. The model errors are assumed to be normally and independently distributed with the variance of model errors unknown but equal for all models. The AIC then becomes

$$\mathrm{AIC} = 2k + n\left(\ln\left(\frac{RSS}{n}\right)\right) \tag{5.33}$$

where RSS is the residual sum of squares and n gives the number of observations. For small sample sizes the AIC requires a bias-adjustment term, the AIC for small samples ($\mathrm{AIC_c}$) being given by

$$\mathrm{AIC_c} = \mathrm{AIC} + \frac{2k(k+1)}{n-k-1} \tag{5.34}$$

As the size n of the data set increases the adjustment term becomes negligible, therefore the small sample adjustment is used for all AIC calculations. AIC differences (Δ_i) were computed for each model and are given in Table 5.10. The AIC was computed both for the entire set of test data (including physiological data) and for just physiological data. Low values of Δ_i

indicate a better model, and zero the best model in AIC terms. The results suggest that the Adapted model provides the best description of all behaviour. The data sets used to compute the AIC values given in Table 5.10 were very large with $n = 46556$ for all test data and $n = 13915$ for kick data. The AIC complexity penalty tends to zero for large data sets, so that the complexity is relatively less important when the sample size is high [160]. Therefore the AIC differences for smaller resampled data sets were also computed. The data was resampled, so that $n = 150$ and the AIC value computed. Resultant values are given in Table 5.11. The AIC differences given in Table 5.11 again suggest that the Adapted model is the best model for describing all test data. For fitting to physiologically relevant kick data the Simplified Adapted and Adapted models perform equally well in terms of their AIC values.

TABLE 5.10: Average AIC differences across 5 locusts (Δ_i = AIC$_i$ - minAIC) for whole data set

Model	No. Params.	Δ_i for all test data	Δ_i for kick data
Linear	4	131000	35200
Wiener	5	52900	10600
Cascade	7	65600	19600
Ding	6	46500	20200
Bobet and Stein	6	9240	530
Simplified Adapted	5	7140	200
Adapted	6	0.00	0.00

TABLE 5.11: Average AIC differences across 5 locusts (Δ_i = AIC$_i$ - minAIC) for resampled data set

Model	No. Params.	Δ_i for all test data	Δ_i for kick data
Linear	4	422	365
Wiener	5	170	112
Cascade	7	214	214
Ding	6	151	218
Bobet and Stein	6	30.1	5.65
Simplified Adapted	5	21.1	0.01
Adapted	6	0.00	0.00

The disadvantage of AIC model selection is that as $n \to \infty$ more complex models tend to be selected as the complexity becomes relatively less important. Bayesian information criteria (BIC) is an asymptotically consistent alternative selection criteria [161]. As the sample size becomes large the probability that BIC will select the correct model tends towards one. BIC has stronger penalties for additional parameters than AIC. The disadvantage of using BIC is that for small or moderately sized samples, due to the complexity penalty, BIC can choose models that are too simple. The general formula for the BIC is

$$\text{BIC} = k \ln(n) - 2 \ln(\ell(\hat{\theta}|x)) \tag{5.35}$$

The model errors are again assumed to be independent and normally distributed with the variance of all models equal and unknown. The BIC is then

$$\text{BIC} = k\ \ln(n) + n\left(\ \ln\left(\frac{RSS}{n}\right)\right) \tag{5.36}$$

Table 5.12 gives the BIC differences for the whole data set. Due to the disadvantages of BIC when using a small sample set, the BIC was not computed for the resampled data set. Table 5.12 indicates that according to the BIC selection criteria the Adapted model is the best model for describing the isometric force response of the locust hind leg extensor. This is in agreement with the AIC selection criteria.

TABLE 5.12: Average BIC differences across 5 locusts (Δ_i = BIC$_i$ - minBIC) for whole data set

Model	No. Params.	Δ_i for all test data	Δ_i for kick data
Linear	4	131000	194000
Wiener	5	52900	78600
Cascade	7	65600	97500
Ding	6	46524	69153
Bobet and Stein	6	9230	13800
Simplified Adapted	5	7130	10600
Adapted	6	0.00	0.00

5.5.3 Response of Individual Pulses

The ability of each model to capture the underlying behaviour and describe the response of each individual pulse is now considered. The experimental response to each individual pulse is given in Chapter 4. Modelled individual pulse contributions were obtained by assuming the behaviour was quasi-linear and subtracting the simulated response to $n-1$ pulses from that to n pulses. The simulated response is presented using parameters relevant to locust LE as an example for each model.

Figures 5.17, 5.18 and 5.19 summarise the modelled response to each individual pulse for a second pulse when the IPF is varied, the n^{th} pulse in a low frequency CFT, and the n^{th} pulse in a high frequency CFT respectively. In each figure the experimentally obtained contribution by each pulse is also given. Due to constraints on the maximum amount of data that can be collected from each locust whilst maintaining repeatability, the experimental response is plotted for a different locust to modelled responses. The qualitative behaviour between locusts is similar, thus the ability of each model to describe the trends (not specific details) seen in experimental data is considered.

No model describes the response to a second pulse well (Fig. 5.17). This is due to the fact that training data did not contain any two pulse trains and so models were not trained to describe

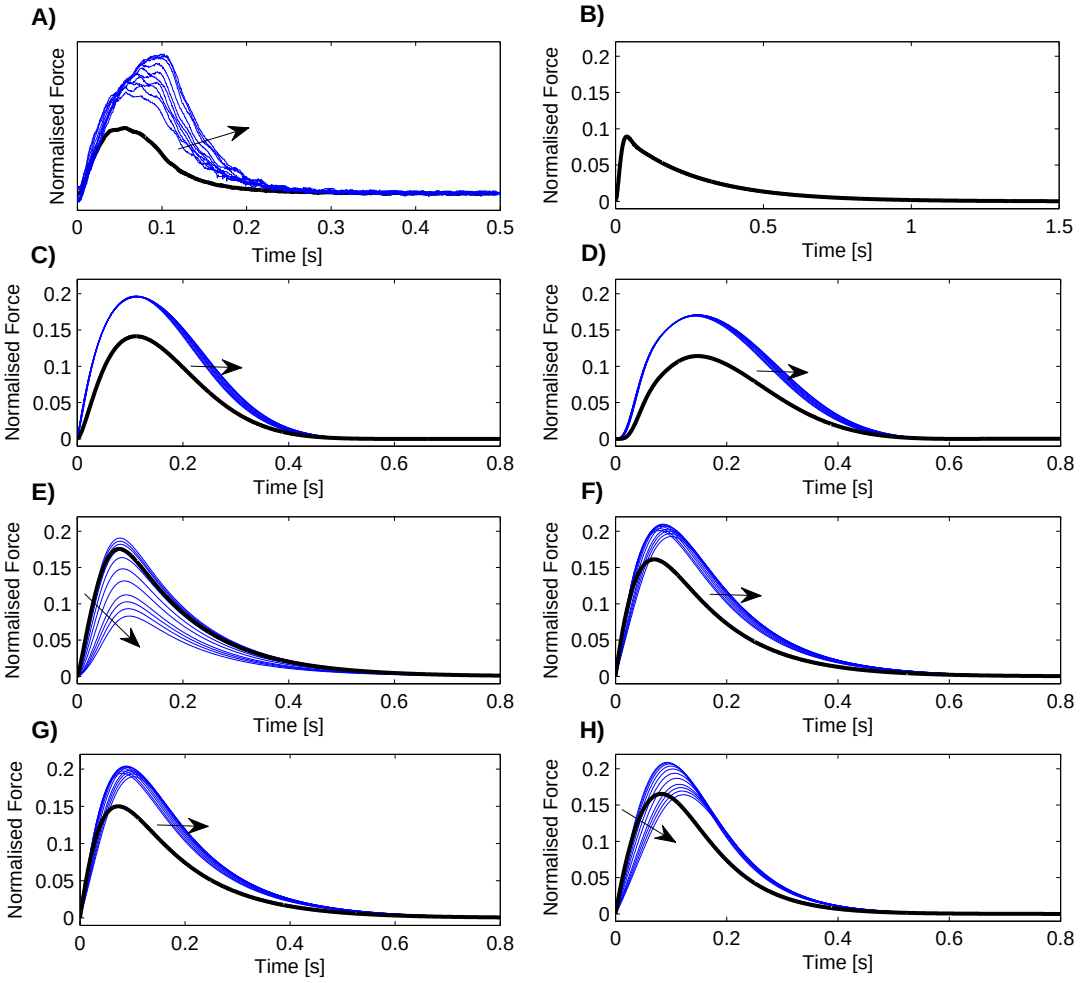

FIGURE 5.17: Comparison between A) Experimental, and B-H) modelled response to a second pulse for a range of IPFs, arrows indicate increasing IPF. The response to a single pulse is given in bold for comparison. Modelled responses are for B) Linear model, C) Wiener Model, D) Cascade Model, E) Ding Model, F) Bobet and Stein model, G) Adapted Simplified Model, H) Adapted Model.

the behaviour of a second pulse. Some models are better able to capture some of the underlying dynamics. The Linear model, as expected, does not capture any of the non-linear dynamics. It performs the worst in terms of goodness of fit, due to this lack of ability to describe the underlying non-linear behaviour. The Cascade and Wiener models are able to describe the fact that the magnitude of the second pulse is increased from the first. These models do not however describe the change in pulse shape or the variation in the response of a second pulse with IPF. The underlying behaviour described by the model of Ding *et al* is very different to that found experimentally, suggesting that the model may not provide an accurate description of the behaviour. As with the goodness of fit, AIC, and BIC findings, the models of Bobet and Stein, Simplified Adapted model and the Adapted model provide the best description of the

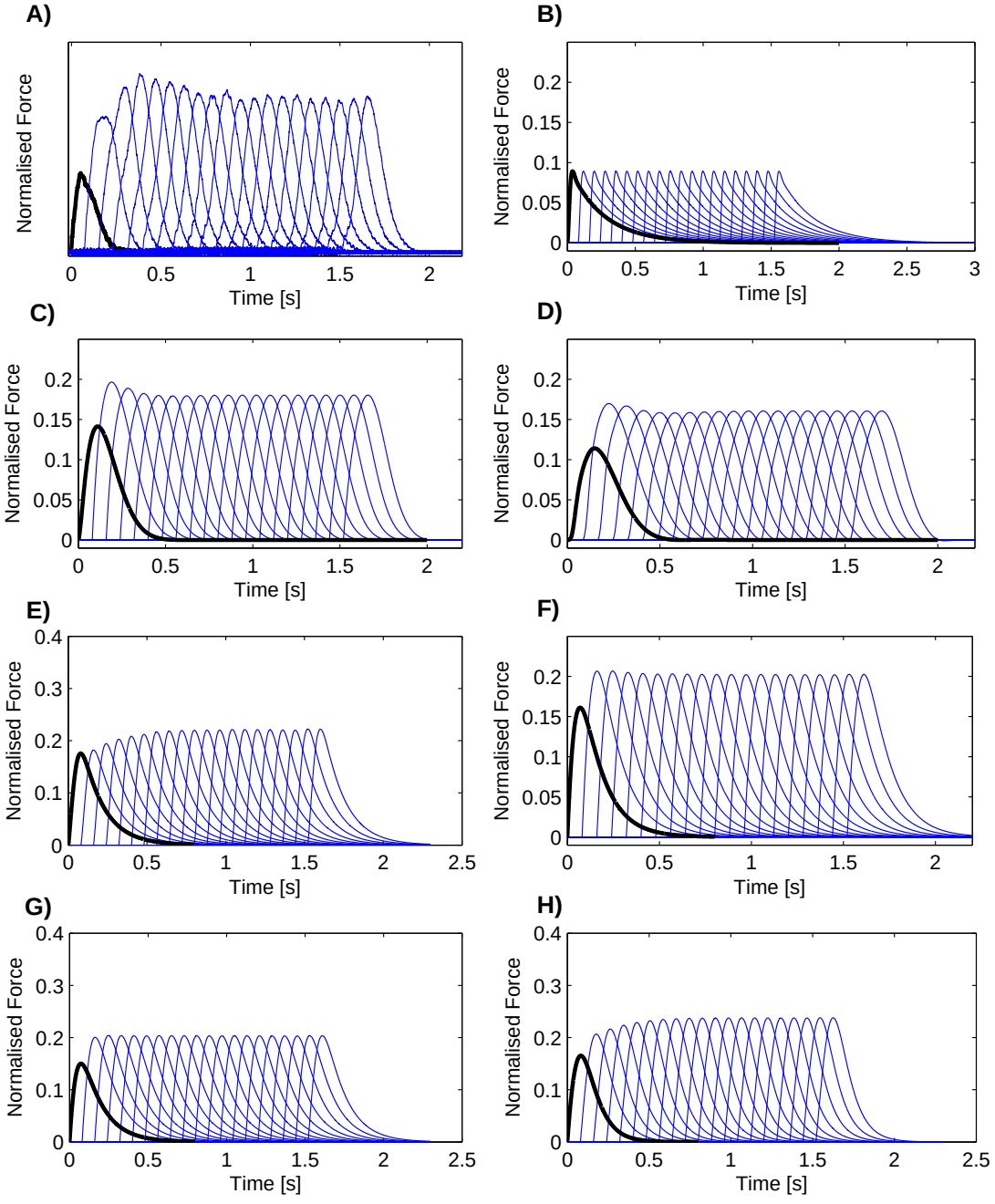

FIGURE 5.18: Comparison between A) Experimental, and B-H) modelled response to the n^{th} pulse for a low frequency IPF (12.5Hz). The response to the first pulse is given in bold. Modelled responses are for B) Linear model, C) Wiener Model, D) Cascade Model, E) Ding Model, F) Bobet and Stein model, G) Adapted Simplified Model, and H) Adapted Model.

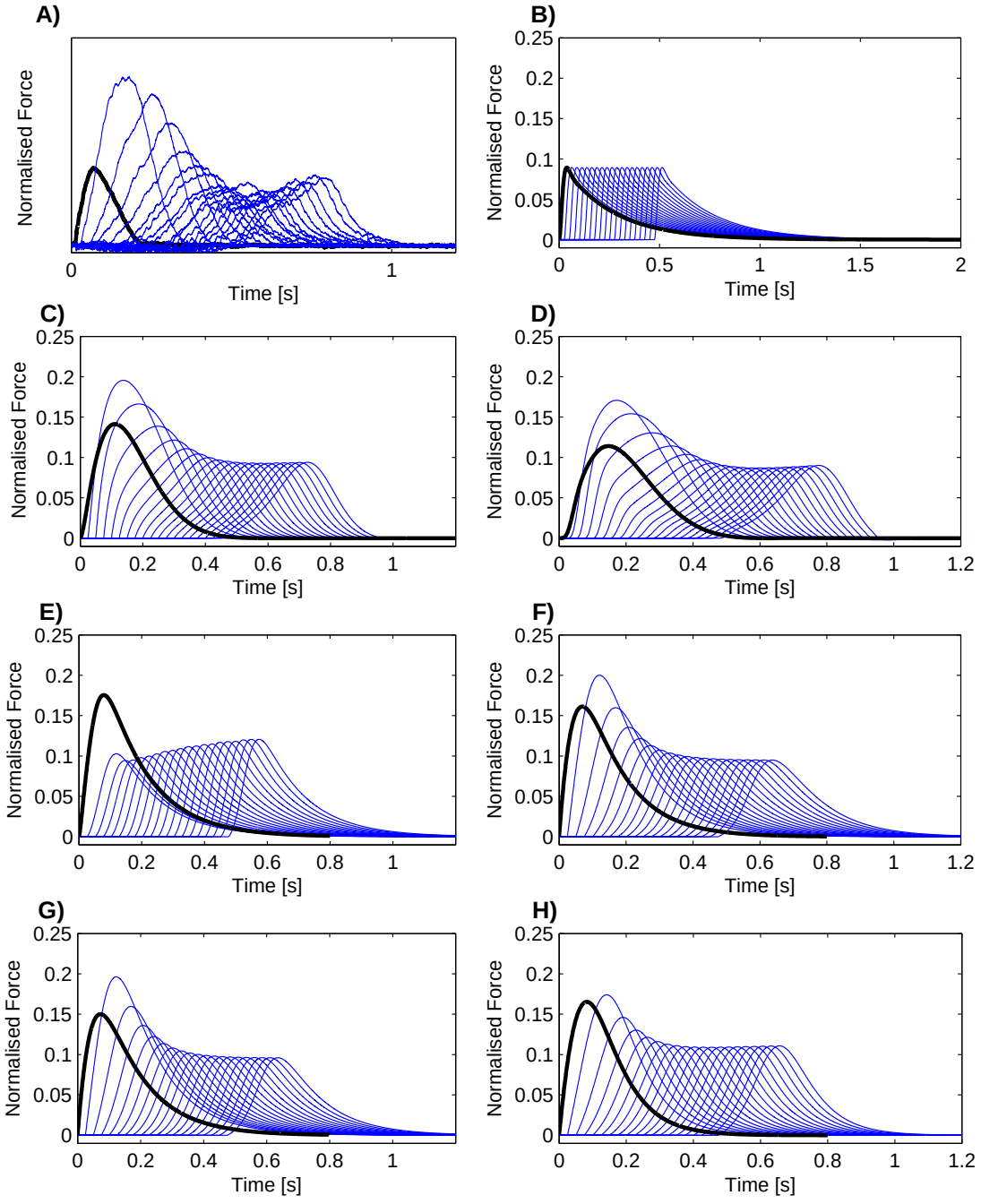

FIGURE 5.19: Comparison between A) Experimental, and B-H) modelled response to the n^{th} pulse for a high frequency IPF (40Hz). The response to the first pulse is given in bold. Modelled responses are for B) Linear model, C) Wiener Model, D) Cascade Model, E) Ding Model, F) Bobet and Stein model, G) Adapted Simplified Model, and H) Adapted Model.

behaviour. The early force depression is well predicted, with this being more evident in the Adapted model. The later force enhancement and increased force enhancement with increasing IPF is not well described by any model.

The response of the n^{th} pulse in a low frequency CFT (Fig. 5.18) is reasonably well described by all models, with exception of the linear model. The main discrepancy between modelled and experimental data is that the modelled amplitude changes are less extreme than those seen in the experimental data.

Examination of the response to each pulse in a high frequency pulse train (Fig. 5.19) it is clear that again, as expected, the linear model cannot describe the underlying behaviour. As with the second pulse (Fig. 5.17), the model of Ding *et al* describes the underlying behaviour poorly, again suggesting that the model does not provide a good description of the behaviour of the locust hind leg extensor muscle. The other models capture the increase and subsequent decrease in the pulse magnitude seen in the experimental data. It is the inclusion of a non-linear saturation function that enables these models to capture this behaviour, and the fact that behaviour is frequency dependent.

Figures 5.17 and 5.19 show that the model of Ding *et al* provides a poor model of the underlying behaviour. This is attributed to the relation used by Ding *et al* to describe the non-linear summation of closely spaced pulses. The form of R_i (Eq. (5.11)) found using average model parameters is shown in Fig. 5.20. It is clear that R_i is not strongly influenced by the pulse separation. The model assumes that the force enhancement always increases with IPF, but this is not the case. For long high IPF trains the magnitudes of later pulses are less than for low IPF trains. In other words the force at the end of high IPF trains is less enhanced than for low IPF trains. Since R_i cannot describe this behaviour, it is thought that the best solution is for R_i not to change much with IPF. This influences the value of τ_c which is used as a time constant in other parts of the model. Furthermore, the expression for R_i is a function of discrete time, while muscle contraction occurs in continuous time. The discrete time model is conceptually less easy to interpret and relate to the processes occurring during contraction. The poor description of the underlying behaviour in the Ding *et al* model is thought to be due to the function describing R_i not providing a good model to describe the force enhancement.

In terms of their ability to describe the underlying behaviour, goodness of fit, AIC and BIC it was seen in the previous section that the 'best' models to describe the behaviour of the locust hind leg extensor muscle are Bobet and Stein's model, the Simplified Adapted model, and the Adapted model. Looking at the response to individual pulses, the most notable weakness of these models is their inability to describe the response of a second pulse in a two pulse train. This could, however, be a weakness in the choice of training data as opposed to the models. In order to test if the models could describe the behaviour of a second pulse better with more

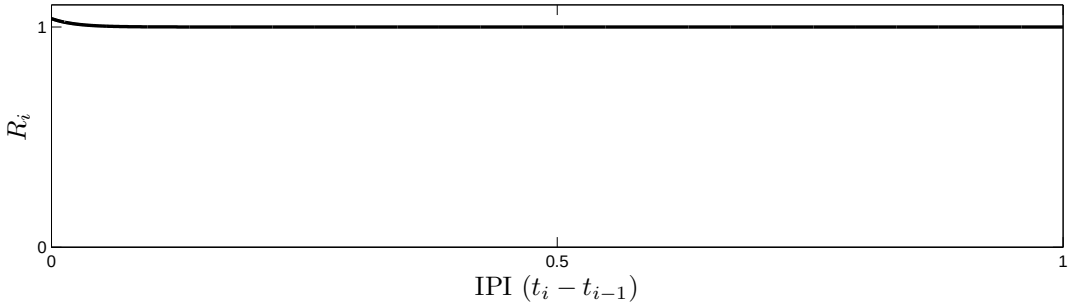

FIGURE 5.20: Dependence of IPI (Eq. (5.11)) on the value of R_i in the model of Ding *et al*, found using average estimated parameters.

appropriate training data, two pulse trains were included in training data. Due to practical constraints on the amount of data that could be collected from one locust, this was done for a different set of locusts. The predicted behaviour of a second pulse for a range of IPFs and for each of the three 'best' models is given in Fig. 5.21. It is evident, by comparing the modelled response in Fig. 5.21 to measured data in Fig. 4.10, that the models are in fact able to capture the behaviour in response to a second pulse. The Simplified Adapted model and Bobet and Stein's model behave similarly. The Adapted model is able to better describe the increasing early depression with increasing IPF.

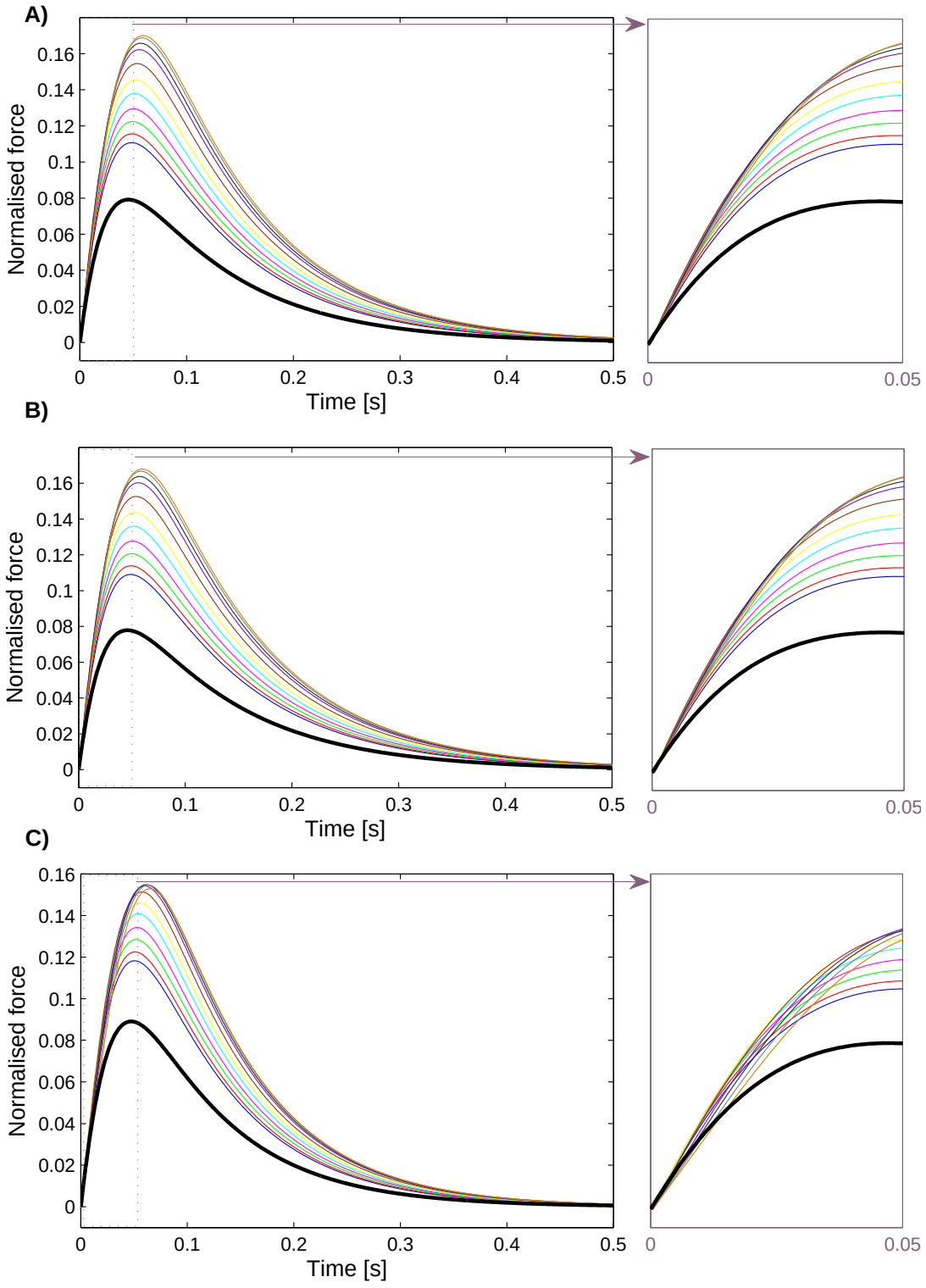

FIGURE 5.21: Response of second pulse in comparison to twitch (—) for A) Bobet and Stein's model, B) Simplified Adapted Model, C) Adapted model. The second pulse for a range of IPIs are shown; 100ms (—), 90ms (—), 80ms (—), 70ms (—), 60ms (—), 50ms (—), 40ms (—), 30ms (—), 25ms (—), 20ms (—), 15ms (—). The graphs on the right hand side show in more detail the section of the force trace up to 0.05s.

5.5.4 Parameter Sensitivity

Parameter sensitivity analysis provides an indication of which parameters contribute most to the output variability, which parameters are highly correlated with outputs and what the result of changing a given input parameter is. It is useful for finding any insignificant parameters that can be eliminated from the model, as well as finding any parameters that require additional research to reduce output uncertainty [82, 162]. Understanding of the system and relationships can be improved by a sensitivity analysis.

A sensitivity analysis was carried out on the Adapted model. The Adapted model was chosen as the AIC and BIC calculations indicated it was the best model. The next best model according to AIC and BIC was the Simplified Adapted model. This model is equivalent to the Adapted model, with $\tau_2 = 0$, and so a Sensitivity Analysis on the Adapted model will also provide some indication of the behaviour of the Simplified Adapted model.

A one-at-a-time approach was used, due to its conceptual simplicity. This approach is similar to that used by Frey Law and Shields [82] and provides a 'local' sensitivity estimate [162]. Each parameter was varied in turn by up to $\pm 10\%$ of its nominal value. Corresponding changes in the force profile were measured by the Frey Law and Shields [82] force characteristics. These characteristics were defined for a twitch in Fig. 4.5. For a pulse train an extra characteristic, the Relative Fusion Index (RFI), is included. This is defined as the mean of the last 4 minima in the pulse responses divided by the corresponding peaks (RFI=1 indicates smooth sustained contraction, RFI=0 indicates no summation of subsequent pulses). For pulse train data the HRT and LRT refer to the decay from the final peak value, and the TPT to the time to reach 90% of the first peak force.

Initial parameter values were set to the average values given in Table 5.7. The model was stimulated by a single input, a low frequency pulse train, a high frequency pulse train, and a kick type input so as to test the model behaviour under a range of conditions. Figures 5.22, 5.24, 5.26 and 5.28 show how the predicted force-time profile is altered by a change in each parameter. Figures 5.23, 5.25, 5.27 and 5.29 indicate the percentage change in each force characteristic as each parameter is changed by up to $\pm 10\%$ from its initial value. The effect on the force response to each different input type is considered in terms of how each parameter in turn affects the response.

The parameter A scales the force response. Percentage changes in A result in equivalent percentage changes in the PF and FTI. Changing A has no effect on the force time measurements (HRT, LRT, TPT) or RFI, as expected. The model is fitted to normalised data, with maximum tetanic force equal to one. To apply the model to actual force data the parameter A would just change by the relevant scale factor, with all other being parameters unchanged.

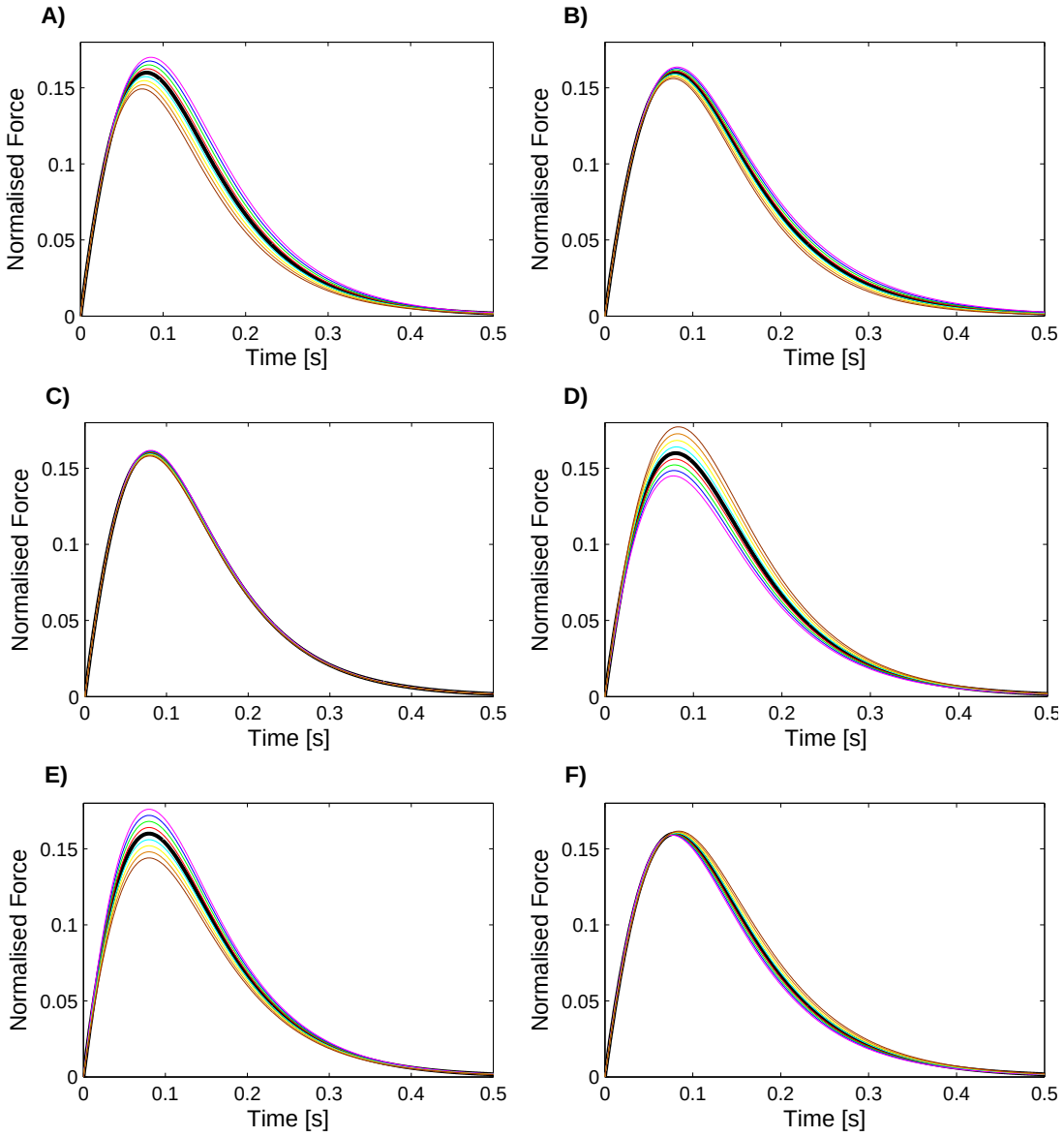

FIGURE 5.22: Change in force-time response to single pulse when each parameter is in turn changed from its average value (—) by up to ±10%. Individual parameter increments are +2.5% (—), +5% (—), +7.5% (—), +10% (—), −2.5% (—), −5% (—), −7.5% (—), −10% (—). A) Changing τ_c, B) changing τ_1, C) changing τ_2, D) changing k, E) changing A, F) changing m.

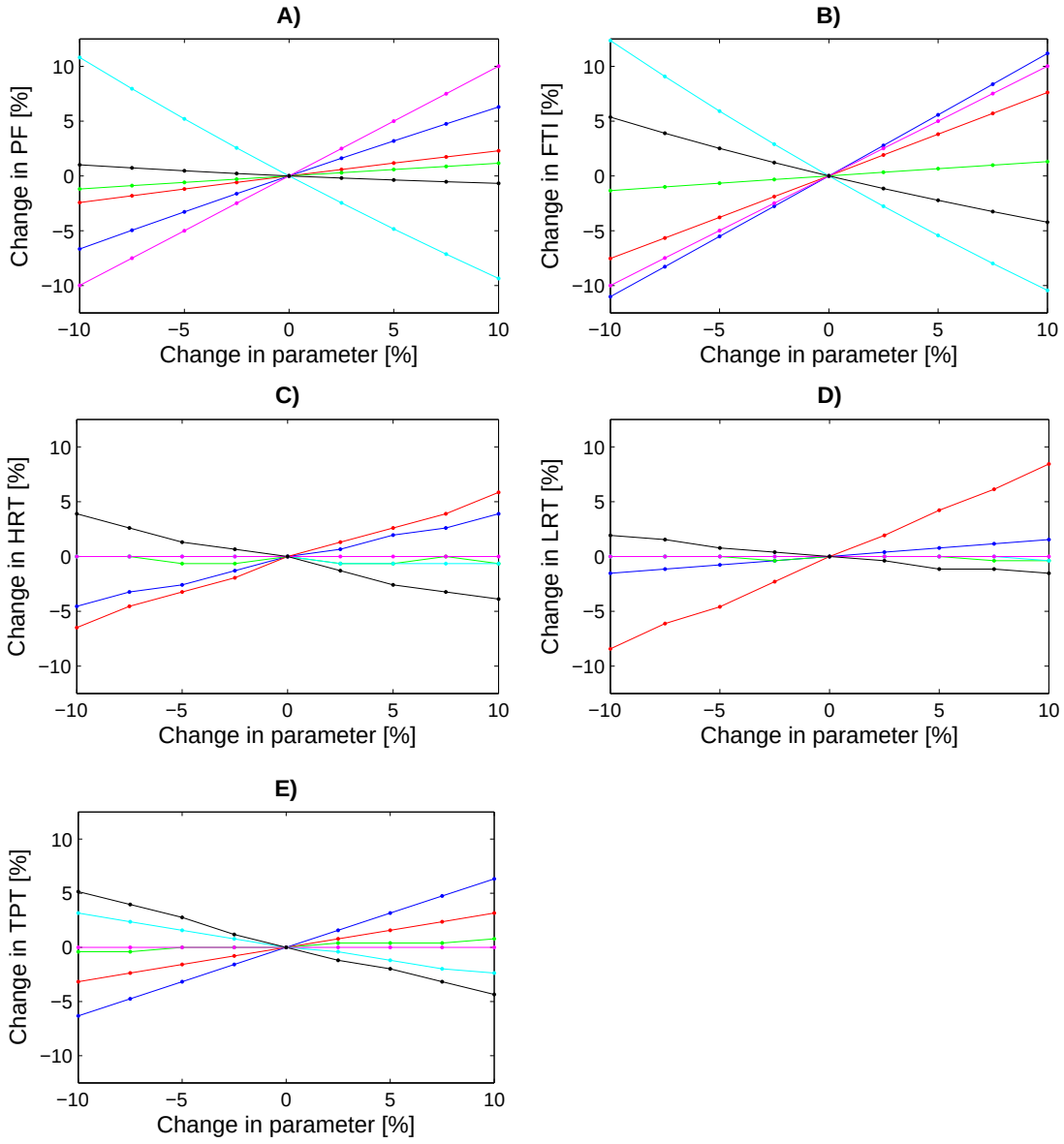

FIGURE 5.23: Percentage change in specific force characteristics and corresponding percentage change in parameter values in response to a single input pulse. A) Peak force, B) Force time integral, C) Half-relaxation time, D) Late-relaxation time, E) Time to peak tension. Parameters are changed one by one and are τ_c(—), τ_1(—), τ_2(—), k(—), A(—), m(—).

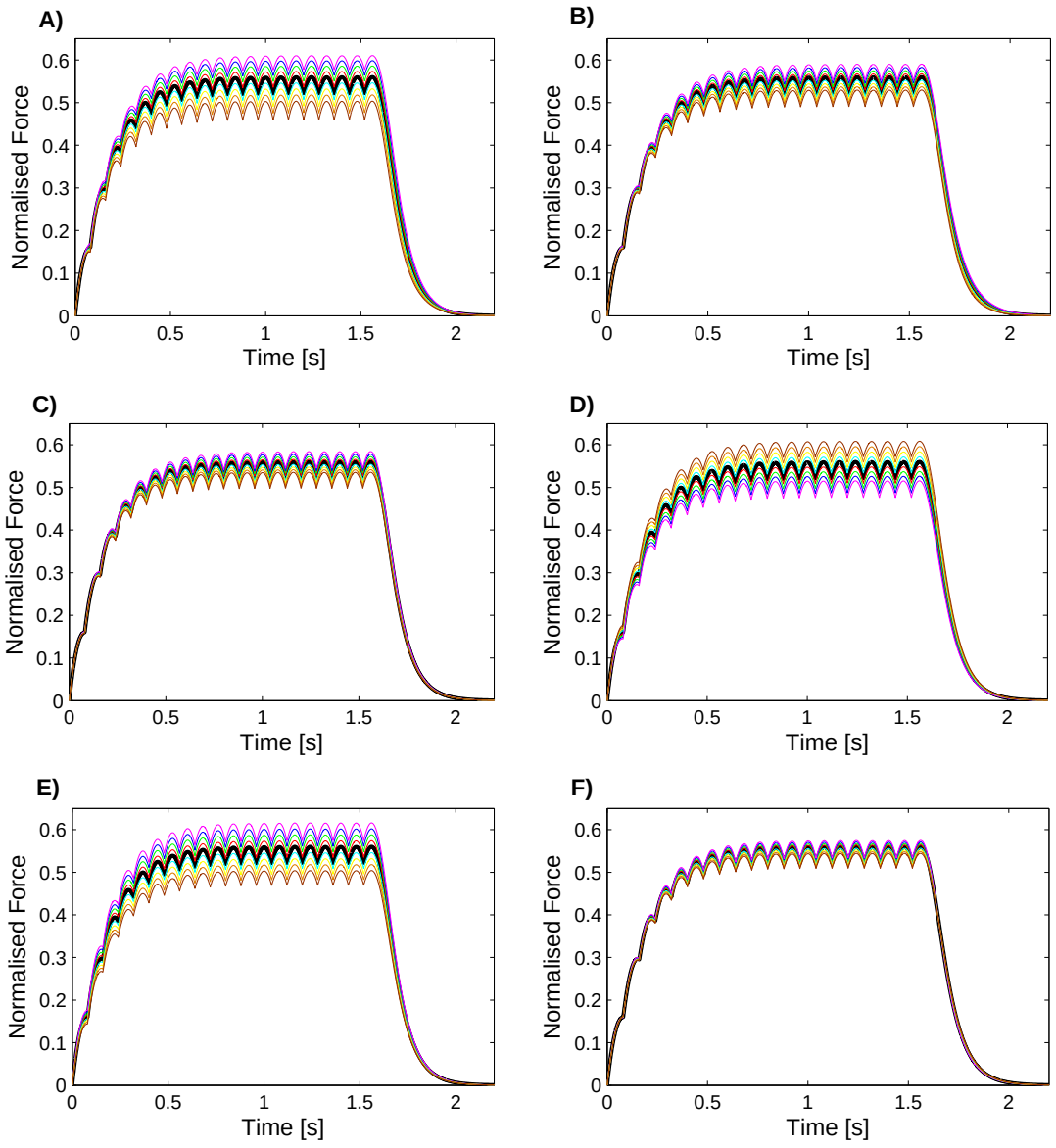

FIGURE 5.24: Change in force-time response to low frequency CFT (12.5Hz) when each parameter is in turn changed from its average value (—) by up to ±10%. Individual parameter increments are +2.5% (—), +5% (—), +7.5% (—), +10% (—), −2.5% (—), −5% (—), −7.5% (—), −10% (—). A) Changing τ_c, B) changing τ_1, C) changing τ_2, D) changing k, E) changing A, F) changing m.

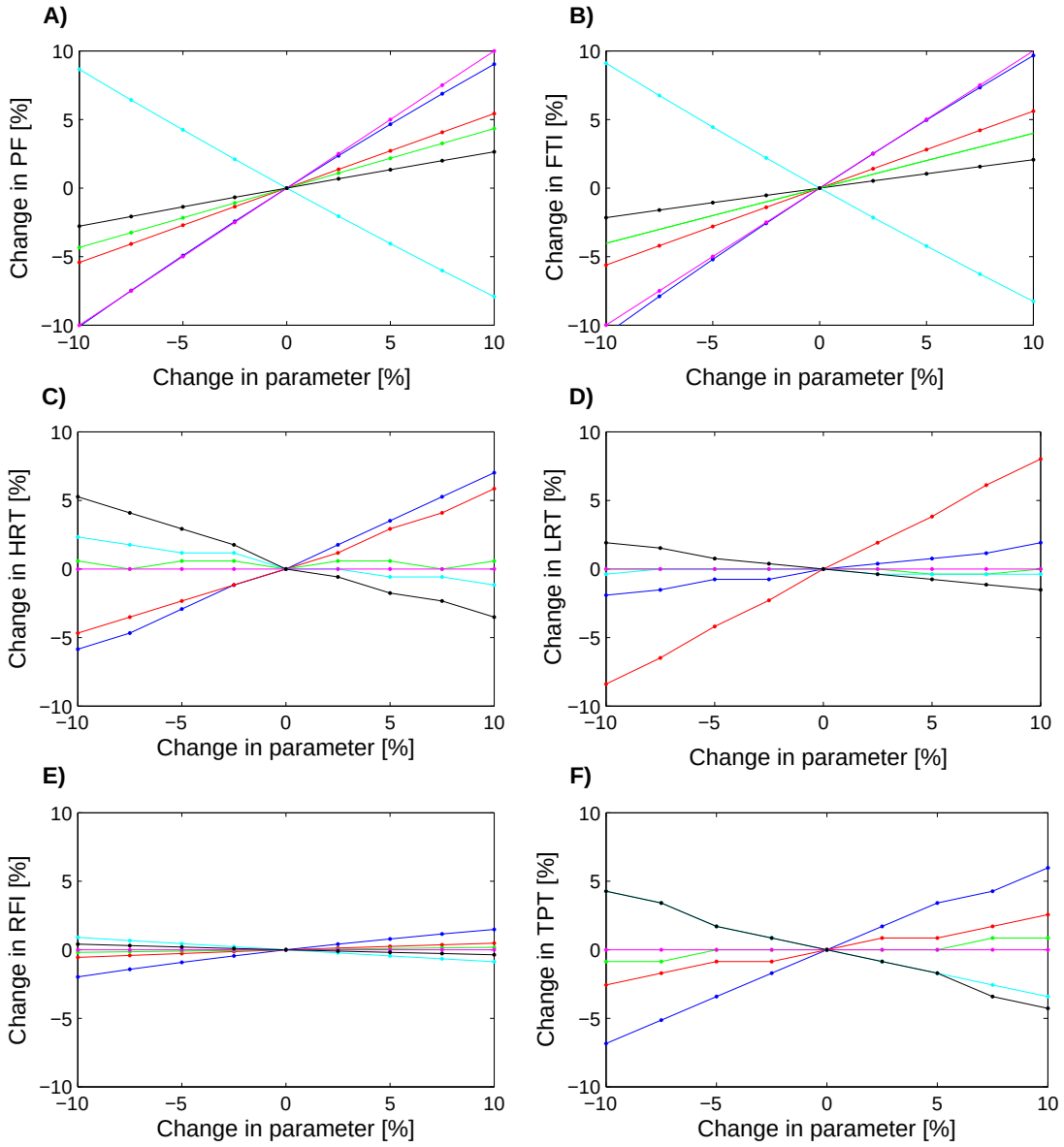

FIGURE 5.25: Percentage change in specific force characteristics and corresponding percentage change in parameter values in response to low frequency CFT (12.5Hz). A) Peak force, B) Force time integral, C) Half-relaxation time, D) Late-relaxation time, E) Relative fusion index, F) Time to peak tension. Parameters are changed one by one and are τ_c(—), τ_1(—), τ_2(—), k(—), A(—), m(—).

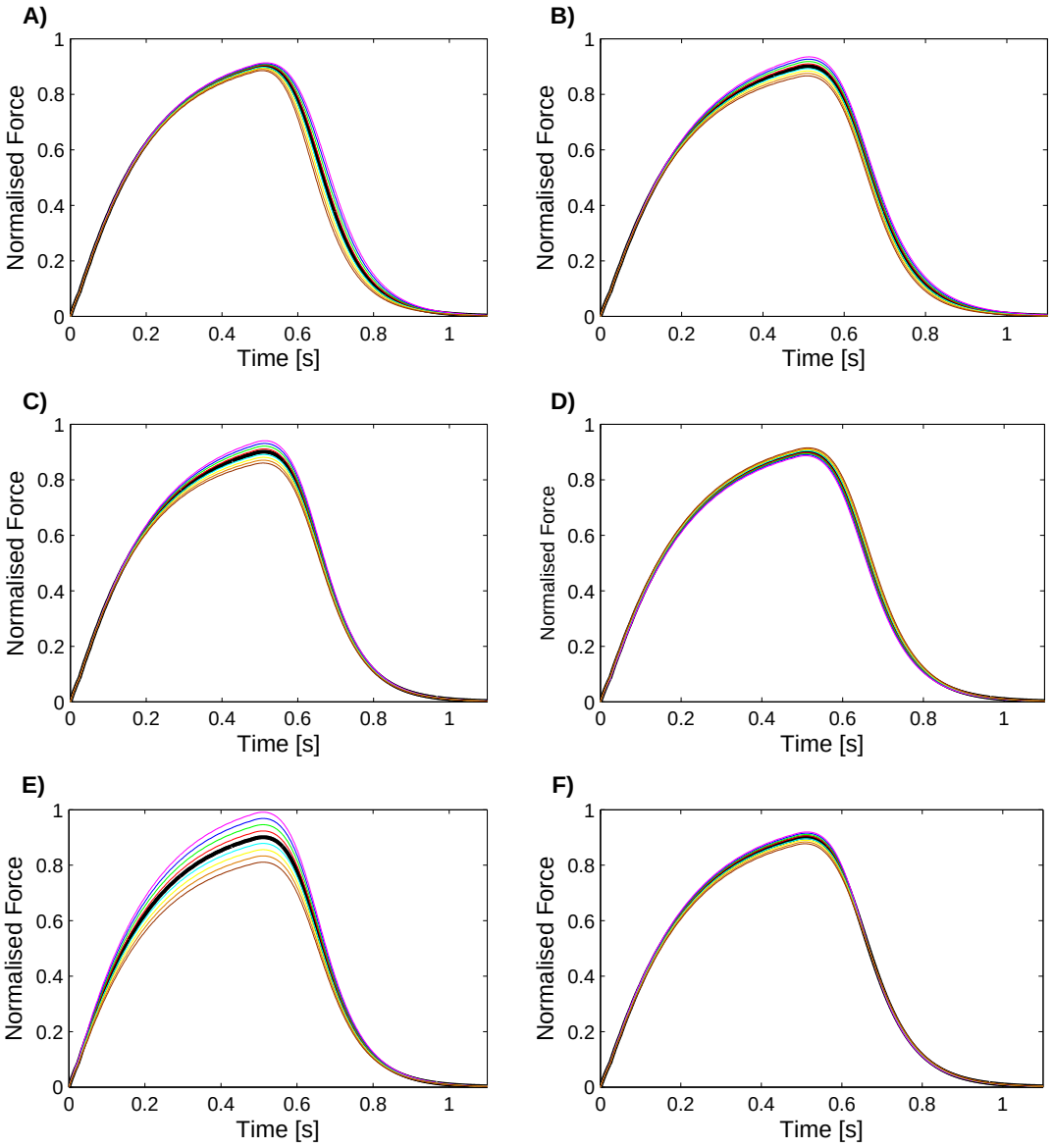

FIGURE 5.26: Change in force-time response to high frequency CFT (40Hz) when each parameter is in turn changed from its average value (—) by up to ±10%. Individual parameter increments are +2.5% (—), +5% (—), +7.5% (—), +10% (—), −2.5% (—), −5% (—), −7.5% (—), −10% (—). A) Changing τ_c, B) changing τ_1, C) changing τ_2, D) changing k, E) changing A, F) changing m.

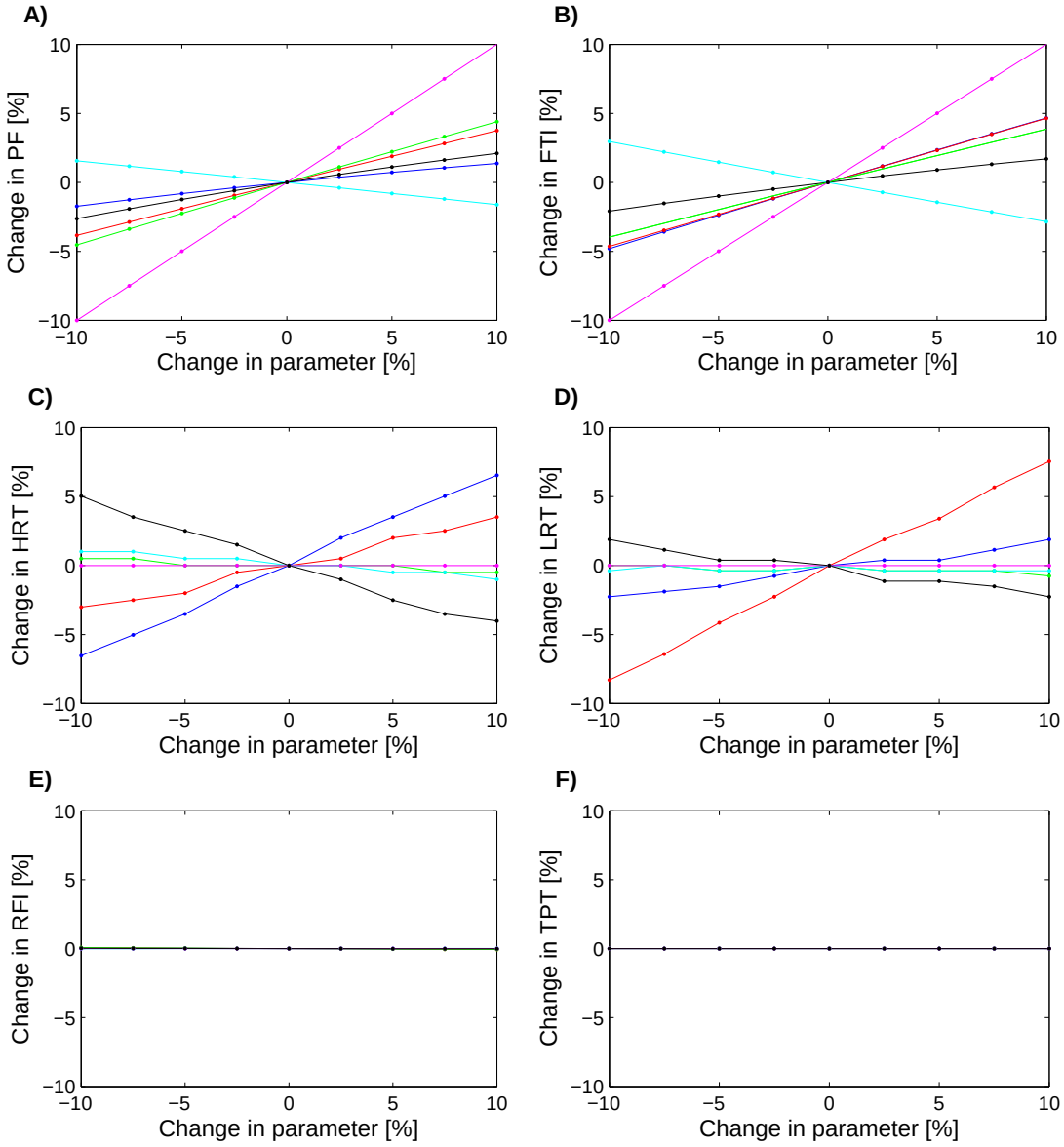

FIGURE 5.27: Percentage change in specific force characteristics and corresponding percentage change in parameter values in response to high frequency CFT (40Hz). A) Peak force, B) Force time integral, C) Half-relaxation time, D) Late-relaxation time, E) Relative fusion index, F) Time to peak tension. Parameters are changed one by one and are τ_c(—), τ_1(—), τ_2(—), k(—), A(—), m(—).

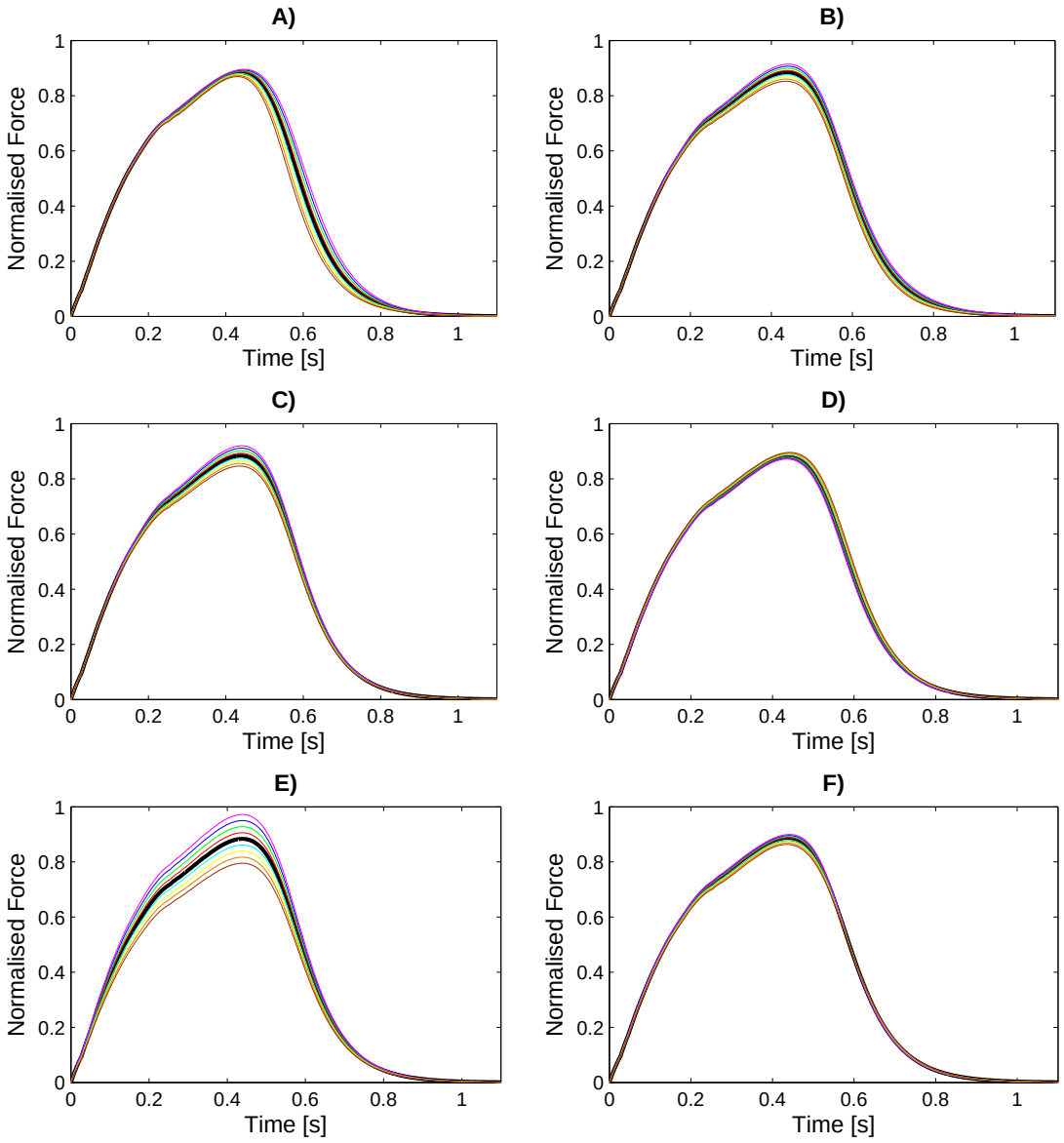

FIGURE 5.28: Change in force-time response to kick type input when each parameter is in turn changed from its average value (—) by up to ±10%. Individual parameter increments are +2.5% (—), +5% (—), +7.5% (—), +10% (—), −2.5% (—), −5% (—), −7.5% (—), −10% (—). A) Changing τ_c, B) changing τ_1, C) changing τ_2, D) changing k, E) changing A, F) changing m.

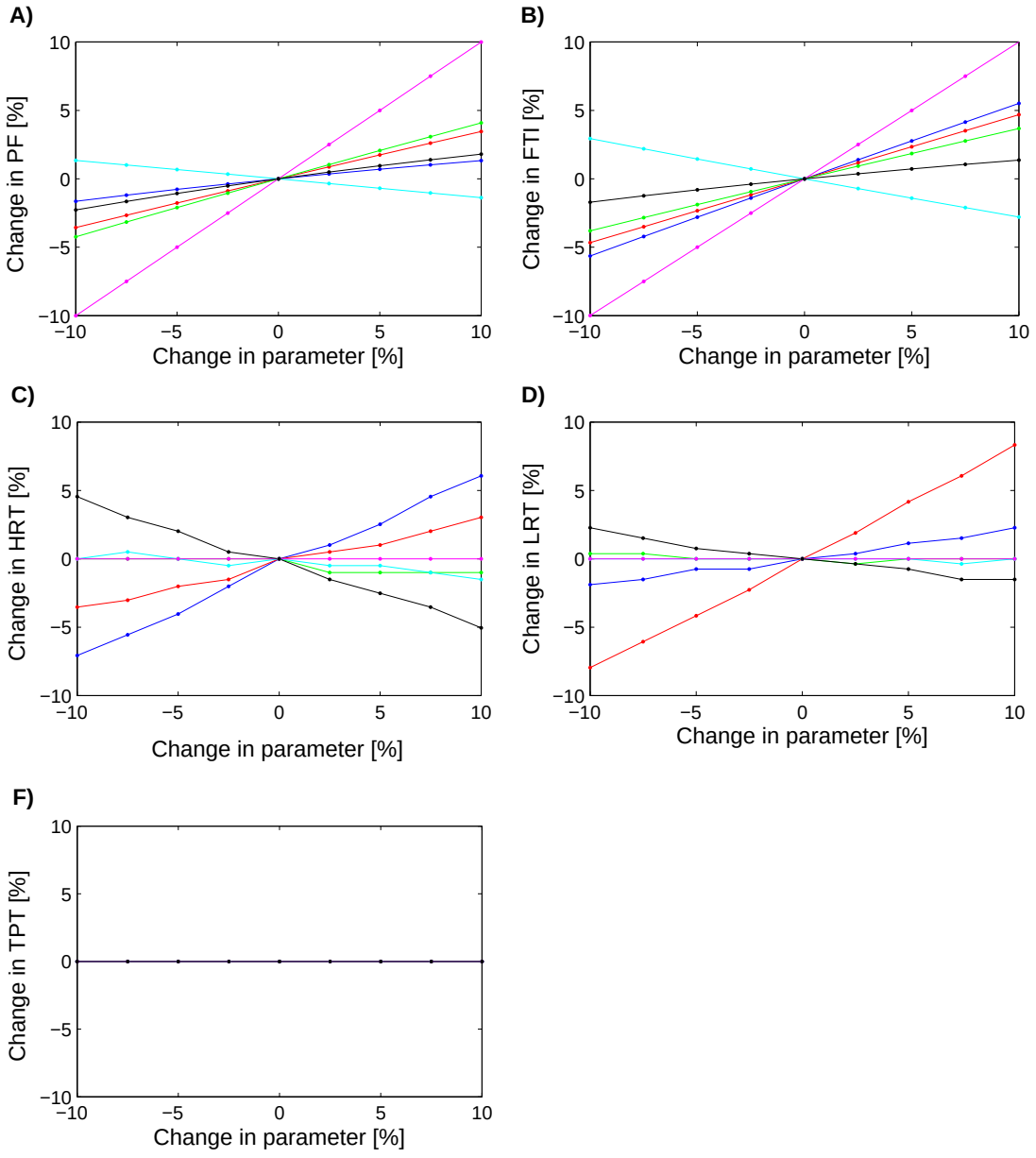

FIGURE 5.29: Percentage change in specific force characteristics and corresponding percentage change in parameter values in response to kick type input. A) Peak force, B) Force time integral, C) Half-relaxation time, D) Late-relaxation time, E) Time to peak tension. Parameters are changed one by one and are τ_c(—), τ_1(—), τ_2(—), k(—), A(—), m(—).

Changes in the parameter k have the most effect on the PF and FTI. An increase in k causes a corresponding decrease in PF and FTI. This is expected, since in Eq. (5.28) a function including the reciprocal of k appears as a scaling factor, multiplying A. Changes in k have a small effect on force-time properties, due to the fact a function of k scales the time constant τ_2. The effect on time properties is small because τ_2 is small.

The parameter m changes all force characteristics a small amount. For a twitch, increasing m decreases the PF and FTI a little, but for other inputs the PF and FTI are increased. This is caused by the fact that m changes the specific shape of the non-linearity as shown in Fig. 5.6. An increase in m decreases the value of the non-linear function for small inputs, yet increases it for high inputs.

The parameter τ_c is the time constant associated with the low pass filtering of the input pulses (Eq. (5.26)). The time constant τ_c is directly associated with the decay time and so increases in τ_c cause increases in HRT and LRT. The change in decay time also affects the peak force and so τ_c has an indirect influence on PF, TPT, FTI and RFI.

The parameter τ_1 is also a time constant, associated with force development. Increases in τ_1 cause increases in HRT and LRT as expected. The time constant in turn affects the force magnitude and increases in τ_1 also result in increases in TPT, RFI (except for high frequency inputs), PF, and FTI.

The parameter τ_2 has less influence on force characteristics. This is expected as from Figs. 5.14 to 5.16 it is evident that the fit is not changed much when τ_2 is not included in the model. The parameter τ_2 has most influence on force magnitude characteristics (PF, FTI).

The force response is not particularly sensitive to changes in any of the parameters. In most cases a $\pm 10\%$ change in input results in a less than $\pm 10\%$ change in output. The exception to this is for a twitch, changing k, but output changes are still low at $\pm 12.5\%$.

It is noted that the TPT and RFI for high frequency inputs are not affected by any changes in parameters. This is attributed to the fact that in these cases the responses are saturated and more extreme changes in parameters are required to change these characteristics.

5.6 Discussion

5.6.1 Optimum Model Behaviour

Both the AIC and BIC indicate that the Adapted model provides the best description of the isometric force response of the locust hind leg extensor muscle. This is further supported by the goodness of fit statistics and the ability of this model to capture the underlying behaviour

reasonably well. The model is relatively simple, has six parameters, and is able to predict the isometric force response to physiologically relevant inputs, as well as to general pulse train inputs.

Adapted model parameters, relevant to the average locust, as given in Table 5.7 were used to simulate each stage of the modelled force generation. The Adapted model consists of two first order differential equations. The first describes a linear relationship between the input pulse and the quantity $C_N(t)$, and acts as a low pass filter. Figures 5.30A, B and C depict how the input pulse train is transformed by Eq. (5.21) into the quantity $C_N(t)$. The second equation (Eq. (5.23)) contains nonlinear terms. These terms act both to restrict the amplitude of the total muscle force and to modify the time constants of the system. Figures 5.30D and E depict how the quantity $C_N(t)$ is transformed into a muscle force.

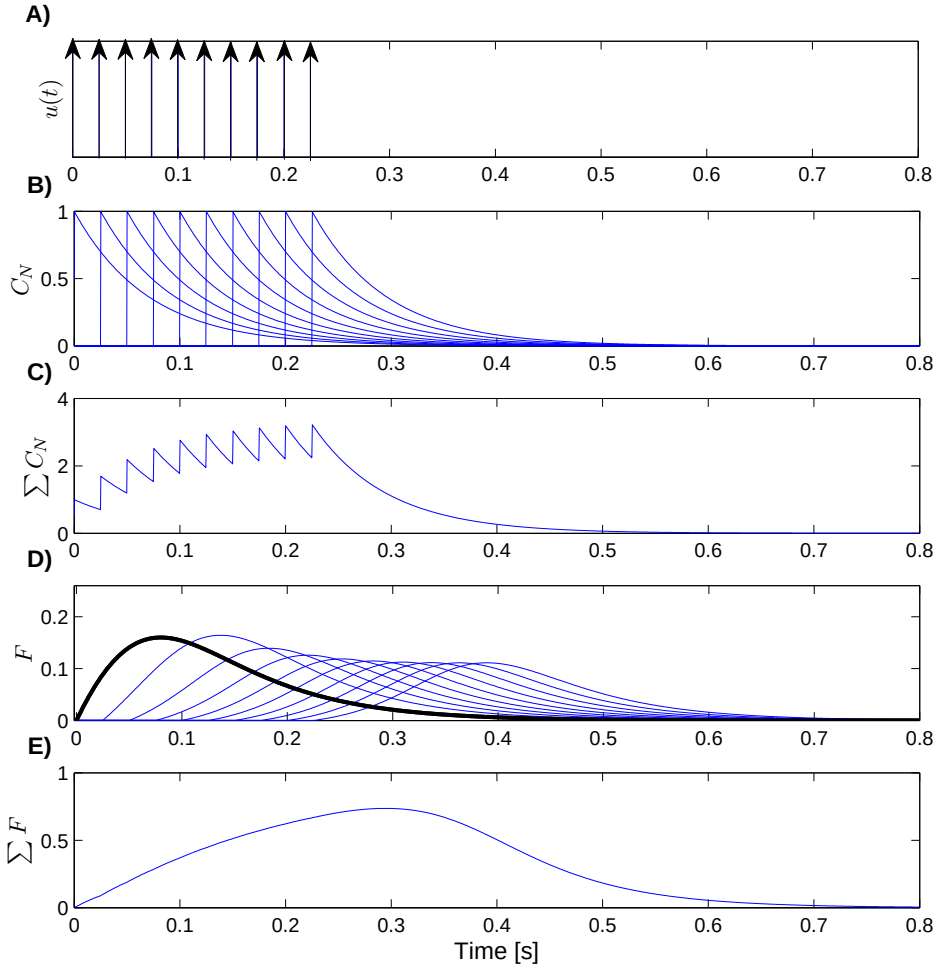

FIGURE 5.30: Behaviour of Adapted model in response to 10 pulse 40Hz CFT broken down into stages, A) Input pulses, $u(t)$, B) Contribution of each pulse to C_N, C) Total C_N, D) Contribution of each pulse to overall force, E) Total isometric force.

5.6.2 Relation of Model to Physiological Processes

The behaviour and form of the Adapted model has physiological relevance. The physical events that occur during muscular contraction are described in Chapter 1. These processes can be summarised as follows [28]: i) Excitation: the arrival of an action potential (AP) releases neurotransmitters, exciting the muscle fibre; ii) Excitation-contraction: the AP propagates through the T-tubuli and gates in the sarcoplasmic reticulum (SR) open and release Ca^{2+} into the muscle filaments; iii) Contraction: Ca^{2+} binds to troponin, freeing binding sites on the thick filaments, a cross-bridge between thin filaments is formed and a subsequent conformal change slides the thin filament over the thick one, shortening the muscle. This is followed by relaxation.

The quantity C_N is thought to represent the calcium concentration in muscle filaments, and the input pulse $u(t)$ the excitation, with the parameter τ_c describing the time constant for calcium release from the SR. The binding of calcium ions to troponin is a saturable nonlinear reaction that occurs during muscle activation; saturation occurs due to the limited number of available binding sites. It is thought that the nonlinear term on the right hand side of Eq. (5.23) reflects the fact that as the calcium concentration increases, eventually the number of cross-bridges reaches a maximum due to there being no more available binding sites, and so the maximum force also reaches a maximum (tetanic force). The nonlinear function on the left of Eq. (5.23) captures the fact that the time constant of the force response to individual pulses within a pulse train changes with time, because it depends on pulse train history. This could be related to the fact that for the muscle to relax, active transport is required to pump calcium out from the muscle filaments and back into the SR. Ebashi [7] recognised the fact that calcium is the key regulatory factor in muscle contraction. This is supported by the general model and by the fact that the calcium concentration C_N plays a key role in determining the overall isometric force response.

The second equation Eq. (5.23) and the time constants τ_1 and τ_2 describe how the free calcium concentration relates to isometric force. The equation is likely to describe the rate-determining step in the formation of a cross-bridge between thick and thin filaments.

The form of the model tends towards that of a simple linear second-order model in the case where there are few, well-separated input pulses (e.g. single pulse input), since the effects of the nonlinear terms become small. Modelling the response to a single input as linear is supported both by previous research [50–53, 156] and the analysis provided in Chapter 4. As the input increases the effects of nonlinearities increase.

5.7 Conclusions

There exist in the literature very few comparisons of existing models, with authors tending to just use their own model. In this chapter seven different isometric models were compared, five taken from the literature and a further two new models adapted from the literature. In comparing models it was clear that a simple Linear model could not describe the inherent nonlinear behaviour of the muscle and, in cases other than where pulses are well separated, provides a poor method of describing the force response to pulse train inputs. The inclusion of a nonlinearity improves the fit as the model is then able to describe some of the nonlinear behaviour. The Cascade model was found to overfit the dynamics, and a better model was one in which the linear part of the model was described by a second order ('Wiener model'), as opposed to a fourth order relation. With the exception of the model of Ding *et al*, models of LNL structure further improved the fit. The model of Ding *et al* performed worse than the Wiener model when describing the response to physiological kick data. It was also found that this model provided a poor description of the underlying behaviour. The best models were Bobet and Stein's model, the Adapted model and the Simple Adapted model. The structures of these models, and hence their modelling capabilities, are similar.

The Adapted model was found to be the best model in terms of goodness of fits, AIC and BIC. A parameter sensitivity analysis on this model found that the force response was not overly sensitive to parameter changes. The structure and model parameters of the Adapted model can be related to the underlying physiological behaviour and the model highlights the key role that calcium plays in muscle contraction.

Chapter 6

Effect of Muscle Length on Force Response

6.1 Introduction

The results given in Chapters 4 and 5 refer to isometric conditions in which the muscle is held at a constant length throughout. All experiments were performed at a fixed muscle length, with the FT angle set to 80°. This chapter investigates the effect on the isometric force of changing the muscle length.

Changing the isometric length is often just assumed to scale the data, as contraction and activation dynamics are commonly assumed uncoupled. In Hill-type models, the relation between maximum tetanic force and muscle length is modelled. This is then used as a scaling factor to describe the isometric behaviour at a range of different lengths (see Ch. 2, Sec. 2.3 for further details). In this chapter the force-length (F_L) relationship of the extensor muscle is investigated. The common method (Sec. 2.3.2.1) of just looking at the maximal isometric force under tetanic conditions is extended. The maximum force vs. muscle length for a range of different stimulation patterns is given. If activation and contraction dynamics are uncoupled these profiles should be scaled versions of each other. Under the uncoupled assumption the type of activation does not affect the contraction dynamics (i.e. the force-length relation). However, it is found that the stimulation type does affect the shape of the force-length curve (FL curve).

As well as looking just at the effect of muscle length on the force-length relationship, as is common practice, the specific shape of the force response at a variety of different lengths is considered. Data, recorded at a number of different muscle lengths, are fitted using the Adapted

model presented in the preceeding chapter. This provides a quantitative measure of how the activation dynamics are effected by muscle length. There have been few previous attempts to quantify the changes in the activation dynamics when the muscle length is changed [87]. By estimating a new set of Adapted model parameters at each length, these changes are tracked and quantified. These findings are used to develop a general isometric model that includes the effect of muscle length in the model.

6.2 Methods

The physical set-up is as described in Chapter 3. Here the specific stimulation protocol used to stimulate the muscle and the angles at which the FT angle was fixed are described in more detail. The main limitation of these experiments was the amount of data that could be collected from each locust.

6.2.1 Stimulation Protocol

The FT angle was set, in the given order to either 80°, 100°, 120°, 60°, 40°, 20°, and 80°; or 90°, 130°, 110°, 90°, 70°, 50°, 30°, and 90°. Two different protocols were used to limit the amount of data being collected from each locust. Using the whole set of angles in one locust did not produce repeatable results. The 80° and 90° measurements were repeated to track the reproducibility and any changes in the response due to the changing input history. At each angle the muscle was stimulated with the training data-set from Chapter 5. This data-set was used because in Chapter 5 it was shown that it can train the model reasonably well whilst keeping the quantity of data small. The amount of data that can be collected from each locust is limited by fatigue (as discussed in Sec. 5.2.2). Unfortunately, due to limits on the amount of data that could be collected and the fact the inputs needed repeating at each different FT angle, the extensor muscle could not be stimulated with additional test data. In this chapter the presented errors and fitted data correspond only to the fit to training data.

6.2.2 Tibial to Muscle Force Conversion

The muscle force was converted into a tibial force at each FT angle using the process described in Chapter 3, Sec 3.4. At each angle the conversion factor changes due to the changing mechanical advantage of the extensor muscle. Results in this chapter, hence refer to the muscle force and are not normalised as in preceding chapters, unless specifically stated.

6.2.3 Non-Uniform Stimulation

Preliminary experiments were performed to set the voltage level used to stimulate the muscle, as described in Chapter 3. In these the stimulus amplitude was increased until a single unitary response was elicited. Similar amplitude levels were then used in experiments. This amplitude level was set at the start of experiments. However, over the course of the stimulation the threshold level to produce a single unitary response to a single input changed. This phenomenum was not seen in data where the angles were not changed. This is possibly due to the decreased time during which the fixed angle experiments took place. This effect meant that within the pulse train response, in some cases, additional neuron stimulation occurred. This phenomenum is demonstrated in Fig. 6.1 which shows the outputs for two repeated inputs for the same locust and FT angle. In one of the responses the extra stimulation response to some of the input spikes is clear. As this happened within the pulse trains the stimulation level could not easily be changed. Data in which extra stimulation occurs were very easy to identify. This data were discarded so that the effects due to the extra stimulation are not included, thus isolating the effects due to changing the isometric length.

Data were collected from eight locusts. However, in data from three of these locusts the effect of non-uniform stimulation was pronounced, so they were not analysed further. The remaining five locusts are termed LV, LW, LX, LY, and LZ. Within these five data-sets results at some angles were discarded due to the presence of non-uniform stimulation.

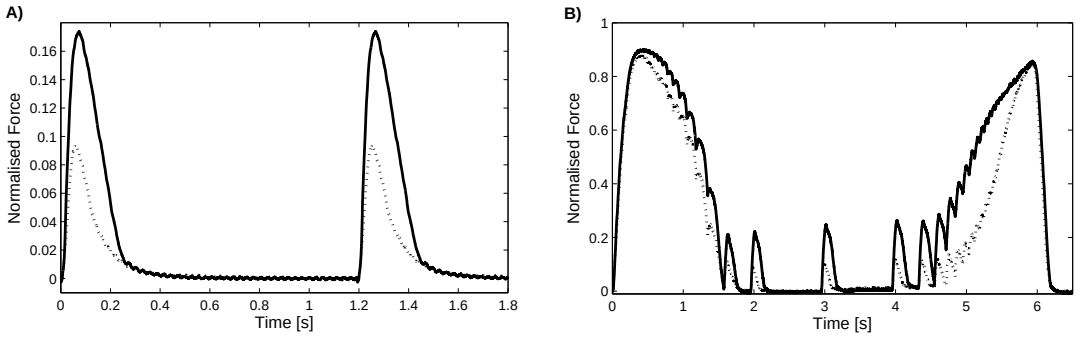

FIGURE 6.1: Problems with stimulation. In one force trace (...) for each case a single, unitary response is elicited. In the other trace (—) for some responses extra stimulation occurs. Presented forces are normalised so the maximum tetanic force recorded in each locust is one.

6.3 Results

6.3.1 Repeatability

The aim of this chapter is to investigate the effect of changing the muscle length on the isometric force response. The changed input history at each length may also cause changes in the force response. Therefore, the repeatability of the response at one angle was assessed to establish which effects are due to the changing input history and which arise from the experimental set up.

6.3.1.1 Angle Unchanged

In order to distinguish the effect of changing the FT angle from history dependent effects, the repeatability of measurements at the same angle was investigated. The training data set was input to the muscle eight times and the resultant force response measured. Figure 6.2 shows the force-time traces for the eight repeats in response to each of the different inputs in one example locust. In a couple of the force responses (corresponding to the first and second repeat) there is some slight deviation in the behaviour, however the broad behaviour is reasonably repeatable. To further investigate and quantify the repeatability, model parameters relevant to the Adapted model were estimated for each set of training data. Figure 6.3 shows the estimated model parameters for each repeat. There is some change in parameters, especially during the first few repeats. This is expected as the force-time traces of these repeats differed slightly. In general the parameter values are very similar and appear to change little over time.

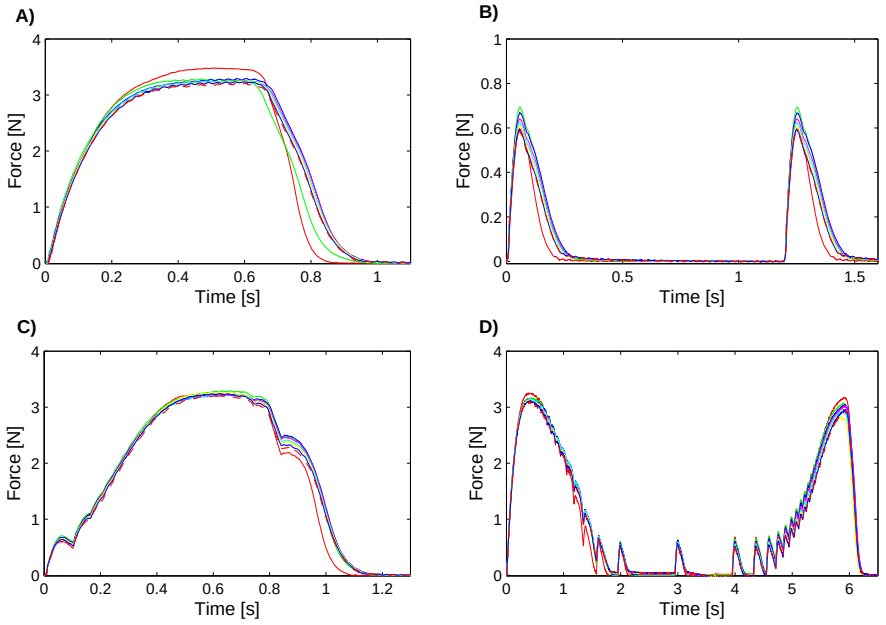

FIGURE 6.2: Repeatability of the data when angle held at 80°. A-D) Give the response to each different input type. Eight repeats are shown and the first (——) and second (——) repeats differ slightly from the other repeats.

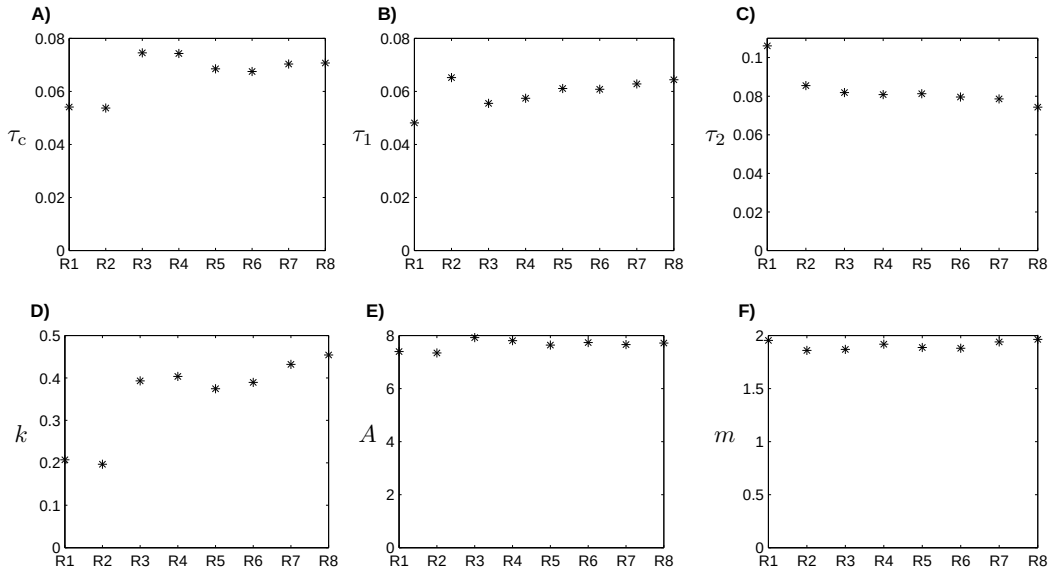

FIGURE 6.3: Estimated Adapted model parameters, found from fitting to 8 repeated sets of normalised training data with the FT angle held at 80°. The estimated parameters are A) τ_c B) τ_1 C) τ_2 D) k E) A F) m.

6.3.1.2 Angle Changed

When the muscle was held at a fixed FT angle of 80° then restimulated, the responses were reasonably repeatable. During force length experiments the FT angle is changed, therefore the effect of changing the FT angle on repeatability is also considered. During experiments the FT angle was set in turn to 80°, 120°, 100°, 80°, 60°, 40°, and 80°; or 90°, 130°, 110°, 90°, 70°, 50°, 30°, and 90° and stimulated using training data at each angle. The repeatability of these 90° and 80° measurements, when all other measurements were also taken, was investigated.

The force-time traces for these repeated angles are shown in Figs. 6.4 to 6.7 for three locusts. The force corresponds to the force exerted by the extensor muscle. The main discrepancy in repeated data is the reduction in magnitude over time. A possible cause for this is muscle damage, caused by muscle movement whilst the stimulation wire is inserted, which arises when the FT angle is changed. The observation that there was no similar force degradation when the angle was not changed supports this. Removal and re-insertion of the wire did not help to improve the repeatability. Inaccuracies may also arise when setting the FT angle; it is estimated that the accuracy in setting the FT joint to a given angle is ± 2.5°.

Aside from the obvious decline in force magnitude, the shape of the force response appears reasonably repeatable. Adapted model parameters were estimated for each repeat and these are given in Fig. 6.8. The largest changes were seen between repeat two and three in the parameter A. In locusts LZ and LW the average normalised standard deviation (n.s.d.) in the parameter A is 39%. Reasonable variations are also seen in the parameter τ_1, with the average n.s.d. 33%. The n.s.d.s of other parameters are significantly lower. The parameter A corresponds to the magnitude and the fact it varies the most supports the observation that it is mainly the magnitudes of responses that are not repeatable. Compared to the case where the angle was not changed, there is also more variation in the other parameters over repeats. These changes in the response over time will be kept in mind when analysing how changes in the FT angle affect results.

Figure 6.9 shows the normalised (so that the maximum tetanic force recorded at each angle is equal to one) and actual muscle force responses to the four different input types at each angle in one locust (LZ). From the normalised data in Fig. 6.9, the shapes of the 80° repeats are similar. This confirms that the main discrepancies in repeated recordings made at the same FT angle relate to the magnitude. The decay in magnitude with repeat number is clear and will be kept in consideration during analysis of results.

Figure 6.9 shows that the shape of the force response depends on the FT angle, and hence on the muscle length. This phenomenum is more clear when considering the normalised force traces. As the FT angle decreases (muscle length increases) the time to reach the peak force

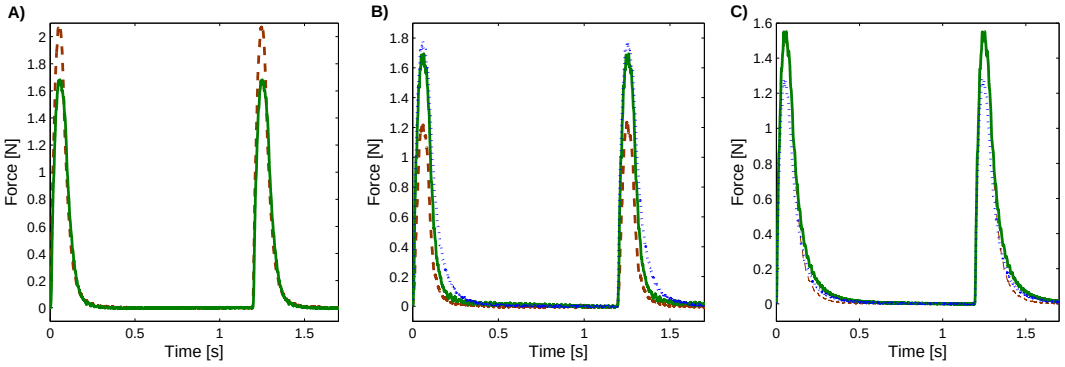

FIGURE 6.4: Repeatability of twitch response in three different locusts (termed LV, LW, LZ) when angle is changed. A) 90° data from LV, only two repeats are shown B) 80° data from LW, C) 80° data from LZ. Up to three repeats are given; Repeat one (- - -), Repeat two (—), Repeat three (...).

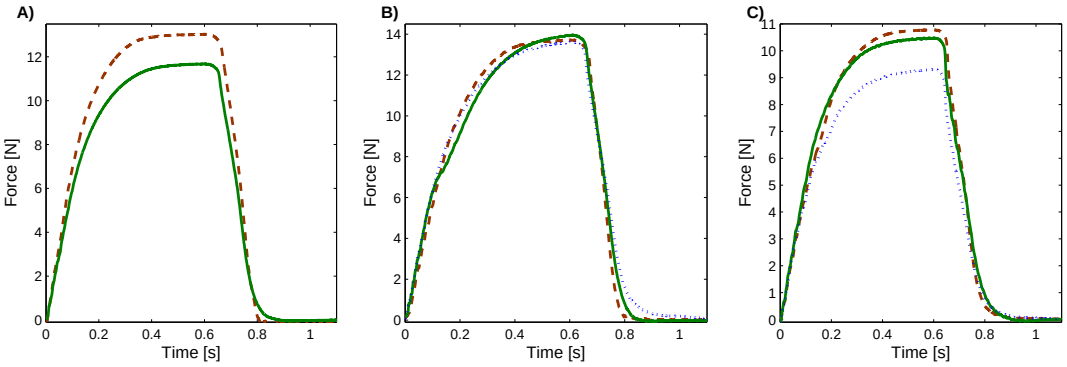

FIGURE 6.5: Repeatability of response to 40pulse, 40Hz CFT in three different locusts (termed LV, LW, LZ) when angle is changed. A) 90° data from LV, only two repeats are shown B) 80° data from LW, C) 80° data from LZ. Up to three repeats are given; Repeat one (- - -), Repeat two (—), Repeat three (...).

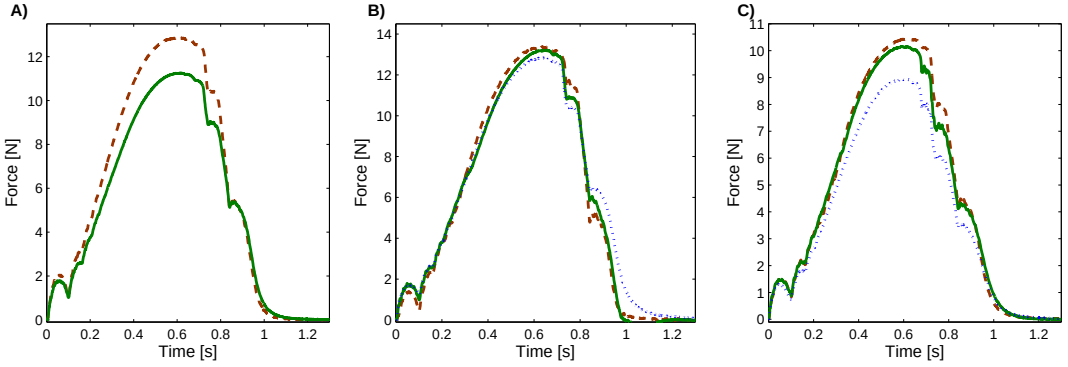

FIGURE 6.6: Repeatability of response to increasing-decreasing frequency pulse train in three different locusts (termed LV, LW, LZ) when angle is changed. A) 90° data from LV, only two repeats are shown B) 80° data from LW, C) 80° data from LZ. Up to three repeats are given; Repeat one (- - -), Repeat two (—), Repeat three (...).

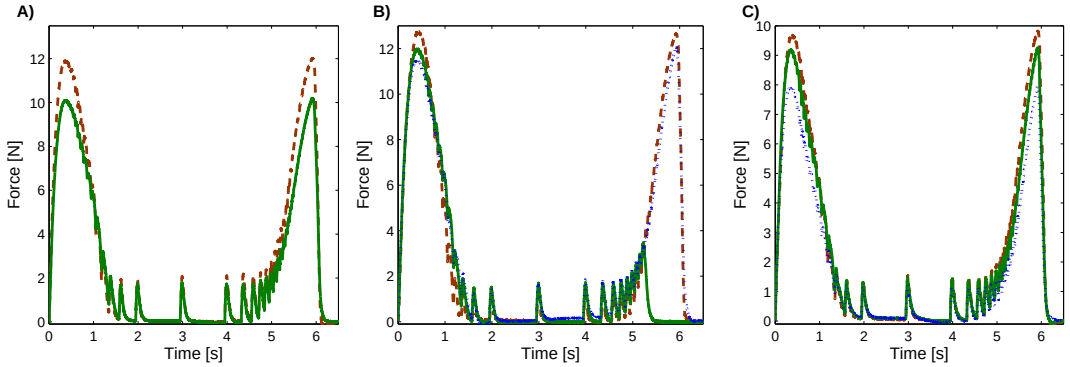

FIGURE 6.7: Repeatability of response to decreasing-increasing frequency pulse train in three different locusts (termed LV, LW, LZ when angle is changed. A) 90° data from LV, only two repeats are shown B) 80° data from LW, C) 80° data from LZ. Up to three repeats are given; Repeat one (- - -), Repeat two (—), Repeat three (...).

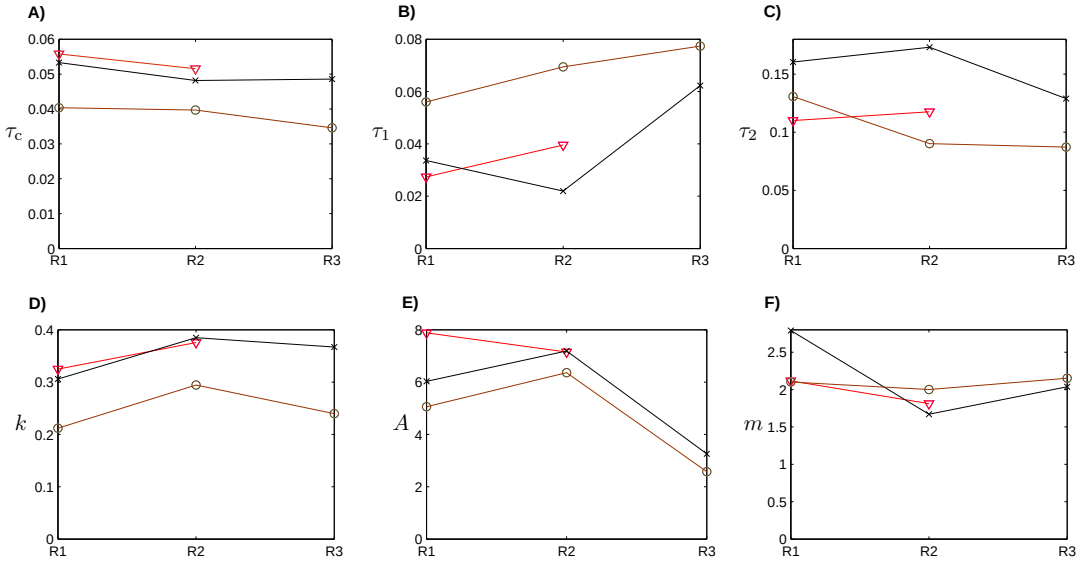

FIGURE 6.8: Estimated Adapted model parameters in three different locusts (LZ○, LW ×, LV ▽) for repeated data where angles changed between repeats.

increases, and the shape of the force response is smoother and 'less square'. This suggests that the activation and contraction dynamics can not be assumed to be uncoupled. This concept is investigated further in the remainder of this chapter.

6.3.2 The Force-Length Relation

As described in Chapter 2, the change in force with muscle length is commonly described by use of a scaling factor which corresponds to the muscle length. A unique scaling factor is used to scale the activation at each length. This factor is obtained from the force-length relation. The force-length relation is found by plotting the maximum isometric tetanic force

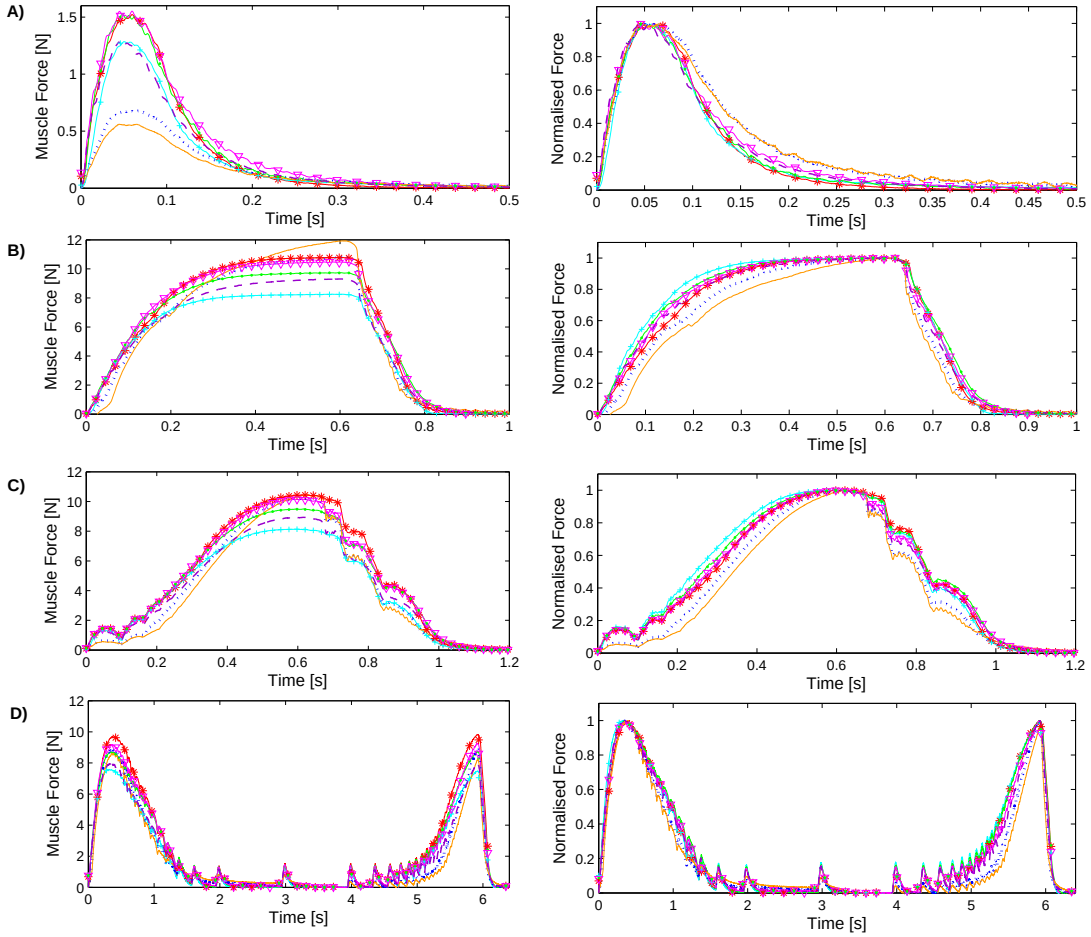

FIGURE 6.9: Example of force-time response recorded in one locust at a range of angles. A) Response to single input, B) response to 40 pulse CFT with IPF=40Hz, C) response to 29 pulse NCFT with IPF=10-100Hz, D) response to 60 pulse NCFT with IPF=10-50Hz. The right hand column shows the normalised force and the left muscle force. The force was recorded in the given order at the following angles: 80°(***), 120°(+++), 100°(.-.-.), 80°(▽▽▽), 60°(...), 40°(—), 80°(- - -).

at a range of different muscle lengths. Commonly, a curve is then fitted to these data to provide a continuous function that relates muscle length to maximal isometric force. This approach assumes that the activation and contractile dynamics are uncoupled. If the activation and contractile dynamics are uncoupled then the shape of the force-length curve should be unaffected by the type of input used to estimate it. The assumption of uncoupled activation and contraction dynamics was tested by plotting the maximum force at each muscle length in response to a range of different inputs. These inputs resulted in both maximal and sub-maximal contractions. Maximal contractions refer to contractions in which the maximum steady-state isometric force (tetanic force) is reached, sub-maximal contractions are all contractions for which maximal activation is not achieved [163]. Figure. 6.10 shows the maximum force at a range of muscle lengths (i.e. FT angles) measured in five different locusts for four different input types. The input types used were equivalent to the training data inputs used in Chapter 5. Of these inputs, the high frequency CFT leads to tetanus and so would be the standard input

type to use in estimating the force-length relation. In response to the increasing-decreasing and decreasing-increasing frequency pulse trains the force reaches the tetanic force at some point, hence these contractions are also termed maximal. In Fig. 6.10 the normalised muscle length is given. The muscle length at 80° was used as a reference point and assumed to be the muscle rest length (l_o). The normalised muscle length was obtained by dividing the current muscle length by the muscle length at 80°.

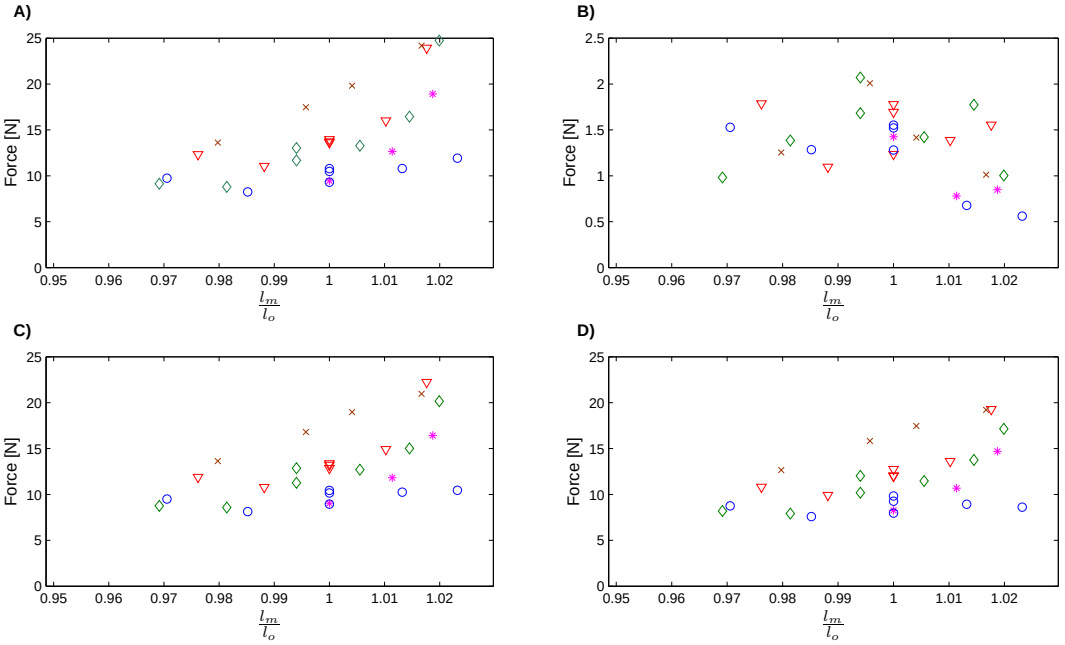

FIGURE 6.10: Maximum force responses at each isometric length for a range of different muscle lengths, given for 5 locusts (x, ▽, ○, ◇, *). A) Response to a 40 pulse 40Hz CFT, B) response to single input, C) response to increasing-decreasing frequency pulse train, D) response to decreasing-increasing frequency pulse train.

At each angle the force is zeroed before the muscle is stimulated, therefore measured forces refer to the contractile force. The passive force is not included in the measurements. In Fig. 6.11 the actual force is normalised by dividing by the maximum force recorded in each locust in response to each specific input. From Figs. 6.10 and 6.11 it is evident that the type of input does influence the shape of the FL curve. The twitch response (Fig. 6.11B) gives a FL curve of similar shape to that seen in the literature (see Fig. 2.12), with the maximum force occurring around the muscle's mid-length. The FL curves from the other input types are similar to each other, but differ from the FL curve for the twitch. The twitch response is an example of a submaximal contraction, as the maximum tetanic force is not reached. The other inputs give rise to maximal contractions. Previous studies [163–165] also found the shape of the FL curve to differ between maximal and submaximal contractions. These studies found that during submaximal levels of stimulation, peak active tension occurs at longer lengths than for maximal stimulation. Rassier [163] suggests that this could be as a result of length-dependent changes in Ca^{2+} sensitivity. The opposite trend is seen in Figs. 6.10 and 6.11. This could be

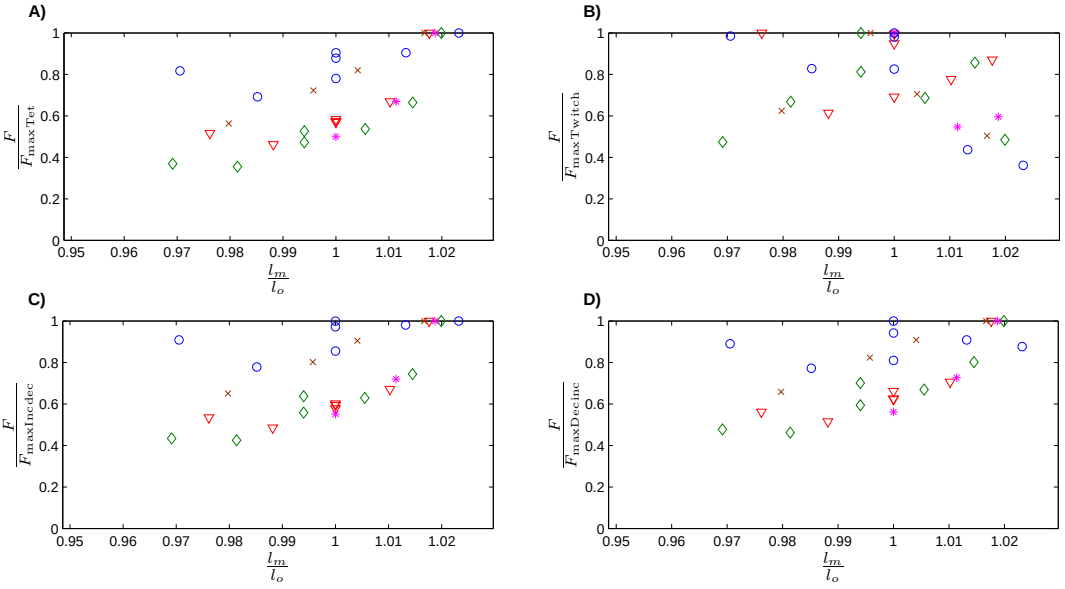

FIGURE 6.11: Normalised (so that maximum response to each input is one in each locust) maximum force responses at each isometric length for a range of different relative muscle lengths, given for 5 locusts. A) Response to a 40 pulse 40Hz CFT, B) response to single input, C) response to increasing-decreasing frequency pulse train, D) response to decreasing-increasing frequency pulse train.

due to repeatability issues, with the decrease in force for longer lengths a result of the decline in force levels over time, as opposed to any internal mechanism. Alternatively, it could be a result of the joint's specific specialisation. In response to maximal stimulation, the force increases as the muscle length increases; there is no subsequent decline in the force magnitude. A possible reason for this could be due to the specialisation of the locust hind leg extensor muscle for jumping and kicking. In response to high frequency sustained contractions the force is maximal when the muscle length is large. This corresponds to a small FT angle. Prior to a jump or kick, co-contraction of the extensor and flexor muscles takes place. During co-contraction the FT angle is small as the tibia is fully flexed. Therefore, it makes physiological sense for the extensor muscle to be optimised to develop the most force when the FT angle is at a minimum (i.e. the muscle at its longest). Single isolated twitch inputs are not used during co-contraction, so the maximum force developed in response to these inputs need not be optimised to occur when the tibia is fully flexed. Furthermore, the FT joint is specialised, and the mechanical advantage of the extensor muscle changes with joint angle. At low or high angles more muscle force is required to produce the same force at the tibia. The locust does not tend to need to produce high tibial forces when the joint is extended, but does prior to a jump when the joint is flexed. Therefore, the mechanics of the joint also mean that the extensor muscle force being maximal at small FT angles (long lengths) is physiologically optimal.

In mammalian muscle the muscle length is assumed to change between 0.5-1.5l_o during a contraction [1] where l_o is the muscle resting length. This is a much larger range than the

changes in length of the locust extensor muscle under the physiological range of movement (i.e. joint rotation from 10°–160°). If it is assumed that the rest length of the locust extensor muscle is at an FT angle of 80°, the expected length changes are of the order of 0.95-1.03l_o. This corresponds to a change in the fibre length of the order of 0.86-1.08l_{of}, where l_{of} is the average fibre length, measured from photographs taken through a microscope. The structure of the locust hind leg extensor muscle (given in Ch. 3) means that the individual fibre lengths are significantly shorter than the total muscle length. It is the individual fibres that contract and result in global contraction of the muscle. Therefore, the change in relative fibre length is perhaps of more significance in this muscle. Although these length changes are much less than those expected in mammalian muscle, they are similar to the ranges measured by Gushlbauer *et al* [5] in the stick insect extensor muscle. They measure a change in muscle length of 0.97-1.03l_o, and in fibre length of 0.80-1.18l_{of} within the physiological range of motion (i.e. 30° - 180°). The differing ranges could be due to the specific muscles and joints of interest, and their specialisations. Zajac's [1] value of maximum length change of 0.5-1.5l_o is based on assumptions from human muscle. These assumptions may not be valid for the locust leg. Mechanics of the joint may restrict the working range. In the present experiment the measurements were recorded at the tibia, with the muscle and joint kept intact. This is not the case in many studies: in these previous studies the muscle can be stretched or shortened beyond its normal working range.

The locust extensor muscle was studied by Zakotnik *et al* [49, 80]. They set the relative extensor muscle length according to the standard model proposed by Zajac [1] to be 1 at an FT angle of 90°, 0.5 for 0° and 1.5 for 180°. These changes were assumed, not measured. It was found in practice that the relative length changes in the locust hind leg extensor muscle are significantly different than the values quoted by Zajac and commonly used to apply to mammalian muscle.

Figures 6.12 and 6.13 show the relative muscle and fibre lengths plotted on axes that range from 0.5-1.5l_o and 0.5-1.5l_{of} respectively. This shows clearly how the measured length changes relate to the values commonly used for mammalian muscle. The reduced range of motion is clear, even when considering the fibre lengths. The different force-length profile in response to high frequency inputs to that seen in the literature could be a result of this reduced range of muscle movement. It is possible that only part of the standard FL curve is replicated as only a section of the standard motion (in mammalian muscle) was used to create it.

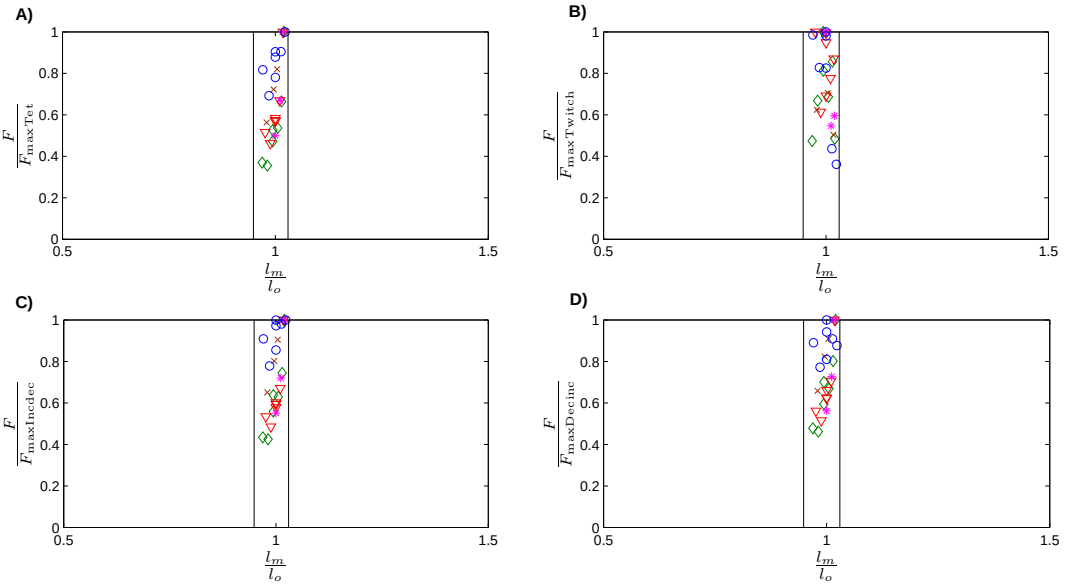

FIGURE 6.12: Normalised (so that maximum response to each input is one in each locust) maximum force responses at each isometric length for a range of different relative muscle lengths, given for 5 locusts. The range of the abscissa is defined by the maximum length change in mammalian muscle; the physiologically possible length change in the locust extensor muscle (vertical lines) is also plotted. A) Response to a 40 pulse 40Hz CFT, B) response to single input, C) response to increasing-decreasing frequency pulse train, D) response to decreasing-increasing frequency pulse train.

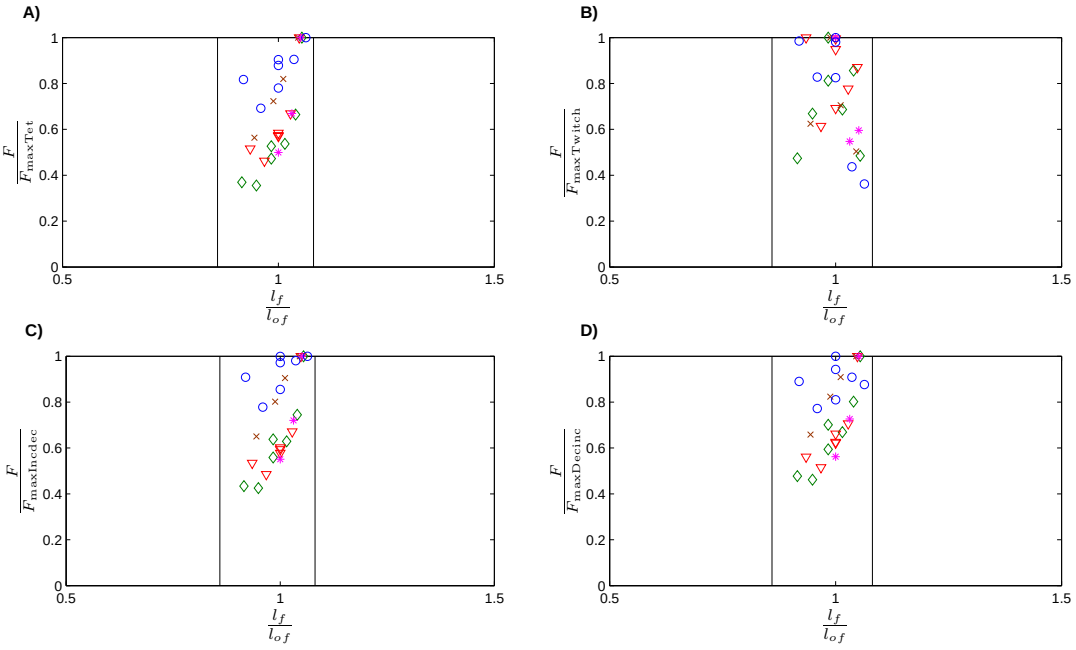

FIGURE 6.13: Normalised (so maximum that response to each input is one in each locust) maximum force responses at each isometric length for a range of different relative fibre lengths, given for 5 locusts. The range of the abscissa is defined by the maximum length change in mammalian muscle; the physiologically possible length change in the locust extensor muscle (vertical lines) is also plotted. A) Response to a 40 pulse 40Hz CFT, B) response to single input, C) response to increasing-decreasing frequency pulse train, D) response to decreasing-increasing frequency pulse train.

6.3.3 Influence of Muscle Length on Force Profile

The fact that the force-length relation depends on the input type suggests that one cannot assume uncoupled activation and contraction dynamics. The differing FL curve shape, dependent on whether the contraction is maximal or submaximal, has also been reported in the literature [163–165]. However, there has been little attempt to characterise how changing the muscle length affects the activation dynamics, either in terms of how the force-time response changes or how a model describing the activation dynamics changes. Perumal *et al* [166] consider how the 'Ding model' is affected by the isometric muscle length by estimating isometric model parameters at a range of different knee flexion angles. They only allow parameter A to change, finding it able to account for most of the changes in force production. In the model A is a scaling factor for force development, hence by allowing only this parameter to change, changes in the specific dynamics, such as the changing shape of the force-time profile, cannot be modelled. In effect, they use A to model the force-length relation. As with Hill-type models, their approach still assumes uncoupled activation and contraction dynamics. The results presented in Figs. 6.10-6.13 suggest that there are changes in the dynamics of the force response, as well as in magnitude. The effect of the muscle length on the specific form of the force response has not been well documented. In this section, along with further examination of the effect of the muscle length on the shape of the force responses, changes in the force response with muscle length are quantified by estimating a different set of Adapted model parameters at each isometric length. From this, the change in Adapted model parameters with muscle length can be established. Trends in model parameters are then assessed, to establish exactly how the activation dynamics are affected by the muscle length.

Figure 6.14 shows the muscle force recorded at a range of different isometric lengths and the modelled response, using the Adapted model for one locust. The model parameters relevant to Fig. 6.14 were estimated by allowing only the parameter A to vary with muscle length and holding the other parameters constant. In effect allowing A to change accounts for the F_L scaling. This method assumes uncoupled activation and contraction dynamics, and is similar to the approach used by Perumal *et al* [166]. The corresponding errors in fit for the given locust are shown in Fig. 6.15. The errors in estimation are reasonable, with all estimated errors across the range of FT angles being less than 3.5% in this particular case. Despite the fact that this method of accounting for muscle length changes gives reasonable errors in the least squares sense, Fig. 6.14 highlights some shortcomings of this modelling method. The peak values are wrongly predicted, with the maximum force being overpredicted at large FT angles and underpredicted at small FT angle. Some of the error in estimating the peak may arise as a result of the decline in force level with time, as discussed in Sec. 6.3.1. In Fig. 6.14 only the parameter A was allowed to change between FT angle, therefore changes in the model dynamics between angles cannot be modelled. However, a change in model dynamics between

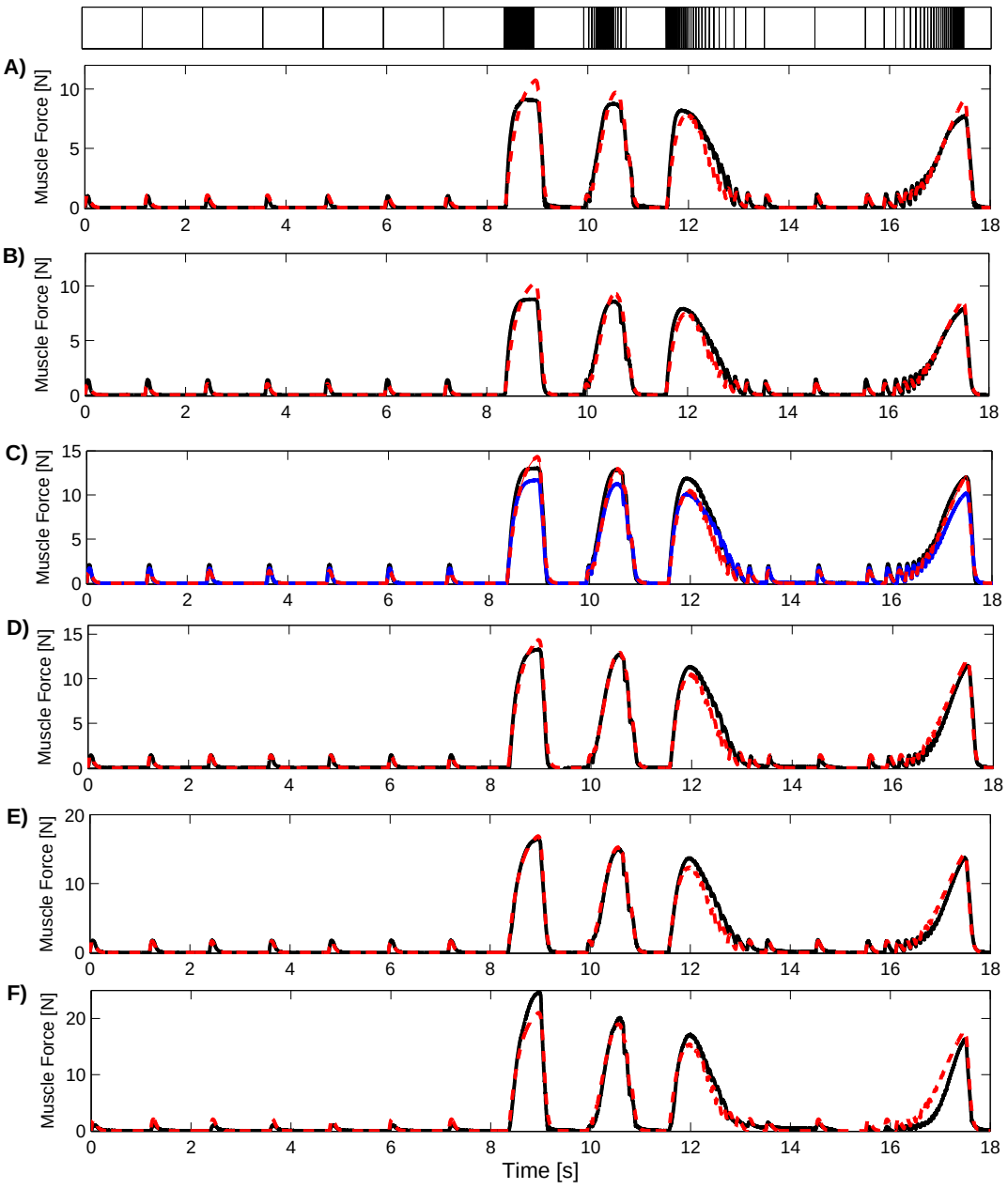

FIGURE 6.14: Measured (—) and modelled (- - -) force response at a range of FT angles for one example locust (LV), the location of stimulus pulses is given at the top of the figure. The modelled trace is fitted to data using the Adapted model, where the parameter A was allowed to vary with FT angle. A) FT=130°, B) FT=110°, C) FT=90° (the measured repeat (—) is also given), D) FT=70°, E) FT=50°, F) FT=30°

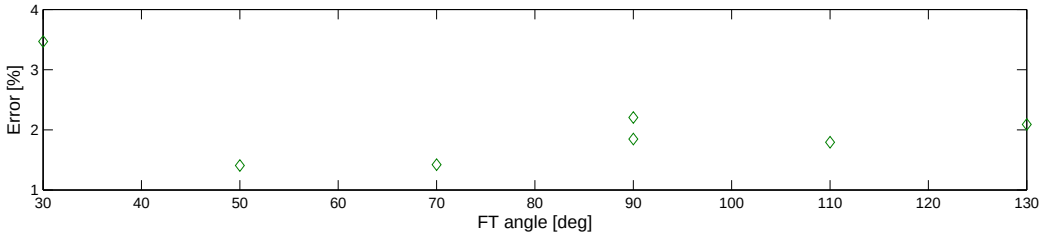

FIGURE 6.15: Errors between measured and modelled data, for locust LV, at a range of FT angles when using the Adapted model and allowing the parameter A to vary between angles.

FT angles is evident in the measured response. The tetanic response at 130° is a lot more square (i.e. maximum force is reached sooner) than the recorded response at 30°. The model is unable to recreate this behaviour.

In order to assess and attempt to quantify changes in the dynamics of the model with muscle length, a different set of adapted model parameters were estimated at each angle, for each locust. The resultant fit to one example locust is shown in Fig. 6.16. It is clear that using this method provides a good fit to the experimental data, however the method requires a large number of parameters to be estimated for each locust. Furthermore, the model only fits the behaviour at a discrete set of FT angles and cannot be utilised to estimate the behaviour at other angles. The estimated errors and parameters in each locust at each FT angle are shown in Figs. 6.17 and 6.18 respectively. The low errors confirm that the fit to data is reasonable. The errors are, as expected, lower than for the case where only the parameter A was allowed to change.

Ideally the dependence of each parameter on the FT angle (or equivalently the muscle length) should be contained within the model, rather than a separate parameter set be estimated at each angle. This would enable the model to predict the response when the FT angle is set to angles other than those measured. Consequently parameters in the model are assumed to be functions of the FT angle and the model fitted across all angles using these relations. The functions used to describe the dependence of each parameter on the FT angle are given by

$$\tau_c = p_1\lambda + p_2 \tag{6.1}$$

$$\tau_1 = \text{const} \tag{6.2}$$

$$\tau_2 = r_1 \exp(r_2\lambda) + r_3 \tag{6.3}$$

$$k = \text{const} \tag{6.4}$$

$$A = s_1\lambda^2 + s_2\lambda + s_3 \tag{6.5}$$

$$m = \text{const} \tag{6.6}$$

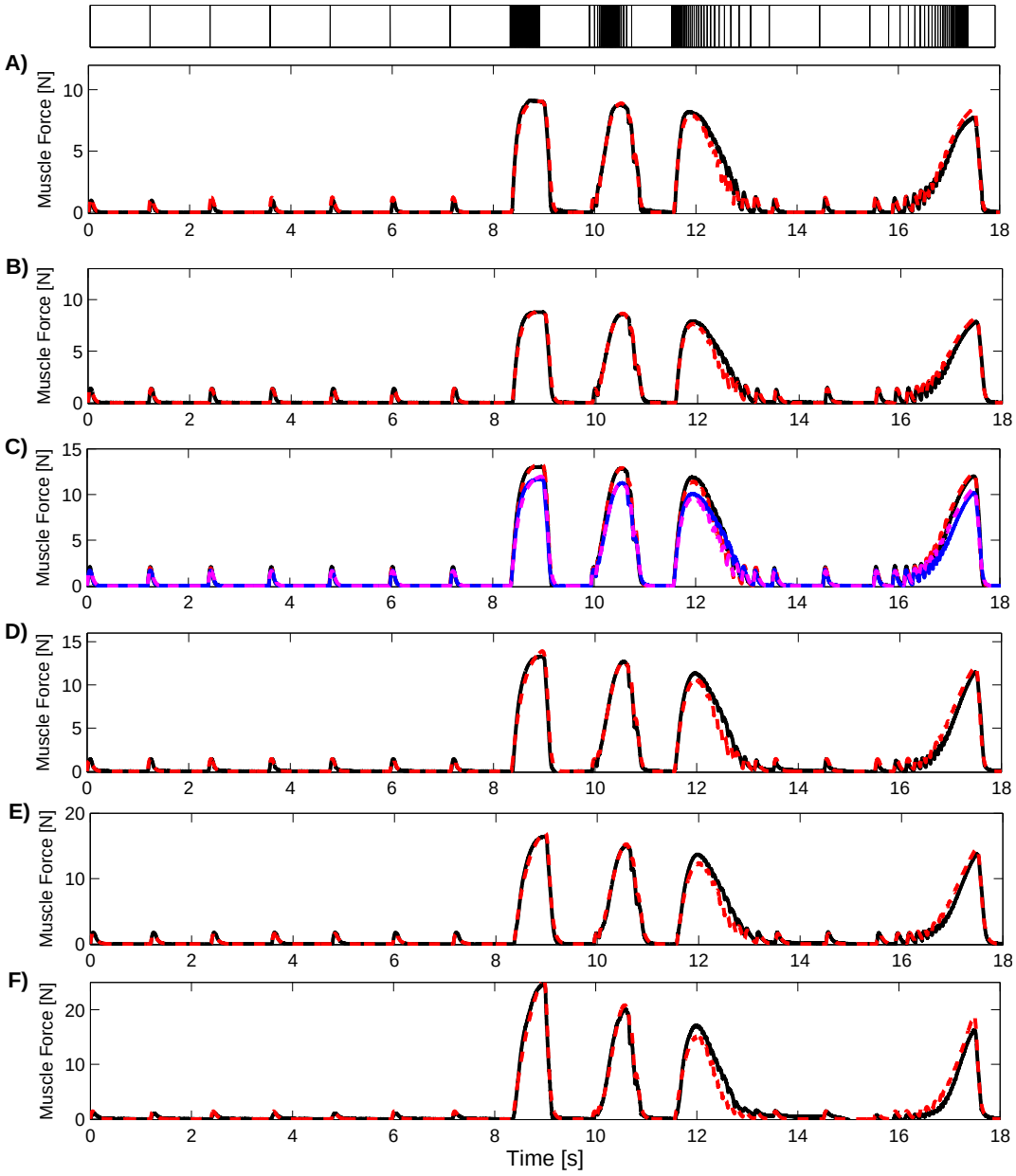

FIGURE 6.16: Measured (—) and modelled (- - -) force response at a range of FT angles for one example locust (LV), the location of stimulus pulses is given at the top of the figure. The modelled traces were obtained using the Adapted model and estimating a new set of parameters at each FT angle using a least-squares fit. A) FT=130°, B) FT=110°, C) FT=90° (the measured repeat (—) and corresponding fit (- - -) are also shown), D) FT=70°, E) FT=50°, F) FT=30°.

where λ is the FT angle in radians. These were found to minimise the fitting errors, while being relatively simple functions. The parameters k and m are assumed to be constant as there are no clear trends in the variations of these parameters with FT angle (Fig. 6.18). Although there is a slight increasing trend in the parameter τ_1 the resultant fit errors were little better than those found by holding τ_1 constant, hence τ_1 is also assumed to be constant. The parameter A is described by a function similar to functions used to estimate the F_L relation in Hill-type

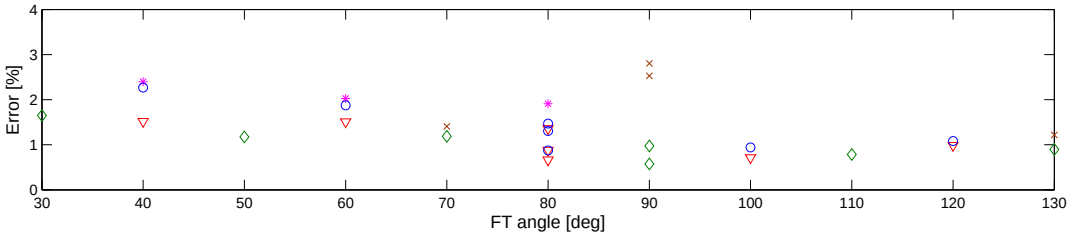

FIGURE 6.17: Errors estimated in 5 locusts (LV (◊), LW (▽), LX (×), LY (*), LZ (○)) when the Adapted model is used and a new set of parameters are estimated at each FT angle.

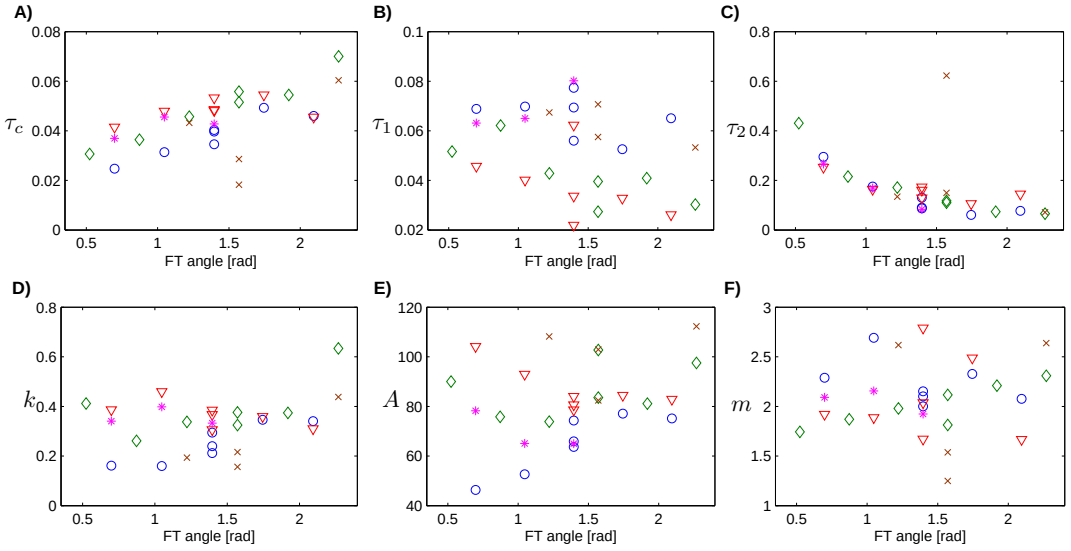

FIGURE 6.18: Estimated Adapted model parameters at different FT angles for 5 locusts (LV (◊), LW (▽), LX (×), LY (*), LZ (○)).

models. Although trends in parameter A are not clear, likely due to repeatability issues, using the given function to describe the parameter A improved fit errors. The relation between τ_2 and the joint angle was assumed to be exponential. An exponential relation was used as when τ_2 was plotted on a log-axis there was an apparently linear trend with the FT angle (see Fig. 6.19).

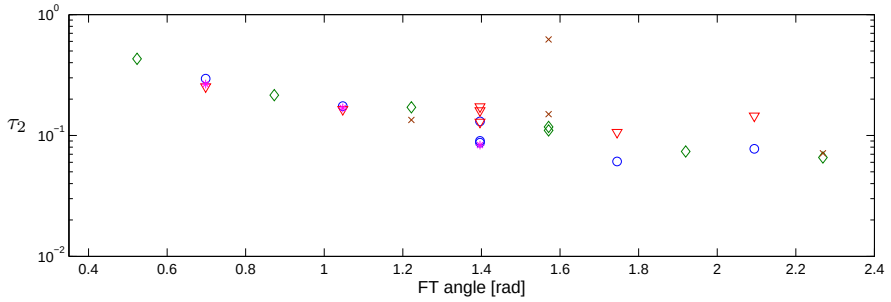

FIGURE 6.19: Estimates for parameter τ_2 at each FT angle, plotted with a logarithmic y-axis. For 5 locusts (LV (◊), LW (▽), LX (×), LY (*), LZ (○)).

Using the parameter dependencies given in Eq. (6.1) to (6.6) the Adapted model was used to estimate the force across all joint angles in each model. The estimates for the Adapted Model parameters at each individual FT angle were not fitted directly to Eq. (6.1) to (6.6); instead the whole data set for all angles (for each locust) was fit to, with the parameters described as the functions in Eq. (6.1) to (6.6). Functions to describe each parameter, with the exception of A, were obtained from the trends shown in Fig. 6.18 as described in the preceding text. The function defining A was chosen to minimise overall fit errors. The resultant fit to experimental data is shown for one locust in Fig. 6.20, with the corresponding errors given in Fig. 6.21. The fit to data appears reasonable with the main source of error coming from scaling the magnitude. The fitted functions describing the dependence of estimated parameters on FT angle are shown in Fig. 6.22, along with the individual parameter estimates for each angle. The trend in the parameter τ_2 with FT angle is clear. The value of τ_2 for locust LY differs significantly for larger angles. This can be attributed to the fact that for this locust no estimates were made for larger angles (because the data showed non-uniform stimulation). Functions describing the parameter τ_c for each locust are broadly consistent, with the exception of locust LY. This could again be due to the lack of data available for Locust LY. Functions describing the parameter A show the most inconsistency, probably due to issues in recording the magnitude. The muscle length is a function of the FT angle and depends on the joint dimensions of each individual locust. Figure 6.23 shows the parameters as functions of the change in muscle length relative to that at an FT angle of 80°.

The experimental data measured for locust LZ are shown in Fig. 6.24. Figures 6.25 and 6.26 show the predicted force response to each input when only parameter A is allowed to depend on the FT angle and when the parameters are defined as functions of the FT angle respectively. The shape and magnitude of the force response can be clearly seen to depend on FT angle in the experimental data. The model where only parameter A is allowed to change is unable to capture this variation as at each angle the data is just a scaled version of data at other angles. With the exception of the twitch data, the model where the parameters depend on the FT angle (Fig. 6.26) provides a reasonable description of the experimental behaviour, and the change in the pulse shape is captured.

The main source of error when using the Adapted model and the functions given in Eq. 6.1 to 6.6 to describe the parameters was the magnitude being wrongly predicted. This could be linked to the repeatability issues discussed in Sec. 6.3.1. The inability of the model to fit to the measured magnitude could be a consequence of the decay in magnitude that was measured over time. There is no merit in having a model that fits to data with smaller errors than the variability than is seen in the data. Figure 6.27 shows the estimated errors for a range of cases. The variability between repeated recordings at 90° is also shown, along with the estimated errors when using: the Adapted model and only allowing the parameter A to change with FT

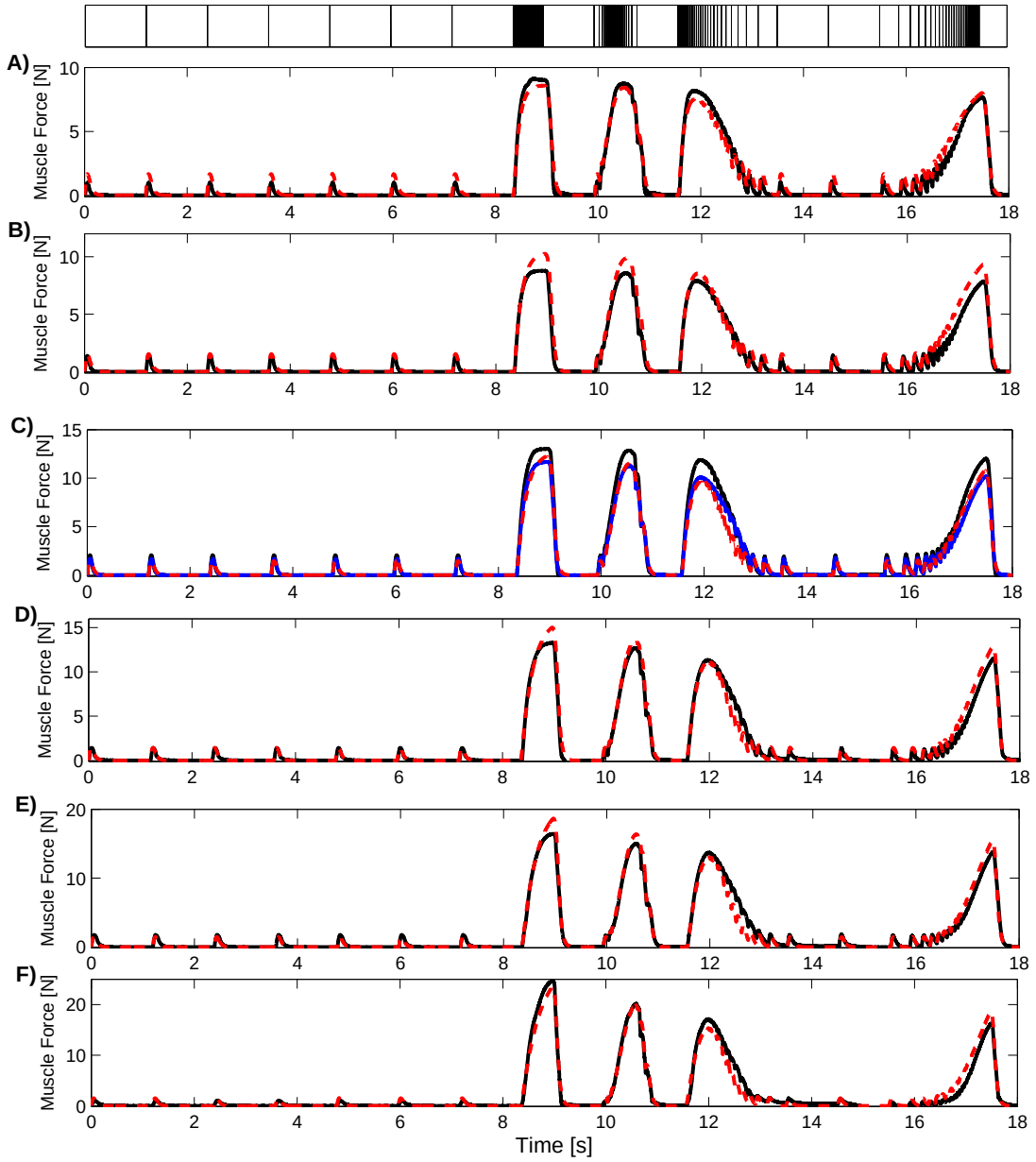

FIGURE 6.20: Measured (—) and modelled (- - -) force response at a range of FT angles for one example locust (LV), the location of stimulus pulses is given at the top of the figure. The modelled traces were obtained using the Adapted model, with parameters described as functions of the FT angle as defined in Eq. (6.1)-(6.6). A) FT=130°, B) FT=110°, C) FT=90° (the measured repeat (—) is also shown), D) FT=70°, E) FT=50°, F) FT=30°.

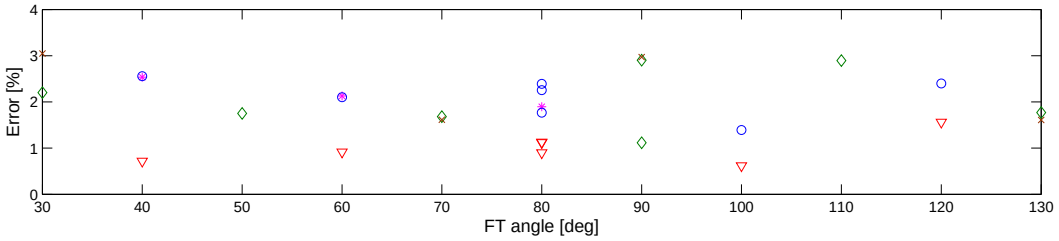

FIGURE 6.21: Estimated errors when using the adapted model and describing parameters as functions of the FT angle. Errors are given for 5 locusts (LV (◊), LW (▽), LX (×), LY (*), LZ (○)).

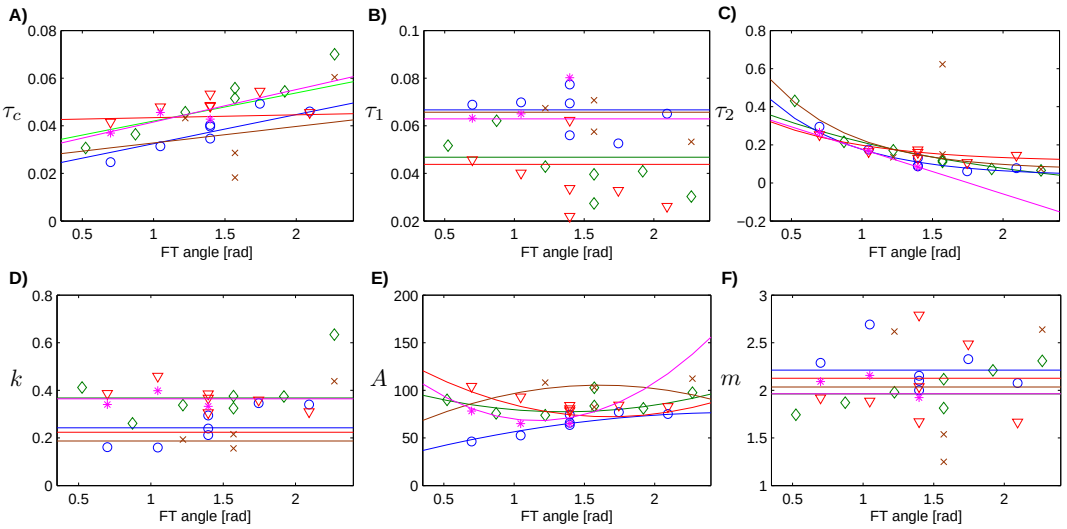

FIGURE 6.22: Fitted parameters of the Adapted model as functions of the FT angle (continuous lines). The individual parameter estimates at each FT angle are also given (*). Results are given for 5 locusts (LV (◊), LW (▽), LX (×), LY (*), LZ (○)).

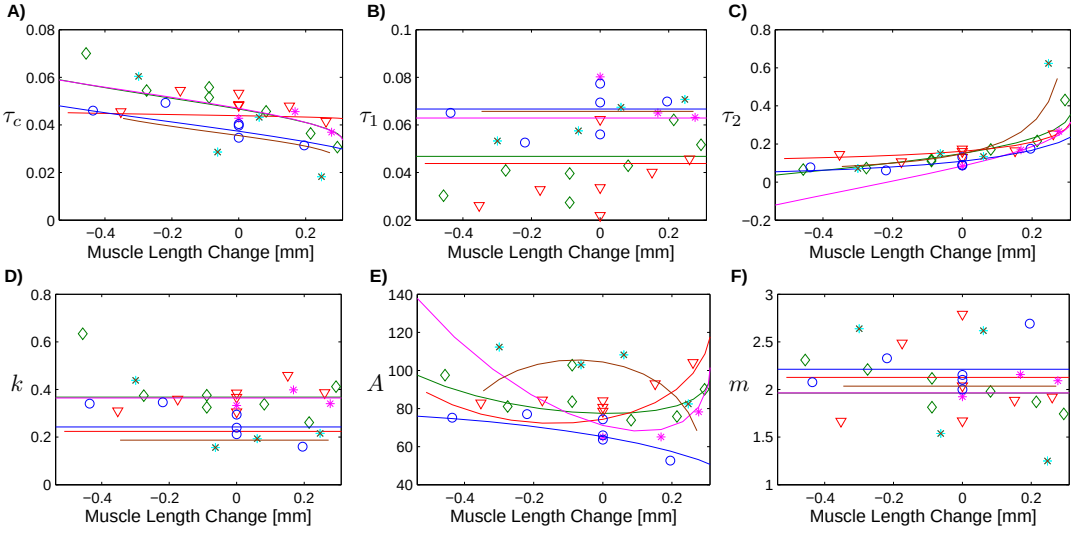

FIGURE 6.23: Relation between estimated parameters and muscle length change. Length changes are measured relative to the muscle length at 80°. Results are given for 5 locusts (LV (◊), LW (▽), LX (×), LY (*), LZ (○)).

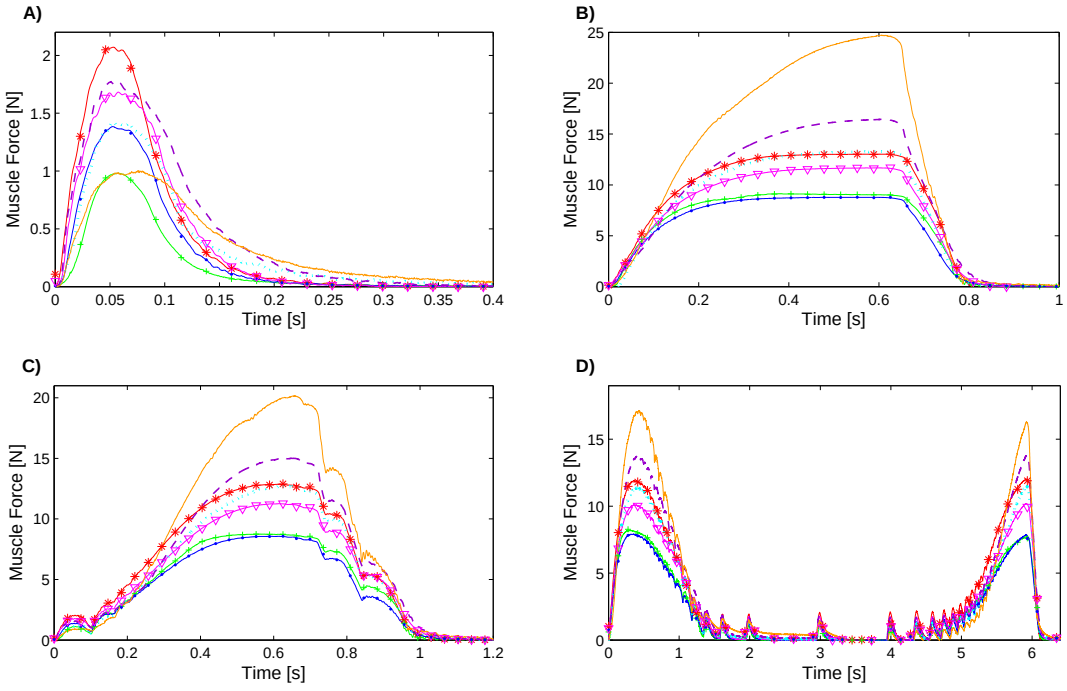

FIGURE 6.24: A-D) Measured force-time traces for locust LY for each input type and angle (130° (+++), 110° (_._._), 90° (***,▽▽▽), 70° (...), 50° (- - -), 30° (—)). A) Response to single input, B) response to 40 pulse CFT with IPF=40Hz, C) response to 29 pulse NCFT with IPF=10-100Hz, D) response to 60 pulse NCFT with IPF=10-50Hz.

angle, the Adapted model when all parameters are allowed to change with FT angle, and the Adapted model when changes in parameters are described by a function of the FT angle. In each case the average estimated model errors are less than the variation due to experimental repeatability. Therefore, these errors do not provide much insight into the suitability of each model. The ability of the model to describe the underlying dynamics and behaviour as the FT angle is changed is thus assessed by studying the predicted form of the force response in the time domain.

In order to show more clearly the changing dynamics and shape of the force response with FT angle, the normalised tetanic force is shown in Fig. 6.28 for both the experimental and modelled cases. The force was normalised so that in each response the maximum force was one. This shows clearly that by only changing A one is unable to capture the changing dynamics. The model where parameters are allowed to change as a function of FT angle provides a good description of the normalised behaviour, further suggesting that the model is good, but the magnitude prediction is affected by the problems of magnitude repeatability in the measured data.

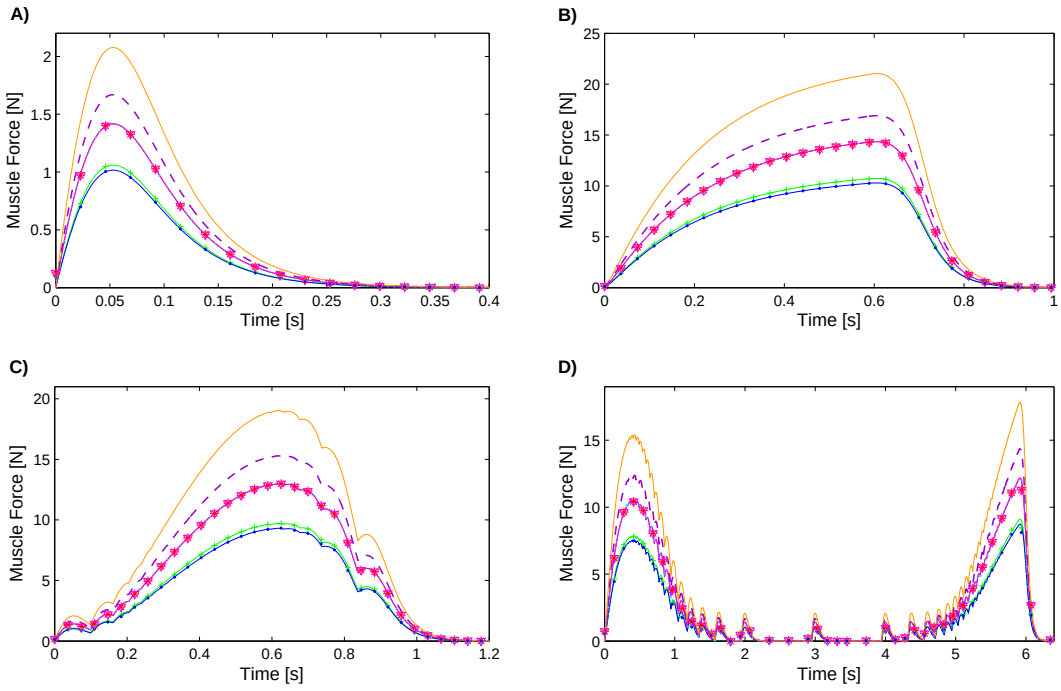

FIGURE 6.25: A-D)Modelled force-time traces, found using the Adapted model and allowing parameter A to depend on the FT angle. Parameters were estimated by minimising the least squares fit to the data in Fig. 6.24. The modelled response to each angle is plotted (130° (+++), 110° (-.-.-), 90° (***,▽▽▽), 70° (...), 50° (- - -), 30° (—)). A) Response to single input, B) response to 40 pulse CFT with IPF=40Hz, C) response to 29 pulse NCFT with IPF=10-100Hz, D) response to 60 pulse NCFT with IPF=10-50Hz.

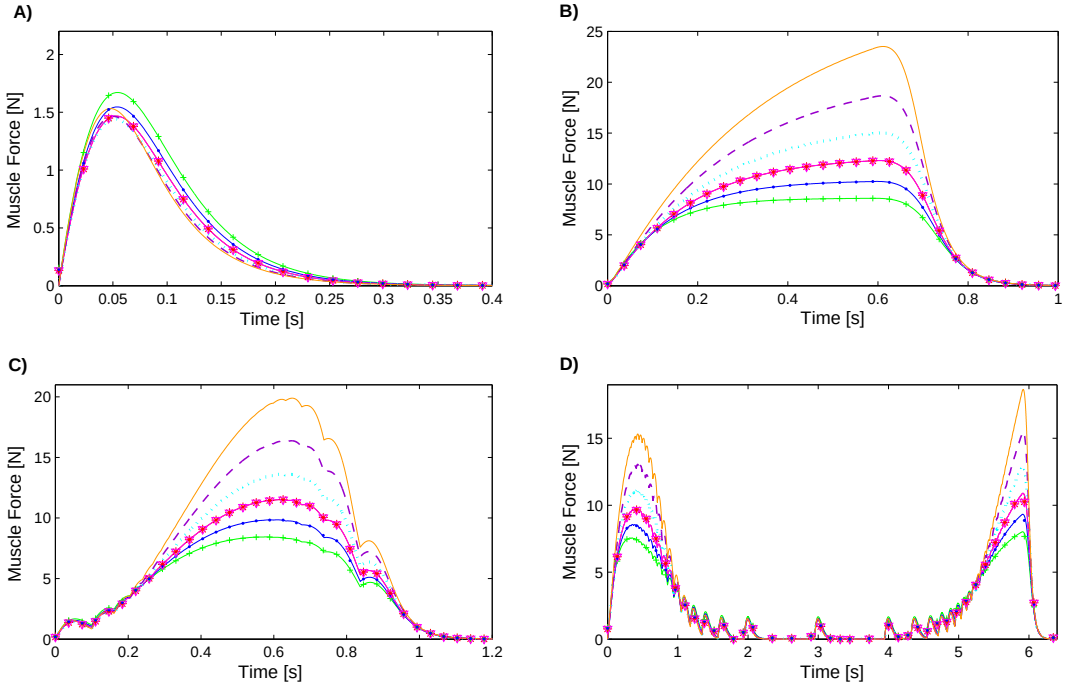

FIGURE 6.26: A-D) Modelled force-time traces, found using the Adapted model and defining the parameters as functions of the FT angle. Parameters were estimated by minimising the least squares fit to the data in Fig. 6.24. The modelled response to each angle is plotted (130° (+++), 110° (-.-.-), 90° (***,▽▽▽), 70° (...), 50° (- - -), 30° (—)). A) Response to single input, B) response to 40 pulse CFT with IPF=40Hz, C) response to 29 pulse NCFT with IPF=10-100Hz, D) response to 60 pulse NCFT with IPF=10-50Hz.

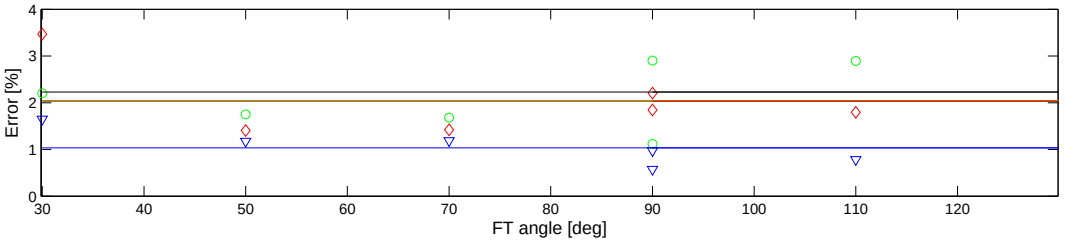

FIGURE 6.27: Errors in fit at different FT angles for each modelling case. The individual errors at each angle and averaged error (continuous line) are given for: the Adapted model when only A is changed (◊), the Adapted model when all parameters are changed (○), and the Adapted model when parameters are changed as functions of the FT angle (▽). The experimental variability, measured at 90°, is also plotted (—).

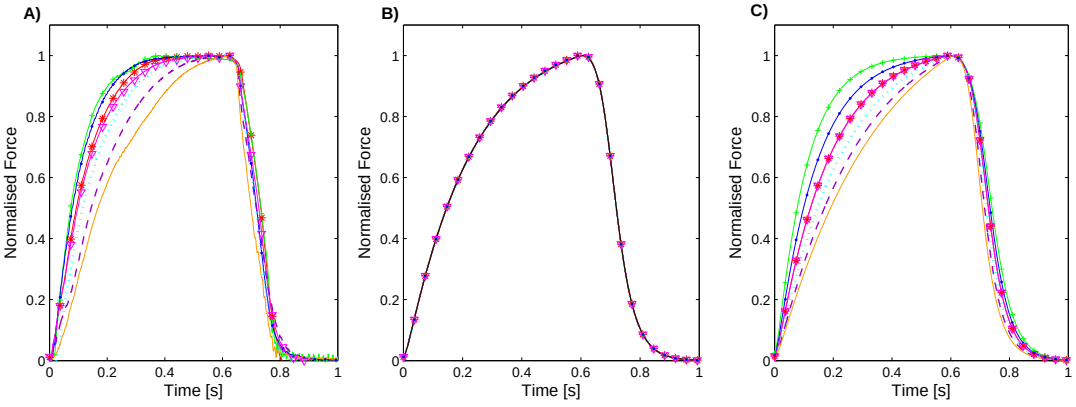

FIGURE 6.28: Normalised tetanic force response at each FT angle (130° (+++), 110° (-.-.-), 90° (***,▽▽▽), 70° (...), 50° (- - -), 30° (—)). A) Experimental data; B) Modelled data when Adapted model is used and only parameter A depends on the FT angle; C) Modelled data when the Adapted model is used and all parameters are defined as functions of the FT angle.

6.4 Discussion

6.4.1 Modifications to Isometric Model as Muscle Length Changes

If the parameters A, τ_c and τ_2 are assumed to be functions of the FT angle, the Adapted model provides a reasonable description of how the force response changes with the muscle length. The overall model's form is

$$\dot{C}_N(t) + \frac{C_N(t)}{\tau_c(\lambda)} = u(t) \tag{6.7}$$

$$\dot{F}(t) + \frac{F(t)}{\tau_1 + \tau_2(\lambda)\frac{C_N(t)^m}{C_N(t)^m + k^m}} = A(\lambda)\frac{C_N(t)^m}{C_N(t)^m + k^m} \tag{6.8}$$

where

$$\tau_c(\lambda) = p_1\lambda + p_2 \tag{6.9}$$

$$\tau_2(\lambda) = r_1 \exp(r_2\lambda) + r_3 \tag{6.10}$$

$$A(\lambda) = s_1\lambda^2 + s_2\lambda + s_3 \tag{6.11}$$

The model has two inputs, the neural stimulus $u(t)$ and the FT angle in radians λ, while the output is muscle force. This model has 11 parameters. Its originality stems from the fact that it contains the dependency of muscle length on isometric force by defining some parameters as functions of the FT angle. A similar approach was used by Perumal *et al* [166] but only for the parameter A which scaled the force response, such that they were unable to capture the changing dynamics.

6.4.2 Changes in Model Parameters

In this section the physical significance of the relations between parameters and FT angle are discussed in more detail. Due to the magnitude repeatability issues, which are reflected in the parameter A, the relation between A and the FT angle is not considered further.

A linear function that increases with increasing FT angle is used to describe the changes in parameter τ_c with FT angle. The value of τ_c defines the time constant associated with the low pass filtering of the input. The parameter is thought to describe the time constant associated with the decay in free calcium concentration C_N after an initial depolarising input $u(t)$. As the muscle length decreases (FT angle increases) the free calcium concentration decay time increases. This finding is in contrast to the work of Balnave and Allen [164] who find

no relation between Ca^{2+} concentration and muscle length in mouse muscle. However, studies [167] in amphibian muscle do find a link between Ca^{2+} concentration and muscle length. These studies report an initial increase in Ca^{2+} concentration with muscle length, then a decrease as the muscle is progressively stretched beyond its slack length. In the results presented here, the initial increase is not evident, but the subsequent decrease in Ca^{2+} concentration with muscle length is evident in the decrease in the parameter τ_c with muscle length. Balnave and Allen [164] suggest that the dependence of length on Ca^{2+} concentration could be species-dependent. Calcium concentrations were not measured during experiments, hence the reported effect of the muscle length changing on the calcium concentration is speculative and only arises as a result of the fitted model parameters.

The importance of the parameter τ_2 increases significantly (exponentially) as the muscle length is stretched beyond its length at 80° (i.e. as the FT angle decreases from 80°) when it is assumed to be slack. This suggests that although in the preceeding chapter the parameter τ_2 was found to have little influence on the force characteristics at 80°, as the FT angle decreases the importance of the parameter τ_2 increases. The parameter τ_2 is a time constant that along with τ_1 describes the transformation from free calcium concentration into a muscle force. The parameter τ_2 is multiplied by a non-linear saturating equation, the resultant non-linear term captures the fact that the time constant of the force responses to individual pulses within a pulse train changes. The fact that the parameter τ_2 increases when the FT angle is below 80° suggests that this non-linear behaviour is more pronounced for longer muscle lengths.

6.4.3 Coupling between Activation and Contraction Dynamics

The results presented here suggest that the activation of the muscle is length dependent, this is supported by [164]. Thus the assumption of uncoupled activation and contraction dynamics is not valid. The fact that the parameters τ_c and τ_2 were strongly dependent on the muscle length suggests that the development of muscle force with time is affected by the muscle length. Without measuring the calcium concentration directly it is difficult to ascertain how physiologically relevant the observed changes in parameters are. It is clear that the model provides a good simple way of modelling the force response of the locust hind leg extensor muscle at a range of physiologically relevant muscle lengths.

6.4.4 Variation in Model Parameters

In the results of this chapter (as in those from preceding chapters) significant variations in the responses between different locusts are evident, these manifest as variations in the model parameters (Fig. 6.18). Previous studies on insect muscle have also found the muscle forces

measured to be variable between animals. Guschlbauer *et al* [5] study the stick insect extensor muscle and find that the maximum tetanic force at 200Hz has a relative s.d. of ±29.8% with the variability greater for lower stimulation frequencies (±72.3% at twitch). Ahn and Full [168] also obtain results with considerable variability of muscle force (relative s.d. of ±38% in muscle 177c at twitch and ±31% at tetanus) in measurements of the cockroach *Blaberus discoidalis* leg. In the locust the peak twitch tension measured by Burns and Usherwood of the mesothoracic leg in response to FETi stimulation varied by ±49% [169]. Hoyle measures a range of twitch tensions for fast fiber stimulation of $29 - 39mN$ at the tibial tip. Zakotnik [49] also observes considerable variability in force measurements. Since the variability has been measured in a range of previous studies in different sets of experiments it is unlikely that the variability in the results presented here is due to systematic errors in preparation. The variability could be a property of the muscle, or be correlated with factors such as age, muscle mass, femur size, and muscle resting length. Correlations between muscle force and other factors have not been studied in detail in either this work or other literature.

There is also variability between measurements in the same locusts (see Fig. 6.18). This is likely to be due to the repeatability issues discussed in section 6.3.1. The sensitivity analysis of the Adapted model given in section 5.5.4 showed that in general, changes in model parameters led to smaller, or equivalent changes in muscle force properties. Conversely this means that in the case where a change in parameter value leads to a smaller change in the properties of the force trace any small differences in measured force traces could be amplified in terms of the change in parameter values.

6.5 Conclusions

This chapter investigated the effect of changing the muscle length on the isometric force. It was found that the dynamics of the isometric force response change depending on the muscle length. The Adapted model, presented in the preceeding chapter, was able to model the changing dynamics if the parameters A, τ_c and τ_2 were assumed to be functions of the FT angle. The changing shape of the force-time profile suggests that the assumption of uncoupled activation and contraction dynamics is poor. This is further confirmed by the fact that the shape of the FL curve was found to be dependent on the type of input used to generate it. Despite these findings the assumption of uncoupled activation and contraction dynamics is common, mainly because this assumption simplifies the problem. The model presented in this chapter provides a mathematically and conceptually simple way of dealing with coupled activation and contraction dynamics.

In this chapter the muscle was held isometrically and the effect of changing the muscle length investigated. The subsequent chapter is concerned with the force response when the muscle velocity is not constrained to be zero so that conditions are not isometric.

Chapter 7

Effect of Muscle Velocity on Force Response

7.1 Introduction

The main body of this thesis focuses on modelling the isometric response, as was considered in the previous chapters. In this chapter, the isometric constraint is removed.

In this chapter the muscle velocity is allowed to be non-zero. The passive response, where the muscle is not stimulated, is considered in detail. A model describing the main components of the passive behaviour is presented. A model describing the active response is an area of work in progress. Some results where the muscle was activated under non-isometric conditions are presented and discussed. An extension to the work presented in this chapter is to develop a general non-isometric model. Protocols to do this are discussed in the following chapter.

7.2 Methods

During experiments the apodeme was grasped directly with forceps mounted on a shaker. The shaker was driven with a voltage to apply a force and hence change the muscle length. Details of the experimental procedure are discussed in more detail in Chapter 3. Specific details regarding inputs and processing of signals are given in this section. Both active and passive experiments were performed. Passive muscle is not stimulated, whereas active muscle is.

7.2.1 Passive Inputs

During passive experiments the shaker was driven with a mainly constant voltage. The resultant force generated by the shaker is approximately proportional to the input voltage. An example of the voltage input used to drive the shaker is shown in Fig. 7.1. The muscle length was set to its rest length prior to the shaker being driven. Different maximum voltages and rates at which the voltage was ramped up and down were used to drive the shaker. This excitation protocol was used as it is simple and provides a good indication of the viscoelastic behaviour. A summary of the voltages used to drive the shaker is provided in Table 7.1. These voltages were amplified before being used to drive the shaker. The amplification was set so that the resultant maximum muscle displacement from rest was of the order of 0.5mm and velocity of the order of 5mms^{-1}. These ranges were used as they are close to the physiological range of motion of the muscle. Further details on how the physiological range was calculated and on the input to the shaker are given in Sec. 3.5.2.3.

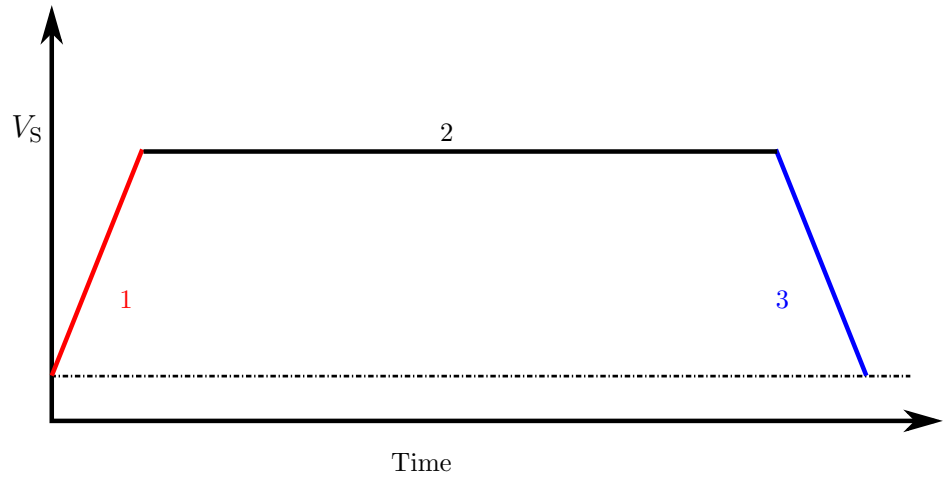

FIGURE 7.1: Example of voltage input to the shaker used during passive experiments.

7.2.2 Active Inputs

Traditionally, the force-velocity curve is obtained from hold and release experiments (see Sec. 2.3.2.1). In these experiments the muscle is maximally activated. The activation and contraction dynamics are assumed uncoupled and so the level of activation is assumed to just scale the force response. In Chapter 6 the effect of muscle length on the force response was investigated. It was found that the level of activation does change the form of the force length relation, and so activation and contraction dynamics cannot be assumed to be uncoupled. It is, therefore, likely that the force velocity curve will be affected by the level of activation. Previous research also suggests this [47]. Force-velocity experiments should, therefore, ideally

Input number	Maximum voltage (V)	Rate of voltage change (Vs^{-1})
1	0.4	1
2	0.4	2
3	0.4	3
4	0.4	4
5	0.4	5
6	0.4	6
7	0.4	7
8	0.1	4
9	0.2	4
10	0.3	4
11	0.4	4
12	0.5	4
13	0.6	4

TABLE 7.1: Voltages that are amplified and used to drive shaker. In inputs 1-7 the maximum voltage is held constant and the rate of change of voltage varied, in 8-13 the rate of voltage change is constant and maximum voltage varied.

take place under a range of different levels of activation to assess and model this effect. In this chapter only the active response of maximally excited muscle is considered. This represents a first step in modelling the muscle behaviour when the velocity is not zero. Investigating the maximally activated case provides a foundation for considering submaximally activated muscle in the future.

During active experiments the muscle was maximally excited, to tetanus. Whilst at tetanus the shaker was activated so that the muscle displacement and velocity were changed. Both chirp and ramp type inputs were used to drive the shaker. The use of these extended inputs is one of the fundamental differences between the experiments presented here and the traditional hold and release experiments. Typically the F_V relation is found by measuring the initial velocity (after transients have decayed) after a step change in force. The method presented in this chapter has the advantage that by using extended inputs and outputs to model the behaviour, history and time dependent effects can be measured.

7.2.3 Processing Signals

In experiments the force and displacement are measured. The velocity and acceleration can then be calculated by differentiating and double differentiating the signal respectively. Numerical differentiation can greatly amplify noise in the data. To reduce this effect, the signal can be low pass filtered prior to differentiation. An alternative approach is to differentiate the sampled data by using discrete wavelet transforms [170]. The wavelet method can also greatly reduce the noise amplification in the differentiation [170]. The velocity and acceleration were calculated using both a wavelet method with a Haar mother wavelet and the level of decomposition set to 5 (developed by Luo *et al* [170]), and using a zero-phase low pass filter. When a third-order

Chebyshev filter with 1dB of ripple in the pass band and a cut off frequency of 40Hz was used the velocity traces using the wavelet and filter method were very similar. The wavelet method was used to find the acceleration and velocity of all signals presented in this chapter. Due to the similar characteristics obtained using a wavelet, or linear filter in this case, the choice of a wavelet method is somewhat arbitrary.

7.3 Passive Response

Under passive conditions the muscle is not activated. The behaviour in response to the ramp up, hold, ramp down changes in the shaker excitation is considered in this section. To date little attempt has been made to characterise the contractile response of passive muscle. Passive models in the literature tend to apply only to muscle as it is stretched beyond its optimal length [28]. These models do not describe the behaviour if the muscle is held passively at a constant length, nor the behaviour if the stretch is decreased and the length returned to the rest length.

7.3.1 Passive Force Data

An example of the muscle displacement and resultant measured force in the time domain are shown in Fig. 7.2 for a range of different voltage inputs. Relaxation, seen as a reduction in force during the period where the input to the shaker is held constant, is apparent in the results. This suggests that the muscle behaves as a viscoelastic material. The main difference between muscle and a conventional viscoelastic material is that there is very little overshoot in the muscle case when the voltage is ramped back down and the muscle is returned to the rest position. Also, during the period where the input to the shaker is held constant there is a slight increase in the displacement. The displacement and corresponding force are shown in Fig. 7.3. There is a clear nonlinear relationship between the force and displacement. During the period where the muscle is stretched rapidly, the force can be well described by a cubic nonlinearity (i.e. $F = k_{l1}x_m + k_{n1}x_m^3$). Previous studies of the response to a passive stretch also find a cubic nonlinearity to provide a good description of the behaviour [28]. The force-displacement relation when the muscle lengthens differs to that when it shortens. This indicates that the passive muscle displays hysteretic behaviour and that during the stretch-shorten cycle energy is dissipated, most likely as heat. The force-displacement traces when the velocities are changed and the maximum stretch is kept the same are similar (Fig. 7.3A, C, E). This suggests that the velocity has little influence on the relation between displacement and force. When the maximum stretch is changed, and velocity held constant, the force-displacement relations over the period of decreasing stretch differ (Fig. 7.3B, D, F).

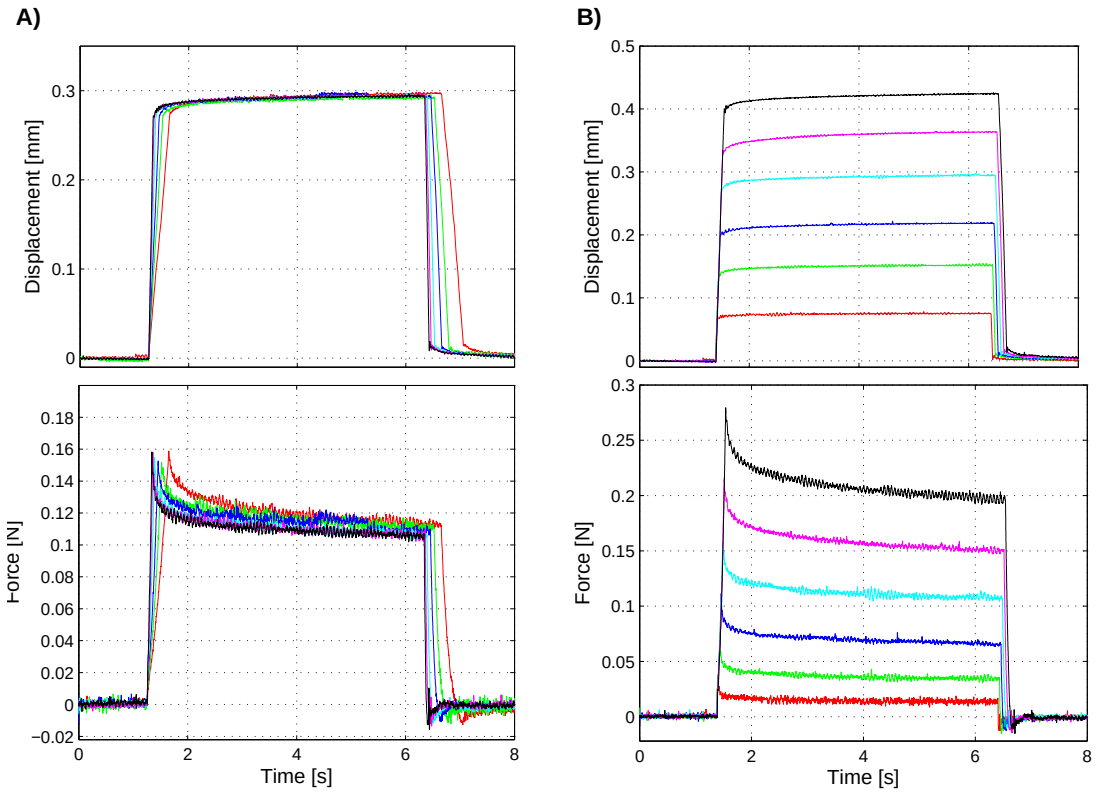

FIGURE 7.2: The displacement and force as functions of time in response to inputs of the form given in Fig. 7.1. A) The voltage rate is varied, but maximum voltage constant, B) the maximum voltage is varied but rate of voltage change held constant.

7.3.2 Theoretical Viscoelastic Model

The ability of the standard linear model (SLM) to capture the trends seen in the data was initially considered. Nonlinear models will be considered in the following sections. A SLM was used, as it is the simplest model that describes both creep and stress relaxation. The model is commonly used to describe the behaviour of viscoelastic materials. The force response of the model shown in Fig 7.4 to displacements of the form shown in Fig. 7.7 was estimated. The force is found from the relation

$$\frac{\dot{F}_m}{k_{l2}} + \frac{F_m}{c_d} = \left(1 + \frac{k_{l1}}{k_{l2}}\right)\dot{x}_m + \frac{k_{l1}}{c_d}x_m \tag{7.1}$$

where k_{l1}, k_{l2} and c_d are the spring and damper coefficients, and F_m and x_m the force and displacement of the muscle, as defined in Fig. 7.4.

If the shaker stiffness is included in the system and the passive muscle is assumed to be described as a SLM the general system is equivalent to that in Fig. 7.5. From Fig. 7.5 the following relation is obtained

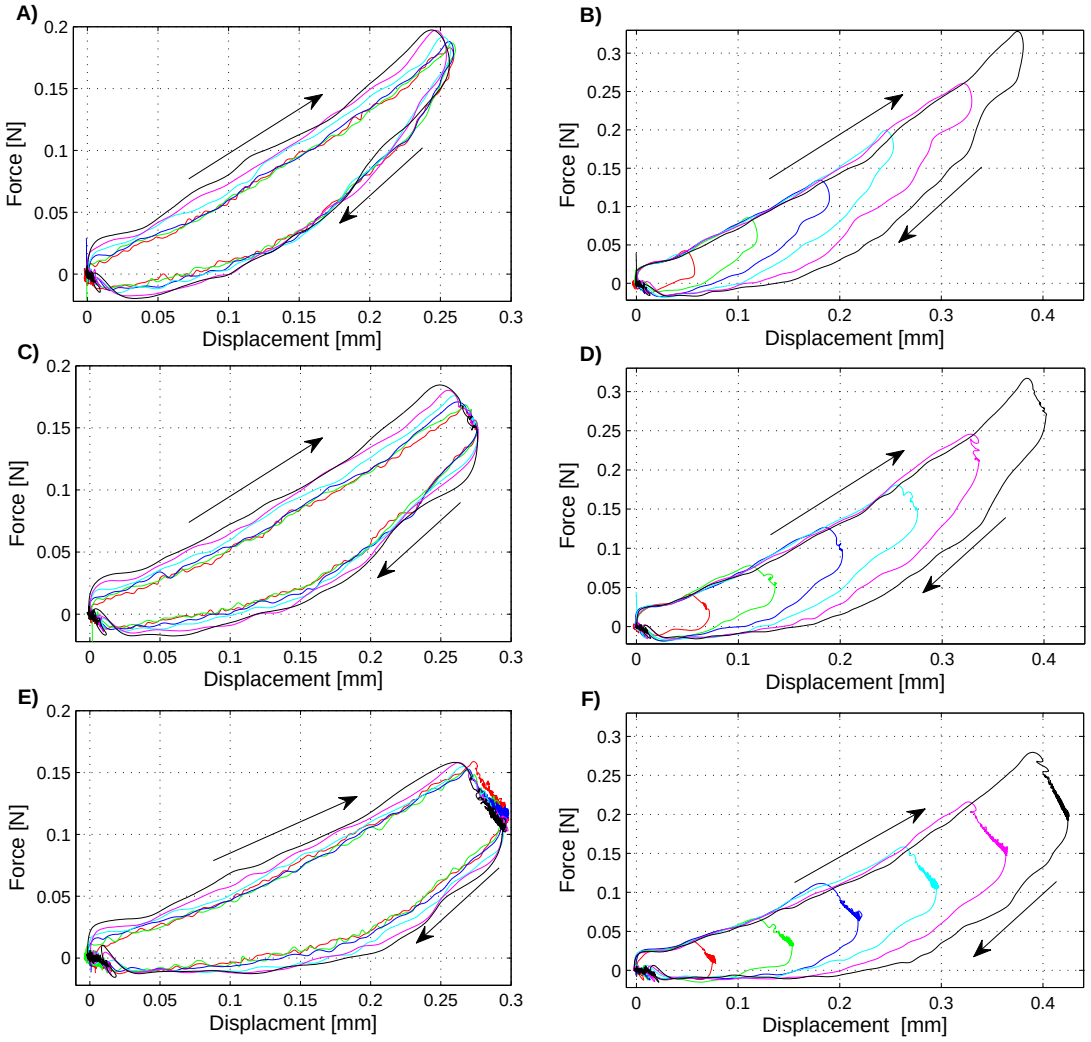

FIGURE 7.3: Measured force-displacement relation in one locust to a range of different shaker inputs. In A), C) and E) the voltage rate is varied but maximum voltage held constant, in B), D) and E) the voltage rate is held constant but maximum voltage is varied. The duration of the hold period is increased from A and B to C and D to E and F. Arrows show the direction of movement.

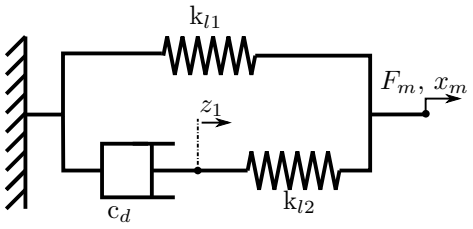

FIGURE 7.4: SLM with linear springs and a linear viscous damper. Model used to simulate force response to a given displacement signal.

$$\frac{\dot{F}_t}{k_{l2}} + \frac{F_t}{c_d} = \left(1 + \frac{k_{l1}}{k_{l2}} + \frac{k_s}{k_{l2}}\right)\dot{x}_m + \left(\frac{k_{l1}}{c_d} + \frac{k_s}{c_d}\right)x_m \tag{7.2}$$

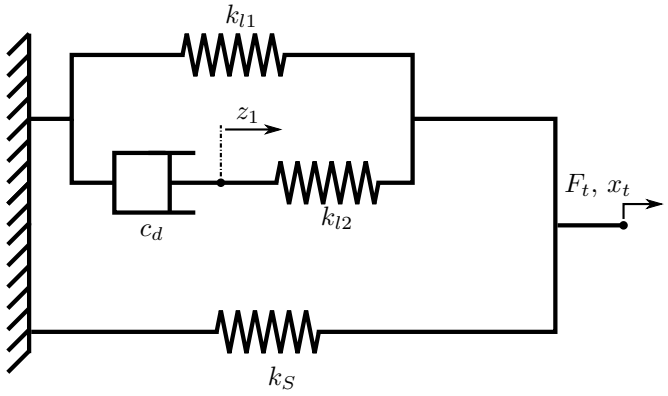

FIGURE 7.5: Model of the shaker and muscle system. The muscle is assumed to be described by a SLM and the shaker to have stiffness k_s.

where F_t is the combined muscle and shaker force. The response is modified if the shaker stiffness is included in the model. During experiments, both the force and displacement of the muscle were measured. These were used in further analysis of the system. This means that the behaviour of the shaker is removed and does not need to be included in the model. The force response of the SLM was simulated using Eq. (7.1). The model coefficients of the SLM, k_{l1}, k_{l2} and c_d, were set arbitrarily to 2Nmm^{-1}, 5Nmm^{-1} and 2Nsmm^{-1} respectively in order to simulate the behaviour of this system. Figure 7.6 shows the force-time response to a range of different displacements (these displacements are also shown). Figure 7.7 shows the corresponding force-displacement relations. When these simulated responses are compared to the experimentally measured responses (Figs. 7.2 and 7.3) some differences are clear. The model has linear springs so is unable to model the nonlinear spring hardening behaviour measured in the muscle. When the length is returned back to the resting length the simulated data shows too much overshoot in comparison to actual data where there is very little overshoot. Also, as a consequence of the input displacement to the simulated model being fixed, the displacement increase during the hold period is not modelled.

Models in the literature, which describe the force response of passive muscle to lengthening from rest, assume that force is generated only when the muscle is stretched beyond the optimal muscle length [28, 39]. The responses given in Figs. 7.6 and 7.7 refer to the response to a stretch, hold, relax input protocol.

When the muscle is passive there are no cross-bridges between the thick and thin filaments. When the muscle is stretched beyond its rest length, passive force is generated as a result of the elasticity of titin [171]. When the muscle is slack, or compressed so that $l_m \leq l_o$, no passive force is generated. Slack muscle is analogous to a slack string under compression. In the experimental response shown in Figs. 7.2 and 7.3 only a very small compressive (negative)

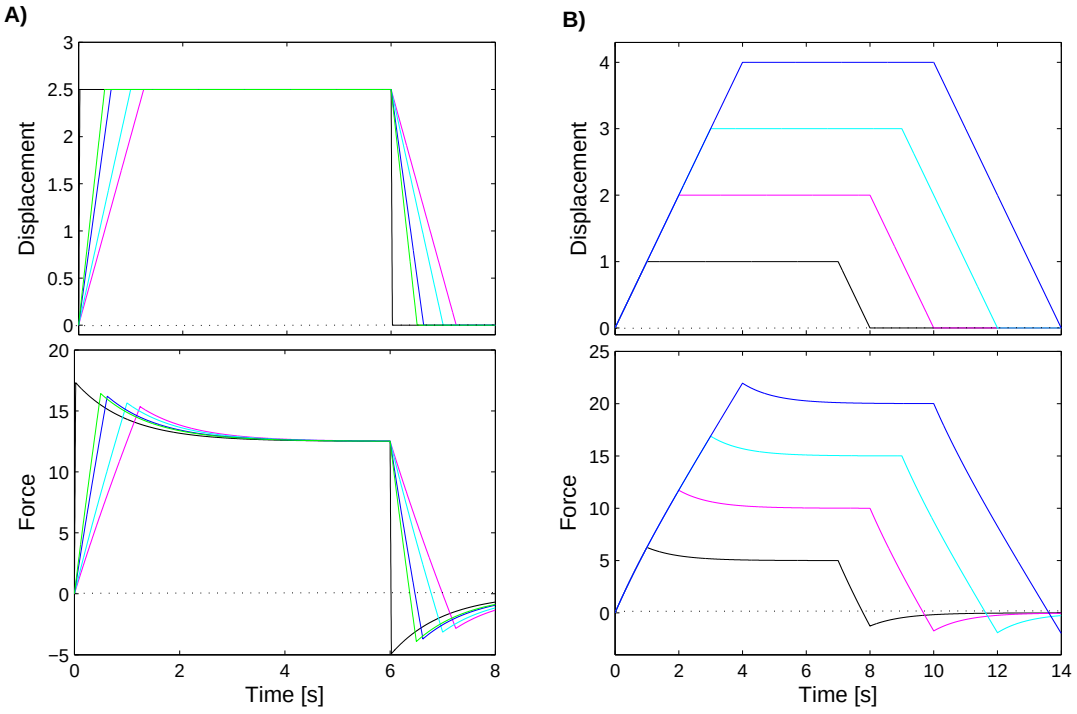

FIGURE 7.6: Simulated force response for a typical viscoelastic material to given displacements in the time domain; A) for varying velocities, B) for varying displacements.

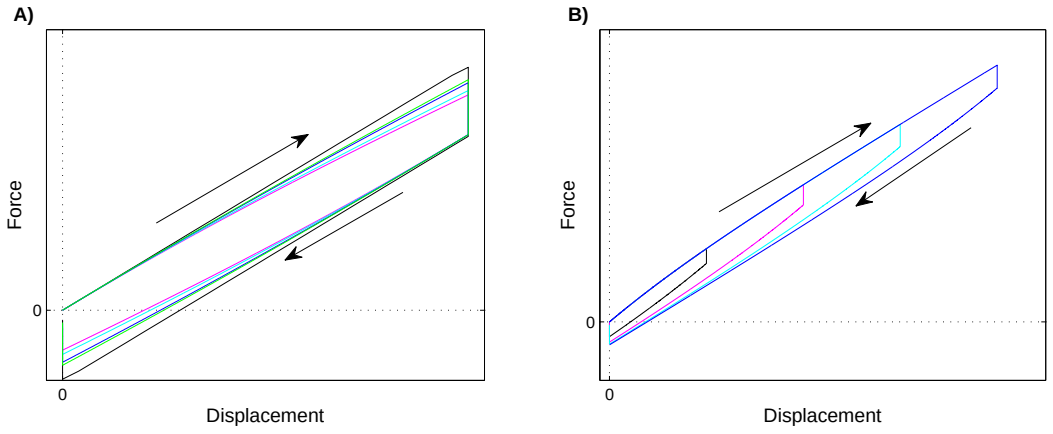

FIGURE 7.7: Simulated force response vs displacements for a typical viscoelastic material, arrows show the direction of movement; A) for varying velocity, B) for varying displacements.

force is generated by the muscle. Due to the structure of the muscle, this force is almost zero. The passive muscle is not able to generate the negative forces predicted by the SLM.

7.3.3 Modelling the Passive Behaviour

Since the ramp up and hold experiments capture the viscoelastic relaxation, data from these were used to develop a model capable of describing the passive force response. From the measured displacement the force was estimated and compared to the measured force. Any model must capture both the force-time relation and the force-displacement relation. Just minimising the error between the estimated force and the measured force as a function of time, as has been done previously in this thesis, is not sufficient. This is due to the fact that the hold period is significantly longer than the sections where the displacement is ramped up or down. This results in the fit to the hold section influencing the error more if all data samples are weighted equally. In estimating the parameters of the springs and dampers a weighted least squares error was used. The weighting function used was

$$w_i = |\dot{x}_m|_i + a_w|x_m|_i \tag{7.3}$$

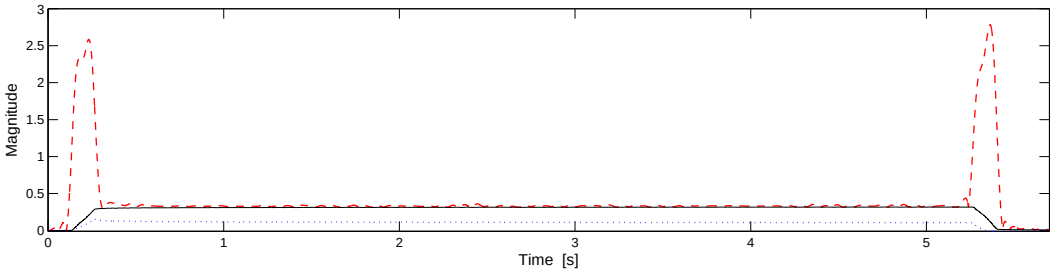

FIGURE 7.8: Weighting function (- - -) for an example input. The corresponding displacement (—) and force response (...) are also shown.

where w_i is the weight for the i^{th} sample, and a_w is a constant with units of s^{-1} to ensure dimensional consistency in the weighting function. By having velocity in the weighting function, increased importance is given to quick changes in displacement. The displacement is also included in the weighting function. The displacement x_m is defined as the change in muscle length from rest length. Including x_m in the weighting function means that a better fit to quasi-steady-state behaviour, during which the velocity is very small, can be obtained. If the muscle velocity is small the force is not necessarily zero if x_m is non-zero. The weighting function could be further optimised by changing the value of a_w, however good fits were obtained with a_w set to 1s^{-1} so this parameter was not further optimised.

As an example, the weighting function is shown in Fig. 7.8 for one input. The weighting function gives increased importance to the ramp up and ramp down sections, to account for the short time for which they occur. When using the weighting function, the error function that is minimised is thus

$$E_w = \frac{\sum_i (w_i F_{m,i} - w_i \hat{F}_{m,i})^2}{\sum_i (w_i F_{m,i})^2} \times 100\% \tag{7.4}$$

The parameters (i.e. the spring and damper coefficients) were estimated by finding the values that gave the smallest weighted errors between the modelled and measured force. This was done using the MATLAB function `lsqnonlin` and a fixed step ODE solver. A range of models with different arrangements of components were investigated. Candidate passive models that display viscoelastic behaviour were used. These models were based on, and adapted from, the form of a SLM. They are shown in Figs. 7.9 to 7.14. In these models S_{n} is used to denote a spring, and $F_{S\mathrm{n}}$ the related spring force. Likewise, D_{n} denotes a damper, with $F_{D\mathrm{n}}$ the related damper force.

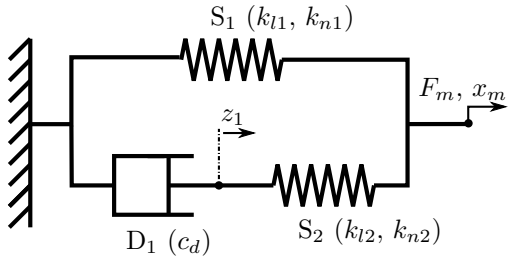

$$F_{S1} = k_{l1} x_m + k_{n1} x_m^3$$
$$F_{S2} = k_{l2}(x_m - z_1) + k_{n2}(x_m - z_1)^3$$
$$F_{D1} = c_d \dot{z}_1$$

FIGURE 7.9: Passive model 1, SLM with nonlinear springs S_1 and S_2, and a linear viscous damper D_1. Coefficients k_{l1}, k_{n1}, k_{l2} and k_{n2} are spring stiffnesses and c_d a damping coefficient.

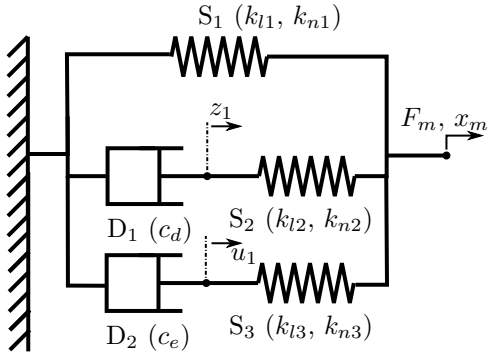

$$F_{S1} = k_{l1} x_m + k_{n1} x_m^3$$
$$F_{S2} = k_{n2}(x_m - z_1) + k_{n2}(x_m - z_1)^3$$
$$F_{D1} = c_d \dot{z}_1$$
$$F_{S3} = k_{l3}(x_m - u_1) + k_{n3}(x_m - u_1)^3$$
$$F_{D2} = c_e \dot{u}_1$$

FIGURE 7.10: Passive model 2, SLM with additional spring and damper in parallel. All springs are nonlinear with stiffnesses k_{l1}, k_{n1}, k_{l2}, k_{n2}, k_{l3} and k_{n3}, dampers are viscous with damping coefficients c_d and c_e.

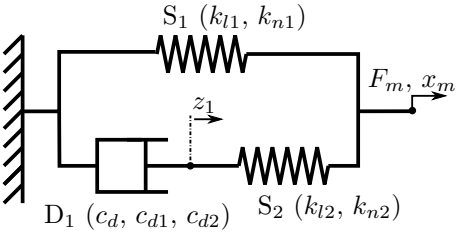

$$F_{S1} = k_{l1}x_m + k_{n1}x_m^3$$
$$F_{S2} = k_{l2}(x_m - z_1) + k_{n2}(x_m - z_1)^3$$
$$F_{D1} = (c_d + c_{d1}z_1 + c_{d2}z_1^2)\dot{z}_1$$

FIGURE 7.11: Passive model 3, SLM with nonlinear springs and nonlinear damper. The spring stiffnesses are k_{l1}, k_{n1}, k_{l2} and k_{n2}. The damper force is assumed to be a function of velocity and displacement, with damping coefficients c_d, c_{d1} and c_{d2}.

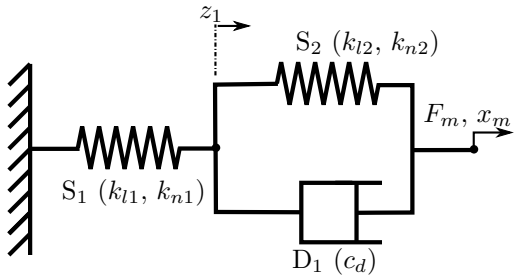

$$F_{S1} = k_{l1}z_1 + k_{n1}z_1^3$$
$$F_{S2} = k_{l2}(x_m - z_1) + k_{n2}(x_m - z_1)^3$$
$$F_{D1} = c_d(\dot{x}_m - \dot{z}_1)$$

FIGURE 7.12: Passive model 4, spring in series with a parallel spring and damper. The springs are nonlinear with stiffnesses k_{l1}, k_{n1}, k_{l2} and k_{n2} and the damper is viscous with damping coefficient c_d.

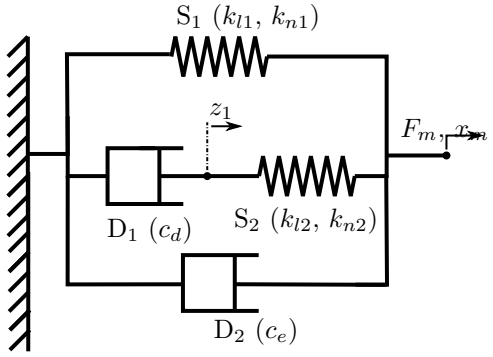

$$F_{S1} = k_{l1}x_m + k_{n1}x_m^3$$
$$F_{S2} = k_{l2}(x_m - z_1) + k_{n2}(x_m - z_1)^3$$
$$F_{D1} = c_d\dot{z}_1$$
$$F_{D2} = c_e x_m \dot{x}_m$$

FIGURE 7.13: Passive model 5, SLM with nonlinear springs and linear damper in parallel with a nonlinear damper. The parallel damper force is a function of the displacement and velocity. Spring stiffnesses are k_{l1}, k_{n1}, k_{l2} and k_{n2} and damping coefficients are c_d and c_e.

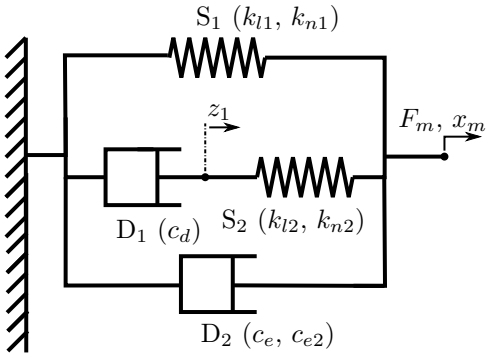

$$F_{S1} = k_{l1}x_m + k_{n1}x_m^3$$
$$F_{S2} = k_{l2}(x_m - z_1) + k_{n2}(x_m - z_1)^3$$
$$F_{D1} = c_d\dot{z}_1$$
$$F_{D2} = (c_e + c_{e2}x_m^2)\dot{x}_m$$

FIGURE 7.14: Passive model 6, SLM with nonlinear springs and linear damper in parallel with a nonlinear damper. The parallel damper force is a function of the displacement and velocity. Spring stiffnesses are k_{l1}, k_{n1}, k_{l2} and k_{n2} and damping coefficients are c_d, c_e and c_{e2}.

In each case, the estimated force F_m cannot be negative because the muscle becomes slack and hence cannot support any compressive force. Models which allowed the force to be negative did not fit the measurements as well. Therefore, in each case the estimated force was given by,

$$\hat{F}_m = \begin{cases} \hat{F}_m & \text{if } \hat{F}_m > 0 \\ 0 & \text{if } \hat{F}_m \leq 0 \end{cases} \tag{7.5}$$

The fitted results to one example locust (termed $\mathrm{L_{na}}$) using each model are summarised in Table 7.2. Model 6 (Fig. 7.14) gives the lowest weighted error and a low total error, with a moderate number of model parameters. The SLM model with nonlinear springs (model 1) is much improved by an extra parallel branch that contains either a spring and damper (model 3) or a damper whose damping factor is dependent on displacement and velocity (models 5 and 6).

Model	Parameters	E_{wt} %	E %
1	5	1.67	9.21
2	8	0.84	7.42
3	7	0.90	7.52
4	5	4.41	7.16
5	6	0.79	7.17
6	7	0.68	7.23

TABLE 7.2: Errors in fit when using each of the candidate passive models in one example locust ($\mathrm{L_{na}}$).

7.3.4 Optimal Passive Model

Model 6 was chosen as the optimal passive model. The fitted parameters and resultant errors for six locusts (termed L_{na}, L_{nb}, L_{nc}, L_{nd}, L_{ne}, L_{nf}) when using model 6 are shown in Table 7.3. The damping factor c_d is estimated as being reasonably large in comparison to c_e, with c_e being close to zero in all locusts. This implies that removing c_e in model 6 would result in a good model with one parameter fewer.

From Table 7.3 it is clear that the errors of the example locust (L_{na}), presented in Table 7.2 are below average. Larger errors occur in some locusts as there is a larger negative component to the force, or due to movement artifacts in the data. Locust L_{na} provides a good representation of the behaviour as data recorded from it do not contain any movement artifacts.

	k_{l1} (Nmm^{-1})	k_{n1} (Nmm^{-3})	c_d ($Nsmm^{-1}$)	k_{l2} (Nmm^{-1})	k_{n2} (Nmm^{-3})	c_e ($Nsmm^{-1}$)	c_{e2} ($Nsmm^{-3}$)	E_{wt} %	E %
L_{na}	0.14	0.18	0.22	0.20	1.1	0.058	0.082	0.68	7.2
L_{nb}	0.070	1.9	0.38	0.16	2.8	0.077	0.19	1.7	10
L_{nc}	0.068	0.22	0.069	0.075	0.78	0.0043	0.028	1.3	12
L_{nd}	0.00	0.55	0.59	0.00	0.76	0.0035	0.028	0.80	10
L_{ne}	0.0036	0.57	0.67	0.021	0.79	0.0062	0.039	0.62	12
L_{nf}	0.012	0.69	0.52	0.0038	1.0	0.0064	0.030	0.63	9.3

TABLE 7.3: Estimated coefficients and errors when model 6 is fitted to passive data from six locusts.

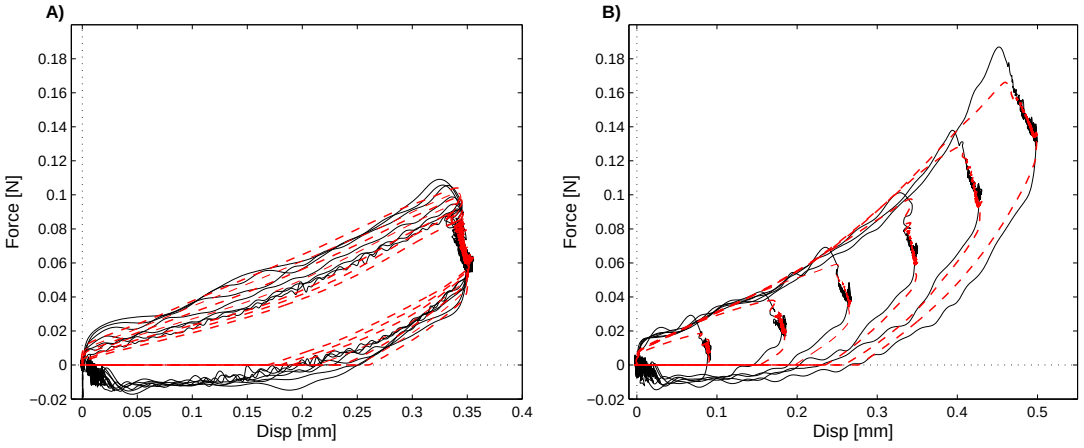

FIGURE 7.15: Measured (—) and modelled (- - -) passive force response vs displacement; A) for varying voltage rates, B) for varying maximum voltage.

The estimated forces for locust L_{nc} using model 6 are shown in Figs. 7.15 to 7.17. It is clear that the main source of error arises due to the assumption that the muscle force cannot be negative, in practice there is some overshoot. Aside from this limitation, the model provides a reasonable description of both the force-time and force-displacement response. It is capable of capturing the force response to a range of different displacements. The measurement of a negative force suggests that the muscle does sustain some negative force. Previous studies on

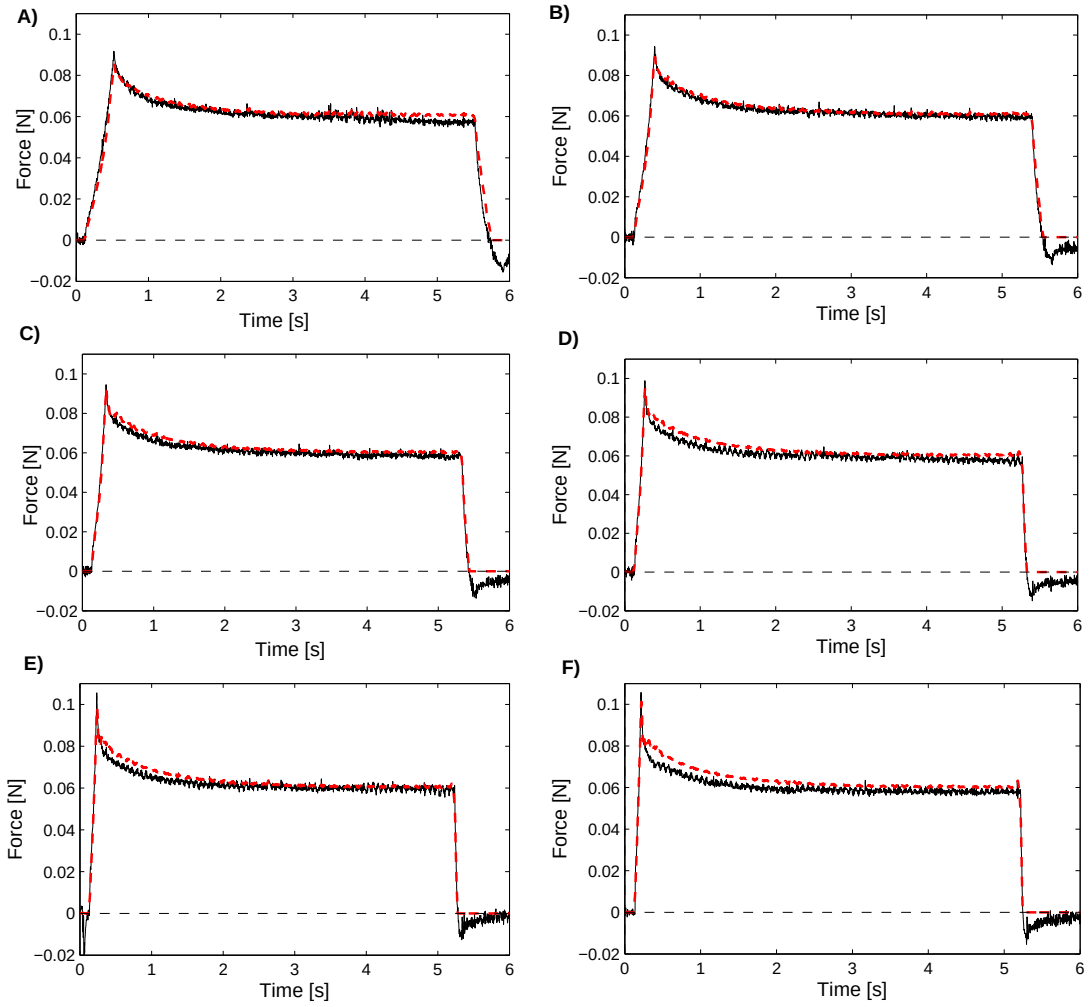

FIGURE 7.16: Measured (—) and modelled (- - -) passive force response in the time domain. The rate of ramp up and down in voltage is varied in A-F, with the rate of voltage change corresponding to input numbers 1-6 in Table 7.1.

passive muscle have not measured any negative force [1, 23]. This is likely to be as a result of these studies only considering the behaviour of passive muscle as it is lengthened, hence the viscoelastic behaviour is not considered. The SLM, which is commonly used to describe a viscoelastic material shows some force overshoot (and so negative force) in simulations that input a displacement profile similar to that measured in experiments (see Fig. 7.7). In the SLM this overshoot is caused by the presence of a damper, which is in series with a spring (Fig. 7.4). It is reasonable to draw analogies between muscle and a viscoelastic material and therefore fair to assume that some of the overshoot is due to a similar mechanism.

The model is comprised of a SLM with nonlinear springs in parallel with an extra nonlinear damper. This extra damper has a damping factor that is dependent upon displacement as well as velocity. The damping has previously been measured to be asymmetric betwen lengthening and shortening [172]. This is also the case in this measured data. The overshoot after shortening is significantly less than the force relaxation after lengthening. Krause *et al* [172]

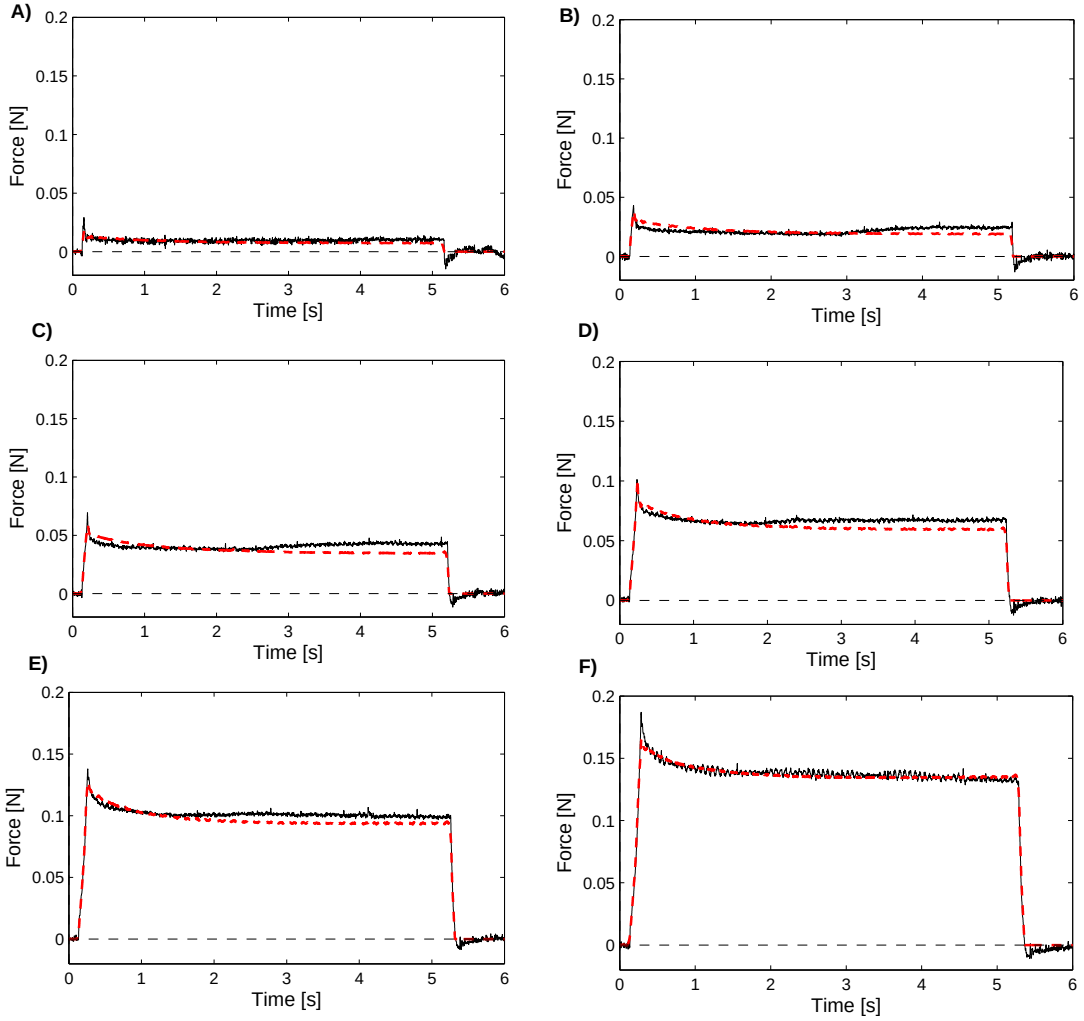

FIGURE 7.17: Measured (—) and modelled (- - -) passive force response in the time domain. The maximum stretch is varied in A-F). Input numbers 8-13 in Table 7.1 summarise the voltages that are amplified then used to drive the shaker.

allow the damping coefficients and spring constants in their model to have different values during lengthening and shortening. This approach could be one way of dealing with the small measured force overshoot.

Results show that the muscle exhibits a lot of hysteresis, which model 6 is able to capture. This measurement of significant hysteresis is in line with previous work on passive tissue [173]. Classical approaches to model hysteresis do not transfer well to the muscle. This is due to the fact that when the length is equivalent to rest length ($x_m = 0$) the force is zero, whether on the assending or descending limb. This is not the case in traditional hysteretic models that predict some force overshoot.

7.4 Active Force

Modelling the force when the muscle is activated and the muscle velocity varies is an area of ongoing research. Some measurements have been made on fully activated muscle and examples of these are presented here. As yet, no model which describes the active force response of the muscle under non-isometric conditions has been developed and no data where the muscle is not fully activated have been collected.

An example of the data collected from the active force experiments is shown in Fig. 7.18. The corresponding input to the shaker is also shown in Fig. 7.18; the spike at 1s triggers the muscle stimulation. As in the passive case, both the muscle force and displacement were recorded during the experiment. Due to movement of the shaker head in response to the applied force, there is a decrease in displacement as the muscle is activated (muscle contracts). Tetanic forces measured at the apodeme using the shaker-load cell-forceps system are substantially lower than those which were measured at the tibia and converted into a muscle force, as in Chapters 4-6. The reason for this is that previous measurements were made under isometric conditions, with the system in static equilibrium. In the current set up, the muscle contracts during activation, causing the shaker platform to move and the muscle length to change. This is shown by the measured change in displacement in Fig. 7.18. The data of most interest are where the muscle is active and the muscle displacement is imposed by the shaker. In the remainder of this chapter, the active force will be presented as the change in force from the tetanic level at the onset of shaking.

Considering the case of maximal activation, the region of interest is the area in which the shaker displacement is varied. These data during this period of time were extracted and the change in force (from tetanus) plotted against the displacement and velocity (Fig. 7.19). For clarity, Fig. 7.20 shows the force-velocity and force-displacement plots on separate axis. The relation between the force and displacement appears to be dependent on the input type and, as with the passive response, some hysteretic viscoelastic behaviour is also evident. Since active muscle appears to behave viscoelastically it is expected that the input type, and the time history of the input, will influence the specific form of the force-displacement relation. The force-velocity relation appears much less clear and the active force appears to be more dependent on the muscle length than the velocity. In experiments both the velocity and displacement were varied simultaneously. In order to isolate the effect of velocity or length on the force Figs. 7.21 and 7.22 show the force-length relation when the velocity is approximately constant and the force-velocity relation for an approximately constant length respectively. In holding the length approximately constant tolerances of ± 0.01mm were used, with tolerances of $\pm 0.05\text{mms}^{-1}$ used for the velocity.

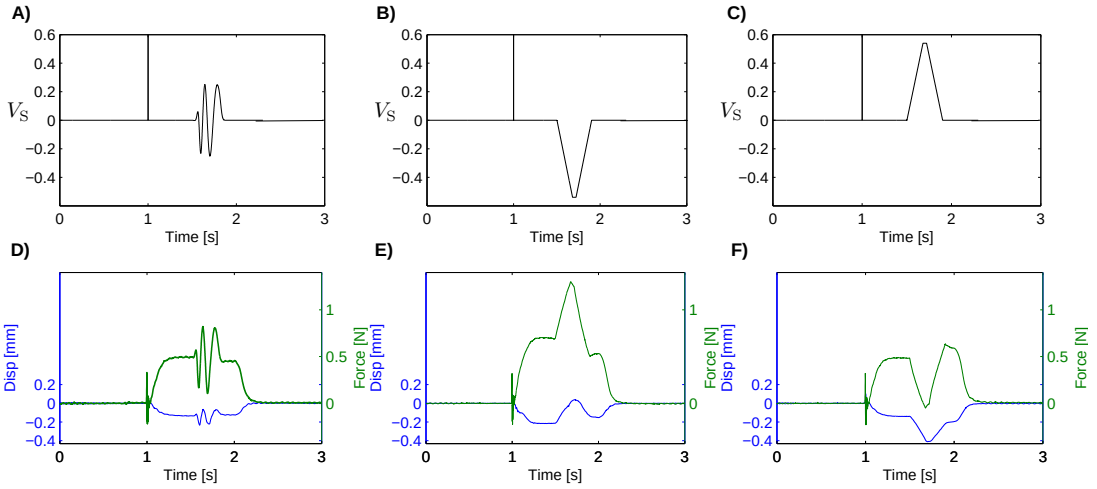

FIGURE 7.18: Example of input (A-C) which is amplified and used to drive the shaker and corresponding outputs (D-F), both force (—) and displacement (—) are measured. A, D) chirp type excitation, B, E) ramp down then up excitation, C, F) ramp up then down excitation.

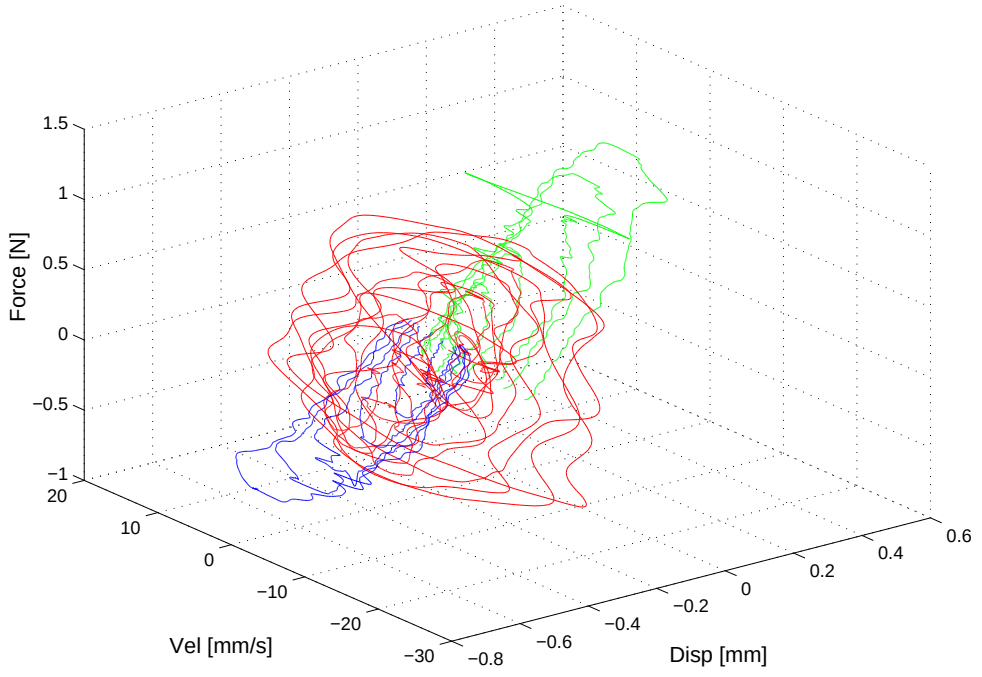

FIGURE 7.19: A 3D plot showing the change in force level from tetanus when the shaker is activated. Data is collected from chirp (—), ramp up-down (—) and ramp down-up (—) inputs.

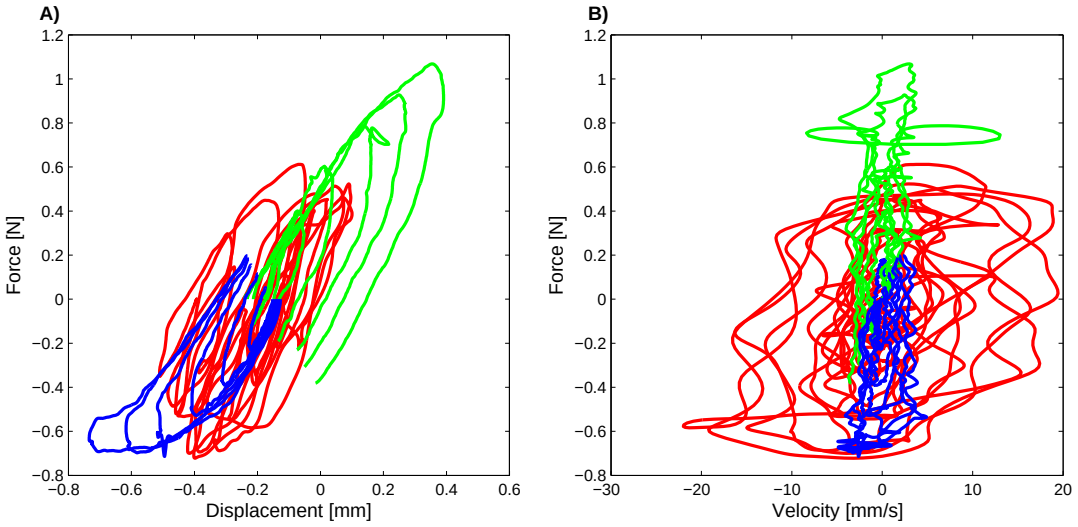

FIGURE 7.20: The A) force-displacement and B) force-velocity response when the muscle is fully activated and both the velocity and displacement are varied. Data is collected from chirp (—), ramp up-down (—) and ramp down-up (—) inputs.

From Fig. 7.21 it can be seen that there is a clear relation between the muscle force and displacement. The force increases with increasing displacement (i.e. muscle length). This is the same trend as was observed in Chapter 6. This is expected because for the case where the velocity is approximately zero this is just a different method of measuring the F_L relation to that presented in Chapter 6. The effect of velocity on force is shown in Fig. 7.22. There are no clear trends between the muscle velocity and the force in the active muscle. This could be due to the force not being dependent on the velocity. Further experiments and analysis are required to investigate this.

7.5 Discussion

Published force-velocity relations are usually obtained using hold and release experiments (see Sec. 2.3.2.1). They generally apply to the initial velocity (measured as soon as transients have subsided) during an isotonic contraction [38]. In obtaining the force-velocity relation the muscle is often fully activated, with activation and contraction dynamics assumed uncoupled. The main issues with this method are the assumption of uncoupled activation and contraction dynamics, measuring isotonic lengthening and that history dependent effects cannot be measured [174]. Furthermore, the results do not necessarily correspond to conditions under which the muscle would normally operate as all conditions are constrained to be isotonic with constant velocity [174]. A new method of obtaining the force-velocity relation is presented in this chapter. This method is similar to the work loop approach to measuring muscle power output. In work loop experiments, the muscle is subjected to sinusoidal length changes and

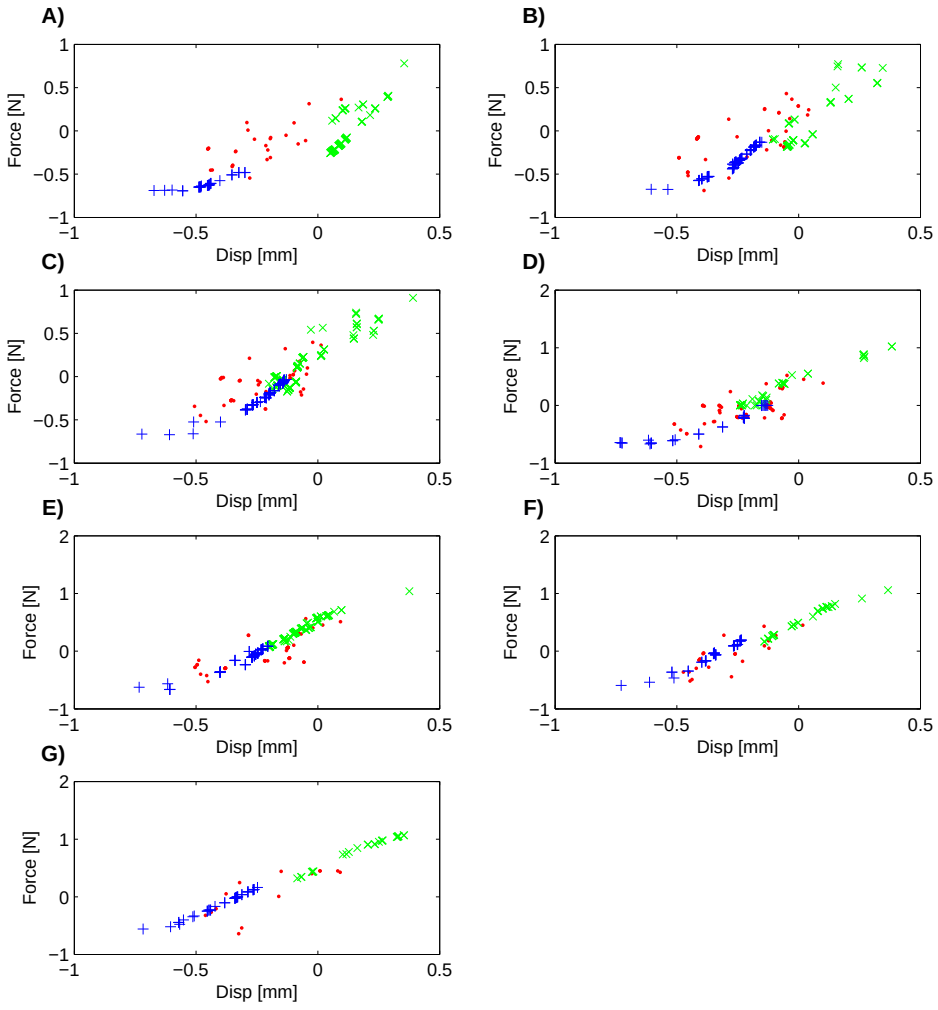

FIGURE 7.21: Force-displacement relation when the velocity v_m is held approximately constant for chirp (.), ramp up-down (×) and ramp down-up (+) inputs. A) $v_m \approx -3\text{mms}^{-1}$, B) $v_m \approx -2\text{mms}^{-1}$, C) $v_m \approx -1\text{mms}^{-1}$, D) $v_m \approx 0\text{mms}^{-1}$, E) $v_m \approx 1\text{mms}^{-1}$, F) $v_m \approx 2\text{mms}^{-1}$, G) $v_m \approx 3\text{mms}^{-1}$,

stimulated with a single stimulus at a chosen phase in the length cycle. A plot of the muscle force against length forms a loop with the area describing the net work per cycle. In the experiments described in this chapter, the muscle was first stimulated and then length changes imposed. This method has advantages as both the lengthening and shortening behaviours can be measured. The imposed length changes can be varied, enabling history dependent effects to be measured.

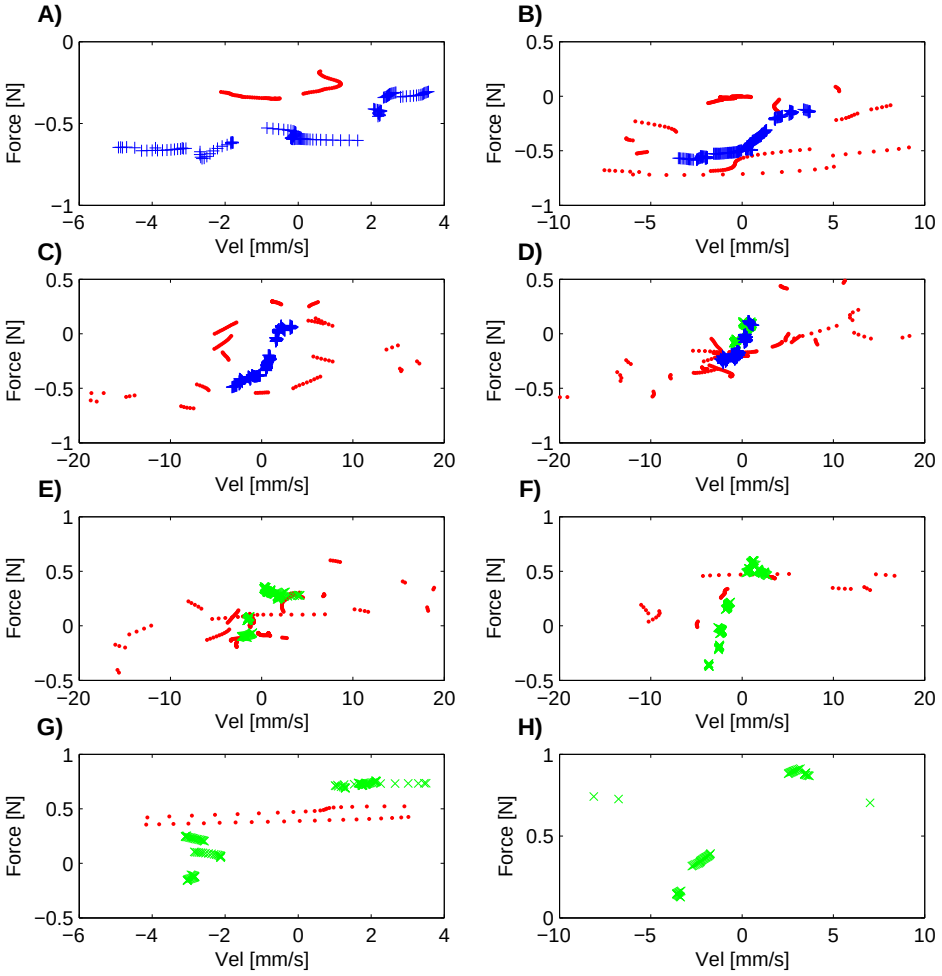

FIGURE 7.22: Force-velocity relation when the displacement x_m is held approximately constant for chirp (.), ramp up-down (×) and ramp down-up (+) inputs. A) $x_m \approx -0.5$mm, B) $x_m \approx -0.4$mm, C) $x_m \approx -0.3$mm, D) $x_m \approx -0.2$mm, E) $x_m \approx -0.1$mm, F) $x_m \approx 0$mm, G) $x_m \approx 0.1$mm, H) $x_m \approx 0.2$mm,

7.5.1 Passive Model

To the author's knowledge, the behaviour of passive skeletal muscle under shortening conditions has not been previously studied. To date passive measurements have commonly been taken on muscle lengthening from rest. In measuring the passive behaviour of the extensor muscle under lengthening and shortening, as in this chapter, the viscoelastic behaviour of the muscle was clear. By using a combination of non-linear cubic springs and dampers, this behaviour could be described well. The slight overshoot and the negative force measured after the muscle is shortened back to its rest length were not well described by the model. It was assumed that the passive muscle could not sustain any negative force, yet a small negative component was measured.

This method results in the force-velocity-length relation arising as a consequence of simpler viscoelastic elements as opposed to being introduced by empirical relations. The advantage of this is that the estimated model has more physical significance.

7.5.2 Active Model

In this thesis no model of the dynamics of the active muscle has been developed, and this remains an area of work in progress. In the presented results, a notable finding is that the force does not seem very dependent upon the muscle velocity. An example of a commonly assumed relation between the contractile force, length and velocity is shown as a F-L-V surface in Fig. 7.23. In Fig. 7.23 the force is a single-valued function of length and velocity. This ignores any history dependent effects, and assumes that the relation between force, length and velocity is single valued. Comparing Fig. 7.23 to the F-L-V surface plotted from results shown in Fig. 7.19, it is clear that the measured relationships between force, length and velocity differ significantly for the locusts in this study. More experiments, with more locusts, that measure the force and displacement (and hence velocity) under maximal stimulation are required to further investigate this finding.

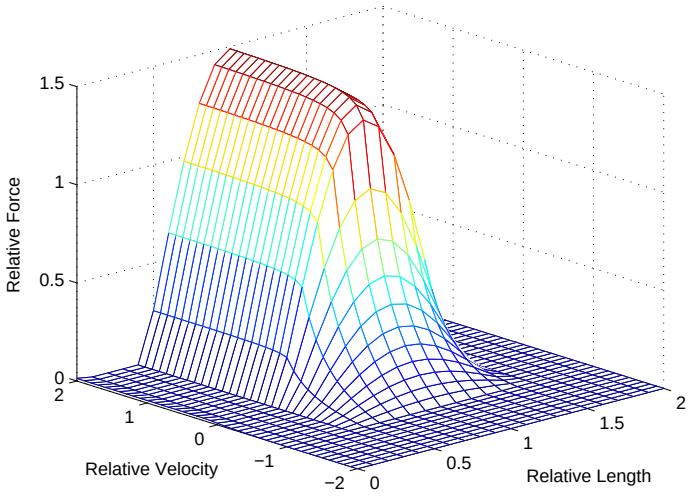

FIGURE 7.23: Standard F-L-V surface from F_L and F_V relations presented in the literature. This particular plot is reconstructed from the relations of Ghigliazza and Holmes [28].

In this section experiments on active muscle were performed under maximal activation. The aim is to first develop a non-isometric model that applies to maximal activation conditions, then to see if and how this model varies dependent upon the level of activation. A similar approach to that described in Chapter 6 for modelling the force-length relation could be utilised.

7.6 Conclusions

This chapter considered contraction under non-isometric conditions. A new method of measuring the force-length-velocity relation was presented. This allows the voltage input to the shaker to be varied in a user defined way, meaning the applied force, and so displacements, can be effectively varied, easing modelling of history dependent effects.

Passive muscle was seen to behave as a viscoelastic material and modelled using a combination of nonlinear springs and dampers. Modelling active muscle under non-isometric conditions remains an area of work in progress; this is discussed along with other future work directions in the following chapter.

Chapter 8

Conclusions and Future Work

In this thesis, the force response of the locust hind leg extensor muscle to input pulses under a range of conditions was investigated. Results presented in this thesis have been discussed in detail in individual chapters. In this last chapter, the main findings of the thesis are concluded. An outline of future work, which would extend the work of this thesis, is also detailed.

Skeletal muscle is a highly complex, nonlinear system. A wide range of models have been used in the literature to describe the muscle force response to a neural stimulus. This is a result of the varying assumptions made by researchers. In this thesis complexity was introduced in the experimental conditions in stages. This meant a model could be built up in parts. This approach reduces the need for questionably valid assumptions. Furthermore, some of the common assumptions made when modelling muscle could be tested. By doing this a greater understanding of the neuromuscular system can be gained. Enhanced understanding of the neuromuscular system leads to more realistic muscle models. This can lead on to more realistic models in the field of modelling movement, as well as improving models used in FES, controlling movement, and in developing devices to restore function after injury [19].

In Chapter 4 the response to individual pulses was investigated. It was found that a second-order linear model provided an adequate description of the response to an isolated input pulse, however the fit using a third-order linear model was better. The fact that the response to isolated pulses could be modelled as linear suggests that much of the non-linear behaviour of the muscle arises as a result of the summation of the responses to closely spaced pulses. As the IPI was decreased and pulses started to sum the behaviour could be approximated as quasi-linear under most conditions. For moderate IPFs the second-order fit deteriorated and the response to each individual input pulse could be modelled using a third-order linear model if parameters describing each pulse were allowed to vary. For long trains at high IPF, the fit

deteriorated, likely due to the assumption of quasi-linear behaviour no longer holding. These findings indicate that the nonlinear behaviour increases with increasing IPF.

The isometric response to each individual pulse was extended by considering predictive models to describe the total force response (Ch. 5). Existing isometric models were fit to data from the locust extensor muscle. Studies that compare existing models are extremely scarce [48]. From this analysis, a new 'Adapted model' was developed. This model builds upon the models of Ding *et al* [20] and Bobet and Stein [73], and has an equivalent number of parameters (six). The Adapted model was found to provide a better fit to data, and to provide a more accurate model of the underlying response to each individual pulse. The model contains two nonlinear saturation terms. These terms are able to capture the nonlinear behaviour of the muscle in response to closely spaced input pulses. When the input is low (e.g. for isolated input pulses) the nonlinearities are weak and the model approximates a linear second-order model, equivalent to that found to provide an adequate fit to individual pulse data.

From the isometric model, developed for a single muscle length, the effect of changing the muscle length on the isometric force was investigated (Ch. 6). A very common assumption in muscle models is that of uncoupled activation and contraction dynamics. However, it was found that the dynamics of the isometric force response depend on the muscle length. This suggests that the assumption of uncoupled activation is poor. The Adapted model was able to model the changing dynamics if the model parameters A, τ_c and τ_2 were described as functions of the FT angle. The overall isometric model for the locust hind leg extensor muscle is given in Chapter 6 as Eq. (6.7) to (6.11).

The isometric case has been thoroughly studied, characterised, and a model to describe the behaviour developed. This thesis contains some additional results regarding the nonisometric case (Ch. 7). The passive response of the muscle could be modelled using an adaption of the SLM, as shown in Fig. 7.14. The passive model is comprised of a SLM with nonlinear springs and a linear damper in parallel with an extra nonlinear damper, where this extra damper has a damping factor which depends on displacement and velocity. The passive muscle was assumed to be unable to sustain any compressive force and so the estimated force was constrained to be greater or equal to zero. The main source of error in the passive model arises as a result of this assumption that the force cannot be negative; in practice the passive muscle does sustain some negative force. The force response of activated muscle, when the velocity is non-zero, has not been fully characterised. This is one area of future work and is discussed in the following section.

8.1 Future work

The muscle system investigated in this thesis is relatively simple, making it ideal to study. In comparison to mammalian muscle, the muscles of invertebrates are innervated by a much smaller number of identifiable neurons. Invertebrate muscle systems lend themselves to the testing and development of muscle models as one can isolate the response to single neurons. Furthermore, in studying muscular function in system where the neural component is well understood, a greater insight into the workings of the neuromuscular system as a whole can be gained. Further work should exploit the benefits of this muscle system, as well as looking at how well the models developed describe the behaviour of mammalian muscle. The main avenues of further investigation are: a) to study the response to each individual neuron and investigate how the force is affected; b) to extend the force-length experiments; c) to investigate how applicable the developed model is to mammalian muscle. These areas are discussed in more detail below.

8.1.1 Study the Response to Each Individual Neuron

The results presented in this thesis refer to the force response to FETi stimulation. One interesting avenue of further investigation would be to do a similar analysis for SETi stimulation. The ability of the model (in Eq. (6.7) to (6.11)) to describe the resultant force response, and the change in any model parameters could be investigated. This might indicate whether the model forms developed in this thesis have much wider generality and applicability.

In mammalian muscle motor units are generally recruited in order of smallest to largest as stimulation increases. In invertebrate muscle individual neurons can be targeted to stimulate particular physiological effects. Stimulating individual neurons is not possible in mammalian muscle. Looking at the effect of stimulation on the force response would provide further insight into the link between the neural and muscular systems. To date the author is not aware of any similar studies.

8.1.2 Extend the Force-Velocity Experiments

The active force experiments, described in Chapter 7, represent an area of work in progress. Some measurements have been made in fully activated muscle. These need extending so that the force response to the physiological range of motion (displacement of ± 0.5mm, velocity of $\pm 10\text{mms}^{-1}$) can be studied. A range of different input types should be used so that any history dependent influences on the force are evident. From these results, the first step is to develop

a model to describe the force response in fully activated muscle when the muscle velocity is non-zero.

Once the fully activated muscle has been characterised, the next step is to investigate how the level of activation affects the force response. This can be achieved by stimulating the muscle to a range of quasi-steady-state submaximal levels of activation and driving the shaker to change the muscle length. From this it could then be established if and how the level of activation affects the nonisometric force response.

The final step would be to couple these results to the isometric model, as was done when the muscle length was varied in Chapter 6, and develop a model able to predict the response to a generalised input when there are no constraints on the motion. A model able to predict physiological behaviour in response to a range of inputs when the muscle is not constrained would be the ultimate goal. The ability to model unconstrained physiological motion is an ideal test of the capability of the resultant model.

8.1.3 Applicability to Mammalian Muscle

The applicability of the developed isometric model to mammalian muscle would provide another interesting avenue for further work. Invertebrate muscle provides a simple system to study and model muscle behaviour. However, many of the benefits of muscle modelling, such as FES, or the development of devices to restore function after injury, are applicable to mammalian muscle. It would therefore be useful to take the isometric model developed for the locust extensor muscle and see how applicable this is to mammalian muscle. Once developed, a similar approach could be used for a non-isometric model.

Mammalian muscle is supplied by a much larger number of nerve fibres and has a correspondingly large number of muscle fibres. In mammalian muscle the number of motor units in a state of active contraction is varied to control the tension developed. When a single motor neuron is activated, all fibres that are innervated by the particular motor neuron contract. The activation of a single motor neuron causes a weak, distributed contraction. Activation of subsequent motor neurons will result in a stronger contraction, as more muscle fibres are activated. One possible way to use the developed model to describe mammalian muscle would be to have a function to describe the recruitment of motor units preceding the model. The resulting contractile force developed by each unit could then be calculated by the model presented in this thesis, and the resultant force given by the sum of the contribution due to each motor unit. Methods that average out the behaviour of each individual motor unit and smear the resulting behaviour may provide a simplification of this approach.

Bibliography

[1] F. E. Zajac. Muscle and tendon: properties, models, scaling, and application to biomechanics and motor control. *Crit Rev Biomed Eng*, 17:359–411, 1989.

[2] R. J. Full and D. E. Koditschek. Templates and anchors: Neuromechanical hypotheses of legged locomotion on land. *J Exp Biol*, 202:3325–3332, 1999.

[3] K. Meijer, M. Rosenthal, and R. J. Full. Muscle-like actuators? A comparison between three electroactive polymers. *Smart Structures and Materials 2001: Electroactive Polymer Actuators and Devices*, 4329:7–15, 2001.

[4] J. M. Winters and S. L-Y. Woo, editors. *Multiple Muscle Systems - Biomechanics and Movements Organization*, chapter 1. Modelling Muscle Mechanics (and Energetics), pages 1–23. Springer, New York, 1990.

[5] C. Guschlbauer, H. Scharstein, and A. Buschges. The extensor tibiae muscle of the stick insect: biomechanical properties of an insect walking leg muscle. *J Exp Biol*, 210:1092–108, 2007.

[6] S. L. Hooper, K. H. Hobbs, and J. B. Thuma. Invertebrate muscles: Thin and thick filament structure; molecular basis of contraction and its regulation, catch and asynchronous muscle. *Prog Neurobiol*, 86:72–127, 2008.

[7] S. Ebashi. The croonian lecture, 1979: Regulation of muscle contraction. *Proc R Soc Lond B Biol Sci*, 207:259–86, 1980.

[8] M. Burrows. *The Neurobiology of an Insect Brain*. Oxford University Press, USA, 1996.

[9] G. Hoyle. Distributions of nerve and muscle fibre types in locust jumping muscle. *J Exp Biol*, 73:205–33, 1978.

[10] G. Hoyle. The anatomy and innervation of locust skeletal muscle. *Proc R Soc Lond B Biol Sci*, 143:281–92, 1955.

[11] G. Hoyle. Neuromuscular mechanisms of a locust skeletal muscle. *Proc R Soc Lond B Biol Sci*, 143:343–367, 1955.

[12] H. C. Bennet-Clark. The energetics of the jump of the locust schistocerca gregaria. *J Exp Biol*, 63:53–83, 1975.

[13] M. Burrows and G. A. Horridge. The organization of inputs to motoneurons of the locust metathoracic leg. *Philos Trans R Soc Lond B Biol Sci*, 269:49–94, 1974.

[14] M. H. Dickinson, C. T. Farley, R. J. Full, M. A. R. Koehl, R. Kram, and S. Lehman. How animals move: An integrative view. *Science*, 288:100–106, 2000.

[15] E. J. Cheng, I. E. Brown, and G. E. Loeb. Virtual muscle: a computational approach to understanding the effects of muscle properties on motor control. *J Neurosci Methods*, 101:117–30, 2000.

[16] J. W. Haefner. *Modeling Biological Systems: Principles and Applications*. Springer, New York, second edition, 2005.

[17] P. A. Huijing. Parameter interdependence and success of skeletal muscle modelling. *Hum Movement Sci*, 14:443–486, 1995.

[18] G. C. Joyce, P. M. Rack, and D. R. Westbury. The mechanical properties of cat soleus muscle during controlled lengthening and shortening movements. *J Physiol*, 204:461–74, 1969.

[19] W. L. Johnson, D. L. Jindrich, R. R. Roy, and V. R. Edgerton. A three-dimensional model of the rat hindlimb: musculoskeletal geometry and muscle moment arms. *J Biomech*, 41:610–9, 2008.

[20] J. Ding, A. S. Wexler, and S. A. Binder-Macleod. A mathematical model that predicts the force-frequency relationship of human skeletal muscle. *Muscle Nerve*, 26:477–85, 2002.

[21] E. Eisenberg, T. L. Hill, and Y. Chen. Cross-bridge model of muscle-contraction - quantitative-analysis. *Biophys J*, 29:195–227, 1980.

[22] G. Theophilidis and M. D. Burns. The innervation of the mesothoracic flexor tibiae muscle of the locust. *J Exp Biol*, 105:373–388, 1983.

[23] Y. C Fung. *Biomechanics Mechanical Properties of Living Tissues*. Springer-Verlag New York, Inc, 1981.

[24] R. L. Lieber. *Skeletal Muscle Structure, Function, and Plasticity*. Lippincott Williams and Wilkins, Baltimore, second edition, 2002.

[25] H. Bader, K. Gietzen, J. Rosenthal, R. Rudel, and H. U. Wolf, editors. *Intracellular Calcium Regulation*. Manchester University Press, Manchester, 1986.

[26] S. Ebashi and M. Endo. Calcium ion and muscle contraction. *Prog Biophys Mol Biol*, 18:123–83, 1968.

[27] A. F. Huxley. Muscular contraction. *J Physiol*, 243:1–43, 1974.

[28] R. M. Ghigliazza and P. Holmes. Towards a neuromechanical model for insect locomotion: Hybrid dynamical systems. *Regular and Chaotic dynamics*, 10:193–225, 2005.

[29] H. E. Huxley. The crossbridge mechanism of muscular-contraction and its implications. *J Exp Biol*, 115:17–30, 1985.

[30] A. F. Huxley and R. Niedergerke. Structural changes in muscle during contraction; interference microscopy of living muscle fibres. *Nature*, 173:971–3, 1954.

[31] H. Huxley and J. Hanson. Changes in the cross-striations of muscle during contraction and stretch and their structural interpretation. *Nature*, 173:973–6, 1954.

[32] D. Basmadjian. *Mathematical Modeling of Physical Systems. An Introduction.* Oxford University Press, New York, 2003.

[33] L. A. Bernotas, P. E. Crago, and H. J. Chizeck. A discrete-time model of electrically stimulated muscle. *IEEE Trans Biomed Eng*, 33:829–838, 1986.

[34] R. M. Alexander. Modelling approaches in biomechanics. *Philos Trans R Soc Lond B Biol Sci*, 358:1429–35, 2003.

[35] R. Riener and J. Quintern. A physiologically based model of muscle activation verified by electrical stimulation. *Bioelectroch Bioener*, 43:257–264, 1997.

[36] A. V. Hill. The heat of shortening and the dynamic constants of muscle. In *Proc R Soc Lond B Biol Sci*, volume 126, pages 136–195, 1938.

[37] A. V. Hill. The heat of activation and the heat of shortening in a muscle twitch. *Proc R Soc Lond B Biol Sci*, 136:195–211, 1949.

[38] J. M. Winters and S. L-Y. Woo, editors. *Multiple Muscle Systems - Biomechanics and Movements Organization*, chapter 5. Hill-Based Muscle Models: A Systems Engineering Perspective, pages 69–93. Springer, 1990.

[39] H. Hatze. A myocybernetic control model of skeletal muscle. *Biol Cybern*, 25:103–19, 1977.

[40] H. Hatze. A general myocybernetic control model of skeletal muscle. *Biol Cybern*, 28:143–57, 1978.

[41] J. P. van Zandwijk, M. F. Bobbert, J. Harlaar, and A. L. Hof. From twitch to tetanus for human muscle: experimental data and model predictions for m-triceps surae. *Biol Cybern*, 79:121–130, 1998.

[42] W. K. Durfee and K. I. Palmer. Estimation of force-activation, force-length, and force-velocity properties in isolated, electrically stimulated muscle. *IEEE Trans Biomed Eng*, 41:205–16, 1994.

[43] P. M. H. Rack and D. R. Westbury. Short-range stiffness of active mammalian muscle and its effect on mechanical-properties. *J Physiol-London*, 240:331–350, 1974.

[44] A. S. Bahler. Series elastic component of mammalian skeletal muscle. *Am J Physiol*, 213:1560–4, 1967.

[45] F. J. Julian and R. L. Moss. Sarcomere length-tension relations of frog skinned muscle-fibers at lengths above the optimum. *J Physiol*, 304:529–539, 1980.

[46] R. L. Moss. Sarcomere length-tension relations of frog skinned muscle fibres during calcium activation at short lengths. *J Physiol*, 292:177–92, 1979.

[47] P. A. Huijing. Muscle, the motor of movement: properties in function, experiment and modelling. *J Electromyography and Kinesiol*, 8:61–77, 1998.

[48] J. Bobet, E. R. Gossen, and R. B. Stein. A comparison of models of force production during stimulated isometric ankle dorsiflexion in humans. *IEEE Trans Neural Syst Rehabil Eng*, 13:444–51, 2005.

[49] J. Zakotnik, T. Matheson, and V. Durr. Co-contraction and passive forces facilitate load compensation of aimed limb movements. *J Neurosci*, 26:4995–5007, 2006.

[50] J. Bobet, R. B. Stein, and M. N. Oguztoreli. A linear time - varying model of force generation in skeletal muscle. *IEEE Trans Biomed Eng*, 40:1000–1006, 1993.

[51] A. Mannard and R. B. Stein. Determination of the frequency response of isometric soleus muscle in the cat using random nerve stimulation. *J Physiol*, 229:275–96, 1973.

[52] P. Bawa, A. Mannard, and R. B. Stein. Effects of elastic loads on the contractions of cat muscles. *Biol Cybern*, 22:129–37, 1976.

[53] P. Bawa, A. Mannard, and R. B. Stein. Predictions and experimental tests of a visco-elastic muscle model using elastic and inertial loads. *Biol Cybern*, 22:139–45, 1976.

[54] R. Baratta and M. Solomonow. The dynamic response model of nine different skeletal muscles. *IEEE Trans Biomed Eng*, 37:243–51, 1990.

[55] R. V. Baratta, M. Solomonow, and B. H. Zhou. Frequency domain-based models of skeletal muscle. *J Electromyogr Kinesiol*, 8:79–91, 1998.

[56] I. E. Brown and G. E. Loeb. Measured and modeled properties of mammalian skeletal muscle. I. the effects of post-activation potentiation on the time course and velocity dependencies of force production. *J Muscle Res Cell Motil*, 20:443–56, 1999.

[57] I. E. Brown, E. J. Cheng, and G. E. Loeb. Measured and modeled properties of mammalian skeletal muscle. ii. the effects of stimulus frequency on force-length and force-velocity relationships. *J Muscle Res Cell Motil*, 20:627–43, 1999.

[58] I. E. Brown and G. E. Loeb. Measured and modeled properties of mammalian skeletal muscle: III. the effects of stimulus frequency on stretch-induced force enhancement and shortening-induced force depression. *J Muscle Res Cell Motil*, 21:21–31, 2000.

[59] I. E. Brown and G. E. Loeb. Measured and modeled properties of mammalian skeletal muscle: IV. dynamics of activation and deactivation. *J Muscle Res Cell Motil*, 21:33–47, 2000.

[60] J. Ding, S. C. Lee, T. E. Johnston, A. S. Wexler, W. B. Scott, and S. A. Binder-Macleod. Mathematical model that predicts isometric muscle forces for individuals with spinal cord injuries. *Muscle Nerve*, 31:702–12, 2005.

[61] A. S. Wexler, J. Ding, and S. A. Binder-Macleod. A mathematical model that predicts skeletal muscle force. *IEEE Trans Biomed Eng*, 44:337–48, 1997.

[62] H. Gollee and K. J. Hunt. Nonlinear modelling and control of electrically stimulated muscle: a local model network approach. *Int. J. Control*, 68:1259–1288, 1997.

[63] H. Gollee, D. J. Murray-Smith, and J. C. Jarvis. A nonlinear approach to modeling of electrically stimulated skeletal muscle. *IEEE Trans Biomed Eng*, 48:406–15, 2001.

[64] K. J. Hunt, M. Munih, N. N. Donaldson, and F. M. Barr. Investigation of the hammerstein hypothesis in the modeling of electrically stimulated muscle. *IEEE Trans Biomed Eng*, 45:998–1009, 1998.

[65] N. de N. Donaldson, H. Gollee, K. J. Hunt, C. Jarvis, and Kwende M. K. N. A radial basis function model of muscle stimulated with irregular inter-pulse intervals. *Med. Eng. Phys.*, 17:431–441, 1995.

[66] A. E. Chapman and P. T. Harrower. Linear approximations of muscle mechanics in isometric contraction. *Biol Cybern*, 27:1–7, 1977.

[67] R. B. Stein, A. S. French, A. Mannard, and R. Yemm. New methods for analysing motor function in man and animals. *Brain Res*, 40:187–92, 1972.

[68] B. H. Zhou, M. Solomonow, R. Baratta, and R. D'Ambrosia. Dynamic performance model of an isometric muscle-joint unit. *Med Eng Phys*, 17:145–50, 1995.

[69] H. E. Huxley. Structural changes during muscle contraction. *Biochem J*, 125:85, 1971.

[70] A. F. Huxley. A note suggesting that the cross-bridge attachment during muscle contraction may take place in two stages. *Proc R Soc Lond B Biol Sci*, 183:83–6, 1973.

[71] R. B. Stein and F. Parmiggiani. Nonlinear summation of contractions in cat muscles. I. early depression. *J Gen Physiol*, 78:277–93, 1981.

[72] F. Parmiggiani and R. B. Stein. Nonlinear summation of contractions in cat muscles. II. later facilitation and stiffness changes. *J Gen Physiol*, 78:295–311, 1981.

[73] J. Bobet and R. B. Stein. A simple model of force generation by skeletal muscle during dynamic isometric contractions. *IEEE Trans Biomed Eng*, 45:1010–6, 1998.

[74] R. Raikova, J. Celichowski, M. Pogrzebna, H. Aladjov, and P. Krutki. Modeling of summation of individual twitches into unfused tetanus for various types of rat motor units. *J Electromyogr Kinesiol*, 17:121–30, 2007.

[75] R. Raikova, M. Pogrzebna, H. Drzymala, J. Celichowski, and H. Aladjov. Variability of successive contractions subtracted from unfused tetanus of fast and slow motor units. *J Electromyogr Kinesiol*, 18:741–51, 2008.

[76] J. Celichowski, R. Raikova, H. Drzymala-Celichowska, I. Ciechanowicz-Kowalczyk, P. Krutki, and R. Rusev. Model-generated decomposition of unfused tetani of motor units evoked by random stimulation. *J Biomech*, 41:3448–54, 2008.

[77] W. K. Durfee and K. E. MacLean. Methods for estimating isometric recruitment curves of electrically stimulated muscle. *IEEE Trans Biomed Eng*, 36:654–67, 1989.

[78] T. L. Chia, P. C. Chow, and H. J. Chizeck. Recursive parameter identification of constrained systems: an application to electrically stimulated muscle. *IEEE Trans Biomed Eng*, 38:429–42, 1991.

[79] P. Holmes, R. J. Full, D. Koditscheck, and J. Guckenheimer. The dynamics of legged locomotion: Models, analyses, and challenges. *SIAM Review*, 48:207–204, 2006.

[80] J. Zakotnik. *Biomechanics and neural control of targeted limb movements in an insect.* PhD thesis, University of Bielfield, Faculty for Biology, 2006.

[81] R. Murray Smith and T. A. Johansen, editors. *Multiple Model Approaches to Modelling and Control*, chapter 3. Modelling Electrically Simulated Muscle, pages 101–120. Taylor and Francis, London, 1997.

[82] L. A. Frey Law and R. K. Shields. Mathematical models use varying parameter strategies to represent paralyzed muscle force properties: a sensitivity analysis. *J Neuroeng Rehabil*, 2:18, 2005.

[83] B. J. van der Linden, H. F. Koopman, H. J. Grootenboer, and P. A. Huijing. Modelling functional effects of muscle geometry. *J Electromyogr Kinesiol*, 8:101–9, 1998.

[84] J. L. Van Leeuwen and C. W. Spoor. Modelling mechanically stable muscle architectures. *Philos Trans R Soc Lond B Biol Sci*, 336:275–92, 1992.

[85] E. Otten. Concepts and models of functional architecture in skeletal muscle. *Exerc Sport Sci Rev*, 16:89–137, 1988.

[86] K. L. Zierler. *Medical Physiology*, volume 1. C.V. Mosby, St. Louis, 13th edition, 1976.

[87] M. Epstein and W. Herzog. *Theoretical Models of Skeletal Muscle*. John Wiley and Sons, New York, 1998.

[88] J. M. Winters. How detailed should muscle models be to understand multijoint movement coordination. *Hum Movement Sci*, 14:401–442, 1995.

[89] H. Hatze. *Myocybernetic control models of skeletal muscle*. University of South Africa, Petoria, 1981.

[90] R. Perumal, A. S. Wexler, and S. A. Binder-Macleod. Mathematical model that predicts lower leg motion in response to electrical stimulation. *J Biomech*, 39:2826–36, 2006.

[91] R. Riener, J. Quintern, and G. Schmidt. Biomechanical model of the human knee evaluated by neuromuscular stimulation. *J Biomech*, 29:1157–67, 1996.

[92] M. F. Bobbert and A. J. Van Soest. Effects of muscle strengthening on vertical jump height: a simulation study. *Med Sci Sports Exerc*, 26:1012–20, 1994.

[93] K. Meijer, H. J. Grootenboer, H. F. J. M. Koopman, B. J. J. J. van der Linden, and P. A. Huijing. A hill type model of rat medial gastrocnemius muscle that accounts for shortening history effects. *J Biomech*, 31:555–563, 1998.

[94] R. Close. Dynamic properties of fast and slow skeletal muscles of the rat during development. *J Physiol*, 173:74–95, 1964.

[95] Y. W. Chang, F. C. Su, H. W. Wu, and K. N. An. Optimum length of muscle contraction. *Clin Biomech*, 14:537–542, 1999.

[96] Y. Giat, J. Mizrahi, and M. Levy. A musculotendon model of the fatigue profiles of paralyzed quadriceps muscle under fes. *IEEE Trans Biomed Eng*, 40:664–74, 1993.

[97] E. J. Perreault, C. J. Heckman, and T. G. Sandercock. Hill muscle model errors during movement are greatest within the physiologically relevant range of motor unit firing rates. *J Biomech*, 36:211–8, 2003.

[98] D. R. Wilkie. The mechanical properties of muscle. *Br Med Bull*, 12:177–82, 1956.

[99] D. R. Wilkie. Muscle function: a personal view. *J Exp Biol*, 115:1–13, 1985.

[100] J. M. Ritchie and D. R. Wilkie. The dynamics of muscular contraction. *J Physiol*, 143:104–13, 1958.

[101] A. M. Gordon, A. F. Huxley, and F. J. Julian. The variation in isometric tension with sarcomere length in vertebrate muscle fibres. *J Physiol*, 184:170–92, 1966.

[102] I. E. Brown, S. H. Scott, and G. E. Loeb. Mechanics of feline soleus: II. design and validation of a mathematical model. *J Muscle Res Cell Motil*, 17:221–33, 1996.

[103] B. Hannaford and L. Stark. Late agonist activation burst (pc) required for optimal head movement - a simulation study. *Biol Cybern*, 57:321–330, 1987.

[104] R. V. Baratta, M. Solomonow, G. Nguyen, and R. D'Ambrosia. Load, length, and velocity of load-moving tibialis anterior muscle of the cat. *J Appl Physiol*, 80:2243–9, 1996.

[105] W. Herzog and T. R. Leonard. Force enhancement following stretching of skeletal muscle: a new mechanism. *J Exp Biol*, 205:1275–1283, 2002.

[106] W. Herzog, R. Schachar, and T. R. Leonard. Characterization of the passive component of force enhancement following active stretching of skeletal muscle. *J Exp Biol*, 206:3635–3643, 2003.

[107] G. J. Ettema, P. A. Huijing, and A. de Haan. The potentiating effect of prestretch on the contractile performance of rat gastrocnemius medialis muscle during subsequent shortening and isometric contractions. *J Exp Biol*, 165:121–36, 1992.

[108] B. C. Abbott and D. R. Wilkie. The relation between velocity of shortening and the tension-length curve of skeletal muscle. *J Physiol*, 117:26 P, 1952.

[109] G. A. Cavagna and G. Citterio. Effect of stretching on the elastic characteristics and the contractile component of frog striated muscle. *J Physiol*, 239:1–14, 1974.

[110] K. A. Edman, G. Elzinga, and M. I. Noble. Enhancement of mechanical performance by stretch during tetanic contractions of vertebrate skeletal muscle fibres. *J Physiol*, 281:139–55, 1978.

[111] K. A. Edman, G. Elzinga, and M. I. Noble. Residual force enhancement after stretch of contracting frog single muscle fibers. *J Gen Physiol*, 80:769–84, 1982.

[112] H. Sugi and T. Tsuchiya. Enhancement of mechanical performance in frog muscle fibres after quick increases in load. *J Physiol*, 319:239–52, 1981.

[113] H. Sugi and T. Tsuchiya. Stiffness changes during enhancement and deficit of isometric force by slow length changes in frog skeletal muscle fibres. *J Physiol*, 407:215–29, 1988.

[114] W. Herzog and T. R. Leonard. Depression of cat soleus-forces following isokinetic shortening. *J Biomech*, 30:865–72, 1997.

[115] I. E. Brown and G. E. Loeb. Post-activation potentiation. a clue for simplifying models of muscle dynamics. *Amer Zool*, 38:743–754, 1998.

[116] G. Shue, P. E. Crago, and H. J. Chizeck. Muscle-joint models incorporating activation dynamics, moment-angle, and moment-velocity properties. *IEEE Trans Biomed Eng*, 42:212–23, 1995.

[117] G. H. Shue and P. E. Crago. Muscle-tendon model with length history-dependent activation-velocity coupling. *Ann Biomed Eng*, 26:369–80, 1998.

[118] D. A. Repperger, C. A. Phillips, A. Neidhard-Doll, D. B. Reynolds, and J. Berlin. Actuator design using biomimicry methods and a pneumatic muscle system. *Control Engineering Practice*, 14:999–1009, 2006.

[119] A. F. Huxley. Muscle structure and theories of contraction. *Prog Biophys Biophys Chem*, 7:255–318, 1957.

[120] A. Minajeva, M. Kulke, J. M. Fernandez, and W. A. Linke. Unfolding of titin domains explains the viscoelastic behavior of skeletal myofibrils. *Biophys J*, 80:1442–1451, 2001.

[121] H. Higuchi. Viscoelasticity and function of connectin/titin filaments in skinned muscle fibers. *Adv Biophys*, 33:159–171, 1996.

[122] H. L. Granzier and K. Wang. Passive tension and stiffness of vertebrate skeletal and insect flight muscles: the contribution of weak cross-bridges and elastic filaments. *Biophys J*, 65:2141–59, 1993.

[123] A. Horowitz, H. P. Wussling, and G. H. Pollack. Effect of small release on force during sarcomere-isometric tetani in frog muscle fibers. *Biophys J*, 63:3–17, 1992.

[124] C. A. Opitz, M. Kulke, M. C. Leake, C. Neagoe, H. Hinssen, R. J. Hajjar, and W. A. Linke. Damped elastic recoil of the titin spring in myofibrils of human myocardium. *Proc Natl Acad Sci U S A*, 100:12688–93, 2003.

[125] M. L. Bartoo, W. A. Linke, and G. H. Pollack. Basis of passive tension and stiffness in isolated rabbit myofibrils. *Am J Physiol*, 273:266–76, 1997.

[126] S. P. Magnusson. Passive properties of human skeletal muscle during stretch maneuvers. a review. *Scand J Med and Sci Spor*, 8:65–77, 1998.

[127] W. A. Linke and M. C. Leake. Multiple sources of passive stress relaxation in muscle fibres. *Phys Med Biol*, 49:3613–27, 2004.

[128] A. L. Dorfmann, W. A. Woods, and B. A. Trimmer. Muscle performance in a soft-bodied terrestrial crawler: constitutive modelling of strain-rate dependency. *J R Soc Interface*, 5:349–62, 2008.

[129] T. M. G. J. van Eijden, S. J. J. Turkawsaki, L. J. van Ruijven, and P. Brugman. Passive force characteristics of an architecturally complex muscle. *J Biomech*, 35:1183–1189, 2002.

[130] Y. F. Heerkens, R. D. Woittiez, P. A. Huijing, A. Huson, G. J. van Ingen Schenau, and R. H. Rozendal. Passive resistance of the human knee: the effect of remobilization. *J Biomed Eng*, 9:69–76, 1987.

[131] J. Tian, T. Iwasaki, and W. O. Friesen. Muscle function in animal movement: passive mechanical properties of leech muscle. *J Comp Physiol A Neuroethol Sens Neural Behav Physiol*, 193:1205–19, 2007.

[132] E. J. Hunter and I. R. Titze. Refinements in modeling the passive properties of laryngeal soft tissue. *J Appl Physiol*, 103:206–19, 2007.

[133] J. E. Speich, K. Quintero, C. Dosier, L. Borgsmiller, H. P. Koo, and P. H. Ratz. A mechanical model for adjustable passive stiffness in rabbit detrusor. *J Appl Physiol*, 101:1189–98, 2006.

[134] J. E. Speich, C. Dosier, L. Borgsmiller, K. Quintero, H. P. Koo, and P. H. Ratz. Adjustable passive length-tension curve in rabbit detrusor smooth muscle. *J Appl Physiol*, 102:1746–55, 2007.

[135] R. J. Full and M. S. Tu. Mechanics of six-legged runners. *J Exp Biol*, 148:129–46, 1990.

[136] R. Josephson and C. Ellington. Power output from a flight muscle of the bumblebee bombus terrestris. I. some features of the dorso-ventral flight muscle. *J Exp Biol*, 200:1215–26, 1997.

[137] J. G. Malamud. The tension in a locust flight-muscle at varied muscle lengths. *J Exp Biol*, 144:479–494, 1989.

[138] K. E. Machin and J. W. S. Pringle. The physiology of insect fibrillar muscle. II. mechanical properties of a beetle flight muscle, 1959.

[139] J. W. Pringle and R. T. Tregear. Mechanical properties of insect fibrillar muscle at large amplitudes of oscillation. *Proc R Soc Lond B Biol Sci*, 174:33–50, 1969.

[140] Usherwood. P. N and H. I. Runion. Analysis of mechanical responses of metathoracic extensor tibiae muscles of free-walking locusts. *J Exp Biol*, 52:39–58, 1970.

[141] M. S. Tu and T. L. Daniel. Cardiac-like behavior of an insect flight muscle. *J Exp Biol*, 207:2455–2464, 2004.

[142] R. Full and A. Ahn. Static forces and moments generated in the insect leg: comparison of a three-dimensional musculo-skeletal computer model with experimental measurements. *J Exp Biol*, 198:1285–98, 1995.

[143] D. Cofer, G. Cymbalyuk, W. J. Heitler, and D. H. Edwards. Neuromechanical simulation of the locust jump. *J Exp Biol*, 213:1060–8, 2010.

[144] M. Burrows and G. Morris. The kinematics and neural control of high-speed kicking movements in the locust. *J Exp Biol*, 204:3471–81, 2001.

[145] W. J. Heitler. Locust jump III. structural specializations of meta-thoracic tibiae. *J Exp Biol*, 67:29–36, 1977.

[146] E. Otten. Inverse and forward dynamics: models of multi-body systems. *Philos Trans R Soc Lond B Biol Sci*, 358:1493–500, 2003.

[147] W. J. Heitler. Locust jump - specializations of metathoracic femoral-tilbial joint. *J Comp Physiol*, 89:93–104, 1974.

[148] J. M. Gabriel. The development of the locust jumping mechanism II. energy storage and muscle mechanics. *J Exp Biol*, 118:327–340, 1985.

[149] P. L. Newland and N. J. Emptage. The central connections and actions during walking of tibial campaniform sensilla in the locust. *J Comp Physiol A Neuroethol Sens Neural Behav Physiol*, 178:749–762, 1996.

[150] A. G. Vidal-Gadea, X. J. Jing, D. Simpson, O. P. Dewhirst, Y. Kondoh, R. Allen, and P. L. Newland. Coding characteristics of spiking local interneurons during imposed limb movements in the locust. *J Neurophysiol*, 103:603–615, 2010.

[151] M. D. Burns. Control of walking in orthoptera .1. leg movements in normal walking. *J Exp Biol*, 58:45–58, 1973.

[152] W. J. Heitler and Braunig P. The role of the fast extensor motor activity in the locust kick reconsidered. *J Exp Biol*, 136:289–309, 1988.

[153] L. Ljung. *System Identification Theory for the User*. Prentice Hal, Englewood Cliffs, NJ, 2nd edition, 1999.

[154] K. Hsu, C. Novara, M. Milanese, and K. Poolla. Parametric and nonparametric curve fitting. *Automatica*, 42:1869–1873, 2006.

[155] K. P. Burnham and D. R. Anderson. *Model Selection and Multimodel Inference A Practical Information - Theoretical Approach*. Springer, New York, second edition, 1998.

[156] E. Wilson, E. Rustighi, B. R. Mace, and P. L. Newland. Isometric force generated by locust skeletal muscle: responses to single stimuli. *Biol Cybern*, 102:503–511, 2010.

[157] The MathWorks. *Curve Fitting Toolbox User's Guide*. The MathWorks, Inc, Natick, 2001.

[158] O. Nelles. *Nonlinear system identification: classical approaches to neural networks and fuzzy models*. Springer-Verlag, Berlin Heidelberg, 2001.

[159] W. J. Heitler and M. Burrows. The locust jump. I. the motor programme. *J Exp Biol*, 66:203–19, 1977.

[160] M. R. Forster. Key concepts in model selection: Performance and generalizability. *Journal of Mathematical Psychology*, 44:205–231, 2000.

[161] H. de G. Acquah. Comparison of akaike information criterion (AIC) and bayesian information criterion (BIC) in selection of an asymmetric price relationship. *JDAE*, 2:1–6, 2010.

[162] D. M. Hamby. A reveiw of techniques for parameter sensitivity analysis of environmental models. *Environ Monit Assess*, 32:135–154, 1994.

[163] D. E. Rassier, B. R. MacIntosh, and W. Herzog. Length dependence of active force production in skeletal muscle. *J Appl Physiol*, 86:1445–57, 1999.

[164] C. D. Balnave and D. G. Allen. The effect of muscle length on intracellular calcium and force in single fibres from mouse skeletal muscle. *J Physiol*, 492:705–713, 1996.

[165] R. I. Close. The relations between sarcomere length and characteristics of isometric twitch contractions of frog satorius muscle. *J Physiol*, 220:745–762, 1972.

[166] R. Perumal, A. S. Wexler, J. Ding, and S. A. Binder-Macleod. Modeling the length dependence of isometric force in human quadriceps muscles. *J Biomech*, 35:919–930, 2002.

[167] J. R. Blinks, R. Rudel, and S. R. Taylor. Calcium transients in isolated amphibian skeletal muscle fibres: detection with aequorin. *J Physiol*, 277:291–323, 1978.

[168] A. N. Ahn and R. J. Full. A motor and a brake: two leg extensor muscles acting at the same joint manage energy differently in a running insect. *J Exp Biol*, 205:379–89, 2002.

[169] M. D. Burns and P. N. R. Usherwood. Mechanical-properties of locust extensor tibiae muscles. *Comp Biochem Phys A*, 61:85–95, 1978.

[170] J. W. Luo, J. Bai, and J. H. Shao. Application of the wavelet transforms on axial strain calculation in ultrasound elastography. *Prog Nat Sci*, 16:942–947, 2006.

[171] R. Horowits. Passive force generation and titin isoforms in mammalian skeletal-muscle. *Biophys J*, 61:392–398, 1992.

[172] P. C. Krause, J. S. Choi, and T. A. Mcmahon. The force-velocity curve in passive whole muscle is asymmetric about zero velocity. *J Biomech*, 28:1035–1043, 1995.

[173] J. M. Mccarter, F. R. N. Nabarro, and C. H. Wyndham. Reversibility of passive length-tension relation in mammalian skeletal muscle. *Archives Internationales De Physiologie Et De Biochimie*, 79:469–479, 1971.

[174] R. K. Josephson. Contraction dynamics and power output of skeletal-muscle. *Ann Rev Physiol*, 55:527–546, 1993.